



Cellulose Interaction with Cationic Polyelectrolyte: Engineering Paper Strength, Structure and Surface

**Thesis in the fulfilment of the requirement for the degree of
Doctor of Philosophy in Chemical Engineering**

by

Jielong Su

M. Eng. (Chem.)

Department of Chemical Engineering

Faculty of Engineering

MONASH UNIVERSITY

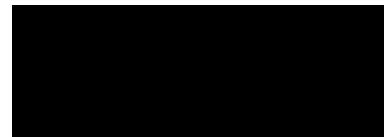
March 2015

This page is intentionally blank

Copyright Notice

Under the Copyright Act 1968, this thesis must be used only under the normal conditions of scholarly fair dealing. In particular no results or conclusions should be extracted from it, nor should it be copied or closely paraphrased in whole or in part without the written consent of the author. Proper written acknowledgement should be made for any assistance obtained from this thesis.

I certify that I have made all reasonable efforts to secure copyright permissions for third party content included in this thesis and have not knowingly added copyright content to my work without the owner's permission.



Jielong Su

This page is intentionally blank

TABLE OF CONTENTS

	Page
Title Page	i
Copyright Notice	iii
General Declaration	vii
Dedication	viii
Acknowledgements	ix
Abstract	xi
List of Publications	xiv
List of Figures	xv
List of Tables	xxi
List of Abbreviations	xxiii
List of Nomenclature	xxiv
Chapter 1	Introduction and Literature Review 25
Chapter 2	Paper strength development and recyclability with polyamideamnie-epichlorohydrin (PAE). 73
Chapter 3	Paper engineered with cellulosic additives: effect of length scale. 93
Chapter 4	Effect of Tethered and Free Microfibrillated Cellulose (MFC) on the Properties of Paper Composites. 117
Chapter 5	Engineering paper as a substrate for blood typing bio-diagnostics. 141
Chapter 6	Adsorption of cationic polyacrylamide at the cellulose-liquid interface: a neutron reflectometry study. 163
Chapter 7	Preparation of smooth deuterated cellulose films for visualisation of adsorbed macromolecules. 203
Chapter 8	Conclusion 233
Appendix	Papers Included in Each Chapter in Their Published Format 239
	I (A) Paper strength development and recyclability with polyamideamnie-epichlorohydrin (PAE).
	I (B) Paper engineered with cellulosic additives: effect of length scale
	I (C) Effect of tethered and free microfibrillated cellulose (MFC) on the properties of paper composites
	I (D) Engineering paper as a substrate for blood typing bio-diagnostics.
	I(E) Adsorption of cationic polyacrylamide at the cellulose-liquid interface: a neutron reflectometry study.

Monash University

Declaration for thesis based or partially based on conjointly published or unpublished work

General Declaration

In accordance with Monash University Doctorate Regulation 17.2 Doctor of Philosophy and Research Master's regulations the following declarations are made:

I hereby declare that this thesis contains no material which has been accepted for the award of any other degree or diploma at any university or equivalent institution and that, to the best of my knowledge and belief, this thesis contains no material previously published or written by another person, except where due reference is made in the text of the thesis.

This thesis includes five original papers published in peer reviewed journals and one manuscript in preparation to be submitted to peer reviewed journals. The core theme of the thesis is to investigate the fundamental science and mechanisms for paper engineering of strength, structure and surface using interactions between cellulose and cationic polyelectrolytes are investigated with the aim of improving paper-based bio-analytical devices. The ideas, development and writing up of all the papers in the thesis were the principal responsibility of myself, the candidate, working within the Department of Chemical Engineering under the supervision of Prof. Gil Garnier and Dr. Warren Batchelor.

The inclusion of co-authors reflects the fact that the work came from active collaboration between researchers and acknowledges input into team-based research.

In the case of six chapters listed below, my contribution to the work involved the following:

Thesis chapter	Publication title	Publication status*	Nature and extent of candidate's contribution
2	Paper strength development and recyclability with polyamideamine-epichlorohydrin (PAE).	Published	Initiation, key ideas, experimental works, analysis works, development and writing up.
3	Paper engineered with cellulosic additives: effect of length scale	Published	
4	Effect of tethered and free microfibrillated cellulose (MFC) on the properties of paper composites	Published	
5	Engineering paper as a substrate for blood typing bio-diagnostics.	Published	
6	Adsorption of cationic polyacrylamide at the cellulose-liquid interface: a neutron reflectometry study.	Published	
7	Preparation of smooth deuterated cellulose films for visualisation of adsorbed macromolecules	Manuscript in Preparation	

I have / have not (circle that which applies) renumbered sections of submitted or published papers in order to generate a consistent presentation within the thesis.

Signed: ... 

Date: 2015-3-12

Dedicated to my family

This page is intentionally blank

ACKNOWLEDGEMENTS

First of all, I would like to present my sincere appreciation and gratitude to my main supervisor Prof. Gil Garnier for providing me an opportunity to conduct this research in the Bioresource Processing Research Institute of Australia (BioPRIA). His insightful guidance and generous support throughout my thesis has allowed me to complete the study. He has always been encouraging and helping me to improve during the whole period of candidature, no matter whether my experiments failed or succeeded. He introduced me not only to the science of celluloses and polymers, but also to many experts and scientists from different disciplines. He has been a model supervisor, from whom I have learned how to work efficiently and to focus on the priorities, although this is very much a ‘work in progress’ from my perspective. His supervision and personality will greatly benefit and enrich my future career development and for that I will be ever grateful.

I am highly appreciative of my co-supervisor Dr. Warren Batchelor. He taught me many fundamentals concerning cellulose fibers and paper physics, as well as giving valuable comments and suggestions about academic writing forms and experimentation. Special thanks to Prof. Wei Shen for his critical discussions during my candidature. I also would like to acknowledge Dr. Christopher J Garvey and Dr. Stephen Holt in Australian National Nuclear Research and Development Organisation for helping me with instrumentation and data analysis. I will never forget Dr. Warwick Raverty for his broad knowledge of cellulose chemistry, his useful guidance on preparation of cellulose derivatives and help in correcting my written English. Associate Prof. Bjorn Winther-Jensen and Dr. Rico F Tabor at Monash University are gratefully acknowledged here for their expertise on cellulose film preparation and characterization.

I would like to express my gratefulness to Dr. Wade Mosse, Dr. Junfei Tian, Dr. Liyuan Zhang, Dr. Ying Hui Ngo, Dr. Ping Peng, Dr. Mohammad Al-Tamimi Dr. Emily Perkins, Dr. Sigappi Narayanan, Dr. Varanasi Swambabu, Dr. Xu Li, Dr. Tina Arbatan, Dr. David Ballerini, Hui Hui Chiam, Whui Lyn Then, Natasha Yeow, Praveena Raj, Uthpala Garusinghe, Zhiyong He, Miaosi Li, Lizi Li, Liyun Guan, Rong Cao, Rosiana Lestiani and Matthew O’Connor who have shared the laboratories in which I have worked. I really cherish their friendship and that of other students at BioPRIA. I also express thanks for the support from the staff at BioPRIA and Department of Chemical Engineering,

particularly Janette Anthony, Lilyanne Price, Jill Crisfield, Kim Phu, Scot Sharman, Heather McLiesh, Harry Bouwmeester and Ron Graham for their assistance throughout my candidature.

I gratefully acknowledge the Australian Research Council for the award of an ARC Linkage Grant that provided me with the living allowance that allowed me to undertake my PhD studies.

Lastly and most importantly, I would like to thank my family for their strong support and encouragement. Only with their love, support, understanding and patience has it been possible for me to enjoy and complete my research.

ABSTRACT

Paper engineering of strength, structure and surface using interactions between cellulose and cationic polyelectrolytes are investigated with the aim of improving paper-based bio-analytical devices (PADs). Advances are described based on fundamental knowledge and engineering aspects in this field that have enable the development of lighter weight papers that have high wet strengths, controlled porosities and multi-functional properties that can be fine tuned.

The influence of reactive cationic polyelectrolyte, polyamideamine-epichlorohydrin (PAE) on paper strength behaviour was studied using hardwood fibers, both with and without inorganic electrolyte. Ion type and concentration in the papermaking process water was found to influence the strength development in different ways. The relationship between repulpability of PAE- strengthened paper and wet strength is described. The effect of blending microfibrillated cellulose (MFC) with hardwood fibers is compared with the refining of hardwood fibers on paper composite properties, with and without PAE addition. Papers incorporating tethered MFC, produced by refining of hardwood fibres, are found to provide equivalent strength properties to papers incorporating untethered MFC with significant drainage benefits and formation uniformity. Air permeability of the composites decreases with untethered and tethered MFC addition.

MFC achieved by ball milling and cellulose micro-particles (CMPs) developed by cryogenic milling softwood fiber are compared with commercial MFC produced by homogenization. The effect of blending two MFCs and CMPs with hardwood fibers on the paper composites properties is investigated in terms of nano/micro cellulose dimensions. CMPs act as mechanical debonding agents and decrease substrate density and strength whereas MFC have higher aspect ratios and smaller size distributions that significantly improve strength and density of composite sheets while decreasing porosities. The addition of MFC combined with PAE can increase both dry and wet strength. The different stress-strain curves under wet conditions are described and these suggest two different mechanisms of strength development: MFC-fiber entanglement and fiber-fiber contact reinforcement.

The role of paper macroscale properties and structure are described in PADs used to type human red blood cells (RBCs). A series of commercial and laboratory-generated papers varying in fibre composition, basis weight, density and porosity are studied and their

abilities to separate antibody agglutinated (specific) from non-agglutinated (non-specific) RBCs are reported. Image analysis is used to measure the intensities of blood spots produced by sequentially absorbing solutions of antibodies and blood samples on paper then eluting with a saline solution. The performance of these papers in blood typing is found to decrease linearly with paper density and thickness and it is inversely proportional to paper pore size. The type of fibres plays a minor role. Porous cellulose webs modified with cationic polyelectrolyte further optimize blood typing analysis.

Cellulose model surfaces, in the form of quasi molecularly smooth thin cellulose films, are investigated to examine the interactions between cellulose, cationic polyelectrolytes and biomolecules. Thin smooth cellulose films are prepared by spin coating either a nanocellulose crystal suspension, or a cellulose acetate solution onto silicon surfaces with subsequent hydrolysis. Film smoothness is greatly improved by controlling the concentration of cellulose acetate and the hydrolysis time in methanolic sodium methoxide. High molecular weight polyacrylamides (CPAM) are used as model polyelectrolytes, and the nanoscale conformation of adsorbed CPAM at the cellulose/water interface is characterized in situ by specular neutron reflectometry. The effect of CPAM charge density and added NaCl (10^{-3} M) is described. At constant molecular weight, the thickness of the CPAM layer adsorbed on cellulose increases with polymer charge density. Addition of NaCl decreases the thickness of a CPAM layer already adsorbed on cellulose. However the thickness of the adsorption layer on cellulose of a CPAM solution pre-equilibrated in NaCl is much higher, because the re-shrunk polymer coils do not relax as much upon adsorption.

Deuterated cellulose film having better contrast for neutron reflectometry is investigated. Incorporation of deuterium into bacterial cellulose is achieved by growing *Gluconacetobacter xylinus* - strain ATCC 53524 in a mixture of deuterated glucose and deuterated glycerol. Two strategies are compared for synthesizing deuterated cellulose derivatives that are soluble in volatile solvents (acetone and toluene) suitable for spin coating: one involves acetylation in acetic anhydride, the other trimethylsilylation in ionic liquid (1-butyl-3-methylimidazolium chloride). The trimethylsilylation of deuterated cellulose results in a much higher yield of product, and is used to prepare toluene solutions for spin-coating onto smooth flat silicon substrates. The resulting thin film is hydrolysed back to deuterated cellulose using hydrogen chloride vapour.

The data generated is used to prepare improved substrate papers for use in PADs with high wet strength, controlled structure and fine-tuned surface properties

LIST OF PUBLICATIONS

Peer-Reviewed Journal Papers

The following published papers are included in this thesis as individual chapters. The sections of these published papers have been renumbered in order to generate a consistent presentation within the thesis. Papers in their published format are included in this thesis as Appendix I.

1. Su, J.L., et al., Paper Strength Development and Recyclability with Polyamideamine-Epichlorohydrin (PAE). *Bioresources*, 2012. 7(1): p. 913-924.
2. Su, J.L., et al., Paper engineered with cellulosic additives: effect of length scale. *Cellulose*, 2014. 21(4): p. 2901-2911.
3. Su, J.L., et al., Effect of tethered and free microfibrillated cellulose (MFC) on the properties of paper composites. *Cellulose*, 2013. 20(4): p. 1925-1935.
4. Su, J.L., M. Al-Tamimi, and G. Garnier, Engineering paper as a substrate for blood typing bio-diagnostics. *Cellulose*, 2012. 19(5): p. 1749-1758.
5. Su, J.L., et al., Adsorption of cationic polyacrylamide at the cellulose–liquid interface: A neutron reflectometry study. *Journal of Colloid and Interface Science*, 2015. 448(0): p. 88-99.

Manuscripts in Preparation

The following manuscripts in preparation are included in this thesis as individual chapters.

1. Su, J.L., et al., Preparation of smooth deuterated cellulose films for visualisation of adsorbed macromolecules. *Manuscript in preparation and to be submitted to Macromolecules*

Conference Papers

The following conference papers have been presented by the author in international and national conferences during this doctoral study, but not included in this thesis.

1. Su, J.L., et al., Engineering paper strength with poly (amideamine) epichlorohydrin-nanoparticle complex, in Chemeca 2011 (39th: 2011: Sydney, N.S.W.).

LIST OF FIGURES

Chapter 1

- Figure 1:** Cationic polyelectrolyte/cellulose composite paper functionalized by nanoparticles (Reproduced with permission of author from reference [30])
- Figure 2:** Schematic representation of the different types of paper diagnostics in: (A) 1D; (B) 2D; and (C) 3D design showing separate testing zones (T) connected to a single sample zone (S) (Reproduced with the author's permission from reference [2]).
- Figure 3:** Experimental system to prepare enzymatic papers – ALP stands for alkaline phosphatase enzyme (Reproduced with the author's permission from reference [26]).
- Figure 4:** Use of paper for determining blood groups relying on antibody-antigen interactions to show agglutinated and non-agglutinated RBCs: (A) via wicking; (B) chromatographically; (C) using the 'result-in-writing' text-reporting paper substrate method (Reproduced with the author's permission from reference [2]).
- Figure 5:** (a) Polymer attains a flat conformation with many trains at the interface. (b) Polymer attains a conformation with many loops and tails tangling out of the surface (Reproduced with the author's permission from reference [28]).
- Figure 6:** Schematic diagram of change in cellulose nanofibers suspension structure with cationic polyelectrolyte addition (Reproduced with the author's permission from reference [61]).
- Figure 7:** Structure of PAE and Schematic presentation of wet strengthening mechanism on paper treated with PAE.
- Figure 8:** Product formation on alkaline phosphatase (ALP) enzymatic paper at different times. The blue purple colour reveals the enzyme (ALP) mediated reaction between 5-bromo-4-chloro-3-indolyl-phosphate and nitro blue tetrazolium dye (Reproduced with the author's permission from reference [41]).
- Figure 9:** Superhydrophobic surface can support liquid drop micro reactors for bioassays (Reproduced with the author's permission from reference [100]).
- Figure 10:** Thesis research components and chapter thesis lists.

Chapter 2

- Figure 1:** Effect of PAE dosage on the wet and dry strength ratio.
- Figure 2:** Effect of PAE concentration on the dry tensile index (a) and wet tensile index (b) of papersheets.
- Figure 3:** Formation of paper sheets with different PAE dosage (scale bar equals 1 centimeter).
- Figure 4:** Effect on PAE concentration on repulpability index (solid line) and wet tensile index (dashed line).
- Figure 5:** Plot of repulpability index versus wet tensile index obtained from sheets strengthened by PAE and a reference without PAE. Data in Fig. 4 were used to calculate the treadline.
- Figure 6:** Effect of salt concentration in stock on paper strength (without PAE addition). a) Dry strength, b) Wet strength.
- Figure 7:** Schematic illustration of salt effect on fibres dimension/swelling and bonding area. The geometry is not drawn to scale.
- Figure 8:** Dry tensile index as a function of (a) NaCl and (b) CaCl₂ concentration at constant addition level of 10 mg PAE /g dry pulp.
- Figure 9:** Wet tensile index as a function of (a) NaCl and (b) CaCl₂ concentration at a constant addition level of 10 mg PAE /g dry pulp.
- Figure 10:** Schematic representation of possible mechanism for cationic-charged PAE being adsorbed to cellulosic fibres in different salt concentrations (a) without salt, (b) Low salt concentration, (c) High salt concentration. The figure is not drawn to scale.

Chapter 3

- Figure 1:** SEM micrographs of cellulosic additives applied to engineer the paper.
- Figure 2:** Streaming current titration measured for the cellulosic products with increasing PAE addition. Lines shown are to guide the eye.
- Figure 3:** Air permeability of paper by addition of 100 mg modified fibers/ g hardwood pulp, without PAE and 10 mg PAE/g hardwood pulp.
- Figure 4:** Morphologies of paper engineered by cellulosic additives, examined by SEM of 3 different magnification (150X, 500X, 10,000X).The bar represents a length of 500, 100 and 5µm.

- Figure 5:** Dry tensile index of paper (a) without PAE and (b) with PAE (10mg/g hardwood fiber) treatment. MFC1, MFC2 and CMPs were added at 100mg/g hardwood fiber.
- Figure 6:** Wet tensile index of paper (a) without PAE and (b) with PAE (10mg/g hardwood fiber) treatment. MFC1, MFC2 and CMPs were added at 100mg/g hardwood fiber.
- Figure 7:** Stress-Strain curve of dry paper (a) without PAE and (b) with PAE (10mg/g hardwood fiber) treatment.
- Figure 8:** Stress-Strain curve of wet paper (a) without PAE and (b) with PAE (10mg/g hardwood fiber) treatment.
- Figure 9:** Proposed mechanisms for paper web reinforcement (a) hardwood fiber web. (b) The addition of MFC, whose mean length is close to the value of hardwood fiber diameter (c) The addition of MFC, whose mean length is lower than the value of hardwood fiber diameter.

Chapter 4

- Figure 1:** SEM micrographs of (left) free MFC from the commercial product and (right) tethered MFC on refined fibers (10,000-revolutions).
- Figure 2:** Relationship between dry tensile index and apparent density for composites made from unrefined hardwood fiber-MFC mixtures and refined hardwood fibers.
- Figure 3:** SEM micrographs of composites made with (left) 75% MFC and (right) refined fiber (10,000-revolutions).
- Figure 4:** Formation of the composites prepared from MFC and refined fibers. Each image is recorded from the area of 6.75cm × 6.75cm.
- Figure 5:** Air permeability-density relationship for composites made of MFC and refined fibers (No PAE addition).
- Figure 6:** Wet tensile-dry tensile relationship for composites made of MFC and refined fibers (No PAE addition).
- Figure 7:** Stress-strain curves of (upper) the dry and (bottom) wet composites prepared by 75% MFC and fibers refined at 10,000 revolutions.
- Figure 8:** Effect of PAE addition on wet-dry tensile relationship of composites prepared from (upper) MFC and (bottom) refined fibers.
- Figure 9:** (a) Dry tensile and (b) wet tensile properties of composites prepared by MFC-fibers and MFC-refined fibers mixture.

Chapter 5

- Figure 1:** Optical density from blood typing on different papers. A) Filter papers. B) Blotting and Kleenex towel papers. C) Experimental papers made from long and short fibres (Average \pm standard deviation of at least 5 measurements).
- Figure 2:** Relationship between blood relative intensity index and particle retention size for different filter papers. The error bars represent the standard deviation from 8 measurements.
- Figure 3:** Relationship between blood relative intensity index and paper thickness. The horizontal error bars represent the standard deviation from 10 measurements. The vertical error bars represent the standard deviation from 8 measurements.
- Figure 4:** Relationship between blood relative intensity index and paper apparent density. The horizontal error bars represent the standard deviation from 10 measurements. The vertical error bars represent the standard deviation from 8 measurements. Lines are shown to guide the eye.
- Figure 5:** Capillary rise of different paper for blood typing. The error bars represent the standard deviation from 3 measurements.
- Figure 6:** Schematic mechanistic diagram for the effect of paper structure during the blood typing process. Comparison of specific and unspecific test over the thin/porous papers.

Chapter 6

- Figure 1:** a) Molecular structure of CPAM. b) Configuration of neutron reflectivity measurement for CPAM absorption at the solid/liquid interface. c) Neutron Reflection from a stratified medium.
- Figure 2:** Appearance of cellulose films made from cellulose nanocrystals aqueous dispersion (6.5 wt %) on silicon wafer (diameter=50.8 mm).
- Figure 3:** a) X-ray reflectometry of the regenerated cellulose films from different cellulose acetate solutions (in acetone). b) Effect of cellulose acetate concentrations on regenerated films thickness and roughness (Lines shown are to guide the eye).
- Figure 4:** a) X-ray reflectometry of cellulose acetate film from cellulose acetate solution (0.13 wt% in acetone) and cellulose films after 1min and 12 hrs

regeneration. b) The effect of regeneration time on the thickness and roughness of the film (Lines shown are to guide the eye).

Figure 5: Contact angle (CA) profile for the cellulose (acetate) films after different regeneration time (CA of cellulose acetate film was measured as $57.1 \pm 3.0^\circ$).

Figure 6: Raman spectra of cellulose acetate film (spin coating from 2.5 % solution) and after 12 hrs regeneration time. The important peaks are labelled.

Figure 7: AFM images and extracted parameters from nanocellulose (a, b), regenerated cellulose acetate (c, d) and pure cellulose acetate (e, f) films. In each case, the left-hand pane (a, c, e) shows height information (wherein the height scale is defined by the line profile in (g) and the right hand pane (b, d, f) shows the phase information. The scale bars represent 100 nm. Line profiles of selected cross-sections are shown in (g), representing the sectional heights defined by the dotted lines in (a, c, e). The two uppermost traces are vertically offset by 10 and 20 nm as indicated by their ‘zero’ lines, for clarity of presentation.

Figure 8: Peak intensity normalized GIWAXS profiles in the specular direction from a regenerated cellulose film on quart substrate as a function of incident angle. The inset shows a typical GIWAXS image. The beam stop is masked by red.

Figure 9: a) Neutron reflectivity from silicon surfaces with regenerated cellulose and CPAM absorbed at two interfaces: Silicon with native oxide layer and cellulose film. b) SLD profile from simultaneous fits to the CPAM F1 on cellulose in part a.

Figure 10: The thickness of CPAM ($M_w=13$ MDa) absorbed at cellulose/D₂O interface with and without NaCl. The data is presented in Table III.

Figure 11: Model fitting for CPAM of a) 40 % and b) 5% charge density adsorption at 1) cellulose surface; 2) diffusion into cellulose layer without changing the cellulose swelling behaviour; 3) diffusion into cellulose layer and the cellulose layer is deswelling 25%. χ^2 indicates the quality of fitting, and the lower value of χ^2 indicate better fits from minimizing the differences between the theoretical and measured reflectivity curves.

Figure 12: The proposed conformation of CPAM absorbed on the cellulose/water interface under different charge density conditions.

Chapter 7

- Figure 1:** Schematic mechanism of blood typing paper on the cellulose interaction with antibodies (IgM).
- Figure 2:** a) Molecular structure of amorphous cellulose (three labile protons from hydroxyl groups) with different deuteration level when immerse in pure H₂O and D₂O .b) Scattering length densities (SLDs) from BMV protein (ref.), protonated and deuterated cellulose (with three labile protons) as a function of D₂O content in the solvent. We assume that all labile protons (from hydroxyl groups) are exchanged in proportion with the D₂O content of the solvent. This figure depends on the value of the specific volume of the molecules used for the calculation. The crossing point of the water line with that of a molecule (protein and cellulose) is called the “matching point” or isopicnic point. $\bar{\rho}$ is called the contrast.
- Figure 3:** Schematic procedure to prepare cellulose films with contrast variation for neutron reflectometry.
- Figure 4:** ATR-FTIR spectra of dried deuterated bacterial cellulose before and after NaOH treatment to remove protein and other cellular material. The spectram has been normalized, for clarity of presentation.
- Figure 5:** ATR-FTIR of bacterial cellulose with and without deuteration. The spectra are normalized and vertically offset, for clarity of presentation. The protonated bacterial cellulose (PBC) has been used as a reference.
- Figure 6:** ATR-FTIR of cellulose derivatives from acetylation of microcrystalline cellulose (MCC) in ILs.
- Figure 7:** Theoretical NR curves for the cellulose films (air/solid interface, assume the thickness=200Å, roughness=4Å) with different SLD.
- Figure 8:** Specular X-ray reflection measurement of deuterated cellulose film and fitting results from two models: single-layer and two-layer.
- Figure 9:** SLD profile from simultaneous fits to deuterated cellulose film on silicon block: a) single-layer model. b) two-layer model.

LIST OF TABLES

Chapter 1

Table I: Filter paper used in paper-based bio-analytical devices.

Chapter 3

Table I: Dimension properties of cellulosic fibers used in this work.

Table II: Paper formation, stress-strain at break and elastic modulus affected by addition of 100 mg cellulosic additives /g hardwood fiber with and without PAE. The target oven-dry grammage for the control sheet is 60 gsm. 95% confidence intervals from 10 measurements indicated in parenthesis.

Chapter 4

Table I: Properties of MFC, primary and secondary fines.

Table II: Properties of 100%MFC, unrefined and refined hardwood (HW) handsheets (basis weight of 60 g/m²).

Table III: Effect of PAE on drainage for (upper) MFC composites preparation and (bottom) air permeability of the composites.

Chapter 5

Table I: Paper properties. The top section presents the commercial papers, the bottom the experimental papers. Standard deviation from 10 measurements indicated in parenthesis.

Table II: Optical density for blood spotted on specific antibodies and non-specific antibodies fixed in different paper substrates (average \pm standard deviation). Standard deviation is from 8 measurements.

Chapter 6

Table I: The estimated properties of copolymer CPAM consisting of uncharged acrylamide (AM) and cationic dimethylaminoethylacrylate methyl chloride (DMA) monomers, with different charge density but constant molecular weight of 13 MDa (supporting information). Φ and ρ present the volume fraction and neutron scattering length density, respectively.

Table II: Properties of cellulose films spin-coating from different raw materials. The thickness and roughness were measured by X-ray reflectometry. The average value and 95% confidence interval were from five samples.

Table III: CPAM adsorption at the solid/D₂O interface was studied by the specular NR measurement. Thickness (δ), roughness (σ), and volume fraction (Φ) of D₂O in the layer were retrieved by fitting the NR curves. The absorbed amount (Γ) of CPAM was calculated with the absorbed layer δ and Φ . χ^2 indicates the quality of fitting, and the lower value of χ^2 indicate better fits from minimizing the differences between the theoretical and measured reflectivity curves. The reflectivity data were co-refined by at least two data sets where the solid substrate was exposed in D₂O without and with CPAM. $\rho_{D_2O}=6.35 \times 10^{-6} \text{ \AA}^{-2}$. The 95% confidence in parenthesis is from three optimal fitting results.

Chapter 7

Table I: Assignment of FTIR spectra of bacterial samples, and the ratio of absorbance of characteristic peaks from figure 2.

Table II: Solubility of cellulose derivatives from acetylation and trimethylsilylation. Complete solubility was confirmed by ensuring lack of any turbidity in the solution being observed when a red laser beam was shone through the solutions following centrifuging. Notes: 1. Figures based on the total weights of acetylated products 2. Calculated from the ratio between toluene-soluble product and the expected theoretical yield of trimethylsilylated cellulose (DS=2.0).

Table III: Deuterated cellulose film on silicon block studied by specular X-ray reflection measurement. Thickness (δ), roughness (σ) and scattering length density (SLD) of the layer were retrieved by fitting the experimental data. χ^2 indicates the quality of fitting, and the lower value of χ^2 indicates better fits from minimizing the differences between the theoretical and measured reflectivity curves. χ^2 , δ , σ and SLD from the best fitting. The 95% confidence in the parenthesis is from three optimal fitting results.

Table IV: X-Ray Scattering length density ($\times 10^{-6} \text{ \AA}^{-2}$) of amorphous cellulose at different level of deuteration and density.

LIST OF ABBREVIATIONS

3D	Three dimensional
AFM	Atomic force microscopy
AKD	Alkyl ketene dimer
ALP	Alkaline phosphatase
BMIM chloride	1-Butyl-3-methylimidazolium chloride
CMPs	Cellulose microparticles
CNC	Cellulose nanocrystal
CPAM	Cationic polyacrylamide
DBC	Deuterated bacterial celluloses
HMDS	Hexamethyldisilazane
Ig	Immunoglobulin
ILs	Ionic liquids
MCC	Microcrystalline cellulose
MFC	Microfibrillated cellulose
NMMO	N-methyl morpholine oxide
NR	Neutron reflection
OH	Hydroxyl
PADs	Paper-based bio-analytical devices
PAE	Polyamideamine-epichlorohydrin
poly-DADMAC	Poly-diallyldimethylammonium chloride
QCM-D	Quartz crystal microbalance with dissipation
RBC	Red blood cell
RFV	Relative formation value
R _g	Radius of gyration
SD	Standard deviation
SLD	Scattering length density
SFA	Surface forces apparatus
SPR	Surface plasmon resonance
TMSC	Trimethylsilylated cellulose
XPS	X-ray photoelectron spectroscopy
XRR	X-ray reflectivity

LIST OF NOMENCLATURE

$^{\circ}\text{C}$	degree Celsius
cm	centimetre
eV	electron volt
kV	kilovolt
mg	milligram
nm	nanometer
mm	millimetre
mL	millilitre
mM	millimolar
mW	milli watt
mV	millivolt
N_{a}	Avogadro's number
μC	microcoulombs
μL	microlitre
M_{R}	relative molecular mass
ρ_{mass}	mass density
t	time
η	viscosity
ρ	density
η	viscosity
γ	surface tension
r	capillary of radius
λ	wavelength
δ	thickness
Γ	adsorbed amount
\AA	angstrom
σ	roughness
q	momentum transfer
Φ	volume fraction
T	temperature

Chapter 1

Introduction and Literature Review

This page is intentionally blank

Content

1.1	Introduction	28
1.2	Literature review	33
1.2.1	Paper-based bio-analytical devices (PADs)	33
1.2.1.1	Fabrication, Utilization and Disposal of PADs	33
1.2.1.2	Critical properties of paper substrates required for analytical purpose	35
1.2.1.2.1	Dry and wet strength.....	35
1.2.1.2.2	Porosity and capillarity	36
1.2.1.2.3	Surface and colloid engineering.....	37
1.2.1.3	Biomolecules and functionality	38
1.2.1.3.1	Enzymes.....	38
1.2.1.3.2	Antibodies.....	39
1.2.1.4	Development of paper-based blood typing biondiagnostics	40
1.2.2	Cationic polyelectrolytes in PADs engineering	42
1.2.2.1	Retention and flocculation	43
1.2.2.2	Wet strength improvement	44
1.2.3	Microfibrillated cellulose (MFC) in paper composites engineering	46
1.2.3.1	Effect of MFC on preparation of paper composites	47
1.2.3.2	Effect of MFC on properties of paper composites	48
1.2.4	Cellulose film as a tool for developing PADs	48
1.2.4.1	Role of cellulose surfaces in PADs	49
1.2.4.2	Preparation of smooth cellulose film as a model surface	51
1.2.4.3	Characterization of the interactions at cellulose surface	53
1.2.4.3.1	Specular X-ray and neutron reflectivity.....	53
1.2.4.3.2	Additional techniques	55
1.2.5	Gaps in knowledge	58
1.3	Research objectives and aims	60
1.4	Thesis outlines	62
1.5	References	65

1.1 Introduction

Nowadays, novel papers engineered with strength, structure and surface properties are still challenging both for papermaking and biomedical industries. For examples, sustainable packaging is appealing for less fiber usage and more fiber re-usage, as well as high strength, light weight and controlled permeability. In clinical practice, paper-based bio-analytical devices (PADs) are designed to be reliable, portable and simple for different biomedical applications [1, 2]. Cationic polyelectrolytes are widely applied in many industries and research laboratories to control the stability of colloids and the interaction properties of surfaces. Traditionally, cationic polyelectrolytes are commonly used as retention aids for process colloids (fillers and fines) and as drainage additives in industries ranging from water treatment to metal and oil recovery. In papermaking, cellulose interaction with cationic polyelectrolytes is used to engineer the manufacturing process (retention and flocculation) and to control paper properties (surface charge, dry and wet strength) of paper.

Paper exhibits strong compatibility with biological systems, offering additional benefits of an inexpensive substrate, porous structure, hydrophilicity and biodegradability. These attributes have given paper major markets in packaging, writing and hygiene, all of which see paper manufactured and sold as a commodity. Paper should not be seen as just a low-cost commodity however and the same properties that make the use of paper advantageous in commodity markets can be utilized in more specialized areas such as paper-based bio-analytical devices (PADs) having higher level functionalities.

Detection and regulation of human diseases has been of great significance all over the world for the last century. A conventional device for biomedical application currently requires elegant instrumentation and specialized training for operation which unfortunately render the cost prohibitive in many regions of the world and in many “non-critical” applications. Nowadays reliable, portable, rapid and inexpensive analytical devices are becoming popular both from the viewpoint of scientific interests and clinical practice. PADs, in the form of cellulosic webs or films, have been developed as a diagnostic platform for many medical applications.

There are four critical aspects for designing high performance PADs: sensitivity, selectivity, simplicity and strength [1, 2]. Hence, paper engineering is required in terms of 1) engineered strength for PADs preparation, application and disposal treatments, 2) sensitive and optimized surface for the affinity of biomolecules (retention, adsorption/desorption, and aging) or other additives (polymers, nanoparticles), and 3) controlled structure (porosity, capillarity) for selective and rapid mass transportation and separation of test fluids [3, 4]. To fulfil these requirements, development of PADs is towards robust (high strength when used in wet or dry conditions), lightweight (less cellulose fiber usage), and multi-functional properties that can be fine tuned. Based on many experimental observations [5-7], a promising approach is to engineer cellulose interactions using cationic polyelectrolytes.

Most PADs are prepared and used in wet or high moisture conditions. Therefore, they must retain a minimum wet strength, while ideally retaining the ability to be repulped and not interfere with normal paper recycling operations. In order to lessen the reduction of the product strength upon contact with water, cationic polyelectrolytes are employed as wet strength additives in papermaking [8-12]. Among such polyelectrolytes, reactive poly-(amideamine) epichlorohydrin (PAE) has been conventionally used because of its efficiency and relative cost benefit. While in practice cellulose/PAE composites are easily prepared and can be expected to act as a wet-strengthened substrate for PADs, a major drawback is a lack of repulpability with adverse effects on paper recycling. In fact there appears to be little published information concerning wet strength and repulpability for high functionality papers. With the aim of developing sustainable and strong PADs, this relationship needs to be quantified in order to guide the disposal strategies following use.

Microfibrillated celluloses (MFC), made by various mechanical, acid hydrolysis or biological processes, have shown high potential in developing novel paper products and renewable composites having unique features [13-15]. The large surface area per volume of MFC considerably improves interfiber bonding, which enables paper products to be significantly thinner at a given tensile strength and permits reductions in raw material usage. Another benefit is the ability to control porosity, allowing new concepts for engineered PADs (permeability, density and strength). Both wet and dry strength of paper is greatly improved by using cellulose nanofibrils together with reactive wet-strength agent such as polyamineamide epichlorohydrin (PAE) [13]. However, very few studies

have attempted to understand the role of dimensional properties of MFC in developing high performance-low cost cellulose composites, with or without PAE. Furthermore, it would be worthwhile making a comparison of the performance of MFC in cellulose/PAE composites and understanding the roles of surface, colloidal and bulk material properties.

In practical terms, paper substrates serve four major functions during biodiagnostics: 1) transportation and storage of sample and biomolecules, 2) accommodation for the specific or non-specific reaction, 3) separation of reactants from products, and 4) communication of the results [16, 17]. A prominent example is paper used to establish blood group, where the blood agglutination is triggered by specific antibody-antigen interaction[18]. Paper-based blood typing is a promising alternative for conventional approaches because of its portability, low cost and rapid test results. Various papers have been designed to improve the accuracy of the test, and different methods were developed for better visual identification [4, 16, 17, 19]. However, paper engineered with controlled properties (fiber composition, hydrophilicity, paper's internal pore size and distribution) and structure (density, permeability) still requires further understanding and optimization in order to create better blood typing PADs.

In biomedical applications, adsorption and desorption of biomolecules at cellulose/water interfaces controls the performance of PADs [16]. Absorption and desorption are also critical for the new platform of cellulose/cationic polyelectrolyte composites. Paper has a complex three-dimension structure and varying characteristics such as porosity, thickness, and chemical composition, which make the analysis of interactions with biomolecules difficult. Hence, smooth cellulose films have been exploited as simpler model substrates on which to examine interfacial fundamentals under various conditions [6, 20, 21]. As a well-defined and non-intrusive technique, neutron reflection (NR) measurement allows investigation of thin-film layers on various substrates, especially under wet conditions. To study interactions between biomolecules and cellulose by NR, the ability to vary contrast experimentally between cellulose and the biomolecule being studied is required. Varying contrast can be achieved by deuteration of the components [22, 23]. Due to the difficulties in controlling deuteration of biomolecules, a practical alternative is to prepare smooth deuterated cellulose films that provide varying levels of contrast [24]. In order to achieve this aim, a series of steps have to be established and optimized for film preparation. These steps include: 1) producing deuterated cellulose derivatives that can be dissolved in

suitable solvents, 2) formation of films of the cellulose derivatives by spin coating these solutions onto suitable flat substrates and 3) reversion of the cellulose derivatives into deuterated cellulose films under mild conditions in which the smoothness of the film is not destroyed by swelling or dimensional contraction of the derivative, or the cellulose.

Cationic polyacrylamides copolymers (CPAM) are among the most commonly used polyelectrolytes and are important because of their efficiency, low cost and availability in a wide range of polymer compositions and structures. CPAM is commercially available with molecular weights and charge densities up to 15 MD and 100%, respectively. These allow CPAM to be used as a model polymer for paper engineering. Recent research applications of CPAM in PADs include the retention of enzymes and nanoparticles on bioactive paper surfaces [25-28] and the development of functional materials and control of biomolecular activities [7]. Although unique properties of paper functionized using CPAM have been discovered for a number of biodiagnostic applications, descriptions of the fundamental conformations adopted by CPAM and quantitative analyses of CPAM on cellulose surfaces remain scarce in the published literature. The hypothesis on which the following investigation is based is that NR can be used to characterize how CPAM behaves at cellulose/water interfaces, and that these studies will elucidate which variables can be used to control and fine tune cellulose/CPAM interactions. This knowledge can serve as a base to both correlate the functionality with the properties of PADs and also to provide a deeper understanding on which further development of PADs can be based.

The overarching aim of this investigation is to address the current research gaps in developing novel paper with engineered strength, structure and surface, particularly for bio-analytical devices. In order to achieve this objective, this thesis concentrates on three length scales in parallel:

- **macroscale** (paper structure and strength),
- **mesoscale** (polymeric wet strength agent/MFC complex in paper composites) and
- **nanoscale** (cellulose surface interaction with model cationic polyelectrolytes) .

Three major objectives are proposed in the research. The first is engineering paper composites by reactive cationic polyelectrolytes (PAE) and MFC (mesoscale). The second is to quantify the effect of paper structure for paper-based diagnostics for blood typing application (macroscale). The third is optimizing smooth cellulose films as model

substrates to measure the cationic polyelectrolyte or biomolecular layer at cellulose/water interface (nanoscale). By conducting these parallel studies and reconciling the three structure length scales, we hope to provide fundamental knowledge to engineer paper strength, structure and surface through better understanding of cellulose interaction with cationic polyelectrolytes, and thus contribute to develop novel paper products, particularly for bio-analytical devices.

The objective of Chapter 1 is to critically review the published literature concerning development of paper-based bio-analytical devices and paper engineering with strength, structure and surface, as well as highlighting the current limitations on paper for bio-analytical use. This chapter consists of three additional sections (Section 1.2, 1.3 and 1.4). Section 1.2 covers three aspects of PADs a) traditional cellulose substrates used for PADs and the variables (strength, structure and surface) that govern their performance; b) cationic polyelectrolyte/cellulose interactions and microfibrillated cellulose (MFC) in paper engineering and c) cellulose films used as model surfaces for study of interactions relevant to PADs. The restrictions current techniques place on the functionality of PADs is reviewed and the critical challenges which need to be addressed are discussed. Finally a perspective on the future directions in this research is provided. The second section (1.3) summarizes how this doctoral study aims to fulfil the current research gaps in paper engineering with strength, structure and surface by studying the interactions between cellulose and cationic polyelectrolytes, and the potential for incorporation in PADs. In the last section (1.4), the organization of the thesis is presented.

1.2 Literature review

1.2.1 Paper-based bio-analytical devices (PADs)

Paper-based bio-analytical devices (PADs), made from cellulosic materials, in the form of porous webs or solid films is attracting wide attention for use as platforms to detect and quantify biomolecules and chemical agents in medical applications. This is because cellulose material is widely available, biocompatible, biodegradable, hydrophilic, and easy to engineer, functionalize and process into diagnostic devices. During the bio-analytical measurement, PADs serve four major functions: 1) transportation and storage of sample and biomolecules, 2) accommodation for the specific or non-specific reaction, 3) separation of reactants from products, and 4) communication of the results. In order to address the current Sensitivity, Selectivity, Simplicity and Strength (4S) limitations of modern paper diagnostics, critical properties and attributes of PADs including strength, porosity and surface chemistry need to be designed and optimized. The proposed strategy for achieving this aim is to engineer cellulose interactions with cationic polyelectrolytes [29] (Figure 1).

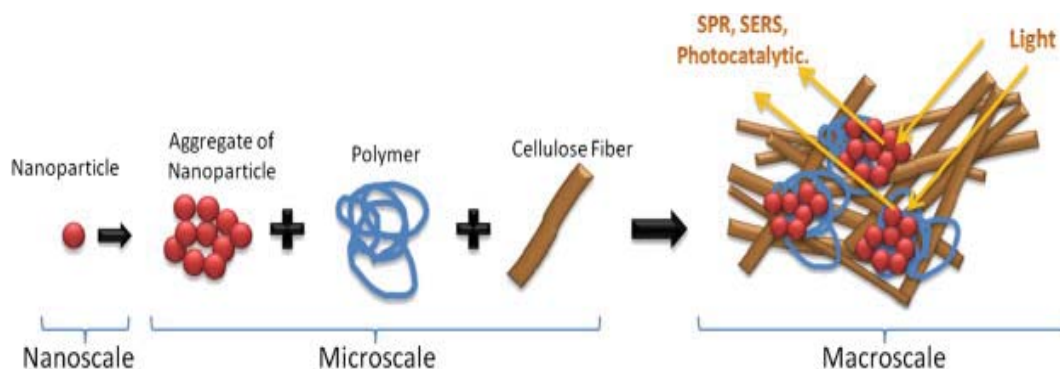


Figure 1. Cationic polyelectrolyte/cellulose composite paper functionalized by nanoparticles (Reproduced with permission of author from reference [29])

1.2.1.1 Fabrication, Utilization and Disposal of PADs

Fabrication of PADs has been extensively explored for various applications in numerous studies [3, 25, 30, 31]. The designs of PADs can be simply classified into three categories according to the way in which the directional flow of fluid is engineered (Figure 2): 1) Fig. 2 A shows the flow of liquid in a single direction that is described as 1D; 2) Fig. 2. B indicates lateral flow of fluid in multiple directions on a plane and is described as 2D; 3) Fig. C shows a design in which fluid flows through multiple planes and this configuration is described as 3D [2]. Different fabrication techniques and their advantages and

drawbacks have been reviewed in articles elsewhere, and the critical strategies have been summarized [2].

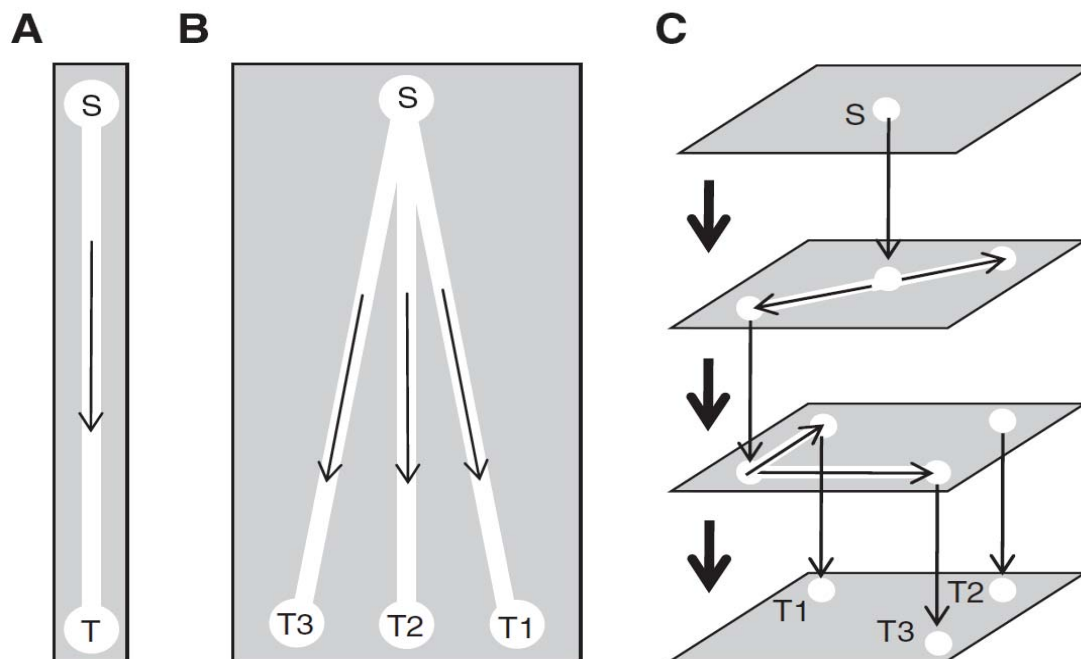


Figure 2. Schematic representation of the different types of paper diagnostics in: (A) 1D; (B) 2D; and (C) 3D design showing separate testing zones (T) connected to a single sample zone (S). (Reproduced with the author's permission from reference [2]).

Even though considerable emphasis has been placed on the preparation of versatile PADs, surprisingly little information has been published on the post-treatment and disposal of these products. Possibly this lack of study is due to the inexpensive and combustible nature of paper. Incineration of used PADs would avoid potential bio-hazards, such as blood containing fatal viruses. From the viewpoint of sustainability, another option would be to recycle the paper waste, and reuse the fibers for low grade products. Currently, paper substrates (filter papers, toweling and tissues) used for PADs contain wet strength polymers that ensure retention of the structure of the substrate in aqueous or high humidity conditions. The repulping behaviour of paper containing wet strength additives is considerably more difficult than the repulping of papers made without them. Special equipment that applies large shearing forces to the papers in aqueous suspension and frequently special chemical additives and processing conditions (pH and temperature) are required, so that recycling high wet strength papers may involve more processing energy and entrained energy in the chemical additives than can be justified by the relatively small

proportion of the waste paper stream that these specialty papers make up [32-34]. Another critical question for PAD engineering concerns the minimum wet-strength and PAE concentration required to meet strength requirements; the less polyelectrolyte strength polymer, the lower the potential of undesired side interactions.

1.2.1.2 Critical properties of paper substrates required for analytical purpose

1.2.1.2.1 Dry and wet strength

Many methods have been explored and developed to prepare ASSURED (Affordable, Sensitive, Specific, User-friendly, Rapid and Robust, Equipment-free, and Deliverable) PADs. During preparation, reagents (enzyme, protein, and chemicals) are introduced into cellulose networks or other substrates in aqueous media by soaking, deposition or functional printing [19, 28, 35]. On the other hand, PADs are handled and used both in dry and wet conditions. Therefore improved paper dry and wet strengths are required in order to optimize the performance of PADs in clinical use.

Dry strength is a mechanical property of the paper web, which stems mainly from the formation of bonds between fibers. The strength of paper products relies on the strengths of the individual fibers and of the bonds between fibers [36]. The Page equation provides theoretical prediction of the tensile failure of paper in terms of two components: 1) fiber strength, measured as zero-span tensile strength, and 2) bond strength as a function of fiber properties and the interaction between fibers [37]:

$$\frac{1}{T} = \frac{9}{8Z} + \frac{12A\rho g}{bPL(R.B.A)}$$

T= tensile strength of the strip expressed as breaking length; P=perimeter of the fiber cross section;
b=shear bond strength per unit bonded area; ρ= density of the fibrous material;
R.B.A=relative bonded area of the sheet; Z=zero-span tensile strength;
A=average fiber cross section; g= acceleration due to gravity; L=fiber length;

In dry paper, hydrogen bonding plays the dominant role in creating tensile strength. As hydrogen bonds act over short distances and are water sensitive, the penetration of water into a dry paper matrix will lead a rapid weakening of fiber-to-fiber hydrogen bonds and a concurrent loss in paper strength [38]. Paper without wet strengthening treatment typically retains around 10% of its original dry strength after being fully soaked in water

primarily because of the energy input required to overcome frictional forces between fibres that are entangled in the web.

Commercial filter paper and towel tissue are commonly reported as substrates used to fabricate PADs [1, 4, 17]. Most of these papers contain strength additives, which improve the fiber-to-fiber bonding under both dry and wet conditions. Experimental paper with or without strength additives has also been explored to engineer PADs (Table I). Practically, by varying the grammage, PADs of different strengths can be made. Furthermore, optimized fiber usage and the performance of PADs may be correlated. Up to now, studies on the role of paper strength in PADs preparation and application remain limited. This lack of study may result from the complex structure of paper in which strength is controlled by fiber-to-fiber interactions that are developed during the process of paper formation, consolidation (pressing), and drying [36, 39]. Development of strong, lightweight and sustainable PADs is attractive both from the standpoints of academic interest and commercial application.

Table I. Filter paper used in paper-based bio-analytical devices.

PADs application	Filter paper used	Wet strengthening	Bursting Strength (psi)		Reference
			Dry	Wet	
Glucose and protein detection	Whatman No.1	None	16	0.3	[3, 30]
Enzyme immobilization	Whatman No. 4	None	21	0.4	[40]
Blood typing	Whatman No. 113	Yes	24	8	[4]

1.2.1.2.2 Porosity and capillarity

Engineering of PADs must take into account not only the cellulose fibrous structure, but also the structure of the void fraction: fibers control the distribution of reagents, while the void fraction controls liquid transportation. The void fraction of paper is calculated from the porosity, which is a function of the various stages of the papermaking process and fiber selection. An increased level of fiber refining causes the fibers bonding together tightly, making the paper denser, and reducing the volume of the void space and thus the porosity [41]. Paper porosity is evaluated quantitatively by the time of penetration of a gas or liquid [42], and the pore size and orientation within the paper significant affects the capillary action.

The common concept of designing PADs is to create microfluidics using the paper structure and to rely on paper capillarity for liquid flow. When an aqueous analyte such as blood is placed on a paper web, the fluid is driven by capillary actions provided by the structure of the hydrophilic cellulose fibers and the fluid is transported by wicking through the inter-fiber voids within the web [4]. The driving force of capillarity is generated by the difference in surface energy between the fluid and the solid. Wicking can be simply described by the liquid flow in a capillary. A velocity (V) for a liquid of viscosity η and surface tension γ flowing in a capillary of radius r and length l can be calculated by the Lucas-Washburn equation [43]:

$$V = \frac{r \cos \theta_E}{8\eta l}$$

Where θ_E is the equilibrium contact angle, which is a function of the chemistries of the liquid, the solid surfaces and the pore wall geometry [42, 44].

1.2.1.2.3 *Surface and colloid engineering*

In the context of modern papermaking, surface and colloid chemistry of cellulose controls the interaction between the cellulosic fibers and other materials (pigment fillers, retention and strength additives, and sizing agents), which influence the final properties of paper (dry strength, wet strength and printability). Three hydroxyl groups in the anhydroglucosidic units of cellulose and the resulting hydrophilic fiber surface allow paper surface modification in the wet state. This property enables fabrication, functionization and application of PADs.

Most of the design of PADs has so far been based on patterned papers in which creation of micro-channels enables controlled multidirectional flow of analytes. A second concept is to build up hydrophobic barriers onto or within the paper structure thereby creating hydrophilic channels between the barriers. This can be realized by functional printing using cellulose non-reactive or reactive compounds such as various waxes and alkylketene-dimer (AKD) sizing agents. Paper diagnostic prototypes have been demonstrated as hydrophilic-hydrophobic contrast patterns on paper, which confine the capillary penetration of aqueous liquids to within paper channels between the hydrophobic barriers [16, 31].

The hydrophilic nature of cellulose makes it particularly compatible with proteins and other biomolecules. Biosensing agents, including biomolecules, can be attached to paper

by printing, or coating on the basis of two major immobilization strategies: 1) physical immobilization using van der Waals and electrostatic forces; 2) chemical immobilization through formation of covalent bonds between atoms in the cellulose and atoms in the biosensing agent. In many cases of physical immobilization the biosensors are not firmly anchored, and are easily desorbed from the surface once immersed in a liquid solution. In order to prevent desorption chemical modification of cellulose can be used to promote formation of covalent bonds [45]. Pelton has summarized different immobilization strategies for biomolecules at cellulose interfaces [46].

An example in which physical immobilization has been successful is treatment of the cellulose surface with water soluble polymeric cationic polyelectrolytes. Cationic polymers can influence both biosensor immobilization and activity on PADs [5, 47]. Peng reported a model PAD engineered using a colloidal system consisting of an enzyme, an inorganic colloid and a cationic polyelectrolyte, which possessed enhanced detecting sensitivity [48]. Systematic studies have also been conducted using cationic polyacrylamides, which were applied to promote the aggregation of gold nanoparticles on bioactive paper [27, 28, 49].

1.2.1.3 Biomolecules and functionality

Paper properties and structure greatly affect the performance and efficiency of PADs, whereas the functionality of PADs is governed almost exclusively by the particular biomolecules that are loaded onto the paper. Two of the most important classes of biomolecules used to create PADs are enzymes and antibodies.

1.2.1.3.1 Enzymes

Enzymes, macromolecular biological catalysts of high selectivity, have been widely immobilized on paper as biosensors [40] (Figure 3). Many macro-scale enzyme-paper interactions and their effects on functionality, reactivity, stability and sensitivity of immobilized enzymes have been well investigated in previous studies [26, 35, 50, 51]. However, at the level of the micro-scale, the role of cellulose surface properties in enzyme-paper functionality and the configuration of enzymes adsorbed at a cellulose interface still need better understanding. Developing techniques such as neutron reflectivity (NR) measurement have the potential to characterize the enzyme configuration quantitatively at model cellulosic surfaces.

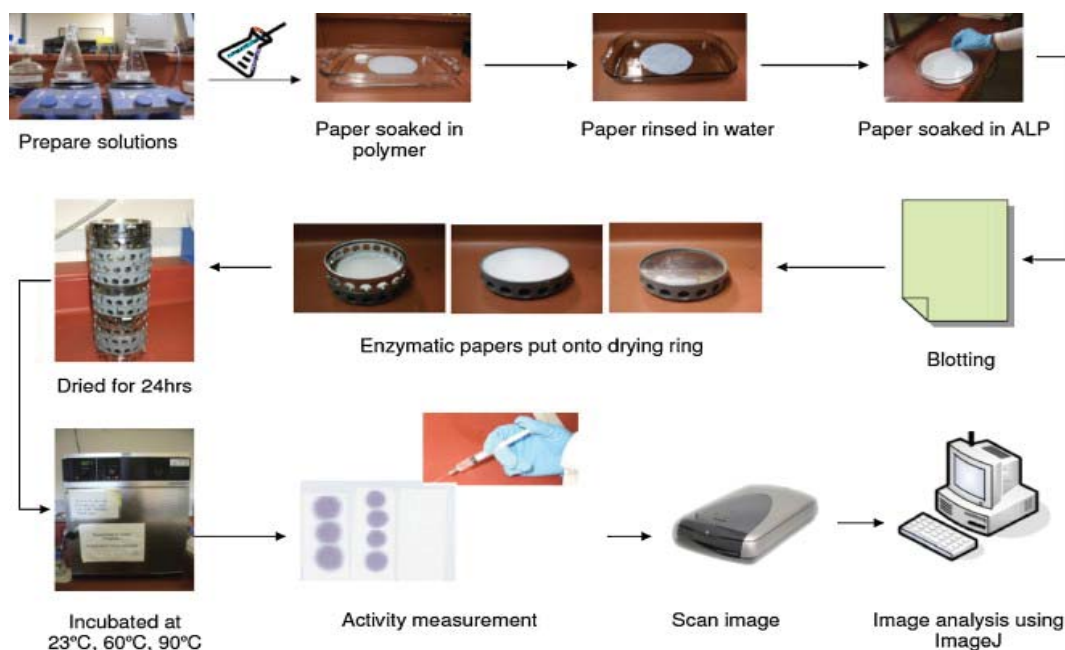


Figure 3. Experimental system to prepare enzymatic papers – ALP stands for alkaline phosphatase enzyme (Reproduced with the author’s permission from reference [25]).

1.2.1.3.2 Antibodies

In many mammals, an antibody (Immunoglobulin, Ig), a Y-shaped protein, is produced by the immune system to identify and neutralize foreign objects. Antibodies can be readily loaded onto paper by spotting, printing or dip-coating from aqueous solution [4, 16, 19]. In humans, there are five isotypes of antibodies, within which the IgM a pentamer, and IgG a monomer, are commonly used in paper diagnostics, particularly for blood typing. Variables such as blood/antibody ratio and antibody concentration significantly affect the sensitivity and selectivity of diagnostic results [4, 19]. Guan reported that the longevity of antibodies sorbed into paper can be improved by mixing with certain synthetic polymers, and that freeze-drying, which preserves the natural tertiary structures of the antibodies, provides a further level of protection over and above that provided by synthetic polymers [7].

The adsorption and desorption of antibodies on paper governs many factors that are critical for the formation and utilization of PADs. The three-dimensional structure of papers, and their varying characteristics, such as porosity, thickness, and chemical composition renders the analysis of adsorption and desorption of antibodies difficult. Experimental information on the structure and density of absorbed antibodies at cellulose

surfaces remains scarce. One way of reducing the difficulties involved in examining the interactions between antibodies and paper is to study fundamental absorption phenomena at model cellulose surfaces that are well characterised, such as smooth cellulose films. The dynamic adsorption and features of absorbed antibodies have been intensively characterized by quartz crystal microbalance with dissipation, atomic force microscopy and surface plasmon resonance [20, 52]. Factors such as cationicity, ionic strength and pH of the solution were reported to control antibody adsorption. There is however limited knowledge available concerning the direct conformation of antibodies at cellulose/water interfaces and therefore details of the nanoscale structures present in the absorbed layers need to be fully examined.

1.2.1.4 Development of paper-based blood typing biodiagnostics

Paper-based bio-analytical devices are designed for broad applications, ranging from clinical diagnostics, such as detection of pathogenic diseases, to physiological disorders and their diagnostic analytes [2]. A prominent recent example of clinical diagnostics is paper-based human red blood cell (RBC) group determination. Accurate assessment of blood group is essential for safe blood transfusion and transplantation medicine [18]. Practically, blood group is determined by the presence or absence of certain antigens on red blood cells (RBCs) [53, 54]. Traditional methods used for blood typing include the slide test, tube test, micro-plate method, gel column agglutination systems and several others [53]. These methods all require sophisticated analytical equipment and professionally trained operators. The tests are also relatively time-consuming.

Paper-based blood typing is a promising alternative because of its portability, low cost and rapid test results. Various papers have been designed to improve the accuracy of the test, and different methods have been developed for better visible identification [4, 16, 19], although all are based on the same principle of haemagglutination of RBCs, where a specific antibody/antigen interaction occurs (Figure 4). The first PADs for blood typing were invented by Khan et al. [4]. These investigators soaked paper strips in antibody solutions, and then added droplets of blood to the centre of the paper strip. A distinct difference was discerned by observing the wicking behaviour of the agglutinated and non-agglutinated blood. Al-Tamimi et al. explored paper blood group typing using the same principle but different testing methodologies, where specific blood agglutination was

differentiated by elution [19]. Recently, user friendly and “result in writing” blood typing PADs have been developed by adapting Al-Tamimi’s method [16]. The paper substrate was patterned with hydrophobic boundaries to surround a hydrophilic channel in the shape of text or symbols, where “invisible writing” is produced using antibody solutions as inks. Haemagglutination of the test sample of blood over one particular symbol renders the symbol visible and a ‘result in writing’ can be observed and recorded easily. A more modern concept of presenting the PADs assay in a barcode-like pattern was demonstrated by Guan et al. [7]. This design allows enhanced adaptability and integration with smartphone-based technologies.

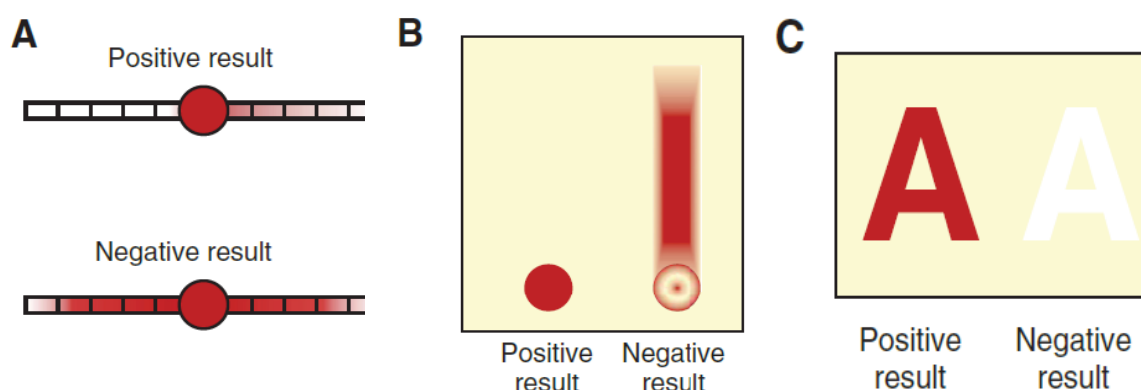


Figure 4. Use of paper for determining blood groups relying on antibody-antigen interactions to show agglutinated and non-agglutinated RBCs: (A) via wicking; (B) chromatographically; (C) using the ‘result-in-writing’ text-reporting paper substrate method. (Reproduced with the author’s permission from reference [2]).

While commercial filter and tissue papers can be used to develop blood typing PADs in the laboratory, once blood typing PADs are produced on a commercial scale for clinical use a very high degree of standardization and reproducibility of test results will be required. In order to achieve the level of standardization required, a specifically engineered paper substrate becomes mandatory. Furthermore, understanding of the transport and immobilisation mechanisms of RBC in PADs and how these are affected by the properties of the paper (fiber composition, hydrophilicity, internal pore size and distribution) and structure (density, permeability) together with how the paper properties affect location, desorption and activity of antibodies is required in order to design an optimally engineered paper substrate [16, 55].

Prototypes of RBC PADs have been successfully fabricated and trialled in the laboratory, however there appear to be little commercial products undergoing clinical trials. One

practical limitation of the methodology stems from the limited longevity of absorbed antibody activities and the shelf life (currently only a matter of days to months- based on antibody) of the product. More experimental data is required to fully compare the performance of conventional analytical techniques with RBC PADs. The future trends on the development of paper blood grouping needs to be targeted on four aspects: 1) Maximising the length of time the antibodies remain active once the product leaves its place of manufacture; 2) Reducing the time taken for a test result to become certain; 3) Maximizing the sensitivity and accuracy of the test by optimizing the fiber usage and paper structure; and 4) Functionalizing the paper surface with patterns that allow integration with electronic devices.

1.2.2 Cationic polyelectrolytes in PADs engineering

Polyelectrolytes are widely used in industry and research laboratories to control the stability of colloids and the interactional properties of surfaces. In papermaking, cationic polyelectrolytes are commonly used as retention aids for process colloids (calcium carbonate or clay fillers and fibre-derived ‘fines’) and as additives that increase the rate at which water can be drained from the fiber web. Other cationic polyelectrolytes containing functional groups that can react with hydroxy groups on the cellulose are used as wet strength additives [12]. Recently, cationic polyelectrolytes have been used to engineer binding of nanoparticles and enzymes on the surfaces of PADs [25, 27, 40] (Figure 5).

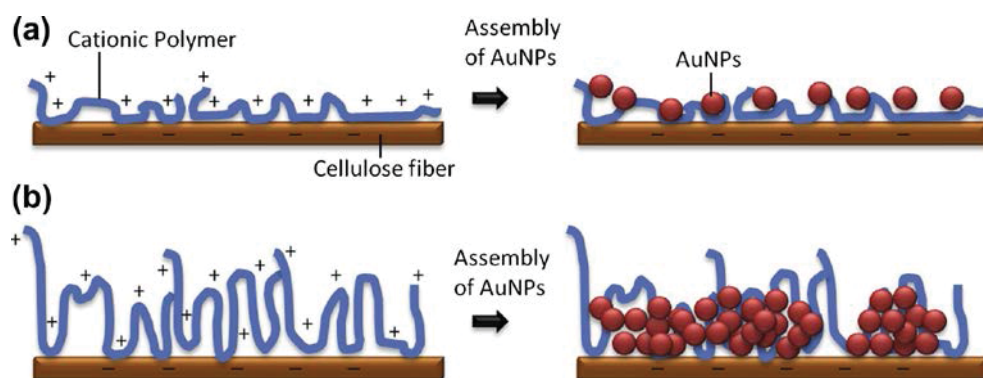


Figure 5. (a) Polymer attains a flat conformation with many trains at the interface. (b) Polymer attains a conformation with many loops and tails tangling out of the surface (Reproduced with the author’s permission from reference [27]).

Typically, a polyelectrolyte is adsorbed from solution onto a surface and remains at the liquid-solid interface. The variables affecting the morphology of the adsorbed layer are

dictated by the properties of the polymer (composition, charge, molecular weight), its affinity for the liquid and for the surface of the solid (Flory-Huggins factor χ), the concentration at which it is present in the liquid, properties of the liquid (temperature, pH, salt concentration and type), surface coverage and kinetics. The theory predicting the basic behaviour of polyelectrolytes in solutions and at solid-liquid interfaces is becoming better understood and can be expressed mathematically as reviewed by Dobrynin and Rubinstein [56] and Fleer *et al.* [57]. These mathematical descriptions only provide a guide to the behaviour observed experimentally and differences between theoretical predictions and experimental observations are often considerable.

Experimental information on the structure and thickness of adsorbed polyelectrolyte layers remains scarce [57]. The structural features of polyelectrolytes adsorbed at the cellulose-liquid interface have been quantified by ellipsometry, neutron reflectometry, atomic force microscopy and surface force apparatus. Three main factors remain poorly understood: 1) the morphology of polymers on cellulose surfaces, 2) the link between the morphology of the polymer in solution and at the cellulose-liquid interface, especially under the kinetically controlled conditions used in industry, and 3) the effect of polymer morphology at the cellulose-liquid interface and colloid stability/surface functionality.

1.2.2.1 Retention and flocculation

Cationic polyacrylamide copolymers (CPAM) are among the most commonly used polyelectrolytes and are important for paper engineering. This is because of their efficiency, low cost and availability in a wide range of polymer compositions and structures. Various grades of CPAM are commercially available with molecular weights and linear charge densities up to 15 MD and 100%, respectively. The linear charge density of CPAM is defined as the percentage of monomers containing a charge; typically a positive charge from incorporation of a quaternary amine in the monomer. Recent research applications of polyelectrolytes include 1) retention of enzymes, antibodies and nanoparticles on surfaces for paper biondiagnostics [27, 49], 2) development of functional materials and control of the activities of biomolecules [58, 59], and 3) engineering the interaction between cellulose nanofibers when preparing composite substrates [60] (Figure 6). However, in spite of their economic and technical importance, the adsorption behaviours of CPAM and the effects of the morphology of the adsorbed layer on the

dynamic stability of colloids are still poorly quantified and understood [57, 61, 62] and as a consequence each application involves considerable trial and error.

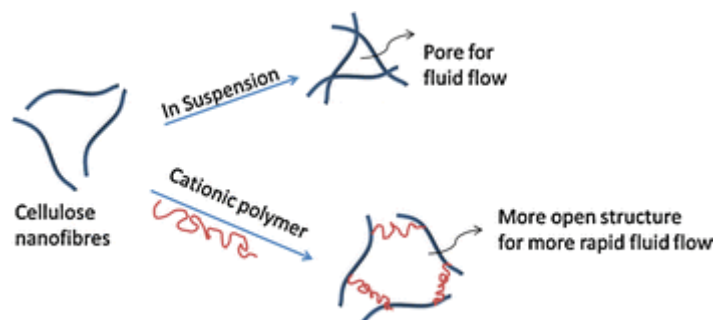


Figure 6. Schematic diagram of change in cellulose nanofibers suspension structure with cationic polyelectrolyte addition (Reproduced with the author's permission from reference [60]).

Lindstrom and Soremark measured the adsorption and surface coverage of CPAM on cellulose fibers under high shear conditions relevant to papermaking [63]. The variables investigated were CPAM charge density, molecular weight and concentration as well as the ionic strength and temperature of the solution. The quantity of polymer adsorbed on fibers was calculated from the CPAM concentration measured in the supernatant liquid using refractive index. An increase in CPAM molecular weight and charge density was found to decrease the amount of CPAM adsorbed on cellulose fibers [63]. The charge stoichiometry (the ratio between the charge on the fibers and the charge on the CPAM) was found to be a governing factor [64]. Wagberg et al. also measured the kinetics of polyelectrolyte adsorption on cellulosic fibers in terms of polymer properties (Mw, charge, concentration) [65].

Cellulose is an important solid surface for paper biondiagnostics in which polyelectrolytes can be used to retain biomolecules (antibodies, enzymes and whole cells) and to retain nanoparticles that can be used to increase the sensitivity of the device. In the absence of published data, it is crucial to quantify the layer thickness of high molecular weight CPAM adsorbed at the cellulose-water interface using a well-defined system in order to better understand why certain PADs work in the way that they do.

1.2.2.2 Wet strength improvement

To lessen the reduction in paper strength upon contact with water, reactive cationic polyelectrolytes such as polyamide-amine-epichlorohydrins (PAEs) are commonly used to improve the bonding between fibres, that constitutes the weak link in wet paper [66] (Figure 7). The generally accepted mechanism of wet-strength development by PAEs in paper is through the establishment of chemical bonds at fibre-fibre contacts. The process involves two steps: 1) retention of the polymer and 2) development of bonds. The main variables affecting PAE efficiency include its azetidinium concentration (see next paragraph), the type of fibres, and the drying conditions [9, 67].

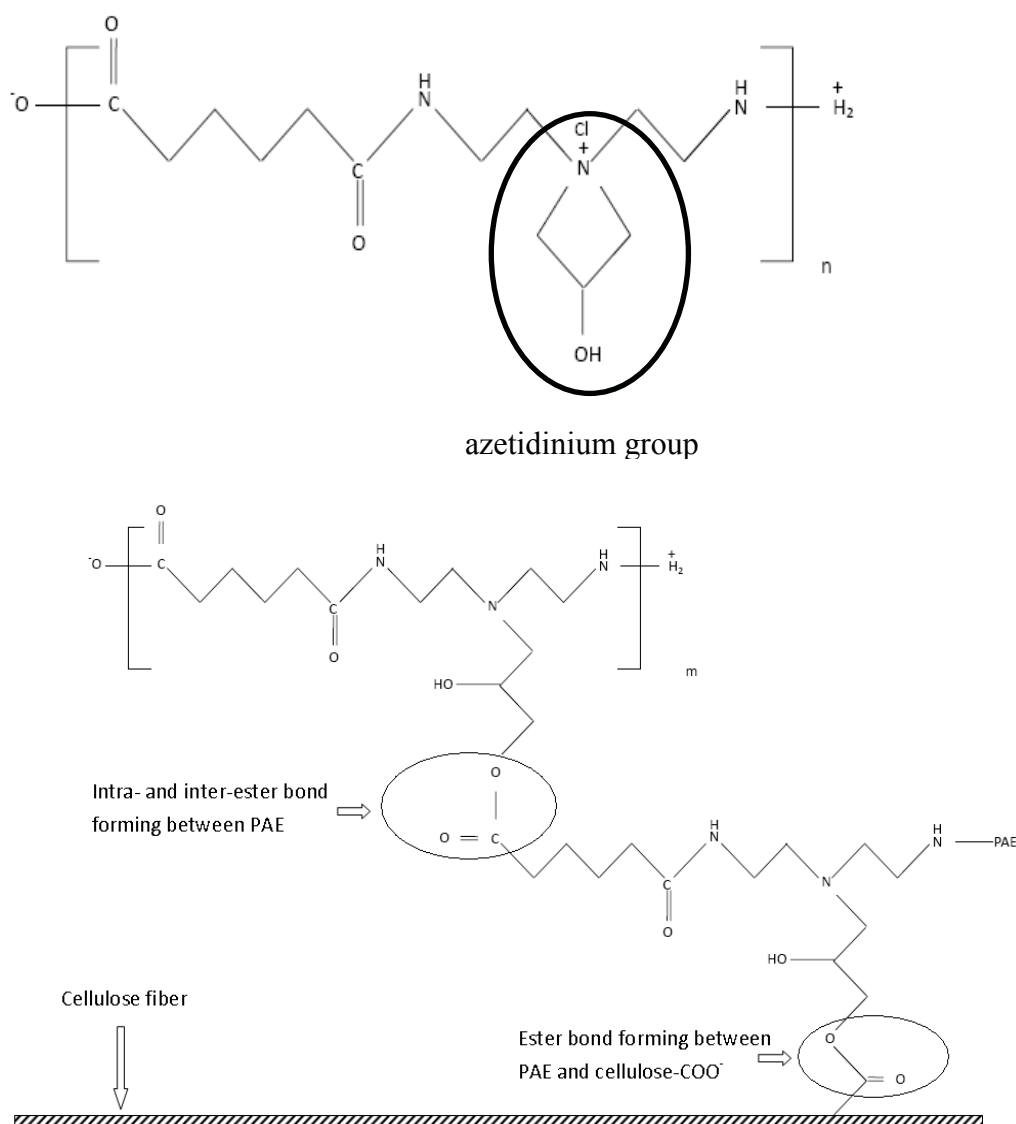


Figure 7. Structure of PAE and Schematic presentation of wet strengthening mechanism on paper treated with PAE.

Carboxyl groups, which significantly affect both PAE retention and reactivity, can be introduced to fibres by kraft pulping and through oxidation during the bleaching process. When adding PAE to a slurry of cellulosic fibres, adsorption is driven by the electrostatic attraction between the anionic carboxylated groups on the fibre surface and the cationic azetidinium groups of the polymer [8, 68]. After PAE adhesion to cellulosic fibres, the curing process facilitates the formation of bonds between fibres and the PAE. These bonds are covalent ester bonds between the carboxyl groups of cellulose or hemicelluloses and the hydroxy groups on the polymer's azetidinium group, resulting in covalent inter-fibre bonds that are not weakened by water [11, 12]. In order to break the covalent inter-fibre bonds, special techniques such as a combination of mechanical energy and oxidizing agents are required for successful repulping [10, 69].

PADs products require wet strength, since most of bio-analysis is carried out in wet or high moisture conditions. PAE can be used in applications requiring long-term wet strength. An additional benefit of using PAE addition is to control the level and sign of the surface charge on the cellulose substrate. The surface of pure cellulose is slightly anionic, and the charge is reversed by treating with excess cationically charged PAE. This feature can obviously be fine tuned to promote the adsorption of either a negatively charged, or a positively charged carrier molecule that is coupled to a biomolecule. Alternatively, PAE on the paper surface may have residual chemically reactive groups that can directly couple to certain biomolecules. Wang et al. reported the influence of PAE treatment on the immobilization of antibodies and their activity on paper. They showed the antibody activity was only slightly decreased by high loadings of PAE, whereas low loadings of PAE improved antibody performance [5]. Despite these benefits, denaturation and deactivation of biomolecules on PAE paper may still occur [47].

1.2.3 Microfibrillated cellulose (MFC) in paper composites engineering

Nanomaterials are bringing significant advantages for designing novel biosensing systems and improvement of existing devices. In PADs, the nanomaterials are applied as carriers or labels with special functions, e.g. surface enhanced Raman scattering, photocatalytic, and antibacterial activity [29]. Microfibrillated cellulose (MFC), made by mechanical [70-72], acid hydrolysis [73], or enzymatic processes [74, 75] have shown strong potential in developing novel paper products and renewable composites having unique

properties. Some of the attributes of MFC composites include improved mechanical properties, improved barrier properties to gases, better biodegradability and better transparency. MFC fibers are interesting as they combine nanoscale fiber diameters (5 ~50 nm) with micron-scale fiber length (1~1000 μm) [76-78]. The advantages of large surface areas and high affinities for biomolecules inherent in MFC fibers can be expected to result in development of improved PADs products that are stronger, lighter in weight and which have better controlled structure, sensitivity and shelf life.

Composites incorporating MFC in the substrate using papermaking processes have already been investigated [13, 79-81]. MFC has been either blended with pulp fibers or used as a pure suspension, with and without polymeric strength agents. MFC composites with high tensile strength have been achieved, with properties depending on material and preparation procedure [82, 83]. However, studies have consistently reported very slow drainage rates that are incompatible with current papermaking practices. Drainage rate is the rate at which water can be removed from the fiber web during the initial (forming) stage of the papermaking process and is one of the most critical parameters that determines whether or not a particular type of fiber can be used to make paper under commercial conditions. Another promising avenue investigated has been the coating of MFC onto paper for improved strength, printability and selective barrier properties [15]. While composites having improved properties have been achieved, two main issues have arisen: the first is again a very slow drainage rate, and the second is the loss of gas barrier and strength properties under conditions of high humidity moisture/or wet conditions [14, 80, 84, 85].

1.2.3.1 Effect of MFC on preparation of paper composites

All paper composites containing MFC are prepared by draining away the water from fiber suspensions. The drainage rate in papermaking is governed by factors such as pH, ionic strength, type and amount of cationic polyelectrolyte used and fiber dimensions. As the surface area of the fiber increases with the reciprocal of the diameter of the average fiber, and the drainage resistance is inversely proportional to the square of the specific surface area [39], the drainage rate is expected to drop at a faster than linear rate with the content of MFC in the furnish, and slow drainage rates are observed in virtually all studies [86, 87].

Fiber refining is a mechanical process that is used to increase the flexibility and degree of fibrillation of papermaking fibers. It is a major factor in virtually all commercial papermaking operations that serves to increase fiber-to-fiber bonding and this results in higher tensile and many other strength indices of the resulting paper sheet. Tethered cellulose microfibrils have been observed on the surface of refined pulp in many studies [74, 88, 89]. Tethered microfibrils are defined as the fibrils delaminated from the outer layers of the fiber that remain attached by a segment or an extremity. Drainage rate is known from experimental practice to drop at a slower than linear rate upon fiber refining [90]. With the aim of developing high performance cellulosic composites for PADs, it is worthwhile investigating the hypothesis that refining creates MFC tethered onto the surface of the fibers, thereby providing equivalent strength but at a significant drainage benefit compared to direct MFC addition that tends to block flow of process water through the wet web during paper manufacture. Studies of PADs produced from paper substrates in which the sole variable is the degree of refining of the pulp used to make the paper appear to be lacking at present.

1.2.3.2 Effect of MFC on properties of paper composites

Films and composites which incorporate MFC and have improved properties have been developed by different approaches. Mechanical strengths, surface smoothness and transparency of films typically all increase as the dimensions of the MFC fibers decrease, while the porosities and gas permeabilities decrease [15, 91]. Arbatan et al. used MFC as a binder for fabrication of superhydrophobic paper [92]. Several studies have demonstrated production of strong paper composites by adding MFC to pulp fiber suspensions, especially in conjunction with a reactive-cationic polymer, such as PAE [13]. The improved properties achieved for these composite papers, namely smoothness and mechanical properties under wet and dry conditions were shown to significantly increase; paper gas permeability to decrease while drainage rates were little changed. Nonetheless, there is little published understanding of the effect of MFC dimension and structure on these paper composites, especially in terms of the strength development mechanism applying in MFC-polymer-fiber composites.

1.2.4 Cellulose film as a tool for developing PADs

In papermaking, many fundamental properties and phenomena rely on colloidal chemistry occurring on the cellulose fiber surfaces. Because natural fibers display quite complex morphologies in paper webs, cellulose model films that have well defined surface compositions and morphologies are much more straightforward substrates that enable use of instrumental techniques that cannot be applied to fiber webs. These techniques include specular X-ray or neutron reflectometry, surface force analysis and atomic force microscopy [13, 52, 93-96].

The supramolecular structure of native cellulose consists of anhydroglucose units linked by 1, 4-glycosidic bonds into linear polymer chains. These chains link together by interchain hydrogen bonding that form both crystalline and amorphous domains within bundles of chains called microfibrils. The degree of crystallinity has a significant effect on the physical, mechanical, and chemical properties of cellulose based products. The crystallinity is also a critical feature when cellulose makes contact with water. Amorphous cellulose domains swell in liquid water and in water vapour as water penetrates inside the spaces in the disordered regions and disrupts the inter-chain hydrogen bonds [97]. Crystalline cellulose domains are highly ordered with few spaces between chains and these are penetrated by water to a much smaller extent. Cellulose thin films with different crystallinities have been prepared by various methods, and mainly applied in swelling, adsorption and surface force studies [98]. Investigations of the interactions between biomolecules and polyelectrolytes at model cellulose film interfaces offer significant opportunities for designing and improving PADs.

1.2.4.1 Role of cellulose surfaces in PADs

Natural cellulosic fibers are porous, hydrophilic materials with high capacities for water absorption. Generally, the cellulose surface serves three functions in PADs: the first is the capacity to retain biomolecules or reagents [20]. Their local distributions and orientations significantly influence the performances and efficiencies in bio-analysis [16]. It is important to keep in mind the difference between cellulose film surfaces and cellulose fiber networks. Paper has a three-dimensional structure, and the thickness (z direction) is a factor to consider in PADs as the reagents and analytes could either spread over the in-plane surface, or penetrate deeper into the thickness direction of paper creating a concentration gradient [55].

The second function is the creation of the necessary change in colour between a negative and a positive result. Such changes may be detected by eye, or by colorimetric analysis. Paper-based dipsticks for analysis of urine and acid-base indicator papers have been widely accepted for many decades as simple paper-based diagnostic devices. Many biochemical reactions that result in colour changes have also been used in conjunction with colorimetric, or spectrophotometric measurements to assay both enzyme and metabolite concentrations. A typical example is the enzymatic reaction shown in Figure 8. Pure cellulose with excellent biocompatibility enables an image analysis technique to quantify the intensity of the coloured products, allowing the evaluation of reaction kinetics and thermal stability [35, 40].

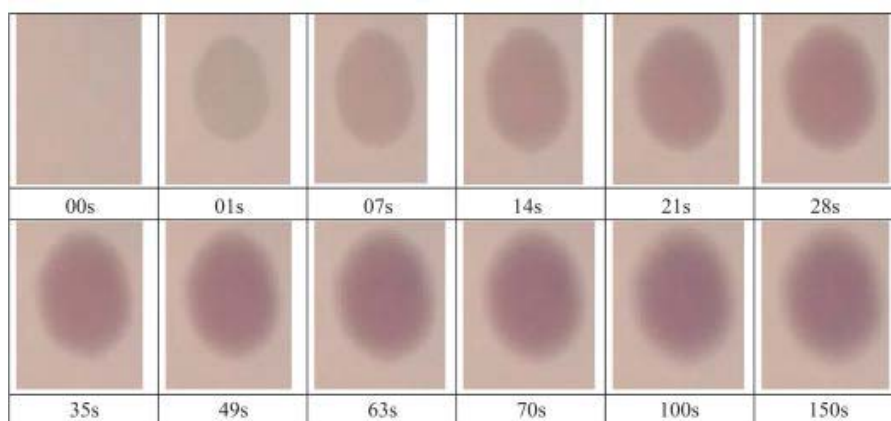


Figure 8. Product formation on alkaline phosphatase (ALP) enzymatic paper at different times. The blue purple colour reveals the enzyme (ALP) mediated reaction between 5-bromo-4-chloro-3-indolyl-phosphate and nitro blue tetrazolium dye (Reproduced with the author's permission from reference [40]).

The third function is alteration of the cellulose surface to form hydrophobic barriers that either create recognizable patterns in the case of a positive test result, or constrain the liquid analyte to flow in particular directions, as illustrated in Figure 2. Hydrophobic cellulose surfaces may be created either by chemical modification or by physical deposition of a hydrophobic material. Chemical modification is achieved using reactive agents that typically react with the hydroxyl groups of cellulose during subsequent high temperature curing. The resulting hydrophobic areas of the paper are usually resistant to extraction with organic solvents, whereas surface hydrophobicity generated by physical

deposition of hydrophobic materials can often be removed by solvents, allowing the possibility of etching to fabricate pattern channels in PADs [16, 31].

Recently there has been an increasing tendency to use solid surfaces and films directly for bio-analytics. Many of these surfaces and films may be incorporated into future PADs. As an example, the prototype of biological assays for human blood typing was conducted on a superhydrophobic polymer surface using a liquid drop micro reactor [99] (see Figure 4). This technique probably inspired the development of a later device supported on a cellulose substrate, where the cellulose surface was made more hydrophobic using conventional paper sizing chemicals. Several different routes for covalent immobilization of antibodies on native or activated cellulosic film have been prepared and evaluated by Orelma et al, in which the antibodies were deposited using standard inkjet printing techniques [20, 21, 52]. Ying reported functionalization of cellulose surfaces with gold nanoparticles and a series of biomolecules. This technique enabled development of a generic surface on which enhanced Raman scattering could be used for antibody-antigen detection [27]. These investigations are expected to open new venues for using cellulose surfaces in immunodiagnostic applications.

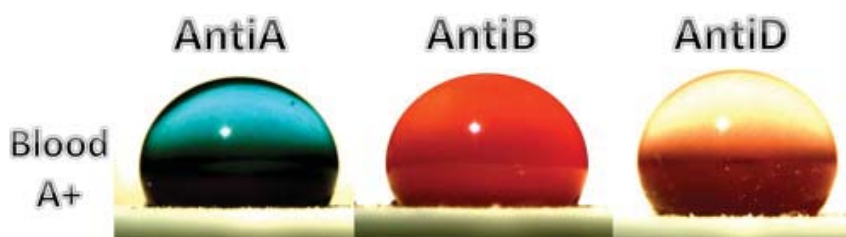


Figure 9. Superhydrophobic surface can support liquid drop micro reactors for bioassays (Reproduced with the author's permission from reference [99]).

1.2.4.2 Preparation of smooth cellulose film as a model surface

Preparation of smooth cellulose model surfaces on supporting substrates can be achieved using two alternative methods: Langmuir-Blodgett (LB) deposition and spin coating [100, 101]. Both methods involve three sequential steps: 1) Preparation of a solution or a suspension of cellulose or a cellulose derivative in a liquid. 2) Deposition of a film of the solution, or suspension on the substrate. 3) Removal of the liquid and purification or regeneration of the cellulose in cases where cellulose derivatives have been used. The

most direct method involves application of a solution or suspension of cellulose onto a substrate to form a film. Because solvents for cellulose all have low volatility and all involve disruption of interchain hydrogen bonding, it is difficult to control the uniformity and roughness of films formed directly from solutions of cellulose [98, 102]. The same limitations apply to films formed from suspensions of cellulose particles where the surface energetics of the particles usually result in aggregation of the particles when the suspending liquid is removed. Indirect methods of film formation involve initial preparation of chemical derivatives of cellulose (e.g. cellulose acetate and trimethylsilylated cellulose) in which interchain hydrogen bonding is reduced to an extent where complete dissolution in volatile solvents becomes possible. Solutions of the derivatives in volatile solvents can be used to create very smooth, uniform films of the derivative once the solvent evaporates. The film of cellulose derivative can then be regenerated back to a cellulose film [94, 103]. Under appropriate conditions, the resulting cellulose films are uniform and smooth, however the whole preparation process is time consuming.

Cellulose films having amorphous regions are widely reported using spin coating techniques, either from cellulose derivative solutions or from nanocellulose suspensions [98]. In spin-coating, the major variables dictating the film thickness and roughness are: 1) the solvent used (particularly its polarity and evaporation rate); 2) concentration and viscosity of the solution (or dispersion); 3) adhesion force between the solution (or dispersion) and the substrate. An anchoring polymer may be used to enhance the adhesion between film and substrate. 4) spinning rate and duration of film deposition; and 5) the purification and regeneration processes used [94, 103-108]. Commercial cellulose acetate and trimethylsilylated cellulose (TMSC) synthesized in the laboratory, are the most common derivatives used for preparing regenerated cellulose films [108, 109].

Cellulose itself occurs in a number of different forms, referred to respectively as cellulose I, cellulose II, cellulose III and cellulose IV, that differ in the arrangement of the interchain hydrogen bonds. Most naturally occurring cellulose is cellulose I, whereas cellulose regenerated from its derivatives is cellulose II. The surfaces of cellulose I have different densities and crystallinities from those formed from amorphous cellulose or cellulose II, leading to dissimilar interfacial properties. Smooth model cellulose I surfaces have been reported to have been produced from colloidal dispersions of cellulose I

nanocrystals [110]. The rod-like nanocrystals in aqueous suspensions can be cast on appropriate surfaces and these reportedly form flat films after water is evaporated. Films in which the rod-like nanocrystals are non-randomly oriented can be achieved by spin-coating or shear.

Bacterial cellulose is also used as raw material to produce cellulose films. In comparison to the cellulose from higher plants, bacterial celluloses produced by some bacteria exhibit many unique properties: excellent biological affinity, high purity and crystallinity [111]. Gao et al. reported preparation of cellulose films from solutions of bacterial cellulose in N-methyl morpholine oxide (NMMO), and reported that the regenerated films have better mechanical and barrier properties than films formed from cellulose derived from wood or cotton [102]. Acetylation of bacterial cellulose using different methods provides other options for producing regenerated cellulose films [112-114].

1.2.4.3 Characterization of the interactions at cellulose surface

Interaction of cellulose surfaces with biomolecules and polyelectrolytes depends on both the interfacial properties of the cellulose and on the morphology of the surface. Various modern techniques have been developed to characterize the interaction at cellulose surface and these are discussed below. Fundamental knowledge concerning interactions at cellulose/liquid (water) interfaces is of great importance as most PADs are prepared and used in the presence of water.

1.2.4.3.1 Specular X-ray and neutron reflectivity

Specular X-ray reflectometry is commonly performed to obtain information on the structure of thin and flat cellulose films in the direction normal to the plane of the film [96, 103, 108, 115]. Specular reflectivity is defined as the ratio of reflected intensity over incident intensity, where the angle of incidence is equal to the angle of reflection. When X-rays are reflected from a film interface which is not perfectly sharp and smooth, the reflected intensity will deviate from that predicted by the Fresnel reflectivity theory. The deviations can be utilized to analyse film properties (density, thickness and roughness) [116]. Although specular X-ray reflectometry is a powerful technique for characterising films based on the interaction with electrons, the major limitation being that X-rays provide insufficient contrast for light atoms such as hydrogen and deuterium [117].

Elastic neutron scattering is a nonintrusive technique for investigating the structures of substances at a nanoscale. The most crucial feature of the technique is contrast variation, relying on the differential ability of hydrogen and deuterium nuclei in the molecular structure of the sample to scatter neutrons in the beam. The technique is particularly useful in the biological sciences as hydrogen-deuterium exchange usually has a minimal effect on the conformation of the sample, but has dramatic effects on the scattering [118]. Controlled incorporation of deuterium into bacterial cellulose has been reported [24], and this allows the scattering length density of the deuterated cellulose to be varied, which enables contrast matching to reveal information about the structure and dynamics of cellulose and its interaction with biomolecules. In the absence of any reports of the use of neutron scattering to study the interactions between cellulose and biomolecules, there is a clear need to prepare smooth cellulose model films having different deuteration levels so that neutron scattering length densities in the cellulose films can be varied in a controlled manner.

The inner structure of materials can be measured by neutron scattering techniques by virtue of the interactions of the nuclei within their component atoms with neutron beams. These interactions can be measured using scattering length density (SLD) profiles. Theoretical SLD (ρ) profiles for the materials can be calculated according to the following formula:

$$\rho = \frac{N_a \rho_{\text{mass}}}{M_R} \times \sum_{i=1}^n b_{ci} \quad (1)$$

In Equation (1), b_{ci} is the bound coherent scattering length of the i th atom of a molecule having n atoms (the value of b_{ci} is different for X-rays and neutron beams). N_a is Avogadro's number, ρ_{mass} is the mass density of the material and M_R is its relative molecular mass (the sum of the relative atomic masses of the constituent atoms of a molecule. Relative atomic mass is the ratio of the average mass of atoms to 1/12 of the mass of an atom of carbon-12).

Specular neutron reflection (NR) is a strong neutron scattering technique that can be used to directly investigate phenomena at surfaces and solid/water interfaces [119], and this technique can be employed to monitor cellulose interfacial interactions under various conditions. The NR measures the ratio of reflected to incident intensity as a function of momentum transfer $q_z = (4\pi/\lambda) \sin\theta$, where θ is the angle of incidence with respect to the

plane of the film and λ is the wavelength of the beam, and the data curve describes the information on the SLD profile normal to an interface. As the thickness of the thin film is well-defined and its roughness is low, the NR spectra of thin films display oscillations (Kiessig fringes) which are directly related to the total thickness of the multilayer film [94]. Roughness is implemented in terms of an error function [120] and defined as the standard deviation of the error function. Hence, the interface and surface properties such as thickness, roughness can be obtained from model fitting analyses.

Swelling behaviour and rearrangements of an amorphous ultrathin cellulose film exposed to water and subsequently dried have been measured by NR [94]. In that study, when the film was immersed in liquid D₂O, the thickness increased by 100% of its original value, whereas there was almost no increase in roughness. Moreover, the uptake of D₂O by the film was 86 wt%. These results demonstrate that amorphous cellulose films can exhibit remarkable swelling properties while maintaining a smooth outer interface. The interaction of cellulase enzymes with amorphous cellulose films has also been characterized by NR [121]. The observed results suggest that 1) substantial H/D exchange occurs upon exposure of cellulose films to D₂O. 2) The swelling behaviour is slightly greater for D₂O than for H₂O and there is no difference in the degree of swelling detected between pure H₂O and D₂O buffer (50 mM sodium acetate pH 5). 3) Without deuteration enrichment of the cellulases, the NR measurement is largely insensitive to the presence of absorbed enzyme as there is insufficient contrast between the enzyme and the water. These findings indicate that the NR technique should be useful in aiding development of PADs, but additionally suggest that meaningful data will only be obtained if both the cellulose film and the biomolecule under study have deuterium incorporated in them in a controlled manner before the NR experiments are undertaken.

1.2.4.3.2 Additional techniques

Topographical and morphological changes on the surface of cellulose film have been widely investigated using atomic force microscopy (AFM). In addition to measuring the film thickness and roughness, AFM is also used to investigate surface interactions with polyelectrolytes. Lefebvre and Gray examined polyelectrolyte layers and multilayers on cellulose nanocrystal films both in water and diluted salt solution [95]. By comparing the deflection-distance curves from different surfaces (silicon, cellulose-coated silicon,

polyelectrolytes adsorbed on the cellulose surface), single and multiple polyelectrolyte bilayers of carboxymethyl cellulose/poly(diallyl-dimethyl-ammonium chloride) presented different force-distance curves, information regarding the nanoscale thicknesses and roughness of multiple layers having diffused repulsive forces was obtained.

Surface force techniques such as colloidal probe microscopy have been developed and used to characterize interactions between pure cellulose surfaces and other materials under aqueous conditions. Rutland et al.[122] found that the forces between cellulose surfaces and certain hydrophobic polymers depend on the electrolyte type and its concentration. In the presence of cationic polyacrylamide, surface adhesion at sub-monolayer coverage resulted from polymer bridging, and sliding friction between cellulose surfaces under these conditions decreased significantly [123, 124].

The Quartz Crystal Microbalance with Dissipation (QCM-D) measures the changes in frequency and dissipation of an oscillating quartz crystal. In principle, the frequency is changed by both mass adsorption on the sensor surface and coupling of the liquid medium to the adsorbed layer, whereas the energy dissipation of the sensor surface is caused by frictional losses in the adsorbed layer [125]. The QCM-D provides in-situ information on the adsorption kinetics and the quantity of water absorbed at the solid/liquid interface. Furthermore, the visco-elastic properties of the formed layer can be retrieved. Model cellulose surfaces deposited on sensor quartz crystals have been well characterized, and used to investigate the dynamics of enzymatic activity, antibody and polyelectrolyte adsorption [20, 126-128] .

Surface Plasmon Resonance (SPR) is used complementally with QCM-D to investigate adsorption kinetics of biomolecules, especially using continuous flow systems. The SPR method is an optical technique applying resonant oscillation of conduction electrons at the interface between a negative and positive permittivity material stimulated by incident light [129]. It is highly sensitive to any alteration of the refractive index on the sensor surface and this characteristic is used to analyse the adsorption of molecules on the sensor surface [6, 52, 130]. In addition, SPR imaging enables observation of the interfacial behaviour in real time, providing a strong tool for characterizing cellulose-biomolecule interactions [93].

The dynamic adsorption and other features of absorbed polyelectrolytes and biomolecules on cellulose films have been intensively characterized by quartz crystal microbalance with dissipation, atomic force microscopy and surface plasmon resonance. Factors such as cationicity, ionic strength and pH of the solution were reported to control their adsorption [6, 21, 52]. There is, however, limited knowledge available concerning the direct conformation of polyelectrolytes and biomolecules at cellulose/water interfaces and therefore details of the nanoscale structures present in the absorbed layers need to be fully examined.

1.2.5 Gaps in knowledge

This literature review has revealed major issues of poorly understood and unknown concepts, and inadequately quantified phenomena. This lack of knowledge currently restricts innovation and development of papers engineered with controlled strengths, structures and surfaces using the interactions between cellulose and cationic polyelectrolytes. Some of the major gaps are:

- Wet strength and ability to repulp PADs after use - little is known about paper substrates that retain high wet strength while maintaining full recyclability
 - 1) What is the influence of cationic wet strength polymer on paper formation and strength development?
 - 2) What are the main variables controlling paper strength development and what are their relationships with repulpability of the papers?
- Paper engineered with high strength and controlled structure (permeability and porosity)
 - 1) What is the role of the physical dimensions of cellulosic additives (MFC and nanocellulose) in paper engineering?
 - 2) What is the strengthening mechanism in the presence of microfibrillated cellulose (MFC), with and without cationic wet strength polymer?
 - 3) How does cationic wet strength polymer/MFC complex affect preparation and structures of cellulose composites?
 - 4) What is the difference between paper substrates incorporating free and tethered MFC, with and without cationic wet strength polymer?
- Paper engineered for human red blood cell typing
 - 1) How does cationic wet strength polymer affect performance of paper-based blood cell typing?
 - 2) How does paper structure affect the sensitivity of paper-based blood typing?
- Nanoscale conformation and thicknesses of biomolecular and polyelectrolyte layers adsorbed at cellulose interfaces - in situ characterizing model cellulose surface interactions with cationic polyelectrolyte or biomolecules by specular neutron reflectometry (NR).
 - 1) Control the smoothness of prepared cellulose films that are suitable for NR measurement.

- 2) Preparation of deuterated cellulose films as model surfaces having varying contrast in NR measurement
- 3) What are the main variables affecting the morphologies of cationic polyelectrolytes and biomolecules absorbed at cellulose/liquid interfaces?
- 4) What are the adsorption kinetics of model polymers and biomolecules, and how is the amount adsorbed best quantified.

1.3 Research objectives and aims

Novel papers suitable for use as generic diagnostic platforms must be strong - particularly when used wet. They must also be easily disposable/recyclable and have a controllable porosity to address the various requirements made by interaction with biological fluids having different viscosities. Porosity must be controllable over different length scales in order to separate biomolecules from aggregates when required. Lastly as mentioned above, biomolecules are the most expensive part of the PAD; they must be fully functional and stable. A better understanding of the effect of the cellulose surface on the interaction/conformation of cationic polyelectrolytes is needed.

This research addresses major problems for paper engineering with strength, structure and surface by studying the interactions between cellulose and cationic polyelectrolytes and the potential for incorporation in PADs. This thesis has four general objectives. First is, using nanocellulose, to develop strong cellulose fibrous composites having controlled properties (porosity and permeability). The second objective is to quantify the effect of paper structure and cationic wet strength polymer on paper-based blood typing diagnostic devices, and to optimize their performance. The third objective is to prepare smooth cellulosic films as model cellulose surfaces, and then measure the thickness and conformation of the adsorbed cationic polyelectrolyte or biomolecule (antibody or enzyme) at the cellulose/water interface. The fourth objective is to investigate the effect of manipulation of the various and complementary length scales on properties of PADs and model PAD systems:

1. Mesoscale: Engineering paper with high strength and controlled structure by cationic wet strength polymer and cellulosic additives.
2. Macroscale: Engineering paper substrate and quantifying the effect of wet strength polymer and paper structure on blood typing biodiagnostics.
3. Nanoscale: Measuring and characterizing the model cationic polyelectrolyte or biomolecules adsorbed at the cellulose/water interface.

To address these objectives, the specific aims of this doctoral study are:

1. To quantify the relationship between wet strength and repulpability of wet-strengthening paper (**Chapter 2**).

2. To investigate the role of microfibrillated cellulose (MFC) dimensions for paper engineering (**Chapter 3**).
3. To engineer paper strength and structure with MFC and polymeric strength agents (**Chapter 4**).
4. To engineer paper for blood typing bio-diagnostics and to quantify the effect of paper structure and cationic wet strength polymer on the analytical performance (**Chapter 5**).
5. To prepare model cellulose surfaces for measurement of the thicknesses and conformations of layers of cationic polyelectrolytes adsorbed at cellulose/water interfaces, as well as investigating the variables affecting the adsorption (**Chapter 6**).
6. To prepare smooth deuterated cellulose surfaces, which enable their contrast under neutron reflectometry experiments to be varied so that measurement of the conformation of biomolecules adsorbed on the surfaces becomes possible (**Chapter 7**).

The relationship between the objectives, the length scales of studies and the chapters of this thesis are illustrated in Figure 10.

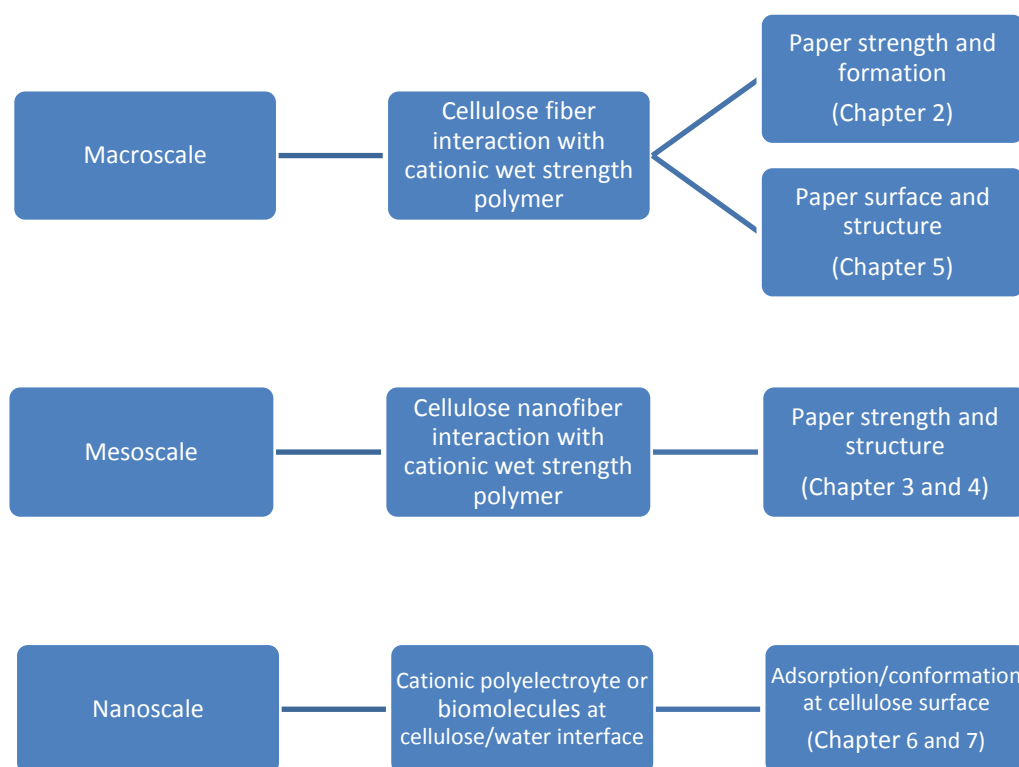


Figure 10. Thesis research components and chapter thesis lists.

1.4 Thesis outlines

The thesis comprises this introductory chapter, five chapters based on published articles and one chapter based on a manuscript in preparation. The objectives and the contributions of each chapter are as follows:

- **Chapter 2:** Paper strength development and recyclability with polyamide-amine-epichlorohydrin (PAE).

(Paper #1, published in *Bioresources*, **7**, 913-924, (2012))

This chapter investigates the tensile strength behavior and recyclability of papers prepared with addition of polyamide-amine-epichlorohydrin (PAE). The dry and wet tensile strengths obtained with different PAE dosages were measured. The repulpabilities of the strengthened papers were correlated directly with their wet strengths. The effect of electrolyte addition on tensile strength was also quantified by varying ionic strength (sodium chloride and calcium chloride concentrations) in the furnish stock. The cation valency and concentration in the process water were important variables which were found to affect the efficiency of PAE in developing wet strength.

- **Chapter 3:** Paper engineered with cellulosic additives: effect of length scale

(Paper #2, published in *Cellulose*, **21**, 2901-2911, (2014))

In this chapter, cellulosic fiber composites produced using laboratory papermaking methods with two types of MFC were studied. The two types of MFC with different length scales were produced respectively by homogenization or by ball milling. Their strengthening effect on blending with hardwood fibers was compared with cellulose microparticles (CMPs) made by cryogenic milling, with and without polyamide-amine-epichlorohydrin (PAE) addition. Their different stress-strain curves in wet conditions suggest two different mechanisms of strength development: MFC-fiber entanglement and fiber-fiber contact reinforcement.

- **Chapter 4:** Effect of tethered and free microfibrillated cellulose (MFC) on the properties of paper composites

(Paper #3, published in *Cellulose*, **20**, 1925-1935, (2013))

In this chapter, high strength and low gas permeability cellulosic composites were produced using laboratory papermaking methods with commercial microfibrillated cellulose (MFC). The effect of blending MFC with hardwood fibers was compared to the direct refining of the fibers with and without polyamide-amine-epichlorohydrin (PAE) addition. The addition of MFC, free or tethered, to pulp fibers combined with PAE can increase the dry and wet strengths of cellulosic fiber webs. Drainage and air permeability of the composites was found to decrease with MFC addition.

- **Chapter 5:** Engineering paper as a substrate for blood typing bio-diagnostics.

(Paper #4, published in *Cellulose*, **19**, 1749-1758, (2012))

This chapter describes quantification of the effect of paper structure on blood typing. Visualization was quantified and analyzed to engineer low-cost diagnostics. Commercial and laboratory-generated papers varying in fibre composition, basis weight, density and porosity were investigated for their ability to separate agglutinated red blood cells(RBC) that had been interacted with antibodies (that are specific to the blood group of the RBC) from non-agglutinated RBC (that had been interacted with antibodies that are not specific for the particular RBC blood group).

- **Chapter 6:** Adsorption of cationic polyacrylamide at the cellulose-liquid interface: a neutron reflectometry study.

(Paper #5, published in *Journal of Colloid and Interface Science*, **448**, 88-99, (2015))

The chapter describes quantification of the layer thickness and density of high molecular weight cationic polyacrylamide (CPAM) adsorbed at the cellulose-water interface by neutron reflectometry. The thicknesses of full monolayers of CPAM of constant molecular weight, but different charge densities, adsorbed with or without NaCl, were studied. Thin and smooth cellulose films were produced by spin coating a solution of cellulose acetate in acetone and regenerating cellulose by alkaline hydrolysis. Film smoothness was greatly improved by controlling the concentration of cellulose acetate and the hydrolysis time in methanolic sodium methoxide. Calculations of the cellulose film and CPAM properties are included in *Appendix A*.

- **Chapter 7:** Preparation of smooth deuterated cellulose films for visualisation of adsorbed macromolecules.

(Manuscript to be submitted to *Macromolecules*)

In this chapter novel approaches to preparing deuterated cellulose films with contrast variation for neutron reflectometry are explored. Incorporation of deuterium into cellulose was successfully achieved by growing cellulose-producing bacteria in D₂O. The bacterial cultures were produced by a colleague who provided the author with raw bacterial celluloses (both native and deuterated) that the author subjected to purification using strong alkali to remove protein contaminants as described in the experimental section. As a second step, two methods for synthesizing different cellulose derivatives which can dissolve in volatile solvents (acetone and toluene) suitable for spin coating were compared. The two approaches were acetylation using acetic anhydride and an acid catalyst; and trimethylsilylation in an ionic liquid solvent. The trimethylsilylation of deuterated cellulose was found to be a more efficient method that results in a high yield of product, and it was used to prepare toluene solutions for spin-coating onto silicon substrates. The resulting thin film was hydrolysed back to deuterated cellulose, and then examined by specular X-ray reflection measurement; full contrast analysis is pending because of limited access to neutron reflectometry equipment during the tenure of the author's scholarship. Nevertheless the method developed may be used by future investigators to conduct NR studies on model deuterated cellulose films.

1.5 References

1. Martinez, A.W., S.T. Phillips, G.M. Whitesides, and E. Carrilho, *Diagnostics for the Developing World: Microfluidic Paper-Based Analytical Devices*. Analytical Chemistry, 2010. **82**(1): p. 3-10.
2. Then Whui, L. and G. Garnier, *Paper diagnostics in biomedicine*, in *Reviews in Analytical Chemistry* 2013. p. 269.
3. Martinez, A.W., S.T. Phillips, E. Carrilho, S.W. Thomas, H. Sindi, and G.M. Whitesides, *Simple telemedicine for developing regions: Camera phones and paper-based microfluidic devices for real-time, off-site diagnosis*. Analytical Chemistry, 2008. **80**(10): p. 3699-3707.
4. Khan, M.S., G. Thouas, W. Shen, G. Whyte, and G. Garnier, *Paper Diagnostic for Instantaneous Blood Typing*. Analytical Chemistry, 2010. **82**(10): p. 4158-4164.
5. Wang, J., R. Pelton, L.J. Veldhuis, C.R. MacKenzie, J.C. Hall, and C.D.M. Filipe, *Wet-strength resins and surface properties affect paper-based antibody assays*. Appita Journal, 2010. **63**(1): p. 32-36.
6. Orelma, H., T. Teerinen, L.S. Johansson, S. Holappa, and J. Laine, *CMC-modified cellulose biointerface for antibody conjugation*. Biomacromolecules, 2012. **13**(4): p. 1051-8.
7. Guan, L.Y., R. Cao, J.F. Tian, H. McLiesh, G. Garnier, and W. Shen, *A preliminary study on the stabilization of blood typing antibodies sorbed into paper*. Cellulose, 2014. **21**(1): p. 717-727.
8. Obokata, T. and A. Isogai, *The mechanism of wet-strength development of cellulose sheets prepared with polyamideamine-epichlorohydrin (PAE) resin*. Colloids and Surfaces a-Physicochemical and Engineering Aspects, 2007. **302**(1-3): p. 525-531.
9. Saito, T. and A. Isogai, *A novel method to improve wet strength of paper*. Tappi Journal, 2005. **4**(3): p. 3-8.
10. Chan, L.L., *Wet-strength resins and their application* 1994, Atlanta, Ga.: TAPPI Press. xii, 120 p.
11. Devore, D.I. and S.A. Fischer, *Wet-strength mechanism of polyaminoamide-epichlorohydrin resins*. Tappi Journal, 1993. **76**(8): p. 121-128.
12. Espy, H.H., *The Mechanism of Wet-Strength Development in Paper - a Review*. Tappi Journal, 1995. **78**(4): p. 90-99.
13. Ahola, S., M. Osterberg, and J. Laine, *Cellulose nanofibrils-adsorption with poly(amideamine) epichlorohydrin studied by QCM-D and application as a paper strength additive*. Cellulose, 2008. **15**(2): p. 303-314.
14. Syverud, K. and P. Stenius, *Strength and barrier properties of MFC films*. Cellulose, 2009. **16**(1): p. 75-85.
15. Aulin, C., M. Gallstedt, and T. Lindstrom, *Oxygen and oil barrier properties of microfibrillated cellulose films and coatings*. Cellulose, 2010. **17**(3): p. 559-574.
16. Jarujamrus, P., J.F. Tian, X. Li, A. Siripinyanond, J. Shiowatana, and W. Shen, *Mechanisms of red blood cells agglutination in antibody-treated paper*. Analyst, 2012. **137**(9): p. 2205-2210.
17. Guan, L., J. Tian, R. Cao, M. Li, Z. Cai, and W. Shen, *Barcode-Like Paper Sensor for Smartphone Diagnostics: An Application of Blood Typing*. Analytical Chemistry, 2014. **86**(22): p. 11362-11367.
18. Daniels, G. and M.E. Reid, *Blood groups: the past 50 years*. Transfusion, 2010. **50**(2): p. 281-289.
19. Al-Tamimi, M., W. Shen, R. Zeineddine, H. Tran, and G. Garnier, *Validation of Paper-Based Assay for Rapid Blood Typing*. Analytical Chemistry, 2012. **84**(3): p. 1661-1668.
20. Orelma, H., I. Filpponen, L.S. Johansson, M. Osterberg, O.J. Rojas, and J. Laine, *Surface Functionalized Nanofibrillar Cellulose (NFC) Film as a Platform for Immunoassays and Diagnostics*. Biointerphases, 2012. **7**(1-4).

21. Orelma, H., L.S. Johansson, I. Filpponen, O.J. Rojas, and J. Laine, *Generic Method for Attaching Biomolecules via Avidin-Biotin Complexes Immobilized on Films of Regenerated and Nanofibrillar Cellulose*. *Biomacromolecules*, 2012. **13**(9): p. 2802-2810.
22. Bali, G., M.B. Foston, H.M. O'Neill, B.R. Evans, J. He, and A.J. Ragauskas, *The effect of deuteration on the structure of bacterial cellulose*. *Carbohydrate Research*, 2013. **374**(0): p. 82-88.
23. Korneev, D., Y. Lvov, G. Decher, J. Schmitt, and S. Yaradaikin, *Neutron reflectivity analysis of self-assembled film superlattices with alternate layers of deuterated and hydrogenated polystyrenesulfonate and polyallylamine*. *Physica B: Condensed Matter*, 1995. **213-214**(0): p. 954-956.
24. He, J., S. Pingali, S.S. Chundawat, A. Pack, A.D. Jones, P. Langan, B. Davison, V. Urban, B. Evans, and H. O'Neill, *Controlled incorporation of deuterium into bacterial cellulose*. *Cellulose*, 2014. **21**(2): p. 927-936.
25. Khan, M.S., S.B.M. Haniffa, A. Slater, and G. Garnier, *Effect of polymers on the retention and aging of enzyme on bioactive papers*. *Colloids and Surfaces B: Biointerfaces*, 2010. **79**(1): p. 88-96.
26. Koga, H., T. Kitaoka, and A. Isogai, *Paper-immobilized enzyme as a green microstructured catalyst*. *Journal of Materials Chemistry*, 2012. **22**(23): p. 11591-11597.
27. Ngo, Y.H., W.L. Then, W. Shen, and G. Garnier, *Gold nanoparticles paper as a SERS bio-diagnostic platform*. *Journal of Colloid and Interface Science*, 2013. **409**: p. 59-65.
28. Ngo, Y.H., D. Li, G.P. Simon, and G. Garnier, *Effect of cationic polyacrylamide dissolution on the adsorption state of gold nanoparticles on paper and their Surface Enhanced Raman Scattering properties*. *Colloids and Surfaces a-Physicochemical and Engineering Aspects*, 2013. **420**: p. 46-52.
29. Ngo, Y.H., D. Li, G.P. Simon, and G. Garnier, *Paper surfaces functionalized by nanoparticles*. *Advances in Colloid and Interface Science*, 2011. **163**(1): p. 23-38.
30. Martinez, A.W., S.T. Phillips, B.J. Wiley, M. Gupta, and G.M. Whitesides, *FLASH: A rapid method for prototyping paper-based microfluidic devices*. *Lab on a Chip*, 2008. **8**(12): p. 2146-2150.
31. Li, X., J.F. Tian, G. Garnier, and W. Shen, *Fabrication of paper-based microfluidic sensors by printing*. *Colloids and Surfaces B-Biointerfaces*, 2010. **76**(2): p. 564-570.
32. Bennington, C.P.J., O.S. Sui, and J.D. Smith, *The effect of mechanical action on waste paper defibering and ink removal in repulping operations*. *Journal of Pulp and Paper Science*, 1998. **24**(11): p. 341-348.
33. Fischer, S.A., *Repulping wet-strength paper*. *Tappi Journal*, 1997. **80**(11): p. 141-147.
34. Bhardwaj, N.K. and V. Rajan, *Wet strength paper repulping: effect of process variables*. *Appita Journal*, 2004. **57**(4): p. 305-310.
35. Khan, M.S., D. Fon, X. Li, J.F. Tian, J. Forsythe, G. Garnier, and W. Shen, *Biosurface engineering through ink jet printing*. *Colloids and Surfaces B-Biointerfaces*, 2010. **75**(2): p. 441-447.
36. Neimo, L., *Papermaking Chemistry*. 4 ed. Papermaking Science and Technology Series, ed. L. Neimo. Vol. 4. 1999: Finnish Paper Engineers's Association and TAPPI.
37. Page, D.H., *A Theory for Tensile Strength of Paper*. *Tappi*, 1969. **52**(4): p. 674-&.
38. Gardner, D.J., G.S. Oporto, R. Mills, and M.A.S.A. Samir, *Adhesion and surface issues in cellulose and nanocellulose*. *Journal of Adhesion Science and Technology*, 2008. **22**(5-6): p. 545-567.
39. Hubbe, M.A. and J.A. Heitmann, *Review of Factors Affecting the Release of Water from Cellulosic Fibers during Paper Manufacture*. *Bioresources*, 2007. **2**(3): p. 500-533.
40. Khan, M.S. and G. Garnier, *Direct measurement of alkaline phosphatase kinetics on bioactive paper*. *Chemical Engineering Science*, 2013. **87**(0): p. 91-99.

41. Laine, C., X. Wang, M. Tenkanen, and A. Varhimo, *Changes in the fiber wall during refining of bleached pine kraft pulp*, in *Holzforschung* 2004. p. 233.
42. Borch, J., *Handbook of physical testing of paper*. 2nd ed 2002, New York: Marcel Dekker. v. <2 >.
43. Cecil, R.L. and T.E. Andreoli, *Cecil essentials of medicine*. 3rd ed 1993, Philadelphia: Saunders. xxviii, 921 p.
44. Cassie, A.B.D. and S. Baxter, *Wettability of porous surfaces*. Transactions of the Faraday Society, 1944. **40**: p. 0546-0550.
45. Su, S.X., R. Nutiu, C.D.M. Filipe, Y.F. Li, and R. Pelton, *Adsorption and covalent coupling of ATP-binding DNA aptamers onto cellulose*. *Langmuir*, 2007. **23**(3): p. 1300-1302.
46. Pelton, R., *Bioactive paper provides a low-cost platform for diagnostics*. *TrAC Trends in Analytical Chemistry*, 2009. **28**(8): p. 925-942.
47. Su, S.X., M. Ali, C.D.M. Filipe, Y.F. Li, and R. Pelton, *Microgel-based inks for paper-supported biosensing applications*. *Biomacromolecules*, 2008. **9**(3): p. 935-941.
48. Peng, P., L. Summers, A. Rodriguez, and G. Garnier, *Colloids engineering and filtration to enhance the sensitivity of paper-based biosensors*. *Colloids and Surfaces B-Biointerfaces*, 2011. **88**(1): p. 271-278.
49. Ngo, Y.H., D. Li, G.P. Simon, and G. Garnier, *Effect of cationic polyacrylamides on the aggregation and SERS performance of gold nanoparticles-treated paper*. *Journal of Colloid and Interface Science*, 2013. **392**: p. 237-246.
50. Tan, S.N., L.Y. Ge, H.Y. Tan, W.K. Loke, J.R. Gao, and W. Wang, *Paper-Based Enzyme Immobilization for Flow Injection Electrochemical Biosensor Integrated with Reagent-Loaded Cartridge toward Portable Modular Device*. *Analytical Chemistry*, 2012. **84**(22): p. 10071-10076.
51. Khan, M.S., X. Li, W. Shen, and G. Garnier, *Thermal stability of bioactive enzymatic papers*. *Colloids and Surfaces B-Biointerfaces*, 2010. **75**(1): p. 239-246.
52. Orelma, H., I. Filpponen, L.S. Johansson, J. Laine, and O.J. Rojas, *Modification of Cellulose Films by Adsorption of CMC and Chitosan for Controlled Attachment of Biomolecules*. *Biomacromolecules*, 2011. **12**(12): p. 4311-4318.
53. Daniels, G. and I. Bromilow, *Essential guide to blood groups*, 2010, Wiley-Blackwell.: Chichester, West Sussex, UK ; Hoboken, NJ. p. 1 online resource (x, 111 p.) col. ill.
54. Malomgre, W. and B. Neumeister, *Recent and future trends in blood group typing*. *Analytical and Bioanalytical Chemistry*, 2009. **393**(5): p. 1443-1451.
55. Li, L.Z., J.F. Tian, D. Ballerini, M.S. Li, and W. Shen, *A study of the transport and immobilisation mechanisms of human red blood cells in a paper-based blood typing device using confocal microscopy*. *Analyst*, 2013. **138**(17): p. 4933-4940.
56. Dobrynin, A.V. and M. Rubinstein, *Theory of polyelectrolytes in solutions and at surfaces*. *Progress in Polymer Science*, 2005. **30**(11): p. 1049-1118.
57. Fler, G.J., M.A. Cohen Stuart, J.M.H.M. Scheutjens, T. Cosgrove, and B. Vincent, *Polymers at interfaces*. 1st ed 1998, London ; New York: Chapman & Hall. 495p.
58. Wang, Y., W. Qi, R. Huang, R. Su, and Z. He, *Jet flow directed supramolecular self-assembly at aqueous liquid-liquid interface*. *RSC Advances*, 2014. **4**(30): p. 15340-15347.
59. Reye, J.T., K. Maxwell, S. Rao, J. Lu, and S. Banerjee, *Cationic polyacrylamides enhance rates of starch and cellulose saccharification*. *Biotechnology letters*, 2009. **31**(10): p. 1613-1616.
60. Varanasi, S. and W. Batchelor, *Superior non-woven sheet forming characteristics of low-density cationic polymer-cellulose nanofibre colloids*. *Cellulose*, 2014. **21**(5): p. 3541-3550.
61. Peng, P. and G. Garnier, *Effect of cationic polyacrylamide on precipitated calcium carbonate flocculation: Kinetics, charge density and ionic strength*. *Colloids and Surfaces A: Physicochemical and Engineering Aspects*, 2012. **408**(0): p. 32-39.

62. Peng, P. and G. Garnier, *Effect of Cationic Polyacrylamide Adsorption Kinetics and Ionic Strength on Precipitated Calcium Carbonate Flocculation*. Langmuir, 2010. **26**(22): p. 16949-16957.
63. Lindstrom, T. and C. Soremark, *Adsorption of Cationic Polyacrylamides on Cellulose*. Journal of Colloid and Interface Science, 1976. **55**(2): p. 305-312.
64. Wågberg, L., L. Winter, L. Ödberg, and T. Lindström, *On the charge stoichiometry upon adsorption of a cationic polyelectrolyte on cellulosic materials*. Colloids and Surfaces, 1987. **27**(1-3): p. 163-173.
65. Wågberg, L. and R. Hägglund, *Kinetics of Polyelectrolyte Adsorption on Cellulosic Fibers*. Langmuir, 2001. **17**(4): p. 1096-1103.
66. Davison, R.W., *Weak link in paper dry strength*. Tappi, 1972. **55**(4): p. 567-573.
67. Obokata, T., A. Isogai, and F. Onabe, *Studies on the mechanism of wet strength development*. Emerging Technologies of Pulping and Papermaking, 2002: p. 613-617.
68. Espy, H.H. and T.W. Rave, *The mechanism of wet-strength development by alkaline-curing amino polymer-epichlorohydrin Resins*. Tappi Journal, 1988. **71**(5): p. 133-137.
69. Espy, H.H. and G.W. Geist, *Persulfates as Repulping Reagents for Neutral Alkaline Wet-Strength Broke*. Tappi Journal, 1993. **76**(2): p. 139-142.
70. Nakagaito, A.N. and H. Yano, *The effect of morphological changes from pulp fiber towards nano-scale fibrillated cellulose on the mechanical properties of high-strength plant fiber based composites*. Applied Physics A, 2004. **78**(4): p. 547-552.
71. Iwamoto, S., A.N. Nakagaito, and H. Yano, *Nano-fibrillation of pulp fibers for the processing of transparent nanocomposites*. Applied Physics A, 2007. **89**(2): p. 461-466.
72. Saito, T., S. Kimura, Y. Nishiyama, and A. Isogai, *Cellulose Nanofibers Prepared by TEMPO-Mediated Oxidation of Native Cellulose*. Biomacromolecules, 2007. **8**(8): p. 2485-2491.
73. Saïd Azizi Samir, M.A., F. Alloin, M. Paillet, and A. Dufresne, *Tangling Effect in Fibrillated Cellulose Reinforced Nanocomposites*. Macromolecules, 2004. **37**(11): p. 4313-4316.
74. Janardhnan, S. and M.M. Sain, *Isolation of Cellulose Microfibrils - an Enzymatic Approach*. Bioresources, 2006. **1**(2): p. 176-188.
75. Henriksson, M., G. Henriksson, L.A. Berglund, and T. Lindstrom, *An environmentally friendly method for enzyme-assisted preparation of microfibrillated cellulose (MFC) nanofibers*. European Polymer Journal, 2007. **43**(8): p. 3434-3441.
76. Dufresne, A., D. Dupeyre, and M.R. Vignon, *Cellulose microfibrils from potato tuber cells: Processing and characterization of starch-cellulose microfibril composites*. Journal of Applied Polymer Science, 2000. **76**(14): p. 2080-2092.
77. Nakagaito, A.N., S. Iwamoto, and H. Yano, *Bacterial cellulose: the ultimate nano-scalar cellulose morphology for the production of high-strength composites*. Applied Physics A, 2005. **80**(1): p. 93-97.
78. Leitner, J., B. Hinterstoisser, M. Wastyn, J. Keckes, and W. Gindl, *Sugar beet cellulose nanofibril-reinforced composites*. Cellulose, 2007. **14**(5): p. 419-425.
79. Eriksen, O., K. Syverud, and O. Gregersen, *The use of microfibrillated cellulose produced from kraft pulp as strength enhancer in TMP paper*. Nordic Pulp & Paper Research Journal, 2008. **23**(3): p. 299-304.
80. Taipale, T., M. Osterberg, A. Nykanen, J. Ruokolainen, and J. Laine, *Effect of microfibrillated cellulose and fines on the drainage of kraft pulp suspension and paper strength*. Cellulose, 2010. **17**(5): p. 1005-1020.
81. Sehaqui, H., A.D. Liu, Q. Zhou, and L.A. Berglund, *Fast Preparation Procedure for Large, Flat Cellulose and Cellulose/Inorganic Nanopaper Structures*. Biomacromolecules, 2010. **11**(9): p. 2195-2198.
82. Siro, I. and D. Plackett, *Microfibrillated cellulose and new nanocomposite materials: a review*. Cellulose, 2010. **17**(3): p. 459-494.

83. Klemm, D., F. Kramer, S. Moritz, T. Lindstrom, M. Ankerfors, D. Gray, and A. Dorris, *Nanocelluloses: A New Family of Nature-Based Materials*. Angewandte Chemie-International Edition, 2011. **50**(24): p. 5438-5466.
84. Miura, S. and T. Kitaoka, *In situ synthesis of gold nanoparticles on zinc oxides preloaded into a cellulosic paper matrix for catalytic applications*. Bioresources, 2011. **6**(4): p. 11.
85. Varanasi, S., H.H. Chiam, and W. Batchelor, *Application and interpretation of zero and short-span testing on nanofibre sheet materials*. Nordic Pulp & Paper Research Journal, 2012. **28**(2): p. 343-351.
86. Taipale, T., M. Österberg, A. Nykänen, J. Ruokolainen, and J. Laine, *Effect of microfibrillated cellulose and fines on the drainage of kraft pulp suspension and paper strength*. Cellulose, 2010. **17**(5): p. 1005-1020.
87. Djafari Petroudy, S.R., K. Syverud, G. Chinga-Carrasco, A. Ghasemian, and H. Resalati, *Effects of bagasse microfibrillated cellulose and cationic polyacrylamide on key properties of bagasse paper*. Carbohydrate Polymers, 2014. **99**(0): p. 311-318.
88. Chakraborty, A., M. Sain, and M. Kortschot, *Cellulose microfibrils: A novel method of preparation using high shear refining and cryocrushing*. Holzforschung, 2005. **59**(1): p. 102-107.
89. Mao, J.L., J.F. Kadla, and R.J. Kerekes, *Retaining surface fibrillation of wet-beaten wood pulp in the dry state*. Tappi Journal, 2009. **8**(7): p. 25-30.
90. Cole, C.A., M.A. Hubbe, and J.A. Heitmann, *Water release from fractionated stock suspensions. Part 1 - Effects of the amounts and types of fiber fines*. Tappi Journal, 2008. **7**(7): p. 28-32.
91. Zhang, L.Y., W. Batchelor, S. Varanasi, T. Tsuzuki, and X.G. Wang, *Effect of cellulose nanofiber dimensions on sheet forming through filtration*. Cellulose, 2012. **19**(2): p. 561-574.
92. Arbatan, T., L. Zhang, X.-Y. Fang, and W. Shen, *Cellulose nanofibers as binder for fabrication of superhydrophobic paper*. Chemical Engineering Journal, 2012. **210**(0): p. 74-79.
93. Allen, S.G., O.M. Tanchak, A. Quirk, A.N. Raegen, K. Reiter, R. Whitney, A.J. Clarke, J. Lipkowski, and J.R. Dutcher, *Surface plasmon resonance imaging of the enzymatic degradation of cellulose microfibrils*. Analytical Methods, 2012. **4**(10): p. 3238-3245.
94. Kontturi, E., M. Suchy, P. Penttilä, B. Jean, K. Pirkkalainen, M. Torkkeli, and R. Serimaa, *Amorphous Characteristics of an Ultrathin Cellulose Film*. Biomacromolecules, 2011. **12**(3): p. 770-777.
95. Lefebvre, J. and D.G. Gray, *AFM of adsorbed polyelectrolytes on cellulose I surfaces spin-coated on silicon wafers*. Cellulose, 2005. **12**(2): p. 127-134.
96. Sczech, R. and H. Riegler, *Molecularly smooth cellulose surfaces for adhesion studies*. Journal of Colloid and Interface Science, 2006. **301**(2): p. 376-385.
97. Muller, M., C. Cihak, H. Schober, Y. Nishiyama, and G. Vogl, *All disordered regions of native cellulose show common low-frequency dynamics*. Macromolecules, 2000. **33**(5): p. 1834-1840.
98. Kontturi, E., T. Tammelin, and M. Osterberg, *Cellulose - model films and the fundamental approach*. Chemical Society Reviews, 2006. **35**(12): p. 1287-1304.
99. Li, L.Z., J.F. Tian, M.S. Li, and W. Shen, *Superhydrophobic surface supported bioassay - An application in blood typing*. Colloids and Surfaces B-Biointerfaces, 2013. **106**: p. 176-180.
100. Roberts, G.G., *Langmuir-Blodgett films* 1990, New York: Plenum Press. xiv, 425 p.
101. Kistler, S.F., P.M. Schweizer, and SpringerLink (Online service), *Liquid Film Coating Scientific principles and their technological implications*, 1997, Springer Netherlands,: Dordrecht. p. 1 online resource (796 pages).
102. Gao, S.S., J.Q. Wang, and Z.W. Jin, *Preparation of cellulose films from solution of bacterial cellulose in NMMO*. Carbohydrate Polymers, 2012. **87**(2): p. 1020-1025.
103. Schaub, M., G. Wenz, G. Wegner, A. Stein, and D. Klemm, *Ultrathin films of cellulose on silicon wafers*. Advanced Materials, 1993. **5**(12): p. 919-922.

104. Gunnars, S., L. Wågberg, and M.A. Cohen Stuart, *Model films of cellulose: I. Method development and initial results*. Cellulose, 2002. **9**(3-4): p. 239-249.
105. Falt, S., L. Wagberg, E.L. Vesterlind, and P.T. Larsson, *Model films of cellulose II - improved preparation method and characterization of the cellulose film*. Cellulose, 2004. **11**(2): p. 151-162.
106. Notley, S.M., M. Eriksson, L. Wagberg, S. Beck, and D.G. Gray, *Surface forces measurements of spin-coated cellulose thin films with different crystallinity*. Langmuir, 2006. **22**(7): p. 3154-3160.
107. Eriksson, M., S.M. Notley, and L. Wagberg, *Cellulose thin films: Degree of cellulose ordering and its influence on adhesion*. Biomacromolecules, 2007. **8**(3): p. 912-919.
108. Buchholz, V., G. Wegner, S. Stemme, and L. Odberg, *Regeneration, derivatization and utilization of cellulose in ultrathin films*. Advanced Materials, 1996. **8**(5): p. 399-&.
109. Shen, W., F. Xu, and I.H. Parker, *An experimental investigation of the redistribution behaviour of alkyl ketene dimers and their corresponding ketones*. Colloids and Surfaces A: Physicochemical and Engineering Aspects, 2003. **212**(2-3): p. 197-209.
110. Edgar, C.D. and D.G. Gray, *Smooth model cellulose I surfaces from nanocrystal suspensions*. Cellulose, 2003. **10**(4): p. 299-306.
111. Iguchi, M., S. Yamanaka, and A. Budhiono, *Bacterial cellulose—a masterpiece of nature's arts*. Journal of Materials Science, 2000. **35**(2): p. 261-270.
112. Tabuchi, M., K. Watanabe, Y. Morinaga, and F. Yoshinaga, *Acetylation of bacterial cellulose: Preparation of cellulose acetate having a high degree of polymerization*. Bioscience Biotechnology and Biochemistry, 1998. **62**(7): p. 1451-1454.
113. Barud, H.S., A.M. de Araujo, D.B. Santos, R.M.N. de Assuncao, C.S. Meireles, D.A. Cerqueira, G. Rodrigues, C.A. Ribeiro, Y. Messaddeq, and S.J.L. Ribeiro, *Thermal behavior of cellulose acetate produced from homogeneous acetylation of bacterial cellulose*. Thermochimica Acta, 2008. **471**(1-2): p. 61-69.
114. Hu, W.L., S.Y. Chen, Q.S. Xu, and H.P. Wang, *Solvent-free acetylation of bacterial cellulose under moderate conditions*. Carbohydrate Polymers, 2011. **83**(4): p. 1575-1581.
115. Rossetti, F.F., P. Panagiotou, F. Rehfeldt, E. Schneck, M. Dommach, S.S. Funari, A. Timmann, P. Muller-Buschbaum, and M. Tanaka, *Structures of regenerated cellulose films revealed by grazing incidence small-angle x-ray scattering*. Biointerphases, 2008. **3**(4): p. 117-127.
116. Daillant, J. and A. Gibaud, *X-ray and Neutron Reflectivity: Principles and Applications* 1999: Springer.
117. Zabel, H., *X-ray and neutron reflectivity analysis of thin films and superlattices*. Applied Physics A, 1994. **58**(3): p. 159-168.
118. Jacrot, B., *The study of biological structures by neutron scattering from solution*. Reports on Progress in Physics, 1976. **39**(10): p. 911.
119. Majkrzak, C.F., *Fundamentals of Specular Neutron Reflectometry*. MRS Online Proceedings Library, 1994. **376**: p. null-null.
120. Nevot, L. and P. Croce, *Characterization of Surfaces by Grazing X-Ray Reflection - Application to Study of Polishing of Some Silicate-Glasses*. Revue De Physique Appliquee, 1980. **15**(3): p. 761-779.
121. Cheng, G., Z.L. Liu, J.K. Murton, M. Jablin, M. Dubey, J. Majewski, C. Halbert, J. Browning, J. Ankner, B. Akgun, C. Wang, A.R. Esker, K.L. Sale, B.A. Simmons, and M.S. Kent, *Neutron Reflectometry and QCM-D Study of the Interaction of Cellulases with Films of Amorphous Cellulose*. Biomacromolecules, 2011. **12**(6): p. 2216-2224.
122. Rutland, M.W., A. Carambassis, G.A. Willing, and R.D. Neuman, *Surface force measurements between cellulose surfaces using scanning probe microscopy*. Colloids and Surfaces A: Physicochemical and Engineering Aspects, 1997. **123-124**(0): p. 369-374.

123. Zauscher, S. and D.J. Klingenberg, *Normal Forces between Cellulose Surfaces Measured with Colloidal Probe Microscopy*. Journal of Colloid and Interface Science, 2000. **229**(2): p. 497-510.
124. Zauscher, S. and D.J. Klingenberg, *Friction between cellulose surfaces measured with colloidal probe microscopy*. Colloids and Surfaces A: Physicochemical and Engineering Aspects, 2001. **178**(1–3): p. 213-229.
125. Rodahl, M., F. Hook, A. Krozer, P. Brzezinski, and B. Kasemo, *Quartz-Crystal Microbalance Setup for Frequency and Q-Factor Measurements in Gaseous and Liquid Environments*. Review of Scientific Instruments, 1995. **66**(7): p. 3924-3930.
126. Tammelin, T., T. Saarinen, M. Osterberg, and J. Laine, *Preparation of Langmuir/Blodgett-cellulose surfaces by using horizontal dipping procedure. Application for polyelectrolyte adsorption studies performed with QCM-D*. Cellulose, 2006. **13**(5): p. 519-535.
127. Holappa, S., K.S. Kontturi, A. Salminen, J. Seppala, and J. Laine, *Adsorption of Hydrophobically End-Capped Poly(ethylene glycol) on Cellulose*. Langmuir, 2013. **29**(45): p. 13750-13759.
128. Suchy, M., M.B. Linder, T. Tammelin, J.M. Campbell, T. Vuorinen, and E. Kontturi, *Quantitative Assessment of the Enzymatic Degradation of Amorphous Cellulose by Using a Quartz Crystal Microbalance with Dissipation Monitoring*. Langmuir, 2011. **27**(14): p. 8819-8828.
129. 3 - *Sensing based on localized surface plasmon resonance in metallic nanoparticles*, in *Nanoparticle Technology Handbook*, M.H.N.N. Yokoyama, Editor 2008, Elsevier: Amsterdam. p. 432-434.
130. Pattnaik, P., *Surface plasmon resonance - Applications in understanding receptor-ligand interaction*. Applied Biochemistry and Biotechnology, 2005. **126**(2): p. 79-92.

This page is intentionally blank

Chapter 2

Paper Strength Development and Recyclability with Polyamideamine-epichlorohydrin (PAE)

This page is intentionally blank

Declaration for Thesis Chapter 2

Declaration by candidate

In the case of Chapter 2, the nature and extent of my contribution to the work was the following:

Nature of contribution	Extent of contribution (%)
Initiation, key ideas, experimental and analysis works, development and writing up of paper	75

The following co-authors contributed to the work. If co-authors are students at Monash University, the extent of their contribution in percentage terms must be stated:

Name	Nature of contribution	Extent of contribution (%) for student co-authors only
Wade K. J. Mosse	Initiation, reviewing and editing of the paper	Research group member
Scot Sharman	Sharing the expertise on papermaking	Research group member
Warren Batchelor	Initiation, reviewing and editing of the paper	Co-supervisor
Gil Garnier *	Initiation, key ideas, reviewing and editing of the paper	Supervisor

The undersigned hereby certify that the above declaration correctly reflects the nature and extent of the candidate's and co-authors' contributions to this work*.

Candidate's Signature		Date 2015-3-6
Main Supervisor's Signature		Date

*Note: Where the responsible author is not the candidate's main supervisor, the main supervisor should consult with the responsible author to agree on the respective contributions of the authors.

This page is intentionally blank

Paper strength development and recyclability with polyamideamine-epichlorohydrin (PAE)

Jielong Su^a, Wade K. J. Mosse^a, Scot Sharman^a, Warren Batchelor^a, and Gil Garnier^{a*}

^a*BioPRIA, Australian Pulp and Paper Institute, Department of Chemical Engineering, Monash University, Wellington Road, Clayton, VIC 3800, Australia.*

*Corresponding author. [REDACTED]

Content

2.1	Abstract	77
2.2	Introduction	78
2.3	Experimental Section	80
2.3.1	Materials	80
2.3.2	Methods	80
2.3.2.1	Handsheets preparation	80
2.3.2.2	Formation test	80
2.3.2.3	Tensile strength test	80
2.3.2.4	Evaluation of recyclability of strengthened sheets	81
2.4	Results and Discussion	81
2.4.1	Effect of PAE Concentration on Paper Strength	81
2.4.2	Recyclability of PAE Strengthened Paper	83
2.4.3	Effect of Electrolyte on Paper Strength	85
2.5	Conclusions	89
2.6	Acknowledgement	89
2.7	References	90

2.1 Abstract

The tensile strength behavior and recyclability of the paper prepared with the addition of polyamideamine-epichlorohydrin (PAE) were investigated. The dry and wet tensile strengths obtained with different PAE dosage were measured. The highest wet-to-dry strength ratio of 35% was obtained at 10 mg/g; above this addition level wet strength dropped slightly and then remained constant. The repulpability of strengthened paper was

correlated directly with wet strength. The effect of electrolyte on tensile strength was also quantified by varying sodium chloride and calcium chloride concentration in the furnish stock. Without PAE, high salt concentrations (100 mM) reduced the tensile strength by 15-20%. At constant PAE addition level of 10 mg/g, low levels of salt addition (of either 10 mM NaCl or 10 mM CaCl₂) slightly improved the strength; paper strength decreased at high salts concentrations. The cation valency and concentration in the process water were important variables which affected the efficiency of PAE. These results present the significance of developing sustainable wet strength agents that can be applied in demanding salty conditions while maintaining the product recyclability.

Keywords: Strength; Repulpability; Polyamideamine-epichlorohydrin (PAE); Recyclability; Paper; Wet-strength.

2.2 Introduction

Strength distribution across paper is ensured by the multiple fibre-fibre bonds and controlled by the bonding area, the adhesion strength, and the fibre strength and size distribution. The Page equation describes the tensile failure of paper in terms of some of these critical variables [1]. The strength of dry and wet paper is crucial to many applications, especially in packaging and tissue products. It has long been established that the tensile strength of paper is directly affected by the swelling behavior of the fibres interacting with water [2]. The strength is controlled by fibre-to-fibre interactions that are developed during the process of paper formation, consolidation, and drying. In dry paper, hydrogen bonding is the dominant adhesive force and only acts over very short distances. As the bonds are water sensitive, the penetration of water into the dry paper matrix leads to a rapid weakening of fibre-to-fibre bonding and a concurrent loss in paper strength [3]. To lessen the reduction of paper strength upon contact with water, reactive water-soluble polymers such as polyamide-amine-epichlorohydrin (PAE) are commonly used to improve the bonding between fibres, which constitutes the weak link in wet paper [4].

The generally accepted mechanism of wet-strength development by PAE in paper is through the establishment of chemical bonds at fibre-fibre contacts. The process involves two steps: retention of the polymer and development of bonds. The main variables affecting PAE efficiency include its azetidinium concentration, the type of fibres, and the

drying conditions [5, 6]. Carboxyl groups, which significantly affect both PAE retention and reactivity, can be introduced to fibres by kraft pulping and through the bleaching process. When adding PAE to a slurry of cellulosic fibres, adsorption is driven by the electrostatic attraction between the anionic carboxylated groups on the fibre surface and the cationic azetidinium groups of the polymer [7, 8]. After PAE adhesion to cellulosic fibres, the curing process facilitates the formation of bonds between fibres. These bonds are covalent between the carboxyl groups of cellulose or hemicelluloses and the polymer's azetidinium group, resulting in inter-fibre bonds that are not water-soluble [9, 10]. Therefore, special techniques such as a combination of mechanical energy and oxidizing agents are required for successful repulping [11, 12].

While the fundamentals of PAE resin strength development mechanism are relatively well understood, the effects of PAE addition on recycling are more obscure. This is especially the case for optimizing water and fibre recycling for sustainability. The direct implications are the necessity to form paper with a furnish having very high salt concentration and the ability to fully and easily repulp PAE-made fibre products to insure full recycling. Indeed, many packaging grades are exclusively made of recycled fibres. In these circumstances, the addition of PAE is expected to fulfill two contradictory requirements. On one hand PAE is requested to provide permanent and strong fibre-fibre bonds; on the other hand, the resulting strengthened paper must remain fully recyclable. Very little quantitative information is available in this realm. It is the objective of this study to quantify the behavior of PAE from the modern perspective of sustainable papermaking.

The first part of this study quantifies the effect of PAE on paper strength development and repulpability. A new methodology was developed to quantify recycling. The second part investigated the effect of salt valency and concentration on paper strength with and without PAE. This study aims at quantifying the potential and limitations of reinforced strength agents in the context of sustainable papermaking.

2.3 Experimental Section

2.3.1 Materials

The commercial PAE (WSR 557 HP) was provided by Nuplex Industries (Australia) Pty Ltd (12.5% w/w solid content solution); PAE solutions were diluted with deionised water prior to each experiment. Analytical grade sodium chloride (NaCl) and calcium chloride (CaCl₂) were purchased from Sigma-Aldrich (Australia). Bleached eucalyptus kraft pulp was obtained from the dry lap sheet (NIST Standard reference material 8946).

2.3.2 Methods

2.3.2.1 Handsheets preparation

Cellulose handsheets were prepared according to the Australian/New Zealand Standard Method 203s. Basically, the dry pulp was thoroughly wetted by soaking in deionized water for about 12 hours. The pulp was transferred to a disintegrator (Model MKIIC, Messmer Instruments Ltd), diluted to 2 L with deionized water, and disinter-grated for 75,000 propeller revolutions. Prior to handsheet forming, the PAE solution was added to the pulp slurry in either salt-free or salt-containing conditions and stirred for 5 min. The pH of the pulp slurry mixture was non-adjusted, and the value was about 5. The addition quantity of PAE was based on oven dry grammage of 60 g/m². After manual couching and wet-pressing at 0.4 MPa for about 15 seconds, the sheets were cured in a drum-dryer at 100 °C for 10 min, in order to activate the bonds between the PAE and the cellulose surface.

2.3.2.2 Formation test

The handsheet uniformity was measured with the Paper Perfect Formation Tester (Op Test Equipment Inc, Canada). The tester classifies formation quality in 10 formation components over a specific range and produces the formation value. The relative formation value (RFV) of each component relates to selected reference sheet (without PAE). RFV values less than 1 means that the formation quality of the tested paper is worse than the formation quality of the reference paper.

2.3.2.3 Tensile strength test

The sheets were equilibrated at 23°C and 50% relative humidity for at least 24 hours before wet and dry tensile testing based on the Australian/New Zealand Standard

Methods 448s and 437s. The test strip was slightly bent and the middle part touched to the surface of the deionised water for 2 seconds. The wetted length is about 25 mm. The width of sample strips was 15 mm and test span was 100 mm. An Instron tensile tester (Instron 5566) was used to record maximum tensile force with constant rate of elongation at 10 mm/min. The tensile index for each sample was calculated as tensile strength (expressed in newtons per metre) divided by basis weight (grams per square meter). The mean value was obtained from seven valid tests and the error bars in figures indicated the 95% confidence interval. T-Test was used to determine statistical significance of data.

2.3.2.4 Evaluation of recyclability of strengthened sheets

The laboratory disintegrator (Model MKIIIC, *Messmer* Instruments Ltd) was used for evaluating the recyclability of the sheets. A 1.2 g handsheet was torn into small pieces of about 1 cm², added to 2 L deionised water, and disintegrated immediately for 3000 revolutions at room temperature (operation time of 1 minute). After repulping, the slurry from the disintegrated handsheet was screened in a fibre classifier (Brecht & Holl type, model BH-6/12) for 20 min through a 0.2 mm slot screen at a water flow rate of 2.5 L/minute. The rejects (fraction that did not pass the screen) were collected, dried at 105 °C for 4 hours and weighed. Repulping and classification were performed at ambient temperature in triplicate and the average was reported.

The repulpability index (R.I.) was defined as:

$$R.I. = \frac{\text{mass of dry sheet} - \text{mass of dry rejects}}{\text{mass of dry sheet}} \times 100 \quad (1)$$

The index represents the percentage of fibres satisfactorily repulped and recovered. A higher value of R.I. indicates easier recycling process of the sheet.

2.4 Results and Discussion

2.4.1 Effect of PAE Concentration on Paper Strength

Paper without PAE retained less than 10% of its original strength (dry) when wetted. Figure 1 shows that wet over dry strength ratio increased significantly to 28% at a PAE concentration of 5 mg/g (mg PAE per g oven dry cellulose fibre), to reach a maximum ratio of 33% at 10 mg/g. The ratio leveled off thereafter, at least to a PAE concentration up to 50 mg/g.

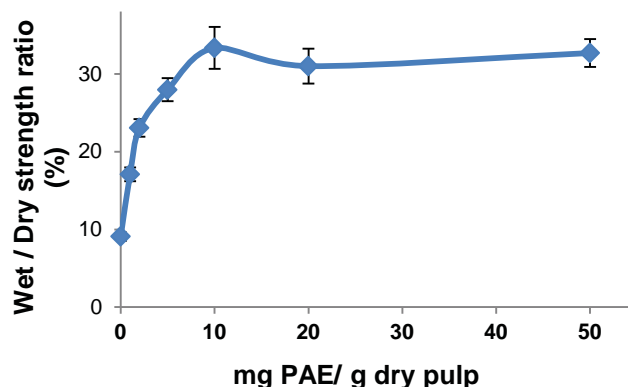


Figure 1: Effect of PAE dosage on the wet and dry strength ratio

The paper wet and dry tensile index both changed non-linearly with the addition of PAE (Fig. 2). At low PAE dosages, the fibre's surface was unsaturated and all polymer adsorbed onto the fibres. Paper strength increased with polymer addition in this regime. The wet tensile index (W.T.I.) increased with PAE addition up to 10 mg/g, to reach a maximum of 4.6 ± 0.1 Nm/g; this was about four times the strength of the reference sheet. The W.T.I. reduced to 4.2 ± 0.1 Nm/g at a PAE dosage of 20 mg/g and leveled off until 50 mg/g. The wet strength improvement is attributed to co-crosslinking with ester bonds forming between pulp carboxyl groups and PAE azetidinium groups. The decrease in paper strength at high PAE concentration could be attributed to homo-crosslinking of PAE, which was very sensitive to water and is weaker than the co-crosslinking involving PAE and fibres [7, 13].

In contrast to wet strength, the maximum dry tensile index of 14.7 ± 0.5 Nm/g was achieved at 2 mg/g; at higher dosages there was a gradual decline in dry tensile index. Paper formation worsened upon PAE addition, especially at larger inspection sizes (Fig. 3). This was probably related to the high cationic charge and the medium molecular weight of PAE, promoting strong fibre flocculation. Therefore PAE has two antagonistic effects on paper strength. The first is a beneficial increase in fibre-fibre bond strength promoted by covalent bonds; the second is a detrimental effect of impaired formation caused by increased fibre flocculation. At low doses of PAE, the covalent bonding

properties of the additive were dominant, and paper strength improved. As polymer addition increased further, fibre flocculation induced by PAE becomes significant and counteracted the strength improvement.

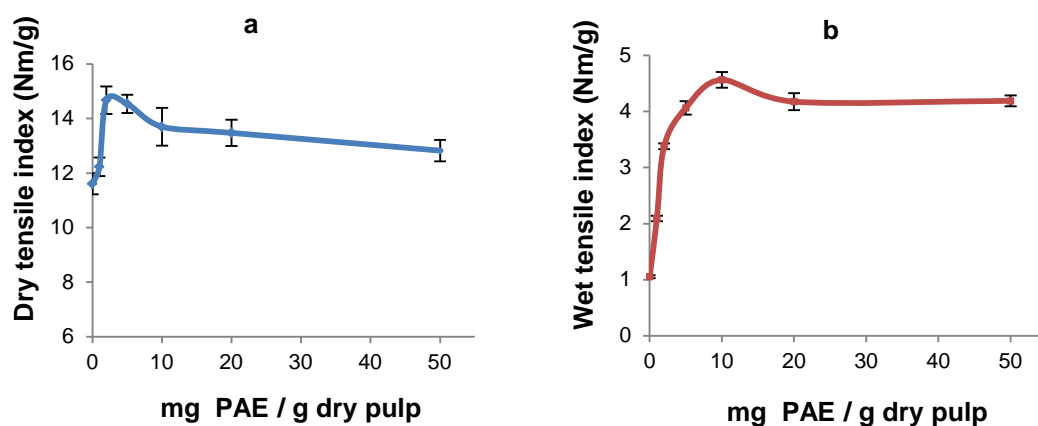


Figure 2: Effect of PAE concentration on the dry tensile index (a) and wet tensile index (b) of papersheets

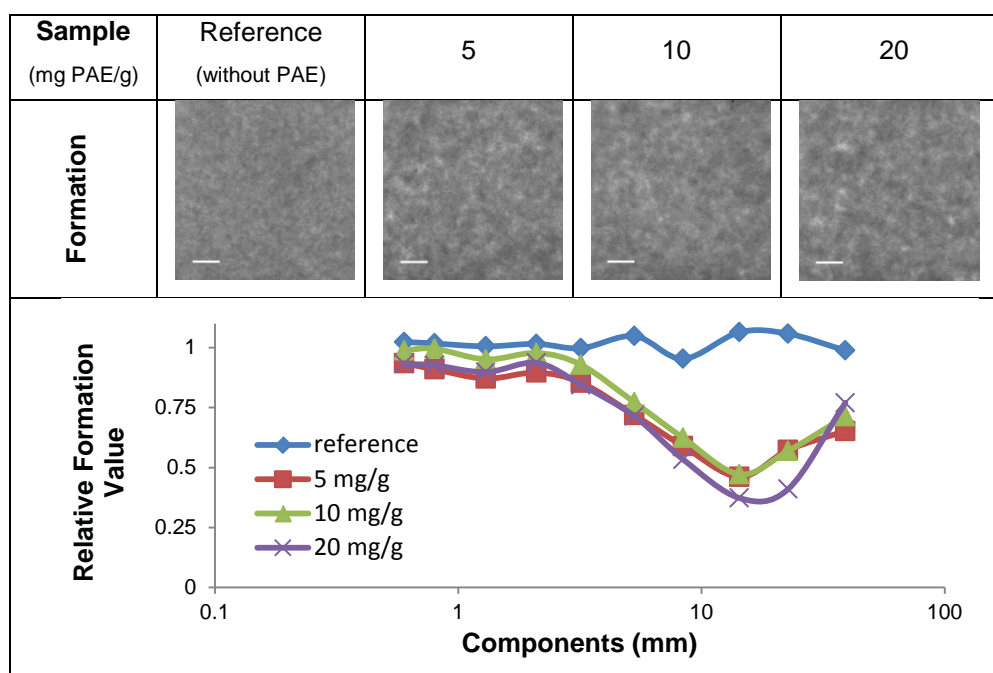


Figure 3: Formation of paper sheets with different PAE dosage (scale bar equals 1 centimeter).

2.4.2 Recyclability of PAE Strengthened Paper

As there is no widely accepted standard test method to evaluate the recyclability of paper; each organization is left to define its own method. Repulping is the process in which

paper is recycled into fibres capable of being used again in papermaking. This is achieved by subjecting a paper slurry to mechanical forces; chemical and bleaching aids are sometimes also used. In this study, a method initially developed by a paper company was modified to rate the sheet recyclability under constant operating parameters.

The effect of PAE concentration on repulpability is shown in Fig. 4. The paper's repulpability decreased in a non-linear fashion with increasing PAE concentration. A repulpability index (R.I.) of 100% for the control sheet indicated that the original sheet was totally recyclable under the experimental conditions. When the control paper sheet was wetted in recycling conditions, the hydrogen bonds between fibres were rapidly disrupted by the competing water molecules, leading to much weaker inter-fibre bonding. Under these circumstances, the paper sheet was very easy to break down into individual fibres upon a short exposure to mechanical shear force.

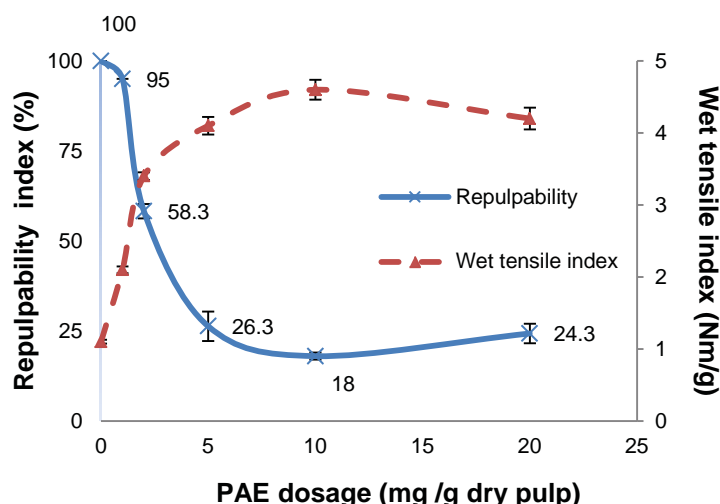


Figure 4: Effect on PAE concentration on repulpability index (solid line) and wet tensile index (dashed line)

Adding PAE increased inter-fibre bonding, thus inhibiting network breakdown and adversely affecting the recycling. The addition of 1 mg PAE /g fibre doubled the wet tensile index to 2.1 Nm/g, and the R.I. decreased to 95%, meaning that a small amount of rejects were left on the screen at end of processing. As the polymer dosage was increased to 2 mg PAE/g fibre, W.T.I. rose to 3.4 Nm/g and the R.I. value dropped sharply to 58%. By further increasing PAE dosage, the R.I. continued to decrease. The sheet was most difficult to repulp at a PAE dosage of 10 mg/g, the PAE concentration at which the

greatest wet tensile index was observed. It was notable that paper sheets exhibited similar repulpability at PAE dosages of 5 mg/g and 20 mg/g, where the W.T.I. was very similar. There was obviously a strong correlation between the paper wet-strength and its repulpability; this relationship was plotted in Fig. 5 in terms of W.T.I and R.I. The relationship was seen to be linear for the samples tested. The initial paper sample with no PAE was excluded from the line, as there are no covalent bonds formed. No paper repulpability was extrapolated to occur at wet strength higher than 5 Nm/g, using the current method. The slope of the line was expected to vary as a function of the ratio of bond strength/mechanical shear; the wet-strength polymer chemical composition, the repulping configuration, and the power would be important variables. Bennington et al. [14] applied a more mechanical analysis to the repulpability process. The proposed model described the repulping process at a pulp mass concentration no less than 1%, and concluded that the rate of defibrization depends on the amount of contact between the rotor and the suspension, the force imparted by the rotor, and the paper strength. In comparison with Bennington's work, the relationship curve from this study was achieved at a much lower fibre concentration (about 0.06%) and constant recycling time.

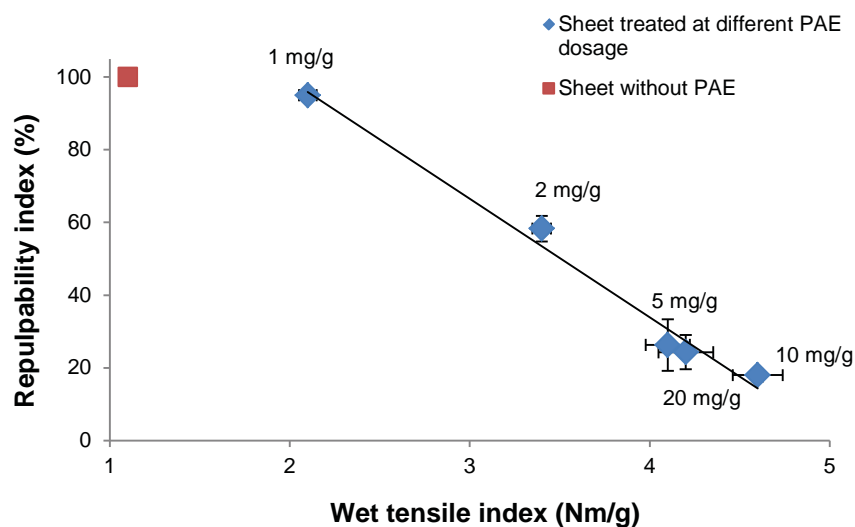


Figure 5: Plot of repulpability index versus wet tensile index obtained from sheets strengthened by PAE and a reference without PAE. Data in Fig. 4 were used to calculate the treadline.

2.4.3 Effect of Electrolyte on Paper Strength

From the standpoint of paper physics, the formation and consolidation of paper structure may be altered by the presence of salt [15]. Figure 6 presents the weakening of both dry

and wet paper without PAE, which was observed when formed with high salt concentration (100mM of NaCl or CaCl₂) in pulp slurry. Dry tensile index declined from 10.7 Nm/g to 8.9 Nm/g with NaCl addition and to 9.1 Nm/g with CaCl₂ addition (Fig 6a). This can be attributed to three factors: reduced inter-fibre strength, reduced pore radius, and increased moisture content. The joint strength that holds fibres together is dependent on ionic strength. A decreased joint strength is expected as salt is added [16]. Also the average pore radii of fibre was reported to decrease at high concentration (100 mM NaCl), and it was suggested that the smaller pores result in a lower molecular contact area between the fibres, reducing the joint strength [17, 18]. Salts are known to affect paper hygroscopy. In this study, the moisture content of paper sheets upon equilibrium in a 50% RH environment was 5.5%, 6.3%, and 6.7% respectively for salt-free, NaCl, and CaCl₂ (100mM).

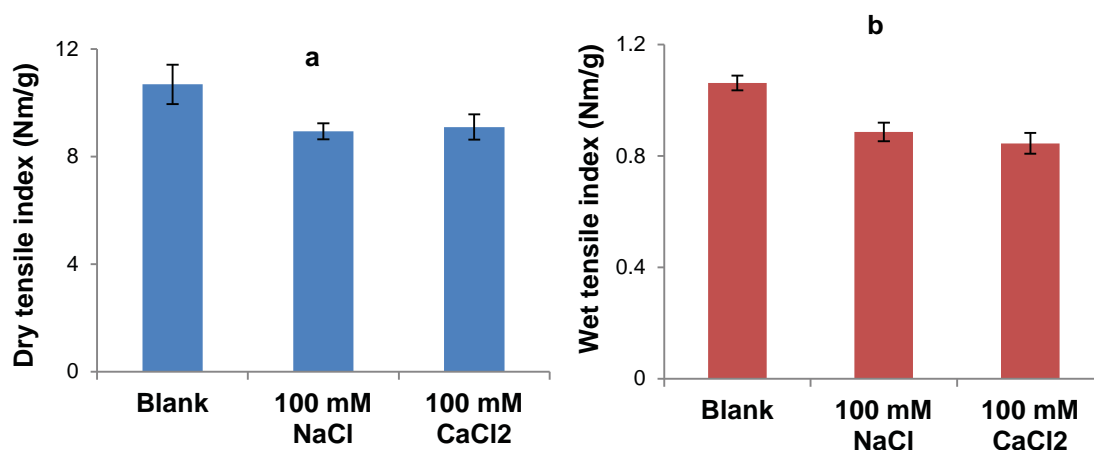


Figure 6: Effect of salt concentration in stock on paper strength (without PAE addition). a) Dry strength, b) Wet strength.

The wet tensile index of paper without PAE was reduced by 17% and 20% with NaCl and CaCl₂ respectively (Fig. 6b). The cellulose fibre surface can be regarded as a hydrogel when saturated in water. The decrease of salt-induced fibre swelling can be caused by an osmotic pressure differential resulting from a difference in concentration of mobile ions between the interior of the gel and the exterior solution [19, 20]. A previous study presented evidence that fibre entanglements and friction are two important mechanisms controlling for the strength of wet paper [21]. For this reason, the lower degree of swelling of fibres in saline environment may create a smaller friction area (Fig. 7), resulting in a paper web of lower wet strength.

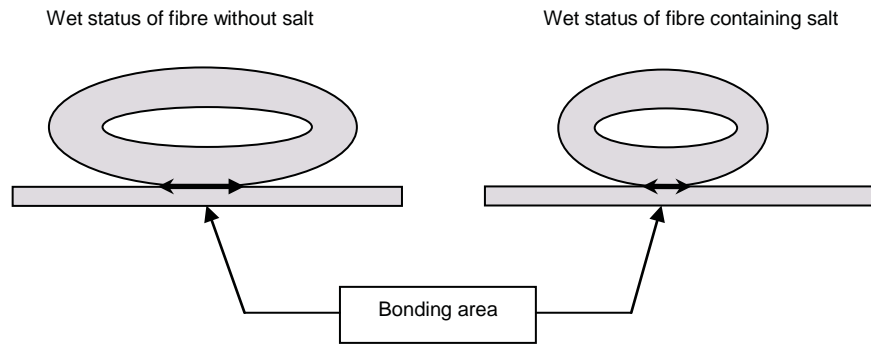


Figure 7: Schematic illustration of salt effect on fibres dimension/swelling and bonding area. The geometry is not drawn to scale.

Salt also influences the strength of PAE-strengthened sheets. Figures 8 and 9 show the effect of the NaCl and CaCl_2 concentration, respectively, on wet and dry paper strength using a PAE dosage of 10 mg/g. The paper wet strength slightly increased at the low concentration of 10 mM, both for NaCl and CaCl_2 . Polyelectrolyte adsorption onto surfaces was previously investigated both in model surface and cellulosic fibre [22-24], and a maximum in the saturation adsorption of cationic polymer was found at a low NaCl concentration of 10 mM. The increase of strength may be linked to a larger amount of PAE adsorbed on fibres in the presence of salt. A small amount of salt may shield the repulsion between the positively charged groups on the PAE chain and allow the macromolecule to coil up into a tighter, less extended conformation which, in turn, enables the PAE chain attach to the fibres more densely and increase the probability of the azetidinium groups forming covalent bonds with fibres. This mechanism is schematically illustrated in Fig. 10.

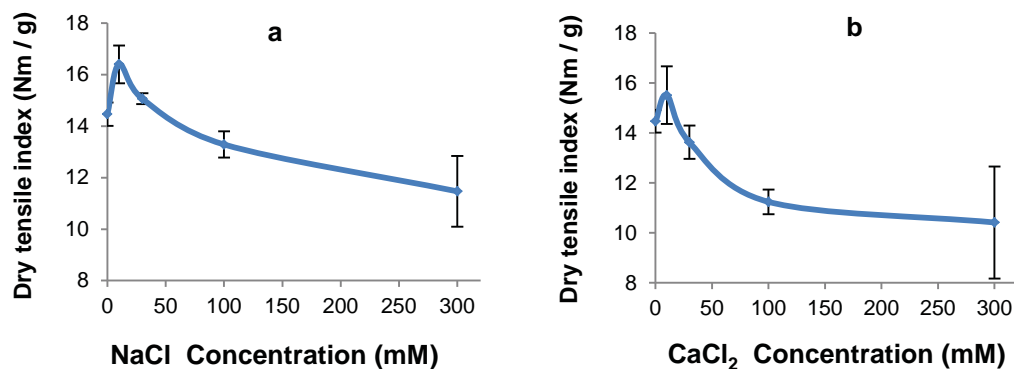


Figure 8: Dry tensile index as a function of (a) NaCl and (b) CaCl_2 concentration at constant addition level of 10 mg PAE /g dry pulp

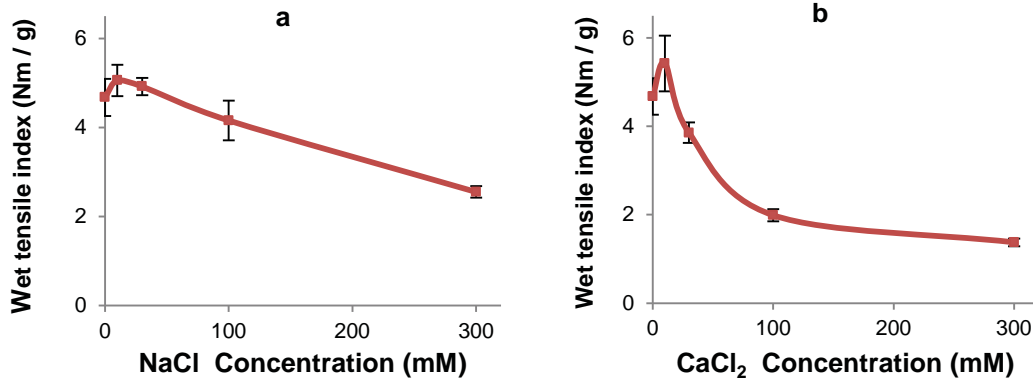


Figure 9: Wet tensile index as a function of (a) NaCl and (b) CaCl₂ concentration at a constant addition level of 10 mg PAE /g dry pulp.

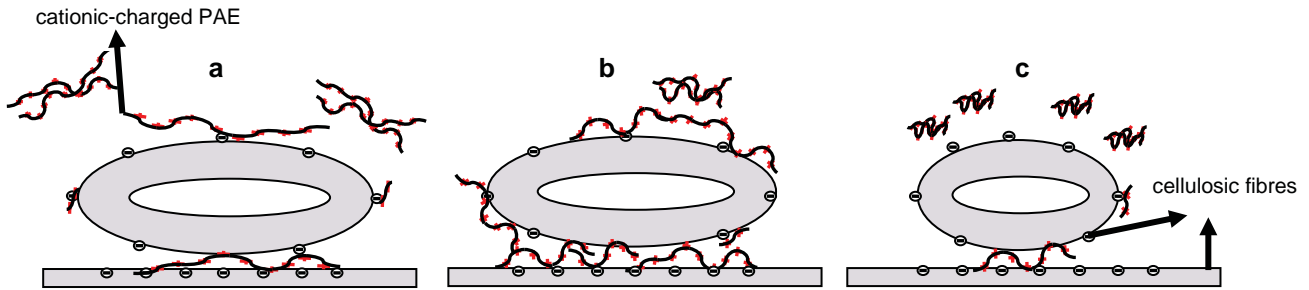


Figure 10: Schematic representation of possible mechanism for cationic-charged PAE being adsorbed to cellulosic fibres in different salt concentrations (a) without salt, (b) Low salt concentration, (c) High salt concentration. The figure is not drawn to scale.

Although the paper's tensile index increased at low salt concentration, for concentrations of 30 mM and above, the strength of the paper sheet declined as increasing salt addition screened the electrostatic interaction required for high polymer adsorption [25]. From the perspective of polymer retention, the adsorbed amount of PAE decreases when salts are added [26]. Considering ion exchange between inorganic cations (Na^+ , Ca^{2+}) and polycations from the dissociation of PAE in solution, the high ionic strength significantly affects the PAE adsorption behavior because the increase in the number of small cationic counterions would interfere with the process [27]. Ca^{2+} ions decreased PAE efficiency more than Na^+ did. Ca^{2+} can not only better compete for the fibres carboxyl sites but also decrease the anionicity of fibres, therefore inhibiting PAE retention.

2.5 Conclusions

1. The ability of polyamideamine-epichlorohydrin (PAE) to improve paper tensile strength was investigated by preparing handsheets with bleached eucalyptus kraft pulp. The maximum enhancement of dry and wet strength properties was achieved at different PAE addition levels; the highest wet to dry strength ratio was obtained at 10 mg/g. Above this addition level, the wet strength falls slightly and then remains constant. Fibre flocculation and poor formation of the paper sheets induced by the cationic polymer were observed during the sheet forming process, which explains why higher PAE doses did not improve tensile strength. The repulpability of PAE- strengthened paper revealed a direct link between wet strength and recyclability. The stronger the paper was in a wet state, the harder it became to repulp, being quantified at the same disintegrator energy.
2. The tensile properties of paper formed in various salt-containing environments with and without PAE were examined. In the absence of PAE, both dry and wet paper strength was decreased at high salt concentration. The strength of sheets reinforced by PAE was also affected by the salt concentration in papermaking stock. At PAE dosage of 10 mg/g, low salt (NaCl and CaCl₂) concentration at 10 mM enhanced the strength of paper while higher salt addition weakened the paper; this can be explained in terms of ionic strength affecting the polymer's conformation and their adsorption density onto fibres. Ion type and concentration in the papermaking process water influenced the strength development in different manners. Experimental results in this study show the need for new wet strength agents that can be applied in demanding salty conditions while maintaining the product recyclability.

2.6 Acknowledgement

The financial contribution of Australian Research Council (LP0990526), Visy and Nopco paper technology is acknowledged.

2.7 References

1. Page, D.H., *A Theory for Tensile Strength of Paper*. Tappi, 1969. **52**(4): p. 674-&.
2. Rowland Stanley, P., *Cellulose: pores, internal surfaces, and the water Interface*, in *Textile and Paper Chemistry and Technology* 1977, American Chemical Society. p. 20-45.
3. Gardner, D.J., G.S. Oporto, R. Mills, and M.A.S.A. Samir, *Adhesion and surface issues in cellulose and nanocellulose*. Journal of Adhesion Science and Technology, 2008. **22**(5-6): p. 545-567.
4. Davison, R.W., *Weak link in paper dry strength*. Tappi, 1972. **55**(4): p. 567-573.
5. Obokata, T., A. Isogai, and F. Onabe, *Studies on the mechanism of wet strength development*. Emerging Technologies of Pulping and Papermaking, 2002: p. 613-617.
6. Saito, T. and A. Isogai, *A novel method to improve wet strength of paper*. Tappi Journal, 2005. **4**(3): p. 3-8.
7. Espy, H.H. and T.W. Rave, *The mechanism of wet-strength development by alkaline-curing amino polymer-epichlorohydrin Resins*. Tappi Journal, 1988. **71**(5): p. 133-137.
8. Obokata, T. and A. Isogai, *The mechanism of wet-strength development of cellulose sheets prepared with polyamideamine-epichlorohydrin (PAE) resin*. Colloids and Surfaces a-Physicochemical and Engineering Aspects, 2007. **302**(1-3): p. 525-531.
9. Devore, D.I. and S.A. Fischer, *Wet-strength mechanism of polyaminoamide-epichlorohydrin resins*. Tappi Journal, 1993. **76**(8): p. 121-128.
10. Espy, H.H., *The Mechanism of Wet-Strength Development in Paper - a Review*. Tappi Journal, 1995. **78**(4): p. 90-99.
11. Espy, H.H. and G.W. Geist, *Persulfates as Repulping Reagents for Neutral Alkaline Wet-Strength Broke*. Tappi Journal, 1993. **76**(2): p. 139-142.
12. Chan, L.L., *Wet-strength resins and their application* 1994, Atlanta, Ga.: TAPPI Press. xii, 120 p.
13. Bates, N.A., *Polyamide-epichlorohydrin wet-strength resin .2. A study of mechanism of wet-strength development in paper*. Tappi, 1969. **52**(6): p. 1162-1169.
14. Bennington, C.P.J., O.S. Sui, and J.D. Smith, *The effect of mechanical action on waste paper defibering and ink removal in repulping operations*. Journal of Pulp and Paper Science, 1998. **24**(11): p. 341-348.
15. Scallan, A.M.a.G., J., *The effect of cations on pulp and paper properties*. Svensk Papperstidning, 1979. **82**: p. 40-47.
16. Torgnysdotter, A. and L. Wagberg, *Influence of electrostatic interactions on fibre/fibre joint and paper strength*. Nordic Pulp and Paper Research Journal, 2004. **19**(4): p. 440-447.
17. Andreasson, B., J. Forsstrom, and L. Wagberg, *Determination of fibre pore structure: influence of salt, pH and conventional wet strength resins*. Cellulose, 2005. **12**(3): p. 253-265.
18. Forsstrom, J., B. Andreasson, and L. Wagberg, *Influence of pore structure and water retaining ability of fibres on the strength of papers from unbleached kraft fibres*. Nordic Pulp and Paper Research Journal, 2005. **20**(2): p. 176-185.
19. Grignon, J. and A.M. Scallan, *Effect of pH and neutral salts upon the swelling of cellulose gels*. Journal of Applied Polymer Science, 1980. **25**(12): p. 2829-2843.
20. Lindström, T., *Chemical factors affecting the behaviour of fibres during papermaking*. Nordic Pulp and Paper Research Journal 1992. **7**(4): p. 181-192.
21. Tejado, A. and T.G.M. van de Ven, *Why does paper get stronger as it dries?* Materials Today, 2010. **13**(9): p. 42-49.
22. Bates, N.A., *Polyamide-epichlorohydrin wet-strength resin .I. retention by pulp*. Tappi, 1969. **52**(6): p. 1157-1161.

23. Enarsson, L.E. and L. Wagberg, *Adsorption kinetics of cationic polyelectrolytes studied with stagnation point adsorption reflectometry and quartz crystal microgravimetry*. Langmuir, 2008. **24**(14): p. 7329-7337.
24. Solberg, D. and L. Wagberg, *Adsorption and flocculation behavior of cationic polyacrylamide and colloidal silica*. Colloids and Surfaces a-Physicochemical and Engineering Aspects, 2003. **219**(1-3): p. 161-172.
25. Enarsson, L.E. and L. Wagberg, *Polyelectrolyte adsorption on thin cellulose films studied with reflectometry and quartz crystal microgravimetry with dissipation*. Biomacromolecules, 2009. **10**(1): p. 134-141.
26. Strazdins, E., *Surface chemical aspects of polymer retention*. Tappi, 1974. **57**(12): p. 76-80.
27. Ampulski, R.S. and C.W. Neal, *The effect of inorganic ions on the adsorption and ion exchange of Kymene 557H by bleached northern softwood kraft pulp* Nordic Pulp and Paper Research Journal, 1989. **04**(2): p. 155-163.

This page is intentionally blank

Chapter 3

Paper Engineered with Cellulosic Additives: Effect of Length Scale

This page is intentionally blank

Declaration for Thesis Chapter 3

Declaration by candidate

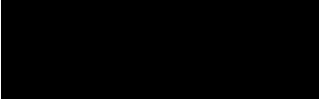
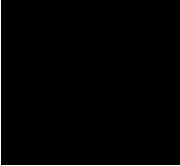
In the case of Chapter 3, the nature and extent of my contribution to the work was the following:

Nature of contribution	Extent of contribution (%)
Initiation, key ideas, experimental and analysis works, development and writing up of paper	80

The following co-authors contributed to the work. If co-authors are students at Monash University, the extent of their contribution in percentage terms must be stated:

Name	Nature of contribution	Extent of contribution (%) for student co-authors only
Liyuan Zhang	Preparation of microfibrillated cellulose from ball milling, reviewing and editing of the paper	External collaboration
Warren Batchelor	Initiation, key ideas, reviewing and editing of the paper	Co-supervisor
Gil Garnier *	Initiation, key ideas, reviewing and editing of the paper	Supervisor

The undersigned hereby certify that the above declaration correctly reflects the nature and extent of the candidate's and co-authors' contributions to this work*.

Candidate's Signature		Date 20/5-3-6
Main Supervisor's Signature		Date

*Note: Where the responsible author is not the candidate's main supervisor, the main supervisor should consult with the responsible author to agree on the respective contributions of the authors.

This page is intentionally blank

Paper engineered with cellulosic additives: effect of length scale

Jielong Su, Liyuan Zhang, Warren Batchelor and Gil Garnier*

Bioprocessing Research Institute of Australia (BioPRIA) Department of Chemical Engineering, Monash University, Clayton, Australia.

*Corresponding author. Email: [REDACTED]

Content

3.1	Abstract	97
3.2	Introduction	98
3.3	Experimental Section	99
3.3.1	Materials	99
3.3.2	Methods	101
3.3.2.1	Handsheets preparation	101
3.3.2.2	Cellulosic fiber and paper properties	101
3.4	Results	103
3.5	Discussion	108
3.5.1	Effect of cellulosic additives on the paper processing	108
3.5.2	Structure and air permeability of paper	110
3.5.3	Strength of paper	111
3.6	Conclusion	113
3.7	Acknowledgement	114
3.8	References	114

3.1 Abstract

High strength and low air permeability cellulosic fiber composites were produced using the paper-making technology with two types of microfibrillated cellulose (MFC), either achieved by homogenization or by ball milling. Their strengthening effect by blending with hardwood fibers was compared to cellulose microparticles (CMPs) made from cryogenic milling, with and without polyamideamine-epichlorohydrin (PAE) addition. MFC from homogenization, due to a broad size distribution, can fully retain on the fibers web; in contrast, the retention ratio for MFC produced from ball milling was lower than

50% because of their smaller size and short aspect ratio, and the resulting paper displayed a compact and dense structure. The significant distinction between the two MFC papers was the elongation at break under wet condition, suggesting two different reinforcement mechanisms. CMPs act as mechanical debonder and could find application in tissue making to increase paper bulk and decrease the density, thus improving tissue softness.

Keywords: MFC, polymer, paper, composite, permeability, strength.

3.2 Introduction

Papers of engineered structure and surface properties are drawing strong interest as a substrate for traditional applications, such as packaging and tissue, and also for novel uses including clear films and bio-diagnostics. Microfibrillated cellulose (MFC) of nano-scale diameter and micro-scale length shows high potential for paper engineering. Their advantages include: abundant natural resources for preparation, the controlled dimensions, being biocompatible and biodegradable. Novel MFC products including composites and films have been prepared [1-3]. The preparation efficiency and properties of the products were directly determined by the dimension of the MFC. However, little is known on the effect of the dimension for nano and micro cellulose used as an additive on the properties and structure of paper composites.

Many approaches have been explored to produce films and composites with MFC. The common one is by filtration of a MFC suspension. Mechanical strength, surface smoothness and transparency of the films typically all increase as the dimension of the MFC fibers decreases, while the porosity and gas permeability decrease [4, 5]. However, the continuous films made by MFC suspension present some serious drawbacks such as low tear strength and poor dimensional stability. A major issue for the preparation is a very slow drainage of water, typical of small, high surface area and electrically charged colloids. Another is cost as MFC materials remain much more expensive than pulp fibers.

A strategy to alleviate these problems is to make paper composites using MFC as additives and relying on the flexible and readily available paper technology. Minimizing the amount of MFC, while maximizing their retention and performance are keys for commercialization. Several studies have demonstrated the process and material benefits

of adding MFC to pulp fiber suspension, especially in conjunction with a reactive-cationic polymer, such as polyamideamine-epichlorohydrin (PAE) [6]. The novel properties achieved for these composites paper: smoothness and mechanical properties under wet and dry conditions were shown to significantly increase; paper gas permeability decrease and suspension drainage was little affected. Nonetheless, there is a poor understanding on the effect of MFC dimension and structure on these paper composites.

In this work, we investigated two types of Microfibrillated cellulose (MFC), produced either by homogenization or by ball milling. This study aims at quantifying the effect of MFC dimension on the paper composite properties. MFC is used as additive with or without a polymeric wet strength additive (PAE). The performance of MFC is also compared to cellulose micro-particles (CMPs) from cryogenic milling. All additives are used in the wet end by direct adsorption onto pulp fibers prior to drainage and web consolidation using the paper making process. It is our objective to develop high performance-low cost paper composites and to better understand the role played by the MFC in terms of surface, colloid and material science.

3.3 Experimental Section

3.3.1 Materials

Commercial microfibrillated cellulose (MFC) was denoted as MFC1 and supplied never dried at a 25% solid content by Daicel chemical Industries Ltd, Japan (Celish KY-100s). MFC1 is made from pure cellulose fibers through high pressure homogenization. Their diameters range from 10 nm to several microns. The dimension properties of the fibers are summarized in Table I. This information was used to calculate their surface area. The charge density of MFC1 is 1.1×10^{-2} $\mu\text{eq/g}$ determined by streaming current titration with poly-diallyldimethylammonium chloride (poly-DADMAC). The titration was performed with a Mutek PCD-02 particle charge detector (BTG Instruments, Germany) and polyDADMAC of average molecular weight of 400,000- 500,000 was purchased from Aldrich. The endpoint of the titration was determined by the signal (mV) reaching zero. Northern softwood bleached kraft pulp (National Institute of Standards & Technology, reference material 8495) was used for preparing cellulose microparticles (CMPs) by cryogenic milling and MFC by ball milling, which was denoted as MFC2.

Table I: Dimension properties of cellulosic fibers used in this work.

Sample	Mean Diameter (μm)	Aspect Ratio	Mean length (μm)
Hardwood fibers	10	65	650
Softwood fibers(Varanasi et al, 2012)	28	72	2000*
MFC1 (Varanasi et al, 2012)	0.073	153	11.2
MFC2 (Zhang et al, 2012)	0.032	146	4.7
Cellulose microparticles (CMPs)	10	/	/

* From estimation

MFC2 were fabricated by ball milling in water, and received in the form of an aqueous dispersion. Specifically, MFC2 were prepared in a SPEX 8000M shaker Mill. Firstly, cellulose pulp sheet (NIST reference material 8495) was torn into 5×5 cm pieces and soaked in deionised water overnight to prepare a 1 wt% solid suspension. The wet cellulose pieces were then shredded using a conventional kitchen blender. Then 20 g of 1 wt% cellulose pulp suspension, 45 g of cerium-doped Zirconium balls (0.5 mm in diameter) and 20 mL of deionised water were placed in a 70 mL polypropylene container and milled using Spex 8000 ball mill for 60 mins. The final suspension was filtered using a polyester mesh (opening size 125 micron) to remove the zirconium balls and any larger remaining fibres. Full information is provided elsewhere by Zhang et al [7].

CMPs were obtained from cryogenic milling (SPEX SamplePrep 6870 Large Freezer Mill). The preparation was conducted by immersing the steel sample vial in liquid nitrogen, and the air dried softwood pulp of 1g in the vial was milled for 100 min through the action of the impactor under the influence of an alternating magnetic field.

The reference sheet with target oven dry (o.d.) basis weight of 60 g eucalyptus kraft hardwood fiber/m², was made from the National Institute of Standards & Technology (NIST) reference material 8496 (Bleached eucalyptus kraft pulp). The charge density of NIST 8496 is 1.54 $\mu\text{eq/g}$ determined by poly-DADMAC titration. The commercial polyamideamine-epichlorohydrin (WSR 557 HP) with an average molecular mass of 500,000 was supplied by Nuplex Industries (Australia) Pty Ltd (12.5% w/w solid content solution). PAE solutions were diluted prior to use for each experiment. Unless specified, deionized water was used in the experiments.

3.3.2 Methods

3.3.2.1 Handsheets preparation

Cellulose handsheets were made using a standard British hand sheet maker according to the Australian/New Zealand Standard Method 203s. Basically, 24g oven dried (o.d.) lap sheet was torn to small pieces and thoroughly wetted by soaking in deionized water for about 12 hours, then transferred to a disintegrator (Model MKIIC, *Messmer* Instruments Ltd). By diluting to 2 L with deionized water and disintegrating for 75 000 propeller revolutions, the pulp stock was prepared for further use. The cellulose additives (CMPs, MFC1 and MFC2) were used in the form of aqueous dispersions, which were directly added into pulp slurry or mixed with PAE solution together prior to adding into the pulp. The resulting furnish was stirred for 5 min prior to handsheet forming. The dewatering time was measured as the time taken to remove all free water from the wet fiber web, starting from when drainage commenced.

The pH of the pulp slurry mixture was about 5 and was not adjusted. The addition of 10mg PAE /g hardwood fiber was based on the target o.d. basis weight of 60 g eucalyptus kraft hardwood fiber/m². After manual couching and wet-pressing at 0.4 MPa for about 15 seconds, the sheets were cured in a drum-dryer at 100 °C for 10 min, in order to activate reactive bonds between the PAE and the cellulose surface.

3.3.2.2 Cellulosic fiber and paper properties

Scanning electron micrographs (SEM) of MFC (MFC1 and MFC2) and engineered paper were obtained using a JEOL 7001 FEG system operating at 5 kV and 180 pA. A drop of diluted MFC dispersion was placed on a silicon wafer, air dried and then platinum coated. The paper composites were also platinum coated prior to SEM imaging. 0.02 g CMPs was dispersed in 10 mL of deionised water, casted on a conductive carbon adhesive tab and air dried prior to platinum coating. Their images were analyzed by Phenom Pro desktop SEM.

Streaming current titration used series of aqueous suspensions consisting of MFC1, MFC2 and eucalyptus kraft hardwood fibers (1% w/v solid) respectively, and PAE solutions prepared at 10 mg/mL. Suitable amounts of PAE solution (no more than 1 mL in total) were added to fiber samples of 100 mL and stirred for 2 min. Finally, a 10 mL

sample was withdrawn and the streaming current titration measured with a Müttek PCD-03 pH particle charge detector (BTG Instruments, Germany).

The retention of cellulose additive was calculated as the ratio of the weight of additive retained in the sheet to the amount of additive used. This was estimated following equation (1). The dosage of additive was kept constant at 100 mg/ g hardwood fiber. The target grammage of the control sheet (without additive) is 60 g hardwood fiber/m² (oven-dried). The sheet weight was measured using a balance (METTLER TOLEDO, model AB304-S) with readability of 0.1mg. The average was measured from 7 replicates.

Retention ratio (%) =

$$\frac{\text{average o.d. weight of sheet with additive} - \text{average o.d. weight of the control sheet}}{\text{weight of additive used}} \times 100 \quad (1)$$

The paper basis weight and thickness were measured from ten replicates according to Australian/New Zealand Standard Methods 426s and 208s. The basis weight of the paper, divided by its thickness was used to calculate the apparent sheet density. Air resistance was assessed by air permeance tester (type 977102, Lorentzen & Wettre, Sweden) according to Australian/New Zealand Standard Method 420s. Both sides of the 7 replicates were measured and the results were valued at the unit of Gurley second/ 100 mL.

The sheets were equilibrated at 23°C and 50% relative humidity for at least 24 hours before wet and dry tensile tests based on the Australian/New Zealand Standard Methods 448s and 437s. For wet tests, the test paper strip was slightly bent and the middle part touched to the surface of the deionised water for 2 seconds. The wetted length is about 25 mm. The width of sample strips were 15 mm and test span was 100 mm. An Instron tensile tester (Instron 5566) was used to record maximum tensile force with constant rate of elongation at 10 mm/min. The tensile index for each sample was calculated as tensile strength (expressed in newtons per metre) divided by basis weight (grams per square meter). The mean value was obtained from seven valid tests and the error bars in the figures indicate the 95% confidence interval. T-Test was used to determine statistical significance of data. The typical stress-strain curve selected for analysis was that from the paper strip having the closest tensile index to the mean value of the series samples.

3.4 Results

The morphology of two MFC and CMPs were compared on Figure 1. MFC1 and MFC2 maintained fibrillar shape after mechanical treatment, and displayed a higher aspect ratio than hardwood and softwood fibers (Table I). The mean length of MFC1 (11.2 μ m) was close to the mean diameter of the hardwood fibers (10 μ m) used for the control paper. CMPs of irregular shape and short aspect ratio were produced by cryogenic milling. Their size ranged from 5-15 μ m with mean diameter of 10 μ m.

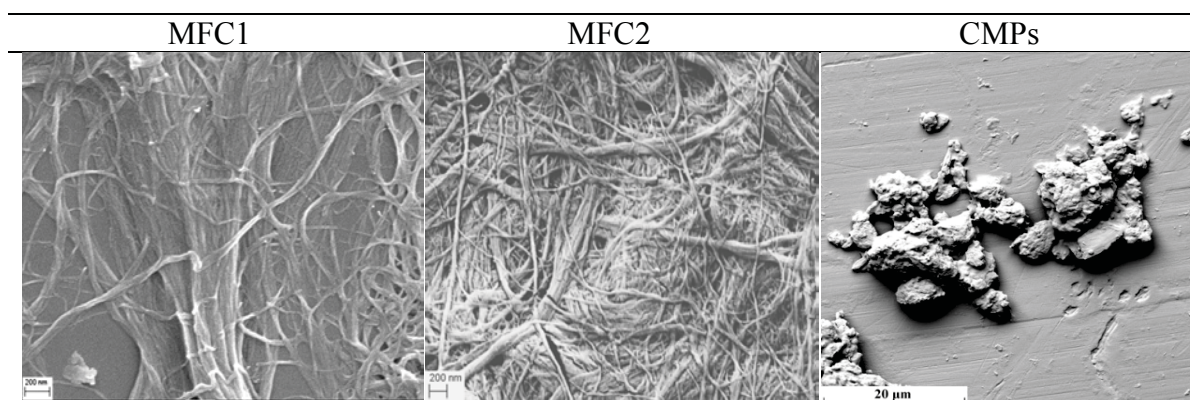


Figure 1: SEM micrographs of cellulosic additives applied to engineer the paper.

Figure 2 shows the streaming current titration of the hardwood pulp and the two nano-sized cellulose additives (MFC1 and MFC2), measured by varying the amounts of PAE. Titration of fiber suspension with PAE first neutralized and then reversed the net charge of the fiber samples. The hardwood pulp reached neutral charge close to 2 mg/g addition level, while MFC1 reached neutral charge at an addition level of approximately 5 mg/g, and a PAE dose at 7.5 mg/g neutralized the charge of MFC2 (Fig 2). Once the cellulose additives (100mg/g hardwood fiber) were blended with PAE (10 mg /g hardwood fiber), their negatively charged surface was reversed to positive, which resulted in the increased retention of MFC2 and CMPs to 67.8% and 88% on the paper web, respectively. However, the dewatering for sheet forming, resultant paper thickness and apparent density were only marginally affected.

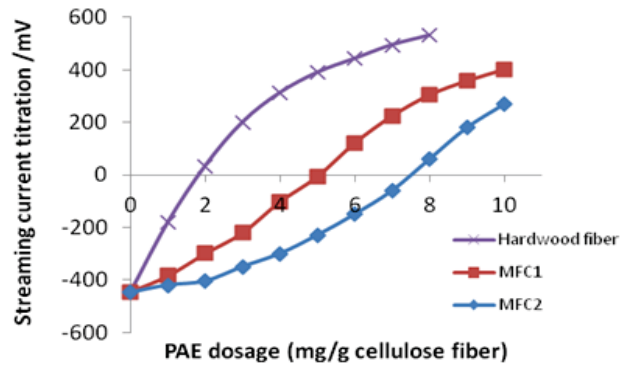


Figure 2: Streaming current titration measured for the cellulosic products with increasing PAE addition. Lines shown are to guide the eye.

Table II: Paper formation, stress-strain at break and elastic modulus affected by addition of 100 mg cellulosic additives /g hardwood fiber with and without PAE. The target oven-dry grammage for the control sheet is 60 gsm.95% confidence intervals from 10 measurements indicated in parenthesis.

	Without PAE				10mg PAE/ g pulp			
	Control	MFC1	MFC2	CMPs	Control	MFC1	MFC2	CMPs
Relative Retention (%)		100 (0)	46.5 (4.1)	71 (3.4)		100 (0)	67.8 (3.8)	88 (4.7)
Dewatering time (s)	<1	1	2	<1	<1	1	2	<1
Thickness (μm)	136 (3)	141 (3)	147 (9)	166 (4)	142 (6)	138 (3)	138 (4)	176 (4)
Apparent density(kg/m ³)	461(19)	495(15)	446(40)	405(19)	449(29)	513(21)	497(28)	395(21)
Stress at break-dry (Mpa)	5.2(0.2)	10.4(0.6)	12.4(0.4)	3.4(0.2)	6.0(0.5)	15.7(0.8)	17.1(0.4)	5.2(0.3)
Stress at break-wet (Mpa)	0.49(0.06)	0.68(0.03)	0.83(0.04)	0.33(0.03)	1.72(0.13)	5.28(0.3)	4.44(0.38)	1.71(0.08)
Strain at break-dry (%)	1.2(0.2)	2.1(0.2)	1.7(0.3)	1.5(0.3)	1.1(0.2)	2.4(0.3)	2.4(0.3)	1.2(0.2)
Strain at break-wet (%)	4.0(0.5)	4.2(0.3)	1.8(0.3)	3.1(0.4)	3.5(0.4)	5.3(0.2)	2.1(0.2)	4.2(0.4)
Elastic modulus-dry (GPa)	0.7(0.07)	1.2(0.11)	1.4(0.13)	0.5(0.02)	0.8(0.08)	1.5(0.05)	1.5(0.1)	0.7(0.07)
Elastic modulus-wet (GPa)	0.05(0.01)	0.08(0.02)	0.13(0.02)	0.05(0.01)	0.1(0.02)	0.2(0.03)	0.4(0.03)	0.1(0.03)

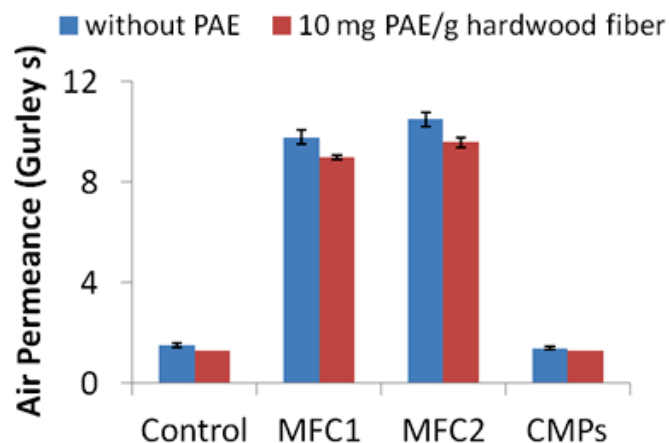


Figure 3: Air permeability of paper by addition of 100 mg modified fibers/ g hardwood pulp, without PAE and 10 mg PAE/g hardwood pulp.

Paper air permeability was recorded from Gurley measurement (Figure 3). Higher air permeability is measured for the control (1.5 ± 0.1 s) and paper with CMPs (1.4 ± 0.1 s). The addition of MFC1 and MFC2 at 100mg/g hardwood fiber dosage into paper critically reduced permeability to 9.8 ± 0.3 s and 10.5 ± 0.3 s. No obvious change in the air permeance resulted simply with PAE addition. The morphology and surface structure of paper made with MFC2 additives are significantly different from those of the other fibrous composites (Figure 4). Paper with MFC2 displays a much smoother surface and more compact configuration. In contrast, the web structure of the control and the paper embedded with CMPs are porous.

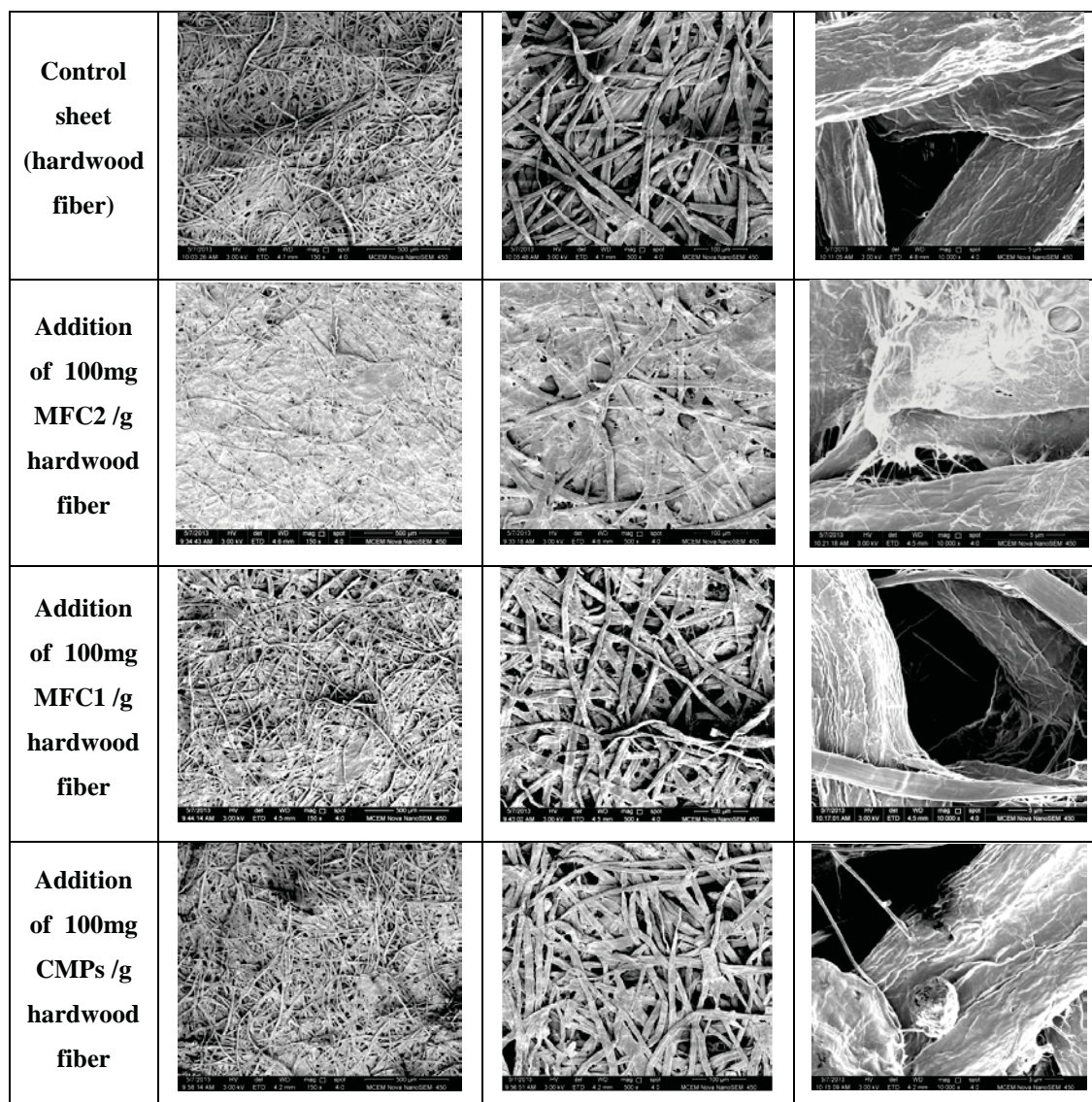


Figure 4: Morphologies of paper engineered by cellulosic additives, examined by SEM of 3 different magnification (150X, 500X, 10,000X). The bar represents a length of 500, 100 and 5 μ m.

Without PAE treatment, MFC1 and MFC2 at dosage of 100 mg/g hardwood fiber considerably increased paper dry strength to 21 ± 1 Nm/g and 28 ± 1 Nm/g, respectively (Figure 5). Comparing with the control (dry tensile of 11.3 ± 0.5 Nm/g), the addition of CMPs significantly weakened the paper strength to 8.4 ± 0.5 Nm/g. Once water penetrated the fiber web, the control paper lost most of its strength to 1.1 ± 0.1 Nm/g (Figure 6). In comparison, paper with MFC2 and MFC1 reached wet tensile index of 1.9 ± 0.1 Nm/g and 1.4 ± 0.1 Nm/g, respectively.

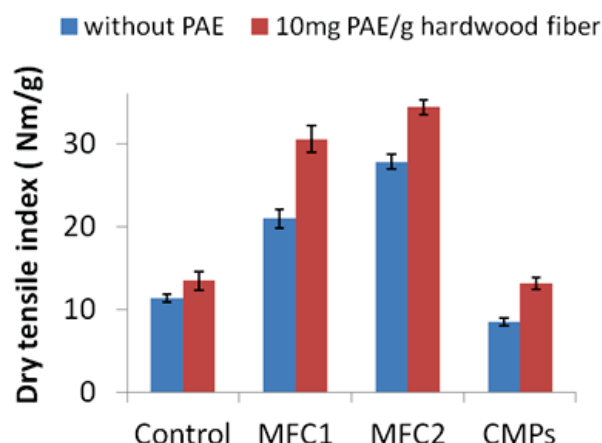


Figure 5: Dry tensile index of paper (a) without PAE and (b) with PAE (10mg/g hardwood fiber) treatment. MFC1, MFC2 and CMPs were added at 100mg/g hardwood fiber.

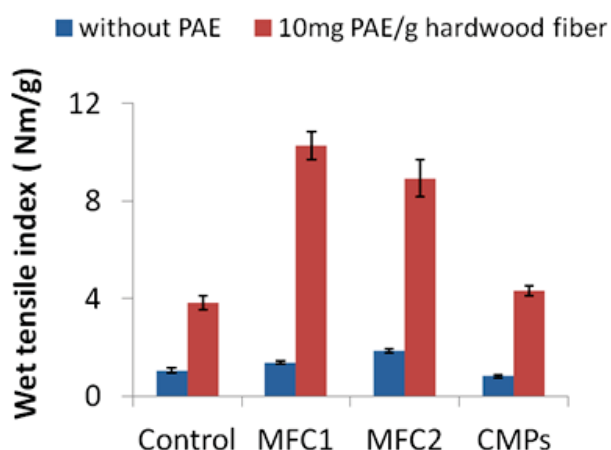


Figure 6: Wet tensile index of paper (a) without PAE and (b) with PAE (10mg/g hardwood fiber) treatment. MFC1, MFC2 and CMPs were added at 100mg/g hardwood fiber.

Addition of PAE (10 mg/g hardwood fiber) to the pulp slurry substantially improved wet strength of the control up to 3.8 ± 0.3 Nm/g. Combining PAE with the addition of MFC1 or MFC2 to the fiber suspension resulted in considerable synergy both for dry and wet strengthening (Figure 5 and 6). Dry tensile indices were drastically increased to 34.4 ± 0.9 Nm/g for MFC2/PAE composite and 30.6 ± 1.6 Nm/g for MFC1/PAE composite, and the corresponding wet tensile indices were 8.9 ± 0.8 Nm/g and 10.3 ± 0.6 Nm/g, respectively.

The stress-strain curve of paper was modified differently by the various cellulose additives (Figure 7 and 8). Elongation of dry paper at failure was prolonged by the addition of MFC1 and MFC2; however, the wet strain at failure was noticeably decreased by MFC2. Dry paper with MFC2/PAE and MFC1/PAE composites stretched in a quite similar way, and both papers exhibit high value of elastic modulus (Table II). Interestingly, in wet conditions, the stress-strain plots of PAE-strengthened paper became linear, and the highest elastic modulus was recorded for paper with MFC2/PAE composite (Table II).

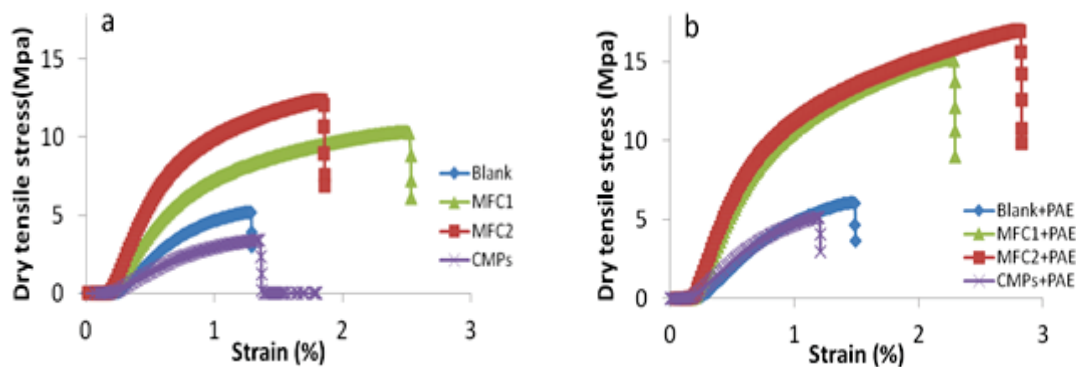


Figure 7: Stress-Strain curve of dry paper (a) without PAE and (b) with PAE (10mg/g hardwood fiber) treatment.

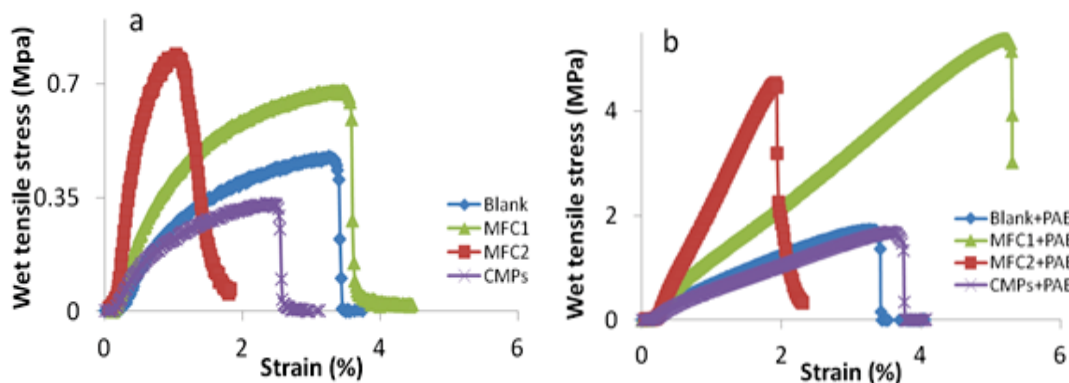


Figure 8: Stress-Strain curve of wet paper (a) without PAE and (b) with PAE (10mg/g hardwood fiber) treatment.

3.5 Discussion

3.5.1 Effect of cellulosic additives on the paper processing

During mechanical processing, morphology and dimension of cellulose fibers are greatly modified by external forces (Figure 1 and Table I). Under the strong shearing force

generated between the milling balls, MFC2 are disintegrated from the bundles of cellulose fibrils of the softwood fiber. By comparison, MFC1 was prepared through microfibrillation of cellulose fibers by a high pressure homogenizer. As the average length of MFC is difficult to measure directly, the aspect ratio and average diameter of the samples are employed to estimate their length. From sedimentation experiments, both MFC1 and MFC2 were found to possess aspect ratio close to 150, higher than the aspect ratio of 72 for softwood fibers [8]. SEM images analyzed by ImageJ showed MFC2 diameters were more uniformly distributed than MFC1 and were smaller with a size of 32 nm [9]. However, the CMPs made from cryogenic milling cellulose fibers consist mostly of irregularly shaped particles of low aspect ratio, which act as debonder in paper by increasing thickness and decreasing its apparent density.

The drainage time of papermaking was reported to be proportional to the MFC ratio in the stock [10, 11]. Bonding of the fibrous network is drastically affected by MFC addition, which also increases shrinkage during drying [12]. In this study, the drainage time was very short: less than three seconds for all handsheets. An increase in drainage resistance was observed for the fiber suspension with the addition of MFC (Table II). This reflects the combined effect of high aspect ratio MFC and low density/deformable fiber flocs, which increase the surface area and contribute to reducing the pore size of the filter mat on the wire. This later mechanism is further supported by the drainage rate remaining constant while MFC retention doubles when PAE is used; this is likely caused by coagulation of MFCs (Table II).

The efficiency of fibers/additives retaining in the paper is important for the papermaking process. The cellulose fiber diameter distributions and aspect ratio are reported to play critical roles during sheet formation [5]. The MFC1 has the higher aspect ratio and an average fiber length of 11.2 μm , which is a dimension similar to the diameter of the hardwood fibers. Hence, the MFC1 is more likely to form physical entanglements than the shorter MFC2 or the CMPs of lower aspect ratio. In comparison to MFC2 and CMPs, MFC1 has a broader size distribution, and mixed with nanofibers, larger fibers and particles [13]. These features explain their full retention on paper without need for a retention aid.

The addition of a cationic polymer to an anionic fiber suspension modifies the interaction between cellulose surfaces via electrostatic force, polymer bridging and steric repulsion; these interaction forces cause dramatic changes in yield stress, floc strength and network strength of the fiber suspension [14]. Two stages were proposed for the adsorption of PAE onto fibers: an initial fast dynamic adsorption (seconds to minutes) and a slow approach to equilibrium (hours to days) [15]. In this study, the surface area of 1g hardwood fibers (close to 1 m²) would be fully covered with 10mg PAE while their surface charge was neutralized at 1.8 mg PAE (Figure 2). 1g MFC1 and MFC2 have much larger surface area (36.5 m² and 83.3 m², respectively), and their charge reversals occur at higher PAE amount (5 mg and 7.5 mg) in spite of their lower surface charge density. There are two possibilities for this observation. The first is the negative charge on the MFC surface being neutralized by cationic PAE addition. Another is the adjacent fibers being bridged by PAE to form relatively strong flocs.

Polymer assisted fiber flocculation is a major factor governing the retention of a fiber suspension. The addition of 10 mg PAE reversed the anionic surface of 1 g MFC fibers (MFC1 and MFC2) to cationic (Figure 2), which promotes the electrostatic interactions with the hardwood fibers. The addition of PAE/cellulosic additives can have 3 main influences: 1) coagulate cellulosic additives into bigger “fine like” structures, 2) co-flocculate fibers with PAE mixture and 3) modify floc properties (density/compressibility and size). In this case, MFC2 and CMPs were flocculated into bigger and denser flocs [16], resulting in the increased retention observed in paper web. The optimization of cationic-polymer assisted flocculation can efficiently improve the retention of cellulosic additives.

3.5.2 Structure and air permeability of paper

Paper properties are greatly affected by the three-dimensional fibers distribution and porous web structure. Fluid and gas transportation in the fiber network closely relates to the porosity, the ratio of void volume and total volume of paper [17, 18], which can be estimated from paper density. In this study, air permeability of paper is not affected by the addition of 100 mg CMPs/g hardwood fiber, but the lower apparent density was recorded. It is anticipated that some fiber-fiber joints were replaced by loose fiber-CMPs contact, thus creating weak bonds and more voids in the fiber web. In contrast, the addition of MFC drastically decreased air permeability of the paper composites. These

results suggest changes in the paper structure: increasing pore tortuosity, decreasing pore area and pore connectivity. This effect is better visualized with the surface morphology illustrated by SEM (Figure 4).

In previous work, air permeance of paper composites was correlated with its drainage period [11]; the time needed for air to diffuse through the dry substrate plane was found proportional to the time required for dewatering pulp fibers into a web; the current study is in good agreement with these previous observations. The air permeability for MFC2 paper composite was lower than that from MFC1, considering a lower retention amount of MFC2 at a given dose of 100 mg/g pulp (Figure 3 and Table II). This result is consistent with the less porous surface morphology observed by scanning electron microscopy (Figure 4). The compact structure of MFC2 composite suggested their greater resistance to air flow from that of porous paper.

3.5.3 Strength of paper

In preliminary experiments, low addition level (less than 2 wt % of pulp fiber) of MFC was explored for paper composites. However, there were no significant strength improvements. This is probably due to a low retention of MFC within the fiber web. By increasing the MFC addition up to 100mg /g fiber, paper displayed higher wet and dry tensile indices without using polymer additives (Figure 5 and 6). Unlike paper made with CMPs, MFC additives not only improved the paper dry strength, but also promoted wet strength. This property allows the fiber web to better retain strength under high moisture or wet conditions. Taking retention amount into account, paper with MFC2 is much stronger than that made with MFC1 (Table II and Figure 5). This can be explained by two reasons. The first is the addition of MFC2 allows more hydrogen bonding by increasing fiber-fiber contacts. When the paper is wetted, MFC2 causes considerable internal friction, which resists the relative motion of the fibers and results in greater wet strength [19]. The second is the lower coarseness of MFC2. The tensile strength of wet web is expected to be inversely proportional to the square of fiber coarseness [20].

Interaction between fibers and polymer greatly affect viscoelasticity and water plasticization of cellulosic composites [21]. Once water penetrates into the cellulosic web, the hydrogen bonding between fibers decreases, leading to a loss of strength [22]. Crosslinking cellulose with the cationic thermal reactive PAE improves bonding

properties, upon drying, against moisture change by creating a network of covalent bonds which restrict fibers swelling [23-25]. Interestingly with PAE, the strength development from MFC2 was quite similar to that of MFC1 sheets (Figure 5 and 6), even with the increased retention of MFC2. Two reasons could account for this observation. First, the surface charge of MFC2 could have been modified upon adsorption of the cationic PAE; MFC2 reoriented during web forming and fibril entanglement would be reduced. Second, wet strength development may be dominated by building up of the covalent bonds network between the fibers and PAE upon drying, which counteracts the influence of MFC2 on fiber friction. For paper made with CMP, the addition of PAE offset the debonding and improved the strength, but without changing the bulk and thickness of the web. These features may find application such as mechanical debonder in tissue making. Traditional tissue making usually combines softeners, typically a cationic surfactant, with wet and dry strength agents, such as PAE and carboxymethyl cellulose (CMC). CMP could provide a non-chemical alternative to cationic surfactants to improve paper bulk, should softness not be affected.

The stress-strain curve of a fiber network indicates the elastic and viscoelastic nature of paper; a linear stress-strain plot suggests that PAE enhances the elasticity of paper. Comparing with the control, both dry MFC1 and MFC2 composites with and without PAE stretched longer at break, and demonstrated higher Young's modulus due to the strong affinity of fibrils bonded to each other (Figure 7). When paper was wetted, the saturated fibers displayed gel-like behaviour, which may account for the extended strain observed [26]. MFC2 composite presents a unique lower strain at failure and a much higher Young's modulus, indicating a brittle material (Figure 8).

The difference of wet elongation between MFC1 and MFC2 composites probably indicates two mechanisms of strengthening (Figure 9). The first is dominated by MFC-fiber entanglement, where MFC length is greater than the fiber diameter, and MFC acts as a bridge to bond the neighbouring fibers. As load is applied to the wet web, the structure deformation mainly relies on MFC entanglements around the fiber joints, explaining the extended failure behaviour. Secondly, in the case of MFC length shorter than fiber diameter, fiber-fiber contact reinforcement controls the strength improvement. When wetted, the MFCs on the fiber surface swell, which causes an initial separation of the fiber web. This would explain the deformation of the web observed at a short strain.

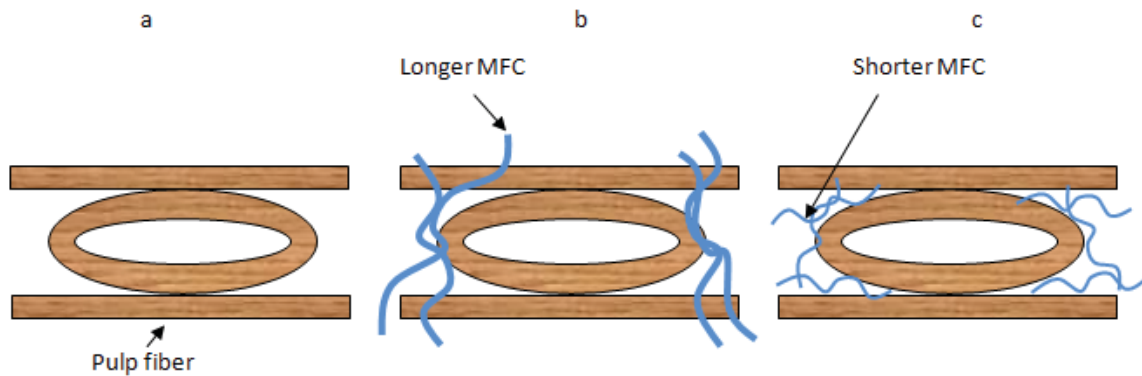


Figure 9: Proposed mechanisms for paper web reinforcement (a) hardwood fiber web. (b) The addition of MFC, whose mean length is close to the value of hardwood fiber diameter (c) The addition of MFC, whose mean length is lower than the value of hardwood fiber diameter.

3.6 Conclusion

Cellulosic fiber web of increased strength and reduced air permeability were produced using the papermaking technology with cellulose additives of length scale ranging from the nano-meter to the micro-meter. Microfibrillated cellulose (MFC) achieved by ball milling and cellulose micro-particles (CMPs) developed by cryogenic milling softwood fiber were compared to commercial MFC produced from homogenization. The effect of blending two MFCs and CMPs with hardwood fibers on the paper properties was investigated in terms of nano/micro cellulose dimension. CMPs act as mechanical debonder and may find application in tissue making to increase paper bulk and decrease the substrate density, thus improving softness. In contrast to cellulose micro-particles (CMPs), microfibrillated cellulose (MFC) having a higher aspect ratio and smaller size significantly improved paper composite strength and decreased its porosity, yielding a denser structure. The retention of MFC was high even without polymeric retention aid thanks to their broad size distribution.

The addition of MFC combined with polyamideamine-epichlorohydrin (PAE) can increase both dry and wet strength of cellulosic materials equivalently by an order of magnitude. Their different stress-strain curves in wet condition suggest two different mechanisms of strength development: MFC-fiber entanglement and fiber-fiber contact reinforcement. Strong and low permeability paper with cellulosic nano-additives can be

produced with a standard paper machine. These composites offer unique possibilities in packaging, tissue and light weight materials.

3.7 Acknowledgement

The financial contribution of Australian Research Council (LP0990526), Visy and Nopco paper technology is acknowledged. Thank to Dr. W K.J. Mosse, P. Chandran and I. Stopka for the cellulose micro-particles, Professor X. Wang and Associate Professor T. Tsuzuki from Deakin University for providing cellulose nanofibrils, and S. Sharman, S. Varanasi, S. Narayanan and H. Chiam for technical help.

3.8 References

1. Siro, I. and D. Plackett, *Microfibrillated cellulose and new nanocomposite materials: a review*. Cellulose, 2010. **17**(3): p. 459-494.
2. Klemm, D., F. Kramer, S. Moritz, T. Lindstrom, M. Ankerfors, D. Gray, and A. Dorris, *Nanocelluloses: A New Family of Nature-Based Materials*. Angewandte Chemie-International Edition, 2011. **50**(24): p. 5438-5466.
3. Koga, H., T. Saito, T. Kitaoka, M. Nogi, K. Suganuma, and A. Isogai, *Transparent, Conductive, and Printable Composites Consisting of TEMPO-Oxidized Nanocellulose and Carbon Nanotube*. Biomacromolecules, 2013. **14**(4): p. 1160-1165.
4. Aulin, C., M. Gallstedt, and T. Lindstrom, *Oxygen and oil barrier properties of microfibrillated cellulose films and coatings*. Cellulose, 2010. **17**(3): p. 559-574.
5. Zhang, L.Y., W. Batchelor, S. Varanasi, T. Tsuzuki, and X.G. Wang, *Effect of cellulose nanofiber dimensions on sheet forming through filtration*. Cellulose, 2012. **19**(2): p. 561-574.
6. Ahola, S., M. Osterberg, and J. Laine, *Cellulose nanofibrils-adsorption with poly(amideamine) epichlorohydrin studied by QCM-D and application as a paper strength additive*. Cellulose, 2008. **15**(2): p. 303-314.
7. Zhang, L.Y., T. Tsuzuki, and X.G. Wang, *Preparation and Characterization on Cellulose Nanofiber Film*. Prizm 7, Pts 1-3, 2010. **654-656**: p. 1760-1763.
8. Varanasi, S., R.L. He, and W. Batchelor, *Estimation of cellulose nanofibre aspect ratio from measurements of fibre suspension gel point*. Cellulose, 2013. **20**(4): p. 1885-1896.
9. Varanasi, S., H.H. Chiam, and W. Batchelor, *Application and interpretation of zero and short-span testing on nanofibre sheet materials*. Nordic Pulp & Paper Research Journal, 2012. **27**(2): p. 343-351.
10. Taipale, T., M. Osterberg, A. Nykanen, J. Ruokolainen, and J. Laine, *Effect of microfibrillated cellulose and fines on the drainage of kraft pulp suspension and paper strength*. Cellulose, 2010. **17**(5): p. 1005-1020.
11. Su, J.L., W.K.J. Mosse, S. Sharman, W.J. Batchelor, and G. Garnier, *Effect of tethered and free microfibrillated cellulose (MFC) on the properties of paper composites*. Cellulose, 2013. **20**(4): p. 1925-1935.
12. Manninen, M., I. Kajanto, J. Happonen, and J. Paltakari, *The effect of microfibrillated cellulose addition on drying shrinkage and dimensional stability of wood-free paper*. Nordic Pulp & Paper Research Journal, 2011. **26**(3): p. 297-305.
13. Varanasi, S. and W.J. Batchelor, *Rapid preparation of cellulose nanofibre sheet*. Cellulose, 2013. **20**(1): p. 211-215.

14. Mosse, W.K.J., D.V. Boger, G.P. Simon, and G. Garnier, *Effect of Cationic Polyacrylamides on the Interactions between Cellulose Fibers*. Langmuir, 2012. **28**(7): p. 3641-3649.
15. Yoon, S.H., *Adsorption kinetics of polyamide-epichlorohydrin on cellulosic fibres suspended in aqueous solution*. Journal of Industrial and Engineering Chemistry, 2006. **12**(6): p. 877-881.
16. Su, J.L., W.K.J. Mosse, S. Sharman, W. Batchelor, and G. Garnier, *Paper Strength Development and Recyclability with Polyamideamine-Epichlorohydrin (Pae)*. Bioresources, 2012. **7**(1): p. 913-924.
17. Jackson, G.W. and D.F. James, *The Permeability of Fibrous Porous-Media*. Canadian Journal of Chemical Engineering, 1986. **64**(3): p. 364-374.
18. Niskanen, K., *Paper physics*. Papermaking science and technology. Vol. 1. 1998: Tappi.
19. Tejado, A. and T.G.M. van de Ven, *Why does paper get stronger as it dries?* Materials Today, 2010. **13**(9): p. 42-49.
20. Seth, R.S., *The Effect of Fiber Length and Coarseness on the Tensile-Strength of Wet Webs - a Statistical Geometry Explanation*. Tappi Journal, 1995. **78**(3): p. 99-102.
21. Myllytie, P., L. Salmen, E. Haimi, and J. Laine, *Viscoelasticity and water plasticization of polymer-cellulose composite films and paper sheets*. Cellulose, 2010. **17**(2): p. 375-385.
22. Gardner, D.J., G.S. Oporto, R. Mills, and M.A.S.A. Samir, *Adhesion and surface issues in cellulose and nanocellulose*. Journal of Adhesion Science and Technology, 2008. **22**(5-6): p. 545-567.
23. Espy, H.H., *The Mechanism of Wet-Strength Development in Paper - a Review*. Tappi Journal, 1995. **78**(4): p. 90-99.
24. Obokata, T. and A. Isogai, *The mechanism of wet-strength development of cellulose sheets prepared with polyamideamine-epichlorohydrin (PAE) resin*. Colloids and Surfaces a-Physicochemical and Engineering Aspects, 2007. **302**(1-3): p. 525-531.
25. Obokata, T. and A. Isogai, *Wet-strength development of cellulose sheets prepared with polyamideamine-epichlorohydrin (PAE) resin by physical interactions*. Nordic Pulp & Paper Research Journal, 2009. **24**(2): p. 135-140.
26. Saarikoski, E., T. Saarinen, J. Salmela, and J. Seppala, *Flocculated flow of microfibrillated cellulose water suspensions: an imaging approach for characterisation of rheological behaviour*. Cellulose, 2012. **19**(3): p. 647-659.

This page is intentionally blank

Chapter 4

Effect of Tethered and Free Microfibrillated Cellulose (MFC) on the Properties of Paper Composites

This page is intentionally blank

Declaration for Thesis Chapter 4

Declaration by candidate

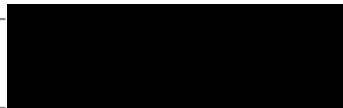
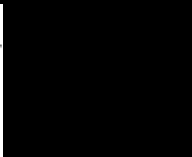
In the case of Chapter 4, the nature and extent of my contribution to the work was the following:

Nature of contribution	Extent of contribution (%)
Initiation, key ideas, experimental and analysis works, development and writing up of paper	75

The following co-authors contributed to the work. If co-authors are students at Monash University, the extent of their contribution in percentage terms must be stated:

Name	Nature of contribution	Extent of contribution (%) for student co-authors only
Wade K. J. Mosse	Initiation, reviewing and editing of the paper	Research group member
Scot Sharman	Sharing the expertise on papermaking	Research group member
Warren Batchelor	Initiation, key ideas, reviewing and editing of the paper	Co-supervisor
Gil Garnier *	Initiation, key ideas, reviewing and editing of the paper	Supervisor

The undersigned hereby certify that the above declaration correctly reflects the nature and extent of the candidate's and co-authors' contributions to this work*.

Candidate's Signature		Date 22/5-3-6
Main Supervisor's Signature		Date

*Note: Where the responsible author is not the candidate's main supervisor, the main supervisor should consult with the responsible author to agree on the respective contributions of the authors.

This page is intentionally blank

Effect of Tethered and Free Microfibrillated Cellulose (MFC) on the Properties of Paper Composites

Jielong Su, Wade K.J. Mosse, Scot Sharman, Warren J. Batchelor and Gil Garnier*

BioPRIA, Australian Pulp and Paper Institute (APPI), Department of Chemical Engineering Monash University, Clayton, VIC 3800, Australia.

*Corresponding author. Email: [REDACTED]

Content

4.1	Abstract	121
4.2	Introduction	122
4.3	Experimental Section	124
4.3.1	Materials	124
4.3.2	Paper refining of the fibers and preparation of cellulosic composites	124
4.3.3	Characterization of the composites	125
4.4	Results	126
4.4.1	MFC composites and refined fiber sheet	126
4.4.2	Polyamideamide-epichlorihydrin (PAE) as additive in Cellulose Composites	132
4.5	Discussion	134
4.5.1	Effect of MFC on composites process	134
4.5.2	Structure and air permeability of MFC composites	135
4.5.3	Strength of MFC composites	136
4.6	Conclusion	138
4.7	Acknowledgement	138
4.8	References	138

4.1 Abstract

High strength and low gas permeability cellulosic composites were produced using the papermaking technology with a commercial microfibrillated cellulose (MFC). The effect of blending MFC with hardwood fibers was compared to the direct refining of the fibers

with and without polyamideamine-epichlorohydrin (PAE) addition. The addition of MFC, free or tethered, to pulp fibers combined with PAE can increase the dry strength and wet strength of cellulosic materials by an order of magnitude. Air permeability of the composites decreases by up to orders 4 of magnitude with MFC addition. The hypothesis that refining wood fibers can produce tethered MFC which provides equivalent strength properties but significant drainage benefits was proven. Furthermore, major benefits in paper formation uniformity (fiber distribution homogeneity) were achieved with refined fibers.

Keywords: Microfibrillated cellulose (MFC), paper, polyamideamine-epichlorohydrin (PAE), refining, hardwood fibers, composites, Tethered microfibrils.

4.2 Introduction

Microfibrillated cellulose (MFC), made by a mechanical [1-3], acid hydrolysis [4] or enzymatic process [5, 6], have shown strong potential in developing novel paper products and renewable composites of unique properties. Some of the MFC composites attributes include high mechanical properties and gas barrier ability, biodegradability and transparency. MFC fibres are interesting as they combine nanoscale diameter (5 to 50 nm) with micron-scale length (1 to 1000 μm) [7-9]. The polyanhydroglucosidic backbone of MFC is capable of strong hydrogen bonding (3 OH/unit) and of adsorbing in a closed packing configuration onto another cellulose surface. MFC has good potential for industrial deployment thanks to the wide availability of cellulosic raw material, the increased production capacity worldwide, and the continuously improving process, which have all contributed to a price steadily decreasing toward the rank of commodity chemical intermediate.

Composites made of MFC using the papermaking process have already been investigated [10-13]. MFC has been either blended with pulp fibers or used as a pure suspension, with and without polymeric strength agents. MFC composites with high tensile strength have been achieved, with properties depending on material and preparation procedure [14, 15]. However, studies have consistently reported a very slow drainage rate incompatible with the current papermaking process. Another promising avenue investigated has been the coating of MFC onto paper for improved strength, printability and selective barrier

properties[16]. While composites of significant properties have been achieved, two main issues have arisen. The first is again a very slow drainage, and the second is the loss of gas barrier and strength properties under conditions of high humidity moisture/or wet conditions [12, 17-19].

The drainage of papermaking is governed by factors such as pH, ionic strength, type of the cationic polyelectrolyte and fiber dimensions. As the surface area of the fiber increases with the reciprocal of the diameter of the average fiber, and the drainage resistance is inversely proportional to the square of the specific surface area [20], the drainage rate is expected to drop at a faster than linear rate with the content of MFC in the furnish. Fiber refining is a current practice in papermaking to increase fiber-fiber bonding through defibrillation of the external surface and increase flexibility of the fiber. Tethered cellulose microfibrils have been observed on the surface of refined pulp in many studies [5, 21, 22]. Tethered microfibrils are defined as the fibrils delaminated from the outer layers of the fiber that remain attached by a segment or an extremity. Drainage rate is known from experimental practice to drop at a slower than linear rate upon fiber refining [23]. We raise the hypothesis that refining creates MFC tethered onto the surface of the fiber able to provide equivalent strength but at a drainage benefit compared to MFC addition which tend to block flow through the wet web. The objective of this study is to probe this hypothesis in the context of high performance cellulosic composites.

In this study, we compare the performance of tethered and free microfibrillated cellulose in paper composites made by standard papermaking technique. Tethered MFC was generated by refining hardwood fibers to different extents. MFC-pulp paper composites were prepared from blending fibers using the regular paper process. The effect of polyamideamine-epichlorohydrin (PAE), a typical wet strength polymer, on the MFC composites was also investigated. The study aims at producing high performance cellulosic composites from the paper process and at better understanding the strength development mechanism of MFC-polymer-fiber composites.

4.3 Experimental Section

4.3.1 Materials

The commercial polyamideamine-epichlorohydrin (PAE) was provided by Nopco Paper Technology Pty Ltd, Australia (33% w/w solid content solution); PAE solutions were diluted with deionised water prior to each experiment. Bleached eucalyptus kraft pulp was obtained from the dry lap sheet (National Institute of Standards & Technology, Standard reference material 8496). Commercially available MFC (free MFC) was purchased from Daicel Chemical Industries Ltd, Japan. This material was made from pure cellulose fibers mechanically treated in a high pressure homogenizer, and was supplied never dried at a 25% solid content. The average length of MFC is 0.5-0.6 mm, fiber diameter range from 10 nanometers to several microns. The MFC was characterized as mean diameter of 73 nanometers and aspect ratio of 147 in previous work [19]. The properties of the MFC used in this study were compared with typical primary and secondary fines from bleached hardwood kraft pulp in Table I.

Table I: Properties of MFC, primary and secondary fines.

Material	Origin	Dimension	Appearance	References
MFC	Micro-fibrillated from high refined pure cellulosic fiber	11 μm in length, and 0.073 μm in width	Fibrillar	Varanasi et al. (2012, 2013)
Primary fines	Originally presented in bleached hardwood kraft pulp	50-92 μm in length, and 14-30 μm in width	Blocky, rectangular	Cole et al. (2008); Chen et al.(2009)
Secondary fines	Refined from fines-free bleached hardwood kraft pulp	121-179 μm in length, and 9-18 μm in width	Slender, transparent	

4.3.2 Paper refining of the fibers and preparation of cellulosic composites

30 g (oven dry weight) NIST 8496 was soaked in 2 liters deionized water overnight and then disintegrated for 75,000 revolutions. The obtained pulp slurry was concentrated into 10% solid consistency by filtration through woven stainless steel wire (mesh aperture of 125 μm). When refined pulp was required, the pulp was refined at different revolutions (500, 1000, 2000, 5000 and 10000) by PFI mill (HAM-JERN, Hamar, Norway) at a load of 1.77 N.mm⁻¹.

Cellulosic composites were prepared according to the Australian/New Zealand Standard Method 203s. The dry pulp was thoroughly wetted by soaking in deionized water overnight. The pulp was transferred to a disintegrator (Model MKIIC, Messmer Instruments Ltd), diluted to 2 L with deionized water, and disintegrated for 75,000 propeller revolutions. The pulp was blended with commercial MFC at different ratios (5, 10, 25, 50, 75 weight %). The prepared pulp-MFC mixture or refined pulps (1.2 g oven dry) in 3 L deionized water were used to construct the composites by handsheet machine (Mavis Engineering Limited, United Kingdom). The forming process is automatically controlled and the drainage time was recorded from 7 replicates. In order to decrease the drainage time for preparation of pure MFC substrate, water jet vacuum attached to the sheet machine was used. Deionized water was used for pulp slurry preparation and also for sheet forming. No salt was added to achieve a specified ionic strength.

The PAE solution was added to the fiber stock slurry and stirred for 10 min. The pH of the pulp slurry mixture was about 6, and no adjustment was made. The quantity of PAE added was based on target oven dry basis weight of 60 g/m². After couching and wet-pressing at 0.4 MPa by sheet press (Type 5-1, AB Lorentzen & Wettre) for 7 minutes, the cellulose composite sheets were placed between two blotting papers, followed by a 10-minutes drum-dryer (Type MR-3, Japo Co., Ltd) treatment at 100 °C; this was to activate the bonds between the PAE and the cellulose surface.

4.3.3 Characterization of the composites

Freeness of the pulp was tested according to Australian/New Zealand Standard Methods 1301.206s:2002. The thickness and apparent density were measured according to Australian/New Zealand Standard Methods 426s and 208s. Air resistance was assessed by air permeance tester (Type 977102, Lorentzen & Wettre, Sweden) according to Australian/New Zealand Standard Method 420s. Both sides of the 7 replicates were measured and the results were determined in Gurley seconds.

The composite uniformity was measured by the Paper Perfect Formation Tester (Op Test Equipment Inc, Canada). The tester classifies formation quality in 10 formation components over a specific range and produces the formation value. The relative

formation value (RFV) of each component relates to selected reference sheet (without PAE). RFV values less than 1 means that the formation quality of the tested paper is worse than the formation quality of the reference paper. Scanning electron micrographs (SEM) were obtained using a JEOL 7001 FEG system operating at 5 kV and 180 pA.

The sheets were equilibrated at 23°C and 50% relative humidity for at least 24 hours before wet and dry tensile testing based on the Australian/New Zealand Standard Methods 448s and 437s. For wet strength measurement, the strips were totally immersed in deionized water for 1 minute, then the excess water was removed from the test piece by a blotter. The width of sample strips was 15 mm and test span was 100 mm. An Instron tensile tester (Instron 5566) was used to record maximum tensile force with constant rate of elongation at 10 mm/min. The tensile index for each sample was calculated as tensile strength (expressed in Nm^{-1}) divided by basis weight (gm^{-2}). The mean value was obtained from seven valid tests and the error bars in figures indicate the 95% confidence interval. Student's T-Test was used to determine statistical significance of data.

4.4 Results

4.4.1 MFC composites and refined fiber sheet

Paper handsheets were constructed from pure MFC and hardwood fibers, used as control, and were tested in tension; their properties are listed in Table II. Dry and wet paper made from 100% MFC was 6 and 14 times stronger, respectively, than the control paper made from the hardwood fibers. The elongation at break of MFC paper was also higher than the control: dry strain was twice as high and wet strength three-fold higher. MFC composites are stronger than the control paper for three reasons. First, MFC has a much higher aspect ratio than eucalyptus fibers (140 versus 60). Second, sheet density is higher for MFC composites, which means more contacts than at lower density, producing a structure more efficient mechanically. Third, hardwood fibers are dried once; without refining, it will have a low bonding potential, producing weak sheet. MFC samples are never-dried which should make a stronger sheet. MFC paper had extremely low permeability compared to the control hardwood fiber paper. The Gurley air permeability test used measures the time required for air, at a given pressure, to pass through a unit area. However, the time required for dewatering the MFC suspension into a paper sheet was also very high (about 15 minutes) and a dense fibrous structure was obtained. Paper entirely made of MFC

cannot practically be drained; it is of interest to investigate whether blending MFC with Hardwood fibers can produce high strength composites that can be drained on a paper machine. An alternative to MFC addition is to refine fibers to increase their fibrillation, thus producing tethered micro-fibrils. Tethered cellulose microfibrils are defined as the fibrils delaminated from the outer layers of the fiber that remain connected by a segment or an extremity. The morphology of microfibrillated fibers (MFC) and tethered fibers obtained from refining are compared on Figure 1. The tethered fibrils on the refined fibers enable binding with the surrounding fibers (Figure 1).

Table II: Properties of 100%MFC, unrefined and refined hardwood (HW) handsheets (basis weight of 60 g/m²)

	Tensile index (Nm/g)		Strain at break (%)		Thickness (μm)	Air permeability (Gurley s)	Apparent density (kg/m ³)	Freeness (ml)
	Dry	Wet	Dry	Wet				
MFC	69.5±5.4	13.6±2.5	3.3±1	11.8±1.2	95±1	42300±562	660±30	-
Unrefined HW	11.1±0.8	1.0±0.1	1.3±0.2	3.4±0.3	127±1	1.4±0.1	461±18	520
500-rev refined HW	17.4±2.6	1.0±0.1	1.4±0.1	3.4±0.4	122±3	1.7±0.2	493±15	520
1,000-rev refined HW	16.9±1.0	1.0±0.1	1.8±0.2	4.3±0.4	105±2	1.8±0.3	535±14	510
2,000-rev refined HW	34.0±4.0	1.3±0.1	3.3±0.4	4.6±0.8	105±2	5.5±1.8	582±12	436
5,000-rev refined HW	40.4±3.6	1.4±0.1	4.3±0.6	4.2±0.7	102±1	18.3±1.9	613±9	343
10,000-rev refined HW	56.8±5.4	1.8±0.1	5.8±0.4	4.0±0.5	97±1	52.2±3.2	620±9	198

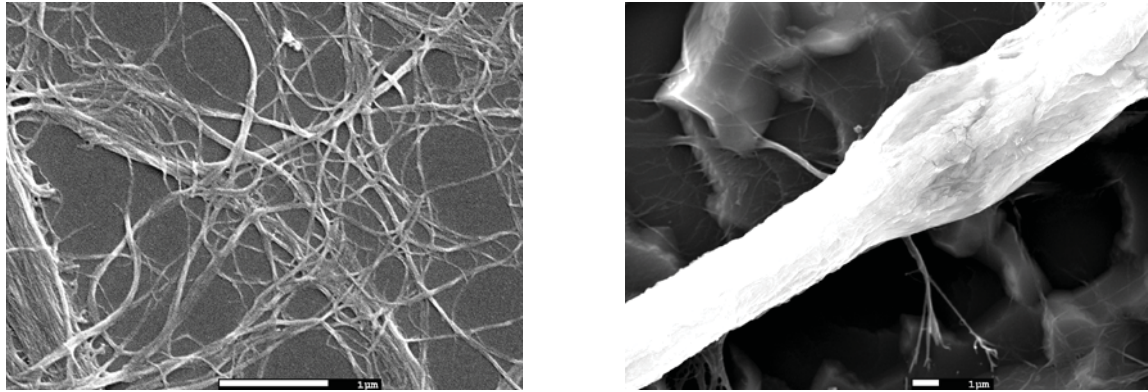


Figure 1: SEM micrographs of (left) free MFC from the commercial product and (right) tethered MFC on refined fibers (10,000-revolutions).

Increasing the MFC ratio in the fiber mixture and using highly refined fibers are two techniques that increase paper density and strength. Two series of paper were prepared and their strength-density relationships are presented in Figure 2. The first series consisted of papers made from fiber blends varying the ratio of MFC/ unrefined

hardwood fibers; the second was achieved by refining hardwood fibers to different extent. The dry tensile indices improved with increased paper density. The strength-density relationship of papers made from MFC and refined fibers paper were both increased up to a density of 625 kg/m^3 , with the MFC composites having a constant slope; strength develops faster than linearly for refined papers of higher density.

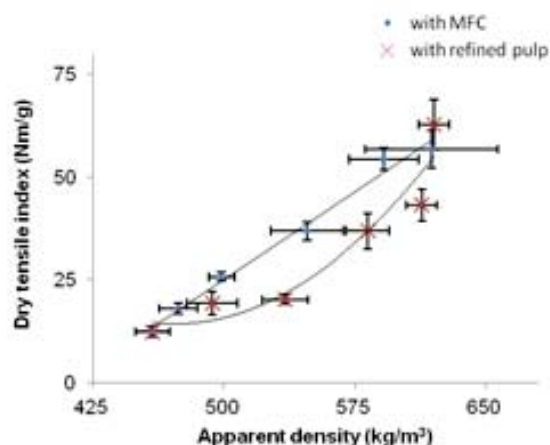


Figure 2: Relationship between dry tensile index and apparent density for composites made from unrefined hardwood fiber-MFC mixtures and refined hardwood fibers.

The morphology and surface structure of composites made from 75% MFC are significantly different from those prepared with highly refined hardwood fibers (10,000-revs) even though both composites have similar strength (Figure 3). MFC (75%) composites have a smoother surface and are more compact than papers made from refined fibers. This might be related to the higher shrinkage of paper made of 75% MFC upon drying; the mean diameter of the handsheet was $155 \pm 2.7 \text{ mm}$, compared to $159 \pm 0.5 \text{ mm}$ for the reference made from 100% unrefined hardwood fiber.

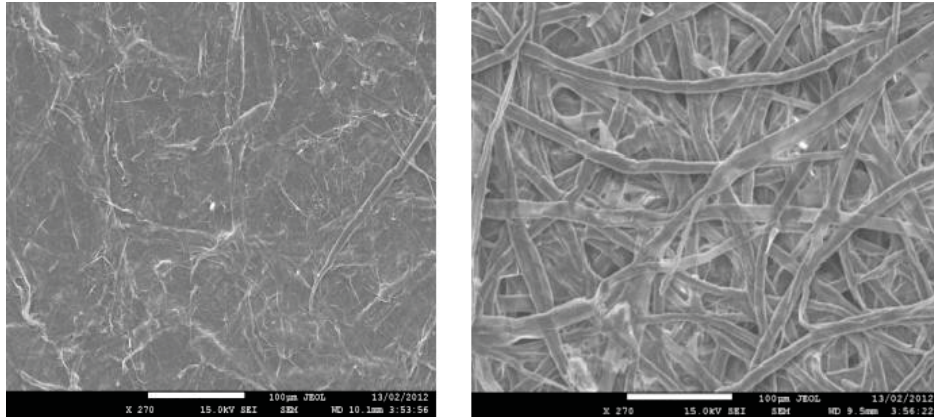


Figure 3: SEM micrographs of composites made with (left) 75% MFC and (right) refined fiber (10,000-revolutions).

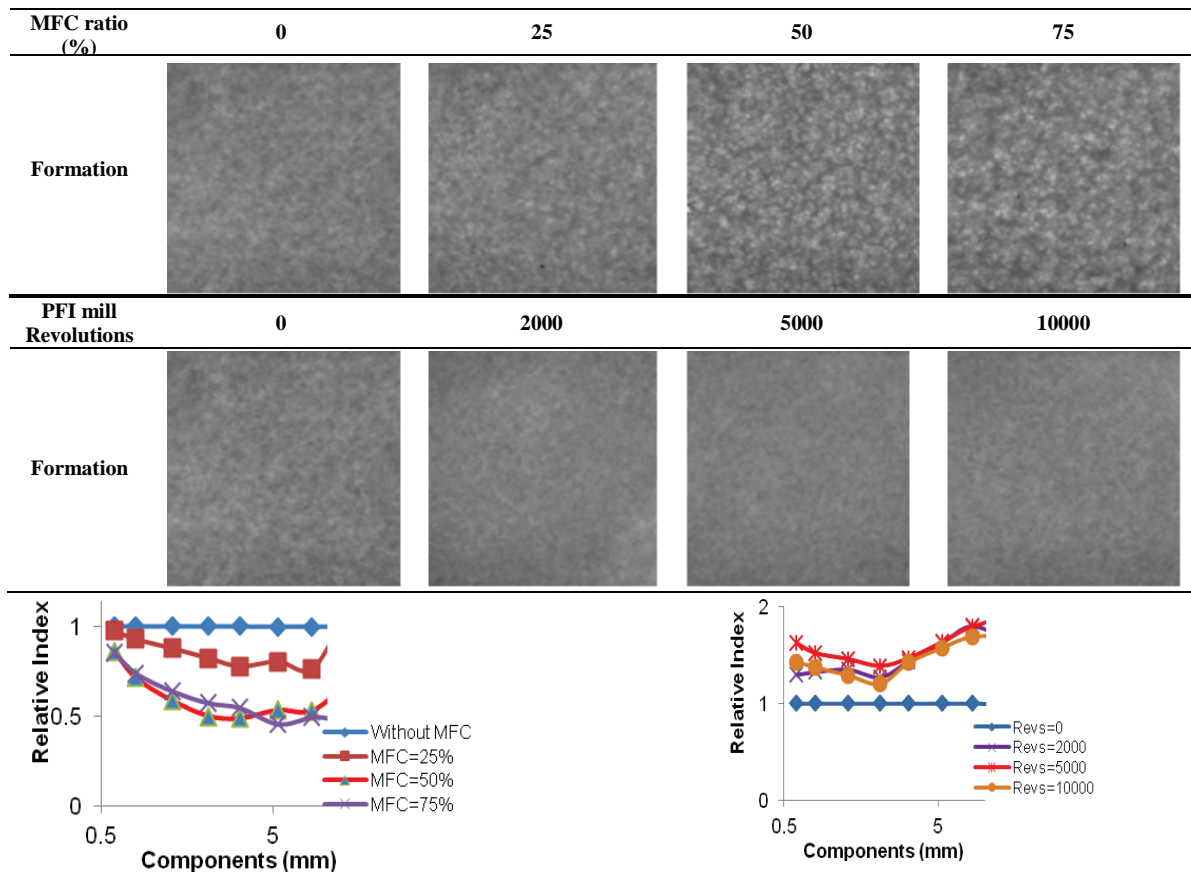


Figure 4: Formation of the composites prepared from MFC and refined fibers. Each image is recorded from the area of 6.75cm ×6.75cm.

The uniformity of paper formation was quantified at different length scales and analyzed with the relative values defined by comparing the sample with a control (Figure 4).

Composite formation uniformity worsened upon MFC addition, especially at the larger inspection sizes around 5 mm corresponding to fiber flocs (Figure 4). In contrast, papers made from refined fibers had improved uniformity of formation at all inspection ranges (0.1-30mm). The air permeability-density relationship of the MFC and refined fibers composites was compared (Figure 5). At a given density, the permeability of papers made from refined fibers was much higher than those containing MFC (lower Gurley values). Air permeability decreased dramatically as the content of MFC increased (Figure 5); by contrast, only a slight decline in air permeability was recorded for the webs made of refined fibers.

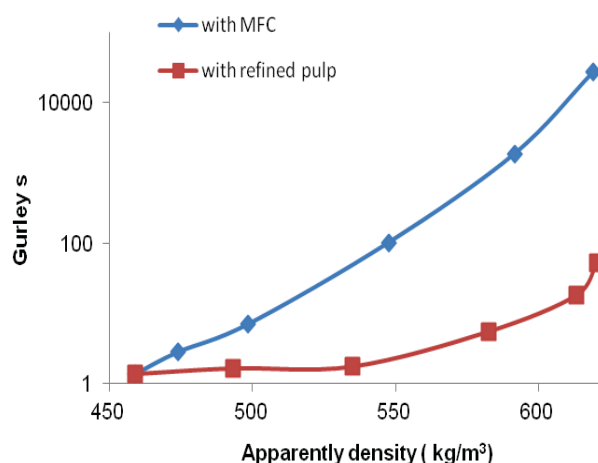


Figure 5: Air permeability-density relationship for composites made of MFC and refined fibers (No PAE addition).

The relationship of wet-dry strength for composites made from MFC and for sheet of refined fibers is presented in Figure 6; it is linear for composite made of refined pulps and exponential for MFC composites. Refining fibers significantly improved the dry tensile index, from 11 ± 1 Nm/g to 63 ± 6 Nm/g, for fibers heavily refined (10,000 revolutions). Refining did not enhance wet tensile to any large extent; a maximum wet strength of 2 ± 0.1 Nm/g was reached compared with 1 ± 0.1 Nm/g for the control. The addition of MFC steadily increased composite strength. The slope of strength development from composites with MFC was higher than that made with refined fibers, indicating that MFC provided significant fibers entanglement frictions in the web. The wet tensile index increased sharply when the MFC ratio rose above 50%. The MFC not only affected the tensile index but also the strain behavior of the papers. Wet composites made of 75%

MFC had higher strain at break than those made from refined fibers (10,000-revs). However, the dry strain of 75% MFC paper was lower (Figure 7).

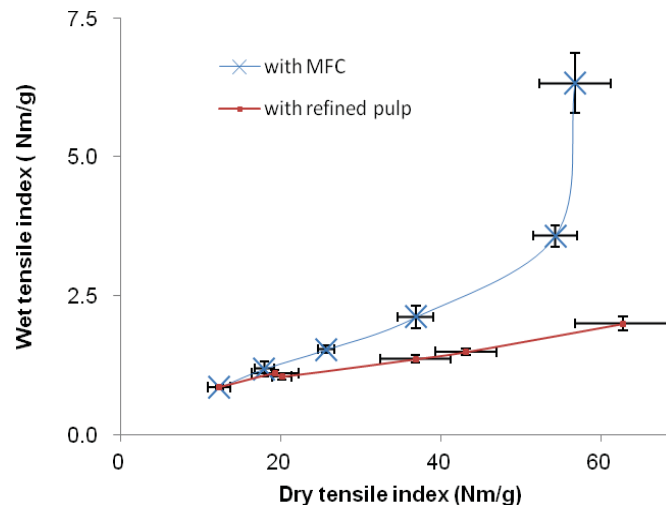


Figure 6: Wet tensile-dry tensile relationship for composites made of MFC and refined fibers (No PAE addition).

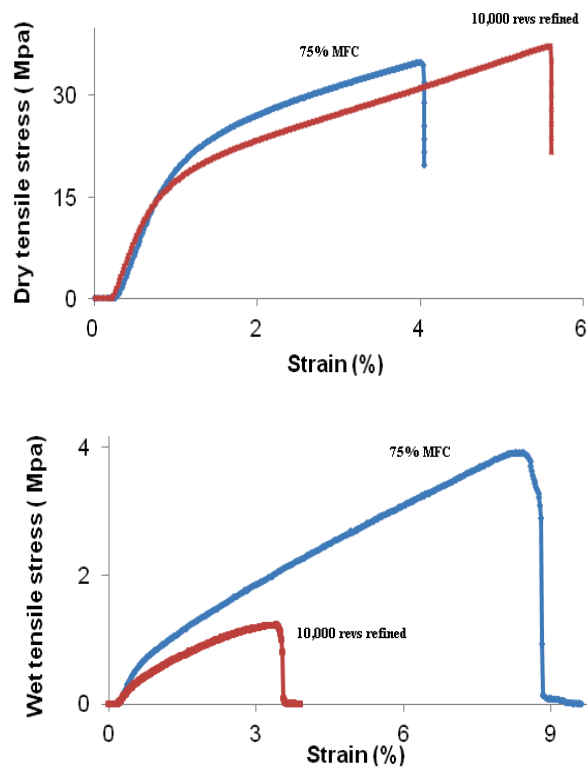


Figure 7: Stress-strain curves of (upper) the dry and (bottom) wet composites prepared by 75% MFC and fibers refined at 10,000 revolutions.

4.4.2 Polyamideamide-epichlorohydrin (PAE) as additive in Cellulose Composites

Polyamideamide-epichlorohydrin (PAE) was adsorbed from solution onto the fibers prior to papermaking for composites made of MFC and refined fibers. Two PAE concentrations were investigated: 2mg/g and 10 mg/g; 2 mg/g corresponds to the theoretical polymer half surface coverage for normal pulp fibers (unrefined) and 10 mg/g is the PAE concentration for maximum wet strength for sheets made of hardwood kraft fibers [24]. PAE addition considerably influenced the dewatering time and air permeability for composites with MFC concentration higher than 10% (Table III). Increased drainage time and reduced composites air permeability were measured with increasing MFC concentration and at 2 mg/g PAE, where the drainage time for paper made with 25% and 50% MFC were 21 ± 3 and 209 ± 16 second, respectively. Interestingly, less time of dewatering and increased air permeability of all MFC composites was achieved at 10mg PAE/g.

The composites dry-wet strength relationships were evaluated with 2 and 10 mg/g for composites made of MFC and refined fibers (Figure 8). With refined fibers and MFC composites, dry strength increased linearly with wet strength, the slope of which was a function of the PAE concentration. The addition of 2 and 10 mg PAE/g substantially improved the composites wet strength and increased the wet over dry strength ratio from 10% to 30%.

Table III: Effect of PAE on drainage for (upper) MFC composites preparation and (bottom) air permeability of the composites.

Drainage time (sec)		MFC ratio (wt %) in unrefined pulp						MFC ratio (wt %) in 10,000-rev refined pulp		
PAE dosage (mg/g)	0	5	10	25	50	75		10	25	50
0	<3	<3	<3	14 ± 0.5	131 ± 8	322 ± 37		8 ± 3	57 ± 14	349 ± 59
2	<3	<3	<3	21 ± 3	209 ± 16	-		-	-	-
10	<3	<3	<3	11 ± 1	100 ± 9	-		6 ± 1	34 ± 2	180 ± 28

Air permeability (Gurley s)		MFC ratio (wt %) in unrefined pulp				Revolutions for refined pulp		
PAE dosage (mg/g)	0	10	25	50		500	2000	5000
0	1.4 ± 0.1	7.1 ± 0.2	103.4 ± 7.6	1905 ± 385		1.7 ± 0.2	5.5 ± 1.8	18.3 ± 1.9
2	1.5 ± 0.2	13.7 ± 1.3	161.1 ± 4.9	2656 ± 55		2.5 ± 0.2	4.1 ± 0.4	10.2 ± 1.2
10	1.3 ± 0	5.7 ± 0.8	60.9 ± 4.1	1279 ± 39		1.6 ± 0.1	2.9 ± 0.2	5.6 ± 0.8

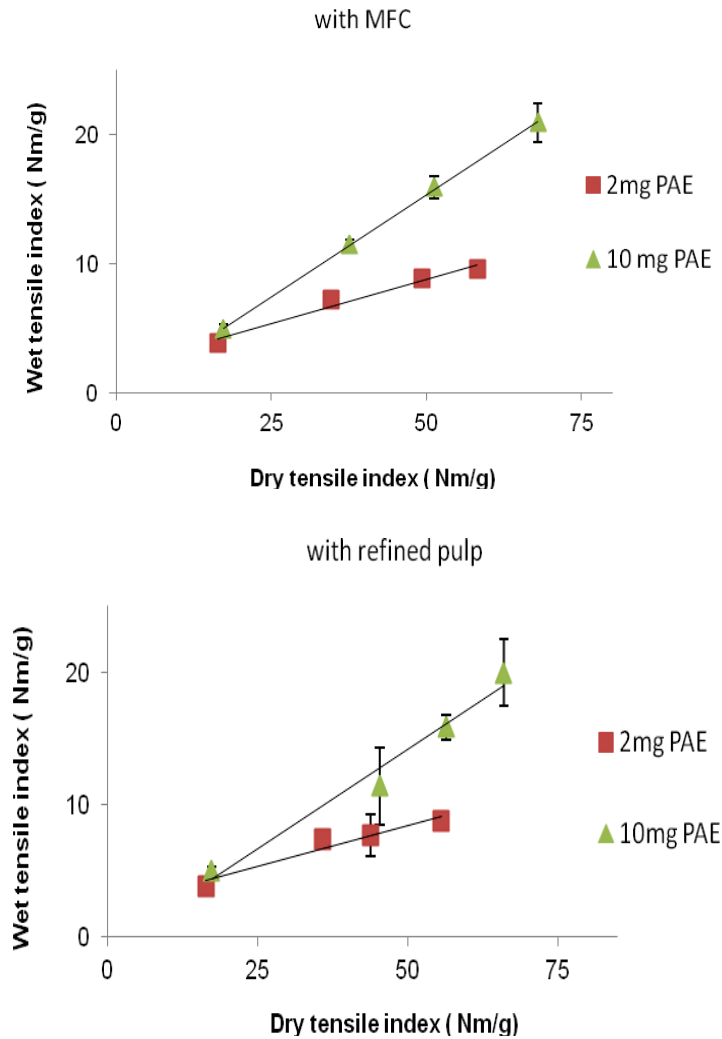


Figure 8: Effect of PAE addition on wet-dry tensile relationship of composites prepared from (upper) MFC and (bottom) refined fibers.

The effect of refining the hardwood fiber fraction on the MFC composites strength properties was investigated. A series of composites were constructed by blending fibers at different MFC/hardwood fiber ratios, with either unrefined or refined (10,000 revs) fibers. These composites were tested for mechanical properties - wet and dry (Figure 9). Without PAE, increasing the ratio of MFC increased strength in all instances. Adding PAE to refined fibers is especially efficient at increasing composite wet-strength. Composites of high and similar wet and dry strength can be achieved by adding PAE to composites made of highly refined (10,000 revs) hardwood fibers and MFC.

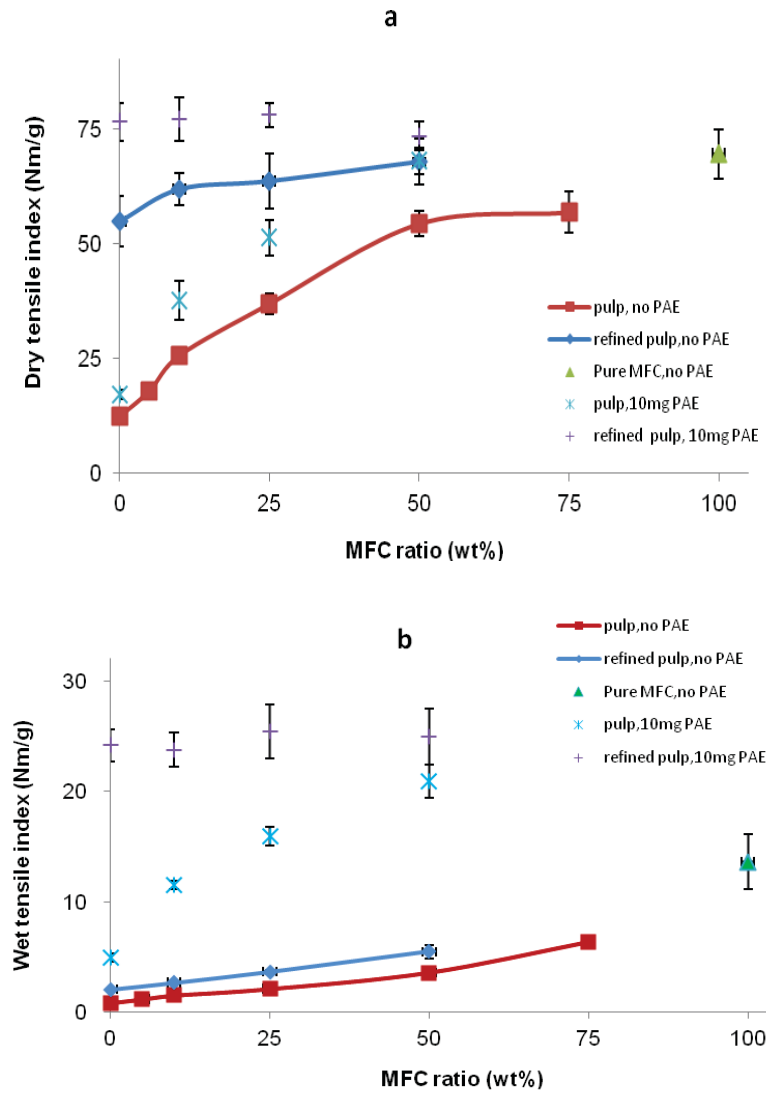


Figure 9: (a) Dry tensile and (b) wet tensile properties of composites prepared by MFC-fibers and MFC-refined fibers mixture.

4.5 Discussion

4.5.1 Effect of MFC on composites process

During refining, the long round cellulose fibers are transformed into collapsed, flexible and flat strips with various levels of surface fibrillation. Meanwhile, some of the primary wall or secondary wall layers are delaminated and become detached from the fibers. More fines are also generated [25]. The contribution of the fines to dewatering increased in inverse proportion to particle size and with increasing surface area [26]. In this study, the drainage time was less than three seconds for all handsheets; their fibers were refined to different extents. The size of the paper remained stable upon unrestrained drying. On the

contrary, the MFC content in the pulp slurry significantly affected the dewatering time (Table III) and the dimensional stability of the paper.

Many methods have been explored to prepare composites made of MFC substrates [13, 14]. The major process consists of dispersing MFC in water and draining using the papermaking process. To achieve a high solid content before pressing and drying, vacuum assisted filtration is commonly used to drain the MFC suspension. Filtration times are very high with drainage times more than half an hour long commonly reported, depending on the final basis weight of the product [13]. This is simply impractical for commercial scaling. Unlike the dimension of traditional fines (Table I), the MFC shows higher aspect ratio (147) and appears to be mainly from the whole of the fiber. The drainage time of our study was proportional to the MFC ratio above 25%, in absence of PAE. This finding is in accordance with literature for MFC (below 10%) monitored by dynamic drainage analyzer [12, 27]. Bonding of the fibrous network is drastically affected by MFC addition, which also increases drying shrinkage [28].

Polymer assisted fiber flocculation is a critical factor governing the drainage of a fiber suspension. The cationic water-soluble polymer also strongly influences the rheological properties of fibrous suspensions. The polymer modifies the interaction between cellulose surfaces via electrostatic force, polymer bridging and steric repulsion. Increasing the PAE concentration to a MFC/fiber fibrous suspension has 3 main effects: 1) coagulate MFC into bigger “fine like” structures, 2) co-flocculate fibers with MFC and 3) modify floc properties (density/compressibility and size). In this study, the increasing drainage resistance observed for the fiber suspension with 2mg PAE/g could indicate the combined effect of free MFC and low density/deformable fiber flocs which can contribute to blocking the wire upon deposition (Table III). At higher PAE dose (10mg/g), most fibers and MFC were flocculated into bigger and especially denser flocs [24], resulting in a fast drainage. The optimization of polymer assisted flocculation can improve paper drainage.

4.5.2 Structure and air permeability of MFC composites

Paper properties are greatly affected by the three-dimensional fibers distribution. Fibers of a nanoscale diameter combined with micron to millimeter length could easily be formed into paper sheets [29]. The uniformity of the composites was analyzed by

transmitted light (Figure 4). The uniformity deteriorated significantly upon MFC addition. However, refining maintained and even improved formation uniformity. Refining has a combined effect of producing fines and increasing fibers flexibility [30]; this could explain the improved uniformity from 2000 revs-refined fibers. However, little additional improvement was observed upon further refining.

Refining fibers did not decrease permeability of composite to a large extent. However, the addition of MFC drastically decreased air permeability of composites by increasing pore tortuosity and decreasing pore area and pore connectivity. MFC films were reported to have similar oxygen transmission rate as common synthetic polymers [17]. Fluid and gas transportation in the fiber network closely relates to the porosity, the ratio of void volume and total volume of paper [31, 32], which can be estimated from density. The air permeability for MFC composites is much lower than those from refined fibers, even at comparable densities (Figure 5). This trend is more obvious at high MFC content, complying with the less porous surface morphology observed by microscopy (Figure 3). The compact structure of MFC composites suggested their distinctive barrier behavior from that of porous paper.

With PAE addition, the air permeance of MFC-containing composites was modified. Air permeance correlated with drainage time (Table III); the longer the time required for dewatering pulp fibers into a web, the longer the period needed for air to diffuse through the dry substrate plane. Although dewatering time reflects the resistance in the dynamic process of wet web forming, it may also indicate the extent of fiber flocculation and substrate structure.

4.5.3 Strength of MFC composites

MFC papers displayed excellent wet and dry tensile indices (Table II) and a higher wet to dry strength ratio (15%) than paper (below 10%) without polymer additives. Unlike paper made of highly refined fibers, increasing the MFC content not only improved the paper dry strength, but considerably promoted wet strength (Figure 6). This property could enable the MFC-made composites to better retain strength under high moisture or wet conditions. An hypothesis is that the larger amount of MFC in the paper web allows more fibers entanglements, and increases inner friction area between fibers, thus leading to

greater wet strength [33]. Another reason is that the much higher aspect ratio of MFC (140) than hardwood fiber (60) produces stronger sheets, as predicted by theory. The dry elongation of MFC and highly-refined fibers composites were similar (Figure 7). Once water penetrates into the cellulosic web, the hydrogen bonding between fibers weakens rapidly [34], leading to a loss in strength and strain of paper from refined pulp (10000 revs). Conversely, the wet MFC composite demonstrates higher strain at break than the dry, The gel-like behavior of swollen MFC may account for the extended strain observed [35].

Viscoelasticity and water plasticization of cellulosic composites are greatly affected by the interaction with polymers [36]. Improved bonding properties against moisture change can be achieved by crosslinking cellulose with cationic-charged, thermal reactive PAE upon drying [37-39]. With PAE, the strength development from MFC composites was similar to that of refined fibers sheets (Figure 8). Two reasons could account for this observation. First, the surface charge of free MFC could have been modified upon cationic PAE adsorption; reorientation of the MFC which occurs during web forming and fiber entanglement would be reduced. Second, wet strength development may be dominated by building up of covalent bonds between the fibers and PAE upon drying, which diminishes the influence of MFC on fiber friction.

MFC blending with unrefined fibers and 10000-revs refined fibers was compared to better understand the role of MFC in strength development (Figure 9). Without PAE, the addition of MFC into unrefined fibers radically increases the relative bonded area and fibers entanglements, resulting in stronger papers. In contrast, the dry strength of composites from the mixture of refined fibers and MFC presented little change despite varying MFC content. This suggests similar MFC and refined fibers bond strength; paper made with 10000-revs refined fibers (tethered MFC) and pure MFC substrate had comparable dry strength (Figure 9a). Yet the mechanism of strength development must be somewhat different as composites made of refined fibers lose much more strength when wet. Refined fibers might allow more hydrogen bonds, and thus closer cellulose-cellulose contacts than MFC addition.

4.6 Conclusion

Novel cellulosic composites of high strength and low gas permeability were produced using the papermaking technology with microfibrillated cellulose (MFC). The effect of blending MFC with hardwood fibers was compared with the refining of the hardwood fibers on the paper composite properties. The hypothesis that refining wood fibers can produce tethered MFC which provide equivalent strength properties but significant drainage benefits was proven. Furthermore, significant benefits in paper formation uniformity (fiber distribution homogeneity) were achieved.

At constant dry strength, composites made with refined fibers had higher density and lower wet strength than those made by blending MFC. This might suggest a higher contribution of hydrogen bonding. The addition of MFC, free or tethered, to pulp fibers combined with polyamideamine-epichlorohydrin (PAE) can increase the dry strength and wet strength of cellulosic materials by an order of magnitude. Air permeability of the composites decreases by up to 4 orders of magnitude with MFC addition, opening new avenues for packaging for food and novel applications.

4.7 Acknowledgement

The financial contribution of Australian Research Council (LP0990526), Visy and Nopco paper technology is acknowledged. The authors would like to thank Misses Sigappi Narayanan and Hui Hui Chiam for experimental assistance, and Mr Swambabu Varanasi for SEM expertise.

4.8 References

1. Nakagaito, A.N. and H. Yano, *The effect of morphological changes from pulp fiber towards nano-scale fibrillated cellulose on the mechanical properties of high-strength plant fiber based composites*. Applied Physics A, 2004. **78**(4): p. 547-552.
2. Iwamoto, S., A.N. Nakagaito, and H. Yano, *Nano-fibrillation of pulp fibers for the processing of transparent nanocomposites*. Applied Physics A, 2007. **89**(2): p. 461-466.
3. Saito, T., S. Kimura, Y. Nishiyama, and A. Isogai, *Cellulose Nanofibers Prepared by TEMPO-Mediated Oxidation of Native Cellulose*. Biomacromolecules, 2007. **8**(8): p. 2485-2491.
4. Saïd Azizi Samir, M.A., F. Alloin, M. Paillet, and A. Dufresne, *Tangling Effect in Fibrillated Cellulose Reinforced Nanocomposites*. Macromolecules, 2004. **37**(11): p. 4313-4316.
5. Janardhnan, S. and M.M. Sain, *Isolation of Cellulose Microfibrils - an Enzymatic Approach*. Bioresources, 2006. **1**(2): p. 176-188.

6. Henriksson, M., G. Henriksson, L.A. Berglund, and T. Lindstrom, *An environmentally friendly method for enzyme-assisted preparation of microfibrillated cellulose (MFC) nanofibers*. European Polymer Journal, 2007. **43**(8): p. 3434-3441.
7. Dufresne, A., D. Dupeyre, and M.R. Vignon, *Cellulose microfibrils from potato tuber cells: Processing and characterization of starch–cellulose microfibril composites*. Journal of Applied Polymer Science, 2000. **76**(14): p. 2080-2092.
8. Nakagaito, A.N., S. Iwamoto, and H. Yano, *Bacterial cellulose: the ultimate nano-scalar cellulose morphology for the production of high-strength composites*. Applied Physics A, 2005. **80**(1): p. 93-97.
9. Leitner, J., B. Hinterstoisser, M. Wastyn, J. Keckes, and W. Gindl, *Sugar beet cellulose nanofibril-reinforced composites*. Cellulose, 2007. **14**(5): p. 419-425.
10. Ahola, S., M. Osterberg, and J. Laine, *Cellulose nanofibrils-adsorption with poly(amideamine) epichlorohydrin studied by QCM-D and application as a paper strength additive*. Cellulose, 2008. **15**(2): p. 303-314.
11. Eriksen, O., K. Syverud, and O. Gregersen, *The use of microfibrillated cellulose produced from kraft pulp as strength enhancer in TMP paper*. Nordic Pulp & Paper Research Journal, 2008. **23**(3): p. 299-304.
12. Taipale, T., M. Osterberg, A. Nykanen, J. Ruokolainen, and J. Laine, *Effect of microfibrillated cellulose and fines on the drainage of kraft pulp suspension and paper strength*. Cellulose, 2010. **17**(5): p. 1005-1020.
13. Sehaqui, H., A.D. Liu, Q. Zhou, and L.A. Berglund, *Fast Preparation Procedure for Large, Flat Cellulose and Cellulose/Inorganic Nanopaper Structures*. Biomacromolecules, 2010. **11**(9): p. 2195-2198.
14. Siro, I. and D. Plackett, *Microfibrillated cellulose and new nanocomposite materials: a review*. Cellulose, 2010. **17**(3): p. 459-494.
15. Klemm, D., F. Kramer, S. Moritz, T. Lindstrom, M. Ankerfors, D. Gray, and A. Dorris, *Nanocelluloses: A New Family of Nature-Based Materials*. Angewandte Chemie-International Edition, 2011. **50**(24): p. 5438-5466.
16. Aulin, C., M. Gällstedt, and T. Lindström, *Oxygen and oil barrier properties of microfibrillated cellulose films and coatings*. Cellulose, 2010. **17**(3): p. 559-574.
17. Syverud, K. and P. Stenius, *Strength and barrier properties of MFC films*. Cellulose, 2009. **16**(1): p. 75-85.
18. Miura, S. and T. Kitaoka, *In situ synthesis of gold nanoparticles on zinc oxides preloaded into a cellulosic paper matrix for catalytic applications*. Bioresources, 2011. **6**(4): p. 11.
19. Varanasi, S., H.H. Chiam, and W. Batchelor, *Application and interpretation of zero and short-span testing on nanofibre sheet materials*. Nordic Pulp & Paper Research Journal, 2012. **28**(2): p. 343-351.
20. Hubbe, M.A. and J.A. Heitmann, *Review of Factors Affecting the Release of Water from Cellulosic Fibers during Paper Manufacture*. Bioresources, 2007. **2**(3): p. 500-533.
21. Chakraborty, A., M. Sain, and M. Kortschot, *Cellulose microfibrils: A novel method of preparation using high shear refining and cryocrushing*. Holzforschung, 2005. **59**(1): p. 102-107.
22. Mao, J.L., J.F. Kadla, and R.J. Kerekes, *Retaining surface fibrillation of wet-beaten wood pulp in the dry state*. Tappi Journal, 2009. **8**(7): p. 25-30.
23. Cole, C.A., M.A. Hubbe, and J.A. Heitmann, *Water release from fractionated stock suspensions. Part 1 - Effects of the amounts and types of fiber fines*. Tappi Journal, 2008. **7**(7): p. 28-32.
24. Su, J., W.K.J. Mosse, S. Sharman, W. Batchelor, and G. Garnier, *Paper strength development and recyclability with polyamineamine-epichlorohydrin (PAE)*. Bioresources, 2012. **7**(1): p. 913-924.

25. Karademir, A. and S. Imamoglu, *Effects of dry strength resin and surfactant addition on the paper made from pulps with different freeness level*. Journal of Applied Sciences, 2007. **7**(4): p. 484-488.
26. Chen, H., A. Park, J.A. Heitmann, and M.A. Hubbe, *Importance of Cellulosic Fines Relative to the Dewatering Rates of Fiber Suspensions*. Industrial & Engineering Chemistry Research, 2009. **48**(20): p. 9106-9112.
27. Varanasi, S. and W. Batchelor, *Rapid preparation of cellulose nanofibre sheet*. Cellulose, 2013. **20**(1): p. 211-215.
28. Manninen, M., I. Kajanto, J. Happonen, and J. Paltakari, *The effect of microfibrillated cellulose addition on drying shrinkage and dimensional stability of wood-free paper*. Nordic Pulp & Paper Research Journal, 2011. **26**(3): p. 297.
29. Zhang, L.Y., W. Batchelor, S. Varanasi, T. Tsuzuki, and X.G. Wang, *Effect of cellulose nanofiber dimensions on sheet forming through filtration*. Cellulose, 2012. **19**(2): p. 561-574.
30. Kontturi, E., M. Suchy, P. Penttilä, B. Jean, K. Pirkkalainen, M. Torkkeli, and R. Serimaa, *Amorphous Characteristics of an Ultrathin Cellulose Film*. Biomacromolecules, 2011. **12**(3): p. 770-777.
31. Jackson, G.W. and D.F. James, *The Permeability of Fibrous Porous-Media*. Canadian Journal of Chemical Engineering, 1986. **64**(3): p. 364-374.
32. Niskanen, K., Suomen Paperi-insinöörien Yhdistys., and Technical Association of the Pulp and Paper Industry., *Paper physics*. Papermaking science and technology 1998, Helsinki ; Atlanta: Published in cooperation with the Finnish Paper Engineers' Association and TAPPI. 324 p.
33. Tejado, A. and T.G.M. van de Ven, *Why does paper get stronger as it dries?* Materials Today, 2010. **13**(9): p. 42-49.
34. Gardner, D.J., G.S. Oporto, R. Mills, and M.A.S.A. Samir, *Adhesion and surface issues in cellulose and nanocellulose*. Journal of Adhesion Science and Technology, 2008. **22**(5-6): p. 545-567.
35. Saarikoski, E., T. Saarinen, J. Salmela, and J. Seppälä, *Flocculated flow of microfibrillated cellulose water suspensions: an imaging approach for characterisation of rheological behaviour*. Cellulose, 2012. **19**(3): p. 647-659.
36. Myllytie, P., L. Salmen, E. Haimi, and J. Laine, *Viscoelasticity and water plasticization of polymer-cellulose composite films and paper sheets*. Cellulose, 2010. **17**(2): p. 375-385.
37. Espy, H.H., *The Mechanism of Wet-Strength Development in Paper - a Review*. Tappi Journal, 1995. **78**(4): p. 90-99.
38. Obokata, T. and A. Isogai, *The mechanism of wet-strength development of cellulose sheets prepared with polyamideamine-epichlorohydrin (PAE) resin*. Colloids and Surfaces a-Physicochemical and Engineering Aspects, 2007. **302**(1-3): p. 525-531.
39. Obokata, T. and A. Isogai, *Wet-strength development of cellulose sheets prepared with polyamideamine-epichlorohydrin (PAE) resin by physical interactions*. Nordic Pulp & Paper Research Journal, 2009. **24**(2): p. 135-140.

Chapter 5

Engineering Paper as a Substrate for Blood Typing Bio-diagnostics

This page is intentionally blank

Declaration for Thesis Chapter 5

Declaration by candidate

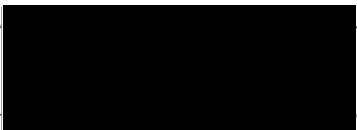
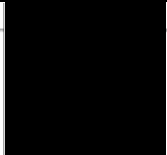
In the case of Chapter 5, the nature and extent of my contribution to the work was the following:

Nature of contribution	Extent of contribution (%)
Initiation, key ideas, experimental and analysis works, development and writing up of paper	70

The following co-authors contributed to the work. If co-authors are students at Monash University, the extent of their contribution in percentage terms must be stated:

Name	Nature of contribution	Extent of contribution (%) for student co-authors only
Mohammad Al-Tamimi	Conducting the experiment of blood typing, key ideas, reviewing and editing of the paper	Research group member
Gil Garnier *	Initiation, key ideas, reviewing and editing of the paper	Supervisor

The undersigned hereby certify that the above declaration correctly reflects the nature and extent of the candidate's and co-authors' contributions to this work*.

Candidate's Signature		Date 2015-3-6
Main Supervisor's Signature		Date

*Note: Where the responsible author is not the candidate's main supervisor, the main supervisor should consult with the responsible author to agree on the respective contributions of the authors.

This page is intentionally blank

Engineering paper as a substrate for blood typing bio-diagnostics

Jielong Su, Mohammad Al-Tamimi and Gil Garnier *

*BioPRIA, Australian Pulp and Paper Institute
Department of Chemical Engineering
Monash University, Clayton, VIC 3800, Australia.*

* Corresponding author: [REDACTED]

Content

5.1	Abstract	145
5.2	Introduction	146
5.3	Experimental Section	148
5.3.1	Blood and Antibodies	148
5.3.2	Paper	148
5.3.3	Method	148
5.3.3.1	Agglutinated RBCs Fixation on Paper.	148
5.3.3.2	Statistical analysis.	149
5.4	Results	149
5.4.1	Agglutinated Blood Fixation on different papers	149
5.4.2	Optimizing Paper properties for blood typing	153
5.5	Discussion	156
5.6	Conclusion	159
5.7	Acknowledgments	160
5.8	References	160

5.1 Abstract

The effect of paper structure on blood typing visualization was quantified and analyzed to engineer low-cost diagnostics. Commercial and experimental papers varying in fibre composition, basis weight, density and porosity were investigated for their ability to separate agglutinated (blood interacted with specific antibodies) from non-agglutinated (blood interacted with non-specific antibodies) red blood cells (RBCs). Antibodies

solutions and blood samples were sequentially absorbed on paper, allowed to interact, eluded with a saline solution, and the intensity of the remaining blood spot was quantified by image analysis. The efficiency and clarity of red blood cell (RBC) separation was quantified with the relative intensity (R.I.) index defined as the intensity ratio of the non-specific test over the specific system; the lower the RI, the better is the separation between a positive from a negative test.

Thick and dense papers are improper for blood typing as they retain indiscriminately both agglutinated and non-agglutinated RBCs. Thin and porous papers provided the best performance. The relative intensity index (the lower the better) increased fairly linearly with paper density and thickness but inversely proportionally with paper pore size. The type of fibres played a minor role. The paper structure is critical in the design of blood typing assay. However, it is only one element of the diagnostic system to engineer with the interactions RBC-antibody-paper.

Keywords: Paper, structure, blood typing, bioassay, diagnostics, antibody, red blood cell (RBC).

5.2 Introduction

Low cost cellulosic blood typing biodiagnostic based on paper and cotton thread have shown great potential for direct medical analysis and reporting. Accurate assessment of blood group is essential for the safe blood transfusion and transplantation medicine [1]. Blood group is determined by the presence or absence of certain antigens on red blood cells (RBCs) [2, 3]. Over 300 different antigens have been identified on RBCs and classified into more than 30 different blood groups, among them the typing ABO and Rhesus D (RhD) blood groups are by far the most important [2, 4]. Every year about 75 million units of blood are collected before a life saving procedure [5]. The identification of ABO and RhD blood group for both blood recipient and donor is essential to prevent incompatible blood transfusion that can lead to fatal haemolytic transfusion reaction [1, 2].

Human blood groups can be identified from the principles of RBCs agglutination using specific antibodies raised against different RBCs antigens. Agglutinated RBCs can be

detected using different assays with reliable sensitivity and specificity rate, including the traditional tube test, microplate and solid phase assays, gel column agglutination and affinity column technology [3, 6-10]. Recently, advanced methods for blood groups identification using gene sequencing and flow cytometry-based assays have been reported [11]. These assays require special laboratory instruments operated by trained laboratory personal which increases the relative cost and test reporting time for these assays [6-8]. Few point-of-care assays can be done without laboratory equipment or blood collection. These assays are associated with higher rate of errors leading to erroneous transfusion [12-20]. Development of simple, rapid and reliable blood grouping assays would be of great value for pre-transfusion compatibility checks and in situations where there is no access to laboratory facilities such as in rural areas and in military applications.

In biodiagnostic for blood typing application, the paper or cotton thread substrates serves three purposes. The first is the driving force to transport by capillarity the blood sample to be analyzed - and reactants if required. The second is to separate the stable RBCs from the agglutinated RBCs by a combination of filtration, size exclusion and chromatography. The third is the simple and direct communication of results. The paper surface and bulk structure and the interactions between paper-antibody-antigen at the liquid-solid interface were previously observed to play critical roles in these three steps [21-23]. However, there has been no systematic study on the effect of paper structure on blood typing analysis.

This study investigates the effect of paper structure for paper-based diagnostics for blood typing applications. Antibodies solutions and blood samples were sequentially adsorbed on the different papers, allowed to rest (30 seconds) before being eluted with a 0.9% saline solution. The papers were dried and the level of RBCs separation was quantified by image analysis. Two types of paper were tested: commercial papers including filter papers, towel and blotting paper, and experimental papers made in our laboratory. The effect of paper basis weight, porosity, density and fibre composition on RBCs separation for specific and non-specific antibody-antigen interactions was analyzed for blood typing applications.

5.3 Experimental Section

5.3.1 Blood and Antibodies

Antibodies against RBC antigens approved for human blood grouping including Anti-A IgM antibodies (clone 51000), Anti-B IgM antibodies (clone 10091) and Anti-D IgM antibodies (clones MS 201) were obtained from Lateral Grifols, Australia. Blood group was identified by a diagnostic laboratory using the standard diagnostic assay (Lateral Grifols, Australia). Blood samples were stored at 4 °C and tested within 7 days of collection. Analytical grades of NaCl, were purchased from Sigma-Aldrich, USA.

5.3.2 Paper

The standard Drink Coster blotting paper 280 gm-2 was from Fibrosystem AB, Sweden. Whatman filter paper (#1, 3, 4, 5, and 113) were purchased from Whatman International Ltd, England. Filter # 2883 was purchased from Adelab Scientific, Australia. Kleenex towel paper manufactured by Kimberly-Clark, Australia was also purchased. The particle retention size of filters was provided by the manufacturers.

Long and short fibres were obtained from disintegration of NIST standard reference material 8495 (Northern Softwood Bleached Kraft Pulp) and 8496 (Eucalyptus Hardwood Bleached Kraft Pulp), respectively. The moving belt sheet former was used to prepare square ($22 \times 22 \text{ cm}^2$) paper. The basis weight and thickness were measured from ten replicates according to Australian/New Zealand Standard Methods 426s and 208s. Capillary rise was determined by Klemm method based on ISO 8787:1986. Basically, papers were cut into $15 \pm 1 \text{ mm} \times 220 \text{ mm}$ strips, which were suspended vertically with their lower end immersed in water. The capillary rise in 10 minutes was measured. The result was the mean value from three measurements.

5.3.3 Method

5.3.3.1 Agglutinated RBCs Fixation on Paper.

Assessment of red colour optical density of blood spotted over specific and non-specific antibodies and subjected to chromatographic elution was essentially performed as previously described (Al-Tamimi et al. 2012). Briefly, Fresh 10 μL droplets of Anti-A,

Anti-B and Anti-D antibody solutions were spotted at 2 cm from the lower edge of blotting, filter or Kleenex and experimental paper strips, followed by the addition of 3 μ L of blood to the center of each antibody spot and allowed to interact for 30 seconds. The paper strip was then suspended vertically with an extremity dipping (about 1cm) in a 0.9% NaCl buffer contained in a thin film chromatography tank for 10 min. The paper was left to dry at room temperature for another 10 min. and a digital picture was recorded using a standard Epson scanner. The intensity of the blood spot after elution was quantified by measuring the mean optical density of the red colour using ImageJ software (National Institute of Health).

5.3.3.2 Statistical analysis.

The optical density of the red colour of blood spot after chromatographic elution was reported as mean \pm standard deviation (SD). Unpaired two-tailed t test was used to compare the mean optical density of blood collected from different donors spotted over specific versus non-specific antibodies, while one way ANOVA test was applied to compare the mean optical density in more than 2 groups. Statistical analysis was performed using GraphPad Prism (version 5) software with $P < 0.05$ considered significant.

5.4 Results

A series of commercial and experimental papers were tested for their ability to separate antibody agglutinated from non-agglutinated blood using a standard technique relying on saline elution and image analysis. The efficiency and clarity of separation was quantified with the relative intensity (R.I.) index defined as the intensity ratio of the non-specific test over the specific system; the lower the RI, the better is the separation between a positive from a negative test. The commercial papers selected included a low density towel, a series of filter papers of different pores size and blotting paper. Experimental papers varying in fibre composition (softwood, hardwood) and basis weight were also tested.

5.4.1 Agglutinated Blood Fixation on different papers

The effect of paper structure on the chromatographic elution of antibody agglutinated and non-agglutinated blood was investigated as technique to identify blood typing (Table I).

A specific and an unspecific droplet of antibody solution were deposited on two different paper strips. A blood droplet of donors with different blood groups (A, B, AB, O, RhD+ and RhD-) was immediately spotted on paper over the typing antibody ring, allowed to interact 30 seconds before the end of the paper strip was contacted with a saline solution and chromatographically eluted for 10 min. The paper was dried, scanned and the colour intensity of the residual blood droplets was measured by image analysis. The optical density of at least 8 replicates was plotted for the filter, blotting & towel and experimental papers in Figure 1. A representative picture of a typical eluted drop of blood group A spotted over specific Anti-A and non-specific Anti-B antibody with different paper substrates is also included in Figure 1. Agglutinated blood, consisting of blood spotted over specific antibodies including blood group A with Anti-A, blood group B with Anti-B, and blood group D with Anti-D, showed a strong fixation on all papers with little variations among the different types of paper. Paper structure had an important effect on the fixation of non-agglutinated blood, which is the blood spotted on a non-specific antibody. For robust blood typing testing, it is critical to avoid any overlap between a specific and an unspecific test, and to maximize their difference in optical density; a low relative index is desired.

The intensity of unspecific and specific blood tests of six filter papers varying in particle size retention was compared (Figure 1A). Good separation between the specific and non-specific tests was achieved with only 3 filters grades (2883, 113 and 4). Blotting paper provided poor intensity differences between specific and non-specific tests, while towel paper yielded near perfect results, with the RBC of non-specific tests almost completely eluding from paper (Figure 1B).

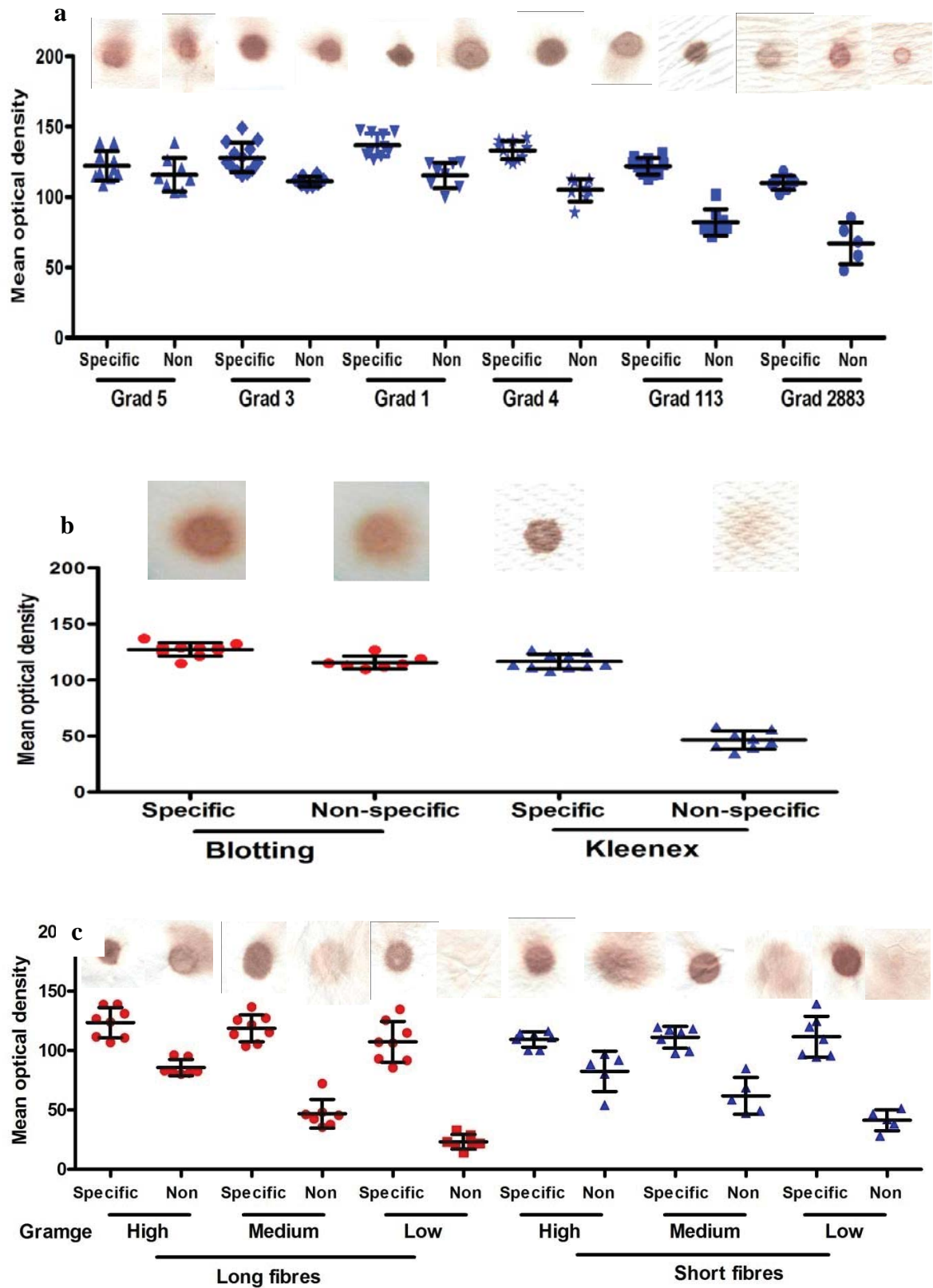


Figure 1: Optical density from blood typing on different papers. A) Filter papers. B) Blotting and Kleenex towel papers. C) Experimental papers made from long and short fibres. (average \pm standard deviation of at least 5 measurements).

Table I: Paper properties. The top section presents the commercial papers, the bottom the experimental papers. Standard deviation from 10 measurements indicated in parenthesis.

paper Properties	Blotting	Grade 5	Grade 3	Grade 1	Grade 4	Grade 113	Grade 2883	Kleenex
Basis weight (g/m ²)	267	96	91	89	94	113	135	28
Thickness (μm)	458(21)	209(3)	221(7)	202(6)	214(2)	396(10)	430 (16)	111(2)
Apparent density (kg/m ³)	582	460	411	439	439	332	315	253
Particle retention size (μm)		2.5	6	11	22.5	30	40	
paper Properties	Long fibre			Short fibre				
	high	medium	low	high	medium	low		
Basis weight (g/m ²)	71	52	25	76	48	24		
Thickness (μm)	127(8)	108(10)	74(11)	192(10)	125(9)	81(5)		
Apparent density (kg/m ³)	559	479	336	396	386	294		

Papers of different basis weights but similar structures were prepared in our laboratory with long (softwood) and short (hardwood) fibres. The orientation of the fibres in paper was kept random to avoid any isotropic effects leading to preferential wicking. These experimental papers were tested for blood typing using the standard technique developed and the optical density from agglutinated and non-agglutinated blood after elution is shown in Figure 1C. Paper basis weight and the type of fibres had very little impact on optical density of the blood dot after saline elution for agglutinated blood (specific) (Table II). However, the mean optical density of blood spotted to non-specific antibodies after elution was significantly lower for low grammage papers (long fibres 23 ± 6 , $P < 0.001$ and short fibres 41 ± 9 , $P < 0.001$) and Kleenex paper (46 ± 8 , $P < 0.001$). There were no overlaps between optical densities for agglutinated and non-agglutinated blood with low grammage papers and the towel.

Table II: Optical density for blood spotted on specific antibodies and non-specific antibodies fixed in different paper substrates. (average \pm standard deviation). Standard deviation is from 8 measurements.

	Optical density for blood spotted on specific antibodies	Optical density for blood spotted on non-specific antibodies	<i>P</i> value
Paper substrate			
Long fibres, 25 g/m ²	107 \pm 17	23 \pm 6	0.0001
Short fibres, 24 g/m ²	112 \pm 17	41 \pm 9	0.0001
Kleenex	116 \pm 7 <i>P</i> = 0.41	46 \pm 8 <i>P</i> < 0.0001	0.0001

**P* < 0.05 considered significant (unpaired two-tailed t test or one way ANOVA).

5.4.2 Optimizing Paper properties for blood typing

Six filter papers of particle size retention ranging from 2.5 to 40 μ m were tested for the relative intensity ratio of their unspecific over specific tests (Figure 2). The size data were provided by the suppliers and the particle retention was rated at 98% efficiency. For filter papers of low particle size retention (lower than 25 μ m), the relative intensities remain high (R.I.>0.75) and decrease slowly with particle retention size. This means the agglutinated and non-agglutinated blood samples were very difficult to distinguish after elution. The relative intensity of blood test decreases steadily, but much faster, for filter papers having a retention size higher than 25 μ m. The most porous filter paper tested, grade 2883 with the size of 40 μ m, had the best relative intensity at around 0.5.

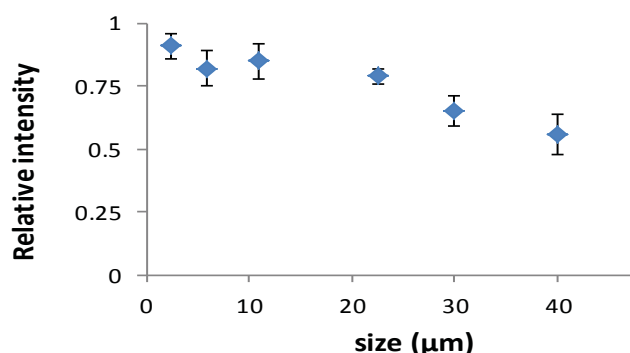


Figure 2: Relationship between blood relative intensity index and particle retention size for different filter papers. The error bars represent the standard deviation from 8 measurements.

The relationship between relative intensity (R.I.) and paper thickness of all papers tested for blood typing was investigated (Figure 3). In general, the thinner substrates have a lower R.I. Thick papers (over 200 μm) retain both individual and aggregated RBC and do not segregate well a positive test from a negative. For thin papers (up to 200 μm) the R.I. linearly increases with the web thickness up to R.I.=0.75 both for long and short fibres papers, forming a master curve. The blotting paper 458 μm thick reached R.I. of 0.88, similar to that of filter grade 5 (thickness of 209 μm). However, two thicker filter papers (#113 with 396 μm and #2883 with 430 μm) demonstrated relatively lower R.I. than those of the other thin filters. These two grades are modified with wet strength polymers.

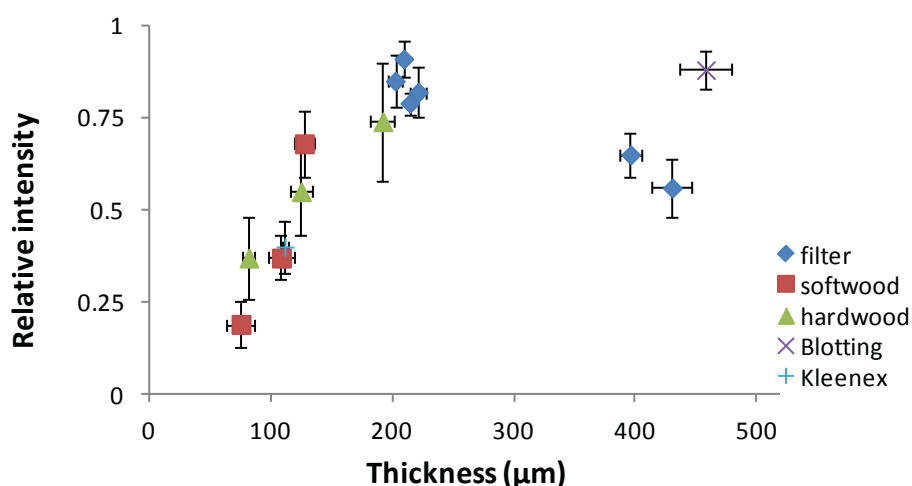


Figure 3: Relationship between blood relative intensity index and paper thickness. The horizontal error bars represent the standard deviation from 10 measurements. The vertical error bars represent the standard deviation from 8 measurements.

For papers made from a given fibre, the R.I. increased linearly with the paper apparent density (Figure 4); papers from each type of fibre yielded a separate curve. The R.I. from long fibres webs gradually raised with density (up to 559 kg/m^3). The minimum R.I. was obtained at 0.19 for a web of long fibres with a density of 336 kg/m^3 , higher than the density of the towel (253 kg/m^3). By comparison with long fibre papers, the R.I. of short fibres papers increased only slightly for basis weight ranging from 48 to 76 g/m^2 . Filters with density above 500 kg/m^3 had high and similar comparable R.I. (0.8 to 0.9) which characterizes poor blood typing. Filter papers with wet-strength additives had lower R.I. with decreased density.

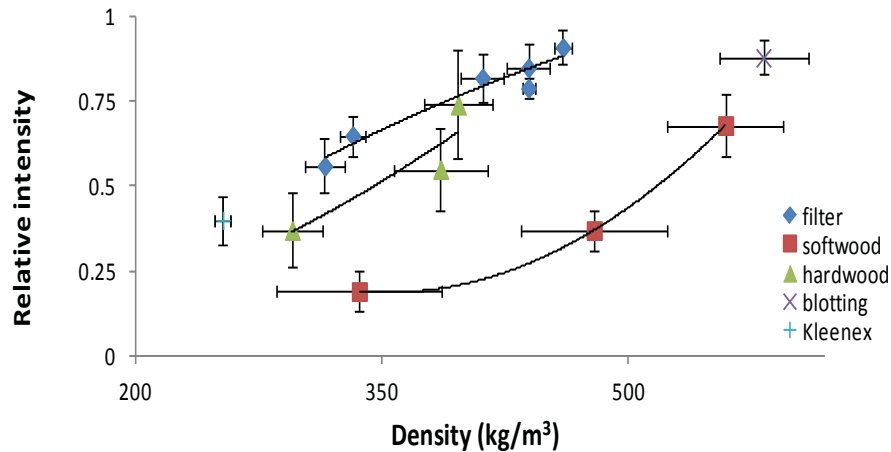


Figure 4: Relationship between blood relative intensity index and paper apparent density. The horizontal error bars represent the standard deviation from 10 measurements. The vertical error bars represent the standard deviation from 8 measurements. Lines are shown to guide the eye.

Paper capillary provides the driving force for elution during blood typing. The capillary rises of water were quantified for the different papers (Figure 5). The blotting paper displayed the lowest rise (60 mm) and the Kleenex towel the highest (104 mm). The experimental papers made from short fibres rose to 97 mm for medium basis weight (48 g/m²), and 102 mm for the high basis weight (76 g/m²). Papers made from long fibres exhibited a lower trend: 82 mm rise for 71 g/m² and 98 mm for 25 g/m².

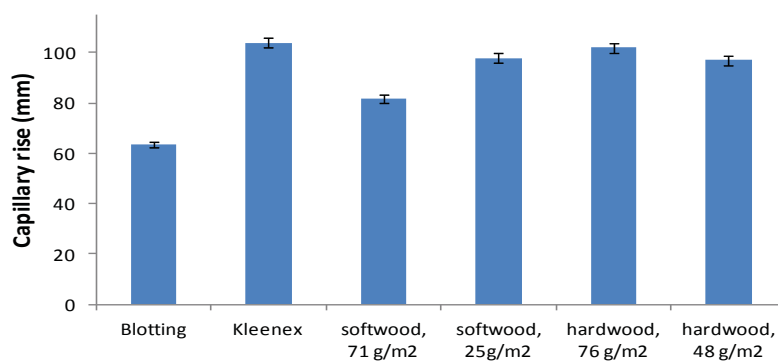


Figure 5: Capillary rise of different paper for blood typing. The error bars represent the standard deviation from 3 measurements.

5.5 Discussion

Measuring the intensity of a blood dot eluded by a saline solution is a convenient and reproducible way to measure the effect of paper structure on blood typing; it is not necessary the preferred embodiment of a commercial paper blood typing diagnostic. The length of the eluded blood can be measured, or better, the test results can directly be printed [24]. This section analyses the role of paper structure on blood typing and the interactions paper-blood-antibody in the context of low cost bio-diagnostics. Specificity is insured by the interaction of the RBC antigen with specific monoclonal antigens triggering blood agglutination.

Paper serves two major functions in blood typing analysis. The first is blood transport, the second is blood separation. Blood transport occurs mostly by wicking along the fibre's long axis and through the inter-fibre spaces [21]. The driving force is capillarity driven by the difference in surface energy between the fluid and the solid. Wicking can be simply described by the liquid flow in a capillary. A velocity (V) for a liquid of viscosity η and surface tension γ flowing in a capillary of radius r and length l can be calculated by the Lucas-Washburn equation [25]:

$$V = \frac{\gamma r \cos \theta_E}{8\eta l} \quad (1)$$

Where θ_E is the equilibrium contact angle, which is a function of chemistry of the liquid, solid surfaces and pore wall geometry [26, 27]. Red blood cell agglutination has two direct effects: a drastic increase in red cell blood viscosity (η) and the reduction of paper capillary (r); both effects decrease the wicking velocity of the red blood cells according to equation 1.

There are a few length scales of interest in paper for blood typing diagnostics. The concept is to agglutinate RBC through specific antibody interaction and to rely on paper for a clear cut segregation between the RBC as aggregates from the stable RBC colloids to communicate typing. It is critical to avoid any overlap between specific interaction and non-specific interaction. Normal red blood cells (RBC) have a diameter ranging from 6 to 8 μm , which is close to the diameter of a eucalyptus (hardwood) fibre (10 μm), and roughly a third of the diameter of a pine radiata (softwood) fibre (30 μm). The hardwood and softwood fibres have lengths of 0.8 and 2 mm, respectively; surface roughness is in the order of the micron [28]. The typing antibodies causing RBC agglutination are

immunoglobulin M (IgM) with diameters of 11 and 40 nm for the individual molecule and the pentamer assembly, respectively [29-31].

Blood separation occurs by a combination of filtration, surface roughness elution and chromatography. For filtration, no significance difference in separation between specific and unspecific tests was recorded for filter papers having a retention size lower than 25 μm . The most porous filter paper tested, with the size of 40 μm , had the best relative intensity of 0.5, meaning that unspecific tests had half the density of RBC of specific test, after elution. Proper dimension of pores are required to immobilize the agglutinated RBCs passing through the cellulose web while allowing the non-agglutinated RBCs to wash away with the solution. The larger pore sizes are likely to enable a better discrimination between the agglutinated from the non-agglutinated RBCs (Figure 1A and 2). We also noticed that the mean optical density from agglutinated blood spots decreased on filter 113 and 2883 (Figure 1a); this suggests that the average substrate pore size (30 and 40 μm , respectively) is only slightly larger than the average RBC diameter, otherwise the agglutinated RBCs would not be sufficiently retained by the substrate. The pore size of the substrate can be designed to optimize the sensitivity and specificity of the test.

The thickness of the substrate is another factor influencing the clarity of blood typing. When antibody solutions were spotted onto different papers, the antibody molecules could either wick and spread over the in-plane surface or penetrate deeper into the thickness of the substrates. We hypothesize that a gradient of antibody concentration was developed along the thickness (z direction) of the substrate. The relationship thickness-R.I. generally reveals that thinner substrates provide more sensitive blood type detection (Figure 3). However, there are exceptions. The thick filters 113 and 2883 showed better performance of blood grouping than the other filters; we believe this was caused by the wet strength polymer, which improved the amount of antibody adsorption on the surface without affecting the antibody activity [32, 33].

The interaction between a specific antibody with red blood cells (RBCc) results in their agglutination. On paper, the antibody can adsorb onto the surface of the fibres and immobilize RBCs through specific antibody-antigen reaction. Once wetted, the antibody, only help by physisorption on paper, can also desorb and diffuse into the blood sample to induce further agglutination of the RBC. This is achieved either by bridging RBCs onto the adsorbed RBC layers on the surface of the cellulose fibre or by the formation of agglutinated RBC particles in the blood sample bulk [21, 23].

The mechanism of interaction between antibody, RBCs and paper to test blood typing is schematically illustrated in Figure 6. The ideal substrate should have a porous structure, where the deposited antibodies could easily interact with specific RBCs while nonspecific RBCs can be easily washed away by solution. This ability may be partially estimated with the apparent density of the substrate. In most cases, low density (high porosity) substrates implied less resistance for mass transportation, thus leading to a clear identification of RBCs (Figure 4). However, the results were obviously affected by the type of fibres, which all possess different surface properties [34].

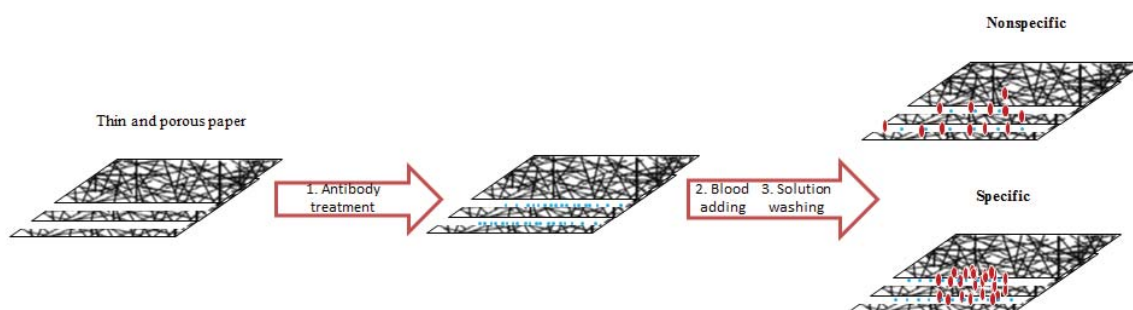


Figure 6: Schematic mechanistic diagram for the effect of paper structure during the blood typing process. Comparison of specific and unspecific test over the thin/porous.

Blood transportation mostly occurs through the interfibre spaces driven by the capillary forces. The capillary rises of water in vertical strips of different substrates were compared using the Klemm method, which is similar to the blood type test studied. A high capillary rise indicates a superior driving force of the fluid into paper; its link to substrate potential for blood typing applications is neither direct nor obvious, and deserves further attention. For paper made of long fibres, blotting and Kleenex paper, a correlation between water rise distance and R.I. of blood typing can be observed by combining Figures 1 and 5; higher water rise distance corresponded to lower R.I. in blood typing. However, papers made from short fibres provide exceptions which emphasize that interactions between fibres, RBCs and antibody must be considered. The paper structure certainly affects blood typing; however, it is only one element of the diagnostic system.

5.6 Conclusion

The effect of paper structure on blood typing visualization was quantified and analyzed in the context of low-cost diagnostics. A series of commercial and experimental papers varying in fibre composition, basis weight, density and porosity was investigated for their ability to separate antibody agglutinated (specific) from non-agglutinated (non-specific) red blood cells (RBCs). Antibodies solutions and blood samples were sequentially absorbed on paper, allowed to interact, eluted with a saline solution, and the intensity of the remaining blood spot was quantified by image analysis. The efficiency and clarity of red blood cell (RBC) separation was quantified with the relative intensity (R.I.) index defined as the intensity ratio of the non-specific test over the specific system; the lower the RI, the better is the separation between a positive from a negative test.

The interaction between a specific antibody with blood results in the agglutination of the red blood cells; the RBCs remain as stable colloids when interacting with their non-specific antibodies. Agglutinated blood remains on paper upon elution with a saline solution disrupting the electrostatic interactions, while the RBCs of non-agglutinated blood simply wash away. This provides the basis for a diagnostic with direct visualization of the cells.

Paper serves three purposes in blood typing diagnostics. The first is to provide, by capillarity, the driving force for the transport of the blood sample and the elution of the saline solution to wash away the non-agglutinated RBCs. The second is to clearly segregate the elution of the agglutinated RBCs (fixed) from that of the non-agglutinated (washed away); this is achieved by a combination of chromatography, surface size exclusion and filtration mechanisms. The third is to directly and visually communicate blood typing results.

Blood typing was best achieved with the low basis weight papers made from softwood fibers. This paper provided a better separation (lower relative intensity) than the commercial Kleenex towel used in our previous work. Thick and dense papers are improper for blood typing as they tend to retain indiscriminately both stable RBCs (non-specific) and aggregated RBCs (specific). Thin and porous papers provided the best performance. The relative intensity index (the lower the better) increased fairly linearly

with paper density, thickness and inversely proportionally with paper pore size. The type of fibres played a minor role. Porous cellulose webs modified with cationic polymers could further optimize blood typing analysis. The paper structure is critical in the design of blood typing assay. However, it is only one element of the diagnostic system that must be engineered along with the control of the multiple interactions of the RBC-antibody-paper system.

5.7 Acknowledgments

Many thanks to Assoc./Prof W. Shen for discussion, and to ARC linkage grants LP0989823 and LP110200973 for funding.

5.8 References

1. Daniels, G. and M.E. Reid, *Blood groups: the past 50 years*. Transfusion, 2010. **50**(2): p. 281-289.
2. Daniels, G. and I. Bromilow, *Essential guide to blood groups*, 2010, Wiley-Blackwell, Chichester, West Sussex, UK ; Hoboken, NJ. p. 1 online resource (x, 111 p.) col. ill.
3. Malomgre, W. and B. Neumeister, *Recent and future trends in blood group typing*. Analytical and Bioanalytical Chemistry, 2009. **393**(5): p. 1443-1451.
4. Daniels, G., L. Castilho, W.A. Flegel, A. Fletcher, G. Garratty, C. Levene, C. Lomas-Francis, J.M. Moulds, J.J. Moulds, M.L. Olsson, M. Overbeeke, J. Poole, M.E. Reid, P. Rouger, E. van der Schoot, M. Scott, P. Sistonen, E. Smart, J.R. Storry, Y. Tani, L.C. Yu, S. Wendel, C. Westhoff, V. Yahalom, and T. Zelinski, *International Society of Blood Transfusion Committee on Terminology for Red Blood Cell Surface Antigens: Macao report*. Vox Sanguinis, 2009. **96**(2): p. 153-156.
5. Klein, H.G., D.R. Spahn, and J.L. Carson, *Transfusion Medicine 1 - Red blood cell transfusion in clinical practice*. Lancet, 2007. **370**(9585): p. 415-426.
6. Beck, M.L., F.V. Plapp, L.T. Sinor, and J.M. Rachel, *Solid-Phase Techniques in Blood-Transfusion Serology*. Crc Critical Reviews in Clinical Laboratory Sciences, 1986. **22**(4): p. 317-342.
7. Lapierre, Y., D. Rigal, J. Adam, D. Josef, F. Meyer, S. Greber, and C. Drot, *The Gel Test - a New Way to Detect Red-Cell Antigen-Antibody Reactions*. Transfusion, 1990. **30**(2): p. 109-113.
8. Harmening, D., *Modern blood banking and transfusion practices*. 4th ed1999, Philadelphia: F.A. Davis. xv, 502 p., 20 col. plates.
9. Knight, R.C. and M. deSilva, *New technologies for red-cell serology*. Blood Reviews, 1996. **10**(2): p. 101-110.
10. Anstee, D.J., *Red cell genotyping and the future of pretransfusion testing*. Blood, 2009. **114**(2): p. 248-256.
11. Roback, J.D., S. Barclay, and C.D. Hillyer, *An automatable format for accurate immunohematology testing by flow cytometry*. Transfusion, 2003. **43**(7): p. 918-927.

12. Eldon, K., *Experience with Abo and Rh Blood-Grouping Cards (Eldon Cards)*. British Medical Journal, 1956. **2**(Nov24): p. 1218-1220.
13. Plapp, F.V., J.M. Rachel, and L.T. Sinor, *Dipsticks for Determining Abo Blood-Groups*. Lancet, 1986. **1**(8496): p. 1465-1466.
14. Blakeley, D., B. Tolliday, C. Colaco, and B. Roser, *Dry Instant Blood Typing Plate for Bedside Use*. Lancet, 1990. **336**(8719): p. 854-855.
15. Giebel, F., S.M. Picker, and B.S. Gathof, *Evaluation of four bedside test systems for card performance, handling and safety*. Transfusion Medicine and Hemotherapy, 2008. **35**(1): p. 33-36.
16. Bienek, D.R. and D.G. Charlton, *Accuracy of User-Friendly Blood Typing Kits Tested Under Simulated Military Field Conditions*. Military Medicine, 2011. **176**(4): p. 454-460.
17. Ingrand, P., N. Surer-Pierres, D. Houssay, and L.R. Salmi, *Reliability of the pretransfusion bedside compatibility test: association with transfusion practice and training*. Transfusion, 1998. **38**(11-12): p. 1030-1036.
18. Dujardin, P.P., L.R. Salmi, and P. Ingrand, *Errors in interpreting the pretransfusion bedside compatibility test - An experimental study*. Vox Sanguinis, 2000. **78**(1): p. 37-43.
19. Ahrens, N., A. Pruss, H. Kieseewetter, and A. Salama, *Failure of bedside ABO testing is still the most common cause of incorrect blood transfusion in the Barcode era*. Transfusion and Apheresis Science, 2005. **33**(1): p. 25-29.
20. Migeot, V., I. Ingrand, L.R. Salmi, and P. Ingrand, *Reliability of bedside ABO testing before transfusion*. Transfusion, 2002. **42**(10): p. 1348-1355.
21. Khan, M.S., G. Thouas, W. Shen, G. Whyte, and G. Garnier, *Paper Diagnostic for Instantaneous Blood Typing*. Analytical Chemistry, 2010. **82**(10): p. 4158-4164.
22. Al-Tamimi, M., W. Shen, R. Zeineddine, H. Tran, and G. Garnier, *Validation of Paper-Based Assay for Rapid Blood Typing*. Analytical Chemistry, 2012. **84**(3): p. 1661-1668.
23. Jarujamrus, P., J. Tian, X. Li, A. Siripinyanond, J. Shiowatana, and W. Shen, *Mechanisms of red blood cells agglutination in antibody-treated paper*. Analyst, 2012. **137**(9): p. 2205-2210.
24. Li, M., J. Tian, M. Al-Tamimi, and W. Shen, *Paper-Based Blood Typing Device That Reports Patient's Blood Type "in Writing"*. Angewandte Chemie International Edition, 2012: p. n/a-n/a.
25. Cecil, R.L. and T.E. Andreoli, *Cecil essentials of medicine*. 3rd ed1993, Philadelphia: Saunders. xxviii, 921 p.
26. Borch, J., *Handbook of physical testing of paper*. 2nd ed2002, New York: Marcel Dekker. v. <2 >.
27. Cassie, A.B.D. and S. Baxter, *Wettability of porous surfaces*. Transactions of the Faraday Society, 1944. **40**: p. 0546-0550.
28. Niskanen, K., Suomen Paperi-insinöörien Yhdistys., and Technical Association of the Pulp and Paper Industry., *Paper physics*. Papermaking science and technology1998, Helsinki ; Atlanta: Published in cooperation with the Finnish Paper Engineers' Association and TAPPI. 324 p.
29. Abe, K., K. Kotera, K. Suzuki, and D. Citterio, *Inkjet-printed paperfluidic immuno-chemical sensing device*. Analytical and Bioanalytical Chemistry, 2010. **398**(2): p. 885-893.
30. Abe, K., K. Suzuki, and D. Citterio, *Inkjet-printed microfluidic multianalyte chemical sensing paper*. Analytical Chemistry, 2008. **80**(18): p. 6928-6934.
31. Di Risio, S. and N. Yan, *Bioactive Paper Through Inkjet Printing*. Journal of Adhesion Science and Technology, 2010. **24**(3): p. 661-684.
32. Pelton, R., *Bioactive paper provides a low-cost platform for diagnostics*. TrAC Trends in Analytical Chemistry, 2009. **28**(8): p. 925-942.
33. Wang, J., R. Pelton, L.J. Veldhuis, C.R. MacKenzie, J.C. Hall, and C.D.M. Filipe, *Wet-strength resins and surface properties affect paper-based antibody assays*. Appita Journal, 2010. **63**(1): p. 32-36.

34. Krueger, J.J. and K.T. Hodgson, *The Relationship between Single-Fiber Contact-Angle and Sizing Performance*. Tappi Journal, 1995. **78**(2): p. 154-161.

Chapter 6

Adsorption of Cationic Polyacrylamide at the Cellulose-liquid Interface: A Neutron Reflectometry Study

This page is intentionally blank

Declaration for Thesis Chapter 6

Declaration by candidate

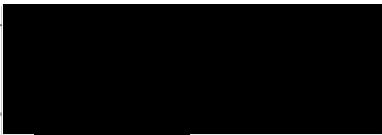
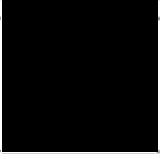
In the case of Chapter 6, the nature and extent of my contribution to the work was the following:

Nature of contribution	Extent of contribution (%)
Initiation, key ideas, experimental and analysis works, development and writing up of paper	70

The following co-authors contributed to the work. If co-authors are students at Monash University, the extent of their contribution in percentage terms must be stated:

Name	Nature of contribution	Extent of contribution (%) for student co-authors only
Christopher J. Garvey	Conducting grazing incidence wide angle X-ray scattering measurement and the data analysis	External collaboration
Stephen Holt	Analysis of specular X ray and neutron reflectometry data	External collaboration
Rico F. Tabor	Conducting atomic force microscopy images measurement and the data analysis, proof reading of manuscript	External collaboration
Bjorn Winther-Jensen	Sharing the expertise on film preparation and film characterization	External collaboration
Warren Batchelor	reviewing the paper	Co-supervisor
Gil Garnier *	Initiation, key ideas, reviewing and editing of the paper	Supervisor

The undersigned hereby certify that the above declaration correctly reflects the nature and extent of the candidate's and co-authors' contributions to this work*.

Candidate's Signature		Date 20/5-3-6
Main Supervisor's Signature		Date

*Note: Where the responsible author is not the candidate's main supervisor, the main supervisor should consult with the responsible author to agree on the respective contributions of the authors.

This page is intentionally blank

Adsorption of cationic polyacrylamide at the cellulose-liquid interface: a neutron reflectometry study

Jielong Su¹, Christopher J. Garvey⁴, Stephen Holt⁴, Rico F. Tabor³, Bjorn Winther-Jensen², Warren Batchelor¹ and Gil Garnier^{1*}

¹BioPRIA- Bioresource Processing Research Institute of Australia, Department of Chemical Engineering, Monash University, ²Department of Material Engineering, Monash University, ³School of Chemistry, Monash University, ⁴Australian Nuclear Science and Technology Organisation (ANSTO).

*Corresponding author. Email: [REDACTED]

Content

6.1	Abstract	168
6.2	Introduction	168
6.3	Experimental Section	171
6.3.1	Materials	171
6.3.2	Method	173
6.3.2.1	Film preparation	173
6.3.2.2	Crystallinity by x ray scattering	173
6.3.2.3	AFM	174
6.3.2.4	X-ray and neutron reflectometry	174
6.4	Results	175
6.4.1	Cellulose film preparation and properties	176
6.4.2	Cationic polyacrylamide (CPAM) absorbed at the D ₂ O/solid interface.	182
6.5	Discussion	188
6.5.1	Smooth Cellulose films	188
6.5.2	CPAM adsorption at the cellulose/D ₂ O interface	190
6.5.2.1	Cellulose swells in D ₂ O	190
6.5.2.2	CPAM absorbed at the cellulose/D ₂ O interface	191
6.6	Conclusion	195
6.7	Acknowledgement	196
6.8	References	196
6.9	Supporting Information	200

6.1 Abstract

The layer thickness and density of high molecular weight cationic polyacrylamide (CPAM) adsorbed at the cellulose-water interface was quantified by neutron reflectometry. The thickness of a full monolayer of CPAM of constant molecular weight (13 MD) but different charge densities, adsorbed with or without NaCl (10^{-3} M), was studied. Thin cellulose films (40 ± 7 Å) of roughness < 10 Å were produced by spin coating a cellulose acetate-acetone solution and regenerating by alkaline hydrolysis. Film smoothness was greatly improved by controlling the concentration of cellulose acetate (0.13 wt%) and the hydrolysis time in sodium methoxide. The adsorption thickness of CPAM (40% charge 13 MD) at the solid-D₂O interface was 43 ± 4 Å on cellulose and 13 ± 2 Å on silicon, an order of magnitude smaller than the CPAM radius of gyration. At constant molecular weight, the thickness of the CPAM layer adsorbed on cellulose increases with polymer charge density (10 ± 1 Å at 5%). Addition of 10^{-3} M NaCl decreased the thickness of CPAM layer already adsorbed on cellulose. However, the adsorption layer on cellulose of a CPAM solution equilibrated in 10^{-3} M NaCl is much thicker (89 ± 11 Å for 40% CPAM). For high molecular weight CPAMs adsorbed from solution under constant conditions, the adsorption layer can be varied by 1 order of magnitude via control of the variables affecting electrostatic intra- and inter- polymer chain interactions.

Keywords: cellulose, CPAM, polymer layer, solid-liquid interface, reflectometry, polyelectrolyte, adsorption

6.2 Introduction

Polyelectrolytes are widely used in industrial and research settings to control the stability of colloids and the interaction properties of surfaces. In papermaking, polyelectrolytes are commonly used as retention aids for process colloids (filler and fines) and as drainage additives. In wastewater treatment, polyelectrolytes coagulate dissolved solids, suspended matter and control the flocculation of sludge; in mining and oil industries, polyelectrolytes improve recovery through selective adsorption. Recent research applications of polyelectrolytes include the retention of enzymes, antibodies and

nanoparticles on surfaces for paper biodiagnostics [1, 2], the development of functional materials, and control of biomolecule activity [3, 4].

Cationic polyacrylamides copolymers (CPAMs) are among the most commonly used polyelectrolytes and are important for industry, because of their efficiency, low cost and availability in a wide range of polymer compositions and structures. CPAM is commercially available with molecular weight and charge densities up to 15 MD and 100%, respectively. The linear charge density of CPAM is defined as the percentage of monomers bearing a formal charge, typically a quaternary amine. However, in spite of their economic and technological importance, the adsorption behaviour of CPAM and the effect of the adsorbed layer morphology on the dynamic stability of colloids are still poorly quantified and understood [5-7], where separate trials are usually needed for each application.

Typically, a polyelectrolyte is adsorbed from solution onto a surface and remains at the liquid-solid interface. The variables affecting the morphology of the adsorbed layer are dictated by the polymer (composition, charge, molecular weight), its affinity for the solvent and surface (Flory-Huggins factor χ), the concentration at which it is adsorbed, solvent properties (temperature, pH, salt concentration and type), surface coverage and kinetics. The theory predicting the basic behaviour of polyelectrolytes in solutions and at interfaces is a topic of active research, and can be expressed mathematically as reviewed by Dobrynin and Rubinstein [8] and Fleer *et al.* [5]; however, the practical behaviour is not well characterised. For polyelectrolytes adsorbed at the interface, Dobrynin and Rubinstein [8] identified 2 regimes. At lower surface charge densities, polyelectrolytes adsorb as two-dimensional layers. For this regime, the balance of the electrostatic attraction between the polymer and charged surface and the electrostatic repulsion between the adsorbed chains control the adsorbed morphology. At high surface charge densities, polyelectrolytes adsorb as three dimensional chains with electrostatic attractions governing the phenomenon [8].

Experimental information on the structure and thickness of adsorbed polyelectrolyte layers remains scarce [5]. The structural features of polyelectrolytes adsorbed at the solid-liquid interface have been quantified by ellipsometry, neutron reflectometry, atomic

force microscopy and the surface forces apparatus. Three key issues remain poorly understood: 1) the morphology of polymers on surfaces, 2) the link between the morphology of the polymer in solution and at the solid-liquid interface, especially under the kinetically controlled conditions used in industry, and 3) the effect of polymer morphology at the solid-liquid interface and colloid stability/surface functionality. This study focuses on the first issue with a special emphasis on CPAM adsorbed onto cellulosic surfaces. Cellulose is an important surface for paper biodiagnostics in which polyelectrolytes can be used to retain biomolecules (antibodies, enzymes, cell) and nanoparticles used to amplify signal. The CPAM-cellulose interaction also plays an important role in industrial processes such as papermaking, painting and coating.

Lindstrom and Soremark measured the adsorption and surface coverage of CPAM on cellulose fibers under the high shear conditions relevant to papermaking [9]. The variables investigated were CPAM charge density, molecular weight and concentration as well as the ionic strength and temperature of the solution. The quantity of polymer adsorbed on fibers was calculated from the CPAM concentration measured in the supernatant by refractive index. An increase in CPAM molecular weight and charge density was found to decrease the amount of CPAM adsorbed on cellulose fibers [9]. The charge stoichiometry was found to be a governing factor [10]. Wagberg et al. also measured the kinetics of polyelectrolyte adsorption on cellulosic fibers, finding a strong correlation with key polymer properties (MW, charge, concentration) [11].

The hydrodynamic thickness (δ) of cationic polyacrylamides on silica is reported to increase as an increasing amount of polymer is adsorbed (Γ) until a plateau is reached. Small cations compete with polymer for surface adsorption and decrease both δ and Γ [5, 12], which represents the typical behavior of electro-sorption of weakly charged polymer chains. A different behavior was reported for hydrolysed polyacrylamides on cationic polystyrene latex with the amount of polymer adsorbed and its layer thickness both increasing with the ionic strength of the solution [13]. This was apparently due to non-electrostatic affinity of the polymer for the surface [5, 13], in contrast to the observation that electrolytes strongly affect electrostatically-driven CPAM adsorption [6, 7, 14-16]. Shubin and Linse reported yet a different behavior for the adsorption of CPAM on silica in which Γ and δ both decreased as a function of the electrolyte concentration. Moreover,

Γ was a function of the type of cation, while δ was mostly independent of this [16]. This was explained by the change in the ratio of adsorbed polymer trains-ends and loops. By competing for the surface, the cations dislodged or prevented trains of polymer from effectively adsorbing on the surface, resulting in a lower adsorbed amount but an increased layer thickness. Solberg and Wagberg reported a similar behavior for the adsorption of CPAM on silica as a function of NaCl concentration using ellipsometry [17].

These previous studies highlight the complex and poorly understood effect of surface chemistry, polymer charge, molecular weight and concentration as well as salt concentration on the morphology of adsorbed polymer. Little is known about the effect of the surface crystallinity, swelling and porosity on the adsorption morphology of polyelectrolyte. Cellulose is the ideal surface to investigate these important variables.

It is the objective of this study to quantify the layer thickness of high molecular weight cationic polyacrylamide (CPAM) adsorbed at the cellulose–water interface using a well-defined system. The thickness of CPAM of different charge densities, but constant molecular weight (13MD) adsorbed with or without NaCl (10^{-3} M), was measured by neutron reflectometry on smooth cellulose films under conditions of full surface coverage. Smooth cellulose films were prepared by spin coating either a nanocellulose crystal suspension or a cellulose acetate solution subsequently regenerated into cellulose by alkaline hydrolysis. The cellulose films were fully characterized and their smoothness and chemical homogeneity were optimized for neutron reflectometry characterisation of their interfaces. In this study, we aim at quantifying how the interaction between cellulose and CPAM can affect the adsorbed polymer morphology, with a view to better understanding the surface interactions involved.

6.3 Experimental Section

6.3.1 Materials

Cellulose acetate ($M_r \sim 29\,000$, acetyl groups substitution $\sim 40\%$), sodium methoxide (purum, $\geq 97.0\%$), methanol (anhydrous, 99.8%) and sodium chloride were purchased from Sigma-Aldrich. Cellulose nanocrystals were graciously provided by U.S. Department of Agriculture in dry powder form. The cationic polyacrylamides (CPAMs) were kindly supplied by AQUA+TECH (Switzerland) and used as received. The specific

polymer formulations were copolymers of uncharged acrylamide with cationic dimethylaminoethylacrylate methyl chloride (Table I and Figure 1a). The charge of CPAM was determined by polyelectrolyte titration from sodium poly(ethylenesulfonate) (Pes-Na, 0.001N, BTG Australia). Polished silicon blocks (50.8 mm diameter, 12 mm and 0.5 mm height, n-type Si:P, [100], El-Cat, Inc. US.) were cleaned for 20 minutes by UV ozonolysis (UVO cleaner ®, model 144AX), and used as substrates for spin coating.

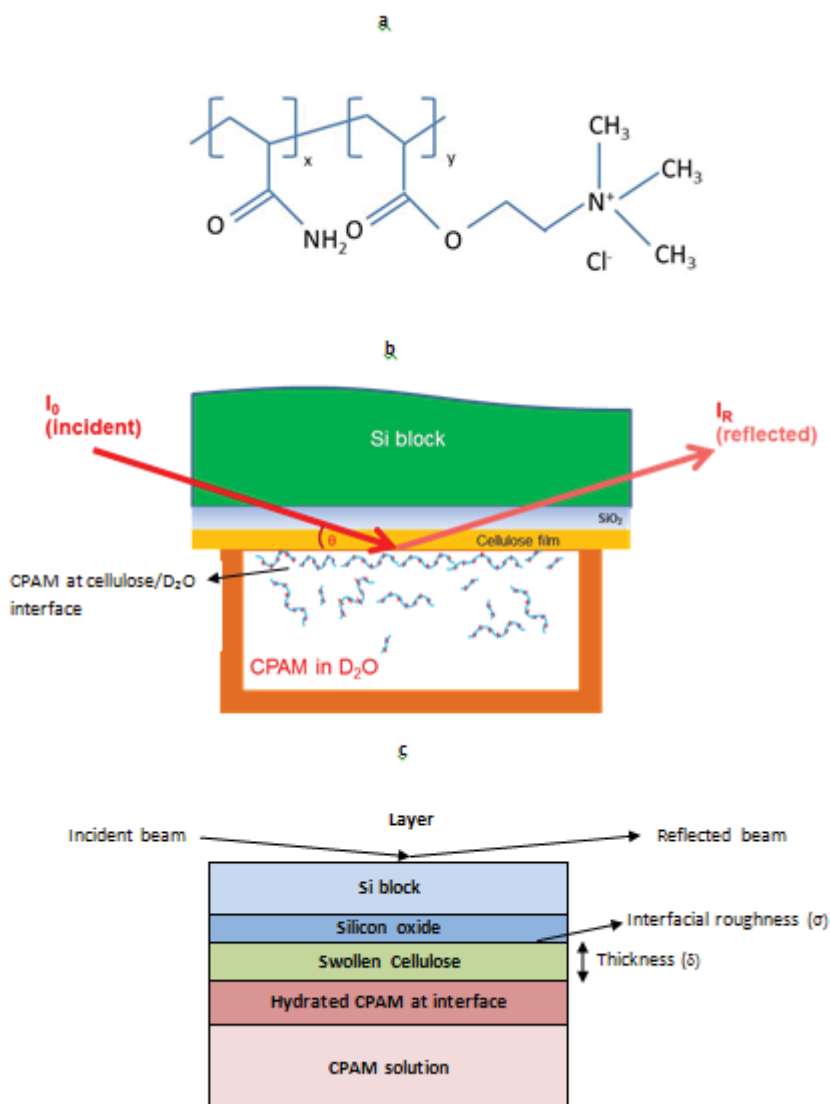


Figure 1: a) Molecular structure of CPAM. b) Configuration of neutron reflectivity measurement for CPAM absorption at the solid/liquid interface. c) Neutron Reflection from a stratified medium.

Table I: The estimated properties of copolymer CPAM consisting of uncharged acrylamide (AM) and cationic dimethylaminoethylacrylate methyl chloride (DMA) monomers, with different charge density but constant molecular weight of 13 MDa (supporting information). Φ and ρ present the volume fraction and neutron scattering length density, respectively.

CPAM	Charge density (wt %)	Molar ratio (AM:DMA)	Φ_{AM} in CPAM (%)	ρ_{CPAM} ($\times 10^{-6} \text{ \AA}^{-2}$)	Radius of gyration (nm)	Chain length (μm)
E1	50	2.7	55.0	1.32	18.1	31.3
F1	40	4.1	64.7	1.42	18.9	34.2
I1	5	51.8	95.9	1.76	21.5	44.4

6.3.2 Method

6.3.2.1 Film preparation

Cellulose acetate (CA) was dissolved in acetone at different concentrations. A 4 mL aliquot of CA solution was placed on the cleaned silicon block and then spin coated (Laurell Technologies Co., PA, model WS400B-6NPP-LITE) at 4000 rpm for 30 seconds. After evaporation of acetone, the cellulose acetate film was hydrolysed to cellulose by soaking it in 0.5% sodium methoxide. The hydrolysis of acetate into hydroxyl was followed using Raman spectroscopy. The CH_3 band around 1375 cm^{-1} , CH_2 band around 1430 cm^{-1} , CH band from 2900 to 3000 cm^{-1} and C=O band from 1730 to 1760 cm^{-1} were monitored [18]. The regenerated cellulose film was washed with deionised water, methanol, and then air dried.

Raman spectra were recorded with a Jobin Yvon T64000 Raman microscope utilizing a 488 nm incident laser with 0.07 mW power at the laser head and a 5% neutral density filter placed between the laser and the instrument. A contact angle measurement system (OCA-230, DataPhysics, Germany) was used to measure water contact angles. To quantify the water contact angle, a water drop of $4 \mu\text{L}$ was placed on the sample and the “Ellipse Fitting” method was used to calculate the contact angle.

6.3.2.2 Crystallinity by x ray scattering

Grazing incidence wide angle X-ray scattering (GIWAXS) measurements were performed on the SAXS/WAXS beam line [19] at the Australian Synchrotron on regenerated cellulose samples on a quartz microscope slide as a substrate. GIWAXS

patterns were accumulated on a Dectris Pilatus 1M detector (DECTRIS Ltd. Switzerland) using 11 keV X-rays and sample to detector distance of 315 mm in grazing incidence geometry. The angle of incidence for GIWAXS measurements were 0.1° , 0.3° and 0.5° . Each GIWAXS image consisted of a composite of 3 images combined to cover the gaps between the modules of Pilatus detector. The 2-dimensional images were processed into the intensity versus scattering vector q using the program Fit2D [20] accounting for the scattering geometry described above, after subtraction of a background (the GIWAXS scattering from a bare quartz slide). A cut, $\pm 5^\circ$, was taken in the specular direction to assess the order of the cellulose chains in the thin film.

6.3.2.3 AFM

Atomic force microscopy images were obtained in AC mode (intermittent contact) using a JPK Nanowizard 3 AFM. The instrument is equipped with capacitive sensors to ensure accurate reporting of height, z , and x - y lateral distances. Cantilevers used were Bruker NCHV model ‘tapping’ mode levers, with nominal resonant frequencies of 340 kHz and spring constants of 20-80 N/m respectively. Imaging was performed with a set-point force of <1 nN. In post-processing, images were ‘flattened’ only by the subtraction of a linear equation from each scan line in the JPK image analysis software; no further manipulations were performed. Height images convert the lateral (z) scale to a colour for ease of presentation. Phase images do the same for the phase information obtained during imaging, *i.e.* the phase difference between the fixed end of the cantilever (driven by the AC piezo) and the free end with the tip where deflection is measured. This phase difference provides information on the way the energy is dissipated by the sample, and can indicate materials with different surface mechanical properties, such as crystalline *versus* amorphous regions, *etc.*

6.3.2.4 X-ray and neutron reflectometry

X-ray Reflectometry Measurements (XRR) and Neutron Reflectometry (NR) were performed at the Australian Nuclear Science and Technology Organization (ANSTO), Lucas Heights, Australia. XRR and NR measurements were made as a function of incident angle (θ), measuring the specularly reflected beam as a function of the momentum change perpendicular to the surface ($q_z = 4\pi \sin \theta / \lambda$, where λ is wavelength of incident beam). The XRR measurements were performed in air on a Panalytical XPert Pro diffractometer operating with $\text{CuK}\alpha 1$ ($\lambda = 1.54056 \text{ \AA}$) radiation using X-rays from a (45

kV) tube source. The q -range corresponds to 0.007 - 0.718 \AA^{-1} and the step size in θ used was 0.01° .

The Platypus time-of-flight neutron reflectometer (ANSTO, Lucas Heights) [21], was used to probe interfacial thickness and density of the CPAM layer in the direction normal to the substrate surface. The reflectometer is on the cold guide CG3 at the OPAL 20 MW research reactor.

Stock CPAM solutions were prepared by first dissolving CPAM at 1 g/L in D_2O for 24 hrs under strong mixing; this solution was then diluted to 0.1 mg/mL in D_2O , with and without NaCl addition, and stirred for at least 12 hrs to ensure proper dissolution of the polymer. For the Neutron reflectometry (NR) measurement, a silicon block (50.8 mm diameter, 12 mm height) coated with regenerated cellulose was fitted in a solid-liquid cell (Figure 1b). 5 mL of CPAM/ D_2O solution was slowly flowed through the cell ($d= 40.5 \text{ mm}$, $z= 0.5 \text{ mm}$, $V= 0.64 \text{ mL}$) which was then closed for measurements. The neutron beam impinged onto the film/water interface by penetrating through the silicon block. Neutron reflectometry (NR) data were collected for a series of conditions where the film was first exposed to pure D_2O , followed by CPAM in D_2O . Cellulose films were swollen in D_2O . The measurements of CPAM absorption were performed at 20°C after at least half an hour further equilibration. Using two angles of incidence, 0.9° and 3.5° , a q -range of ~ 0.010 - 0.265 \AA^{-1} was achieved in this work. The MOTOFIT macro for Igor Pro 6.32A (Wavemetrics, Inc., Lake Oswego, USA) was used to model the XRR and NR data [22] in terms of a minimum of layers of defined thickness, scattering length density (chemical and isotopic composition and density) and roughness between the layers.

6.4 Results

Smooth cellulose films were spin coated on silicon wafer and quartz surfaces and characterized by X-ray reflectometry, AFM, contact angle measurement, and Raman spectroscopy. CPAM was adsorbed from solution onto the cellulose and silicon surfaces, and the thickness of the polymer layer at the solid-liquid layer was measured by neutron reflectometry. The effect of the CPAM charge density and solution ionic strength on the thickness of the CPAM adsorption layer was investigated. The influence of the control variables within the spin coating and cellulose regeneration processes on the cellulose

film properties was first studied. Cellulose films were then prepared under the conditions providing optimal smoothness, and these films used as substrates for the CPAM adsorption study.

6.4.1 Cellulose film preparation and properties

Thin and smooth cellulose films of roughness (variability) lower than the length scale of the adsorbed CPAM layer thickness to be measured (nm range) are required in order to obtain meaningful reflectometry data. A cellulose film roughness lower than 10 Å was targeted. Two types of cellulose films were made by spin coating: cellulose nanocrystals and regenerated cellulose films. Cellulose nanocrystals films form a mostly crystalline surface that does not swell in water; films of regenerated cellulose are expected to be mostly amorphous and show significant swelling in water.

The dry cellulose nanocrystal (CNC) film spin coated on silicon wafers displayed characteristic non-uniform interference colours (Figure 2). The small dark blue spots resulted from large CNC aggregates. The colour surrounding the spots faded out along the radial direction, which represents rough surface coverage. The colour blue of the CNC film is caused by its thickness and also by colour interference reflected by the heterogeneously distributed CNC [23]. The radial arrangement of nanocrystals on the wafer (Figure 2) is similar to that reported on glass and mica [24]. A 57 ± 19 Å roughness was measured by X-ray reflectometry (Table II).



Figure 2: Appearance of cellulose films made from cellulose nanocrystals aqueous dispersion (6.5 wt %) on silicon wafer (diameter=50.8 mm).

Table II: Properties of cellulose films spin-coating from different raw materials. The thickness and roughness were measured by X-ray reflectometry. The average value and 95% confidence interval were from five samples.

Raw material	Concentration (wt %)	Thickness (Å)	Roughness (Å)	Appearance	Reproducibility
Cellulose acetate solution (acetone)	2.5	471±96	28±11	dark blue	Good
	0.4	127±26	19±3	transparent	
	0.13	40±7	7±1	transparent	
Cellulose nanocrystals aqueous dispersion	6.5	133±57	57±19	blue	Poor

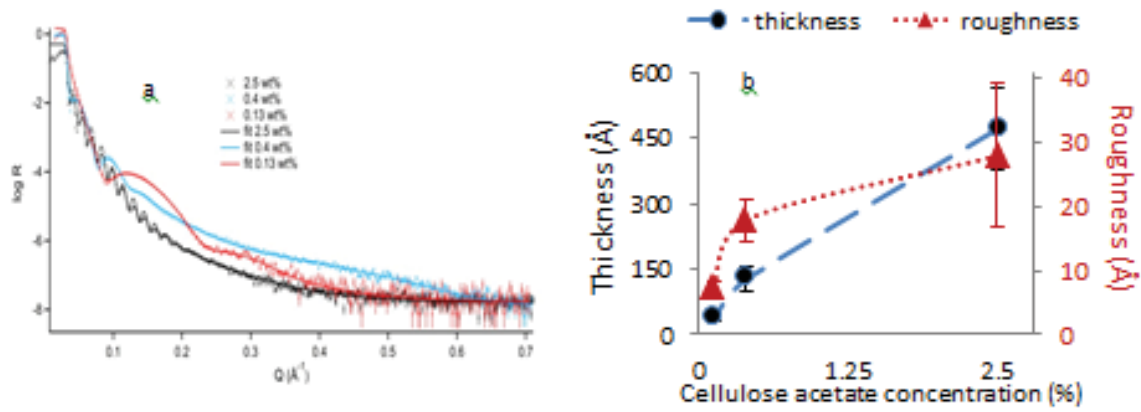


Figure 3: a) X-ray reflectometry of the regenerated cellulose films from different cellulose acetate solutions (in acetone). b) Effect of cellulose acetate concentrations on regenerated films thickness and roughness (Lines shown are to guide the eye).

The preparation of regenerated cellulose films was more reproducible than the CNC film. Spin coating a 2.5 wt% cellulose acetate in acetone solution onto silicon wafers produced regenerated cellulose films 471±96 Å thick, which is greater than the 133±57 Å of CNC films made from a 6.5 wt% aqueous dispersion. We assumed the presence of a surface oxide layer on the silicon block; the roughness and thickness of the silicon oxide layer were 0.2 Å and 4 Å, respectively. However, these regenerated cellulose films were very smooth with a roughness of 28±11 Å, significantly smoother than the CNC films (57±19

Å). Decreasing the cellulose acetate concentration produced thinner and smoother cellulose films (Table II and Figure 3). The thinnest (40 ± 7 Å) and smoothest (roughness of 7 ± 1 Å) cellulose film was achieved at the lowest cellulose acetate concentration of 0.13 wt%, which was selected to prepare all the regenerated films for the neutron reflectometry study.

Cellulose films can be regenerated from acetate cellulose through hydrolysis with a strong base such as sodium methoxide. Most previous studies have used equilibrium conditions to ensure full hydrolysis into cellulose. However, few studies have analysed the impact the regeneration process might have on the cellulose film quality. As part of this study we addressed two questions: 1) what is the effect of regeneration on film thickness and smoothness? and 2) what is the minimum hydrolysis time required to ensure full conversion of the acetate groups into hydroxyls? The effect of regeneration time was studied to optimise the quality of the cellulose films.

The cellulose acetate film thickness of 64 ± 5 Å and roughness of 3 ± 1 Å were measured by X-ray reflectometry (Figure 4A). After 10 mins regeneration by soaking in a sodium methoxide solution, the film thickness was reduced to 40 ± 7 Å, and the roughness considerably increased to 12 Å. As the regeneration period further increased, the film thickness became constant, but the roughness slightly decreased with time (Figure 4B).

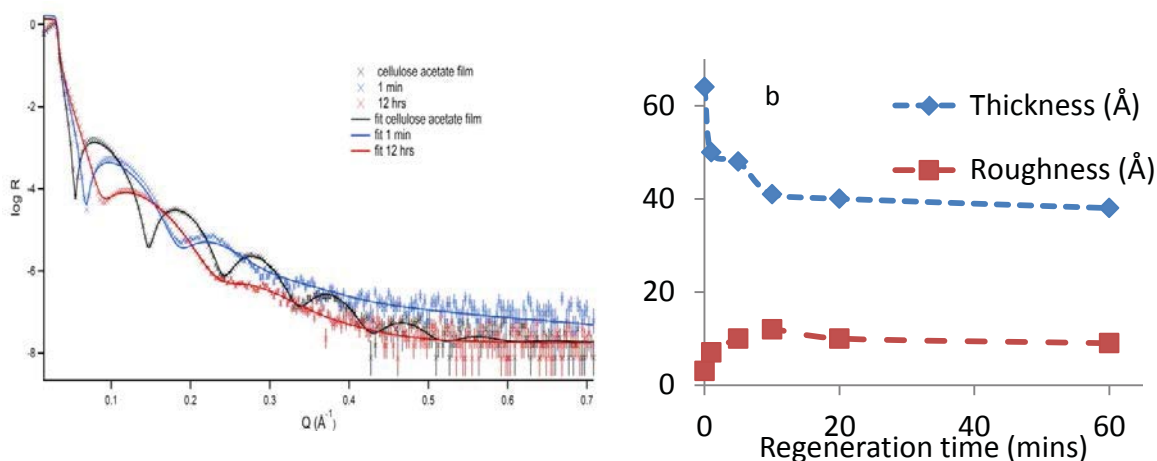


Figure 4: a) X-ray reflectometry of cellulose acetate film from cellulose acetate solution^a (0.13 wt% in acetone) and cellulose films after 1min and 12 hrs regeneration. b) The effect of regeneration time on the thickness and roughness of the film (Lines shown are to guide the eye).

The effect of regeneration time on the surface chemical composition of the cellulosic film was characterized by measuring the equilibrium contact angle formed by water droplets on the surfaces. The contact angle of water on the original cellulose acetate film was $57.1 \pm 3.0^\circ$, characteristic of a moderately wettable surface and in good agreement with literature [25]. After only 1 min of regeneration, the water contact angle of the cellulosic film sharply increased to $76.4 \pm 2.0^\circ$; this was followed by a steady decrease to $31.1 \pm 2.8^\circ$ after 60 mins regeneration (Figure 5). The contact angle of water on the cellulosic film did not significantly change thereafter. The chemical composition of the cellulosic films was also analysed by Raman spectroscopy (Figure 6). After 12 hrs regeneration, decrease of C=O band around 1750 cm^{-1} , CH_3 band around 1375 cm^{-1} , CH_2 band around 1430 cm^{-1} and band of C-H stretching vibration at $2930\text{--}2960\text{ cm}^{-1}$ were confirmed by Raman spectroscopy [18]. This indicates completion of the hydrolysis of acetate into hydroxyl [26].

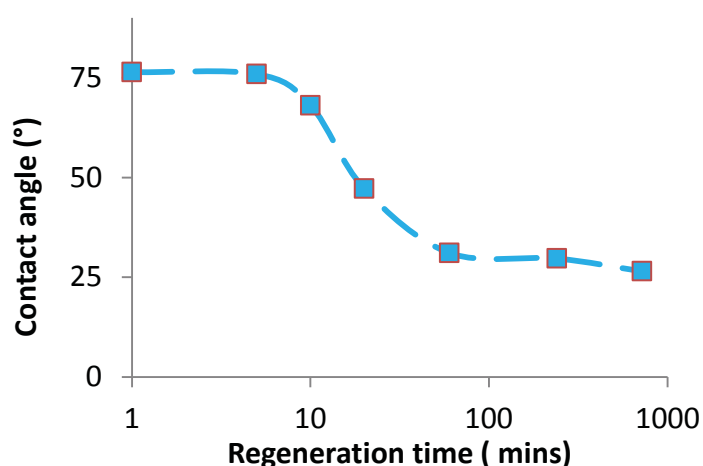


Figure 5: Contact angle (CA) profile for the cellulose (acetate) films after different regeneration time (CA of cellulose acetate film was measured as $57.1 \pm 3.0^\circ$).

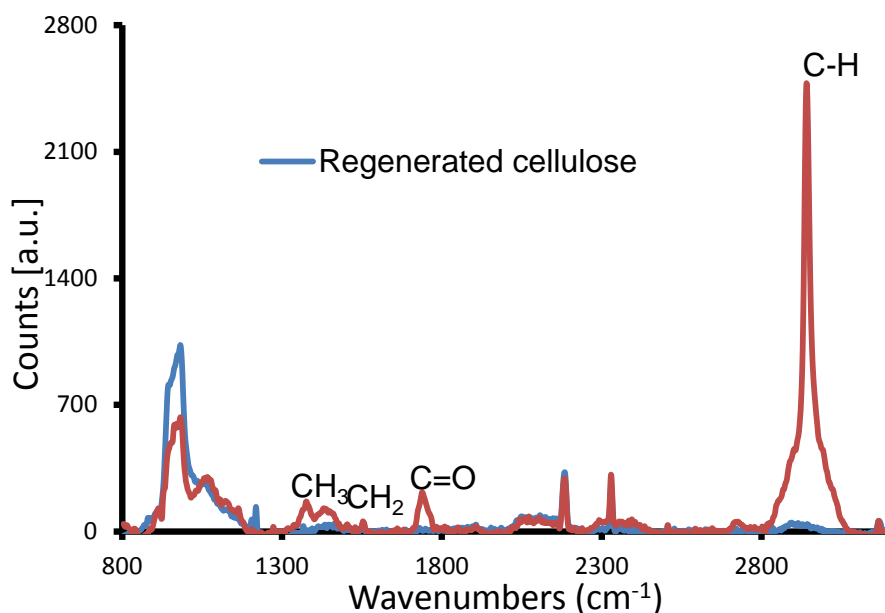


Figure 6: Raman spectra of cellulose acetate film (spin coating from 2.5 % solution) and after 12 hrs regeneration time. The important peaks are labelled.

The morphology of the three types of cellulosic films spin coated on quartz (cellulose acetate, regenerated cellulose and cellulose nanocrystals) was analyzed by AFM (Figure 7) in intermittent contact mode. Root-mean-square (RMS) roughness values across a $1\mu\text{m}^2$ area were: 3.5 nm (CNC), 1.1 nm (regenerated cellulose acetate), and 1.6 nm (cellulose acetate). The length scale of heterogeneity varies among the 3 surfaces, and in the case of CNC films corresponds to the size of the CNC crystals. Phase information from measurements of the CNC films also revealed preferential orientation of the crystals induced by spin coating.

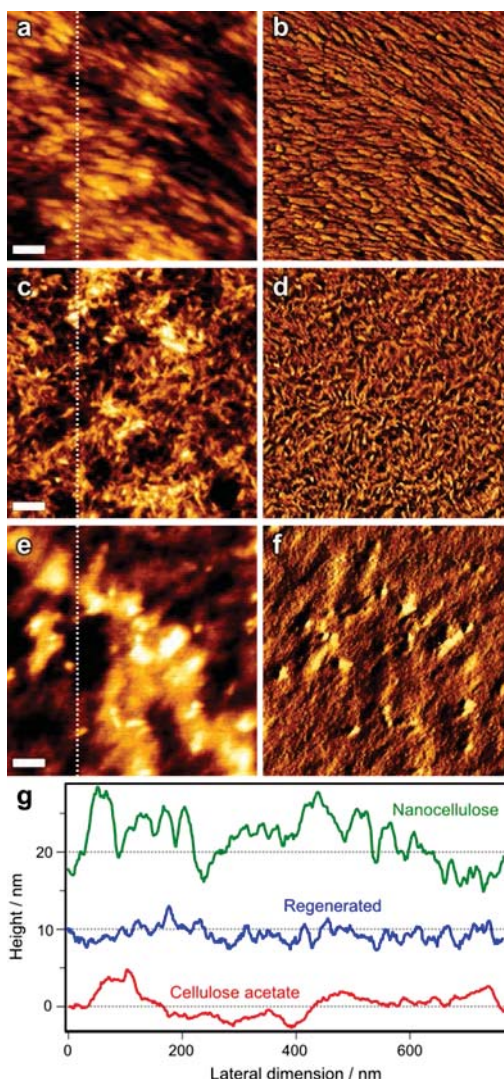


Figure 7: AFM images and extracted parameters from nanocellulose (a, b), regenerated cellulose acetate (c, d) and pure cellulose acetate (e, f) films. In each case, the left-hand pane (a, c, e) shows height information (wherein the height scale is defined by the line profile in (g) and the right hand pane (b, d, f) shows the phase information. The scale bars represent 100 nm. Line profiles of selected cross-sections are shown in (g), representing the sectional heights defined by the dotted lines in (a, c, e). The two uppermost traces are vertically offset by 10 and 20 nm as indicated by their ‘zero’ lines, for clarity of presentation.

The major feature of the specular cut of GIWAXS 2d data images (Figure 8) is a very broad peak centred at 1.44 \AA^{-1} . The feature does not change in shape with increasing incident angle but shifts to slightly higher q values with increasing incident angle. This is the correct value for the position of the amorphous halo. The most intense reflections of

cellulose II occur at $q = 1.5 \text{ \AA}^{-1}$, there is no evidence of cellulose II diffraction peaks [27]. Within the range of depths probed by the evanescent X-ray beam [28], the cellulose film is completely and homogeneously amorphous. GIWAXS measurement of the cellulose nanocrystal film revealed high crystallinity (Fig S2, Supplementary information).

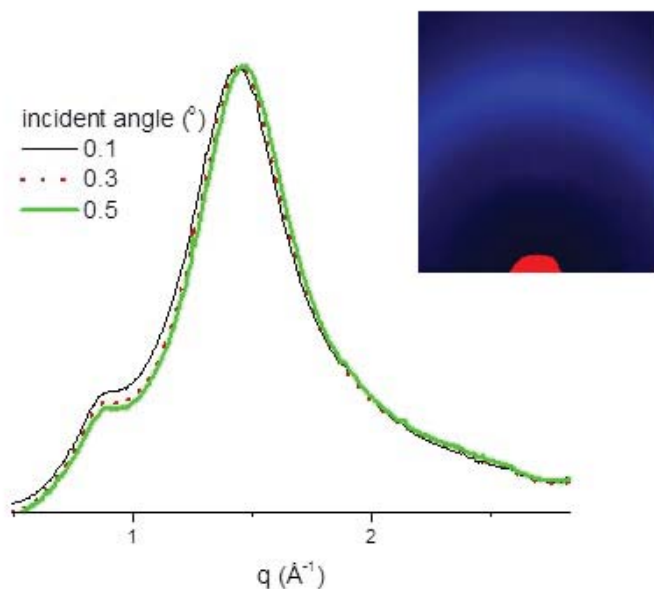


Figure 8: Peak intensity normalized GIWAXS profiles in the specular direction from a regenerated cellulose film on quartz substrate as a function of incident angle. The inset shows a typical GIWAXS image. The beam stop is masked by red.

6.4.2 Cationic polyacrylamide (CPAM) adsorbed at the D₂O/solid interface.

CPAM was adsorbed from solution onto smooth regenerated cellulose films, and the thickness of the polymer layer at the liquid-solid interface was measured by neutron reflectometry. This was achieved under conditions of CPAM surface excess expected to produce a full polymer monolayer, and polymer concentration and molecular weight were kept constant at 0.1 mg/mL and 13 MD, respectively. From the CPAM charge density and molecular weight (13 MDa), the radius of gyration (R_g), end-to-end distance and scattering length density (SLD) of the polymers were calculated (Table I & Fig S1, supporting information).

Specular neutron reflectometry data were fitted using the solvent penetration mode in Motofit, with the Abeles Formalism to fit multiple contrast neutron and X-ray reflectometry data. The measured reflectivity depends on the variation in the scattering length density (SLD) profile, ($\rho(z)$) perpendicular to the interface. The interfacial structure was approximated by a slab model with layers of thickness (δ), roughness (σ), SLD (ρ) and volume fraction (Φ) of solvent.

Motofit minimises the difference between the theoretical and measured reflectivity curves, by changing the parameters (δ , σ , ρ , Φ) that describe each layer (Figure 1c). As the thickness of the thin film is well-defined and its roughness is low, the NR spectra of thin films display oscillations (Kiessig fringes) which are directly related to the total thickness of the multilayer film [29]. Roughness is implemented in terms of an error function [30] and defined as the standard deviation of the erf function. The scattering length density profile SLD (ρ) of the materials forming the layers is calculated with:

$$\rho = \frac{N_a \rho_{\text{mass}}}{M_R} \times \sum_{i=1}^n b_{\text{ci}} \quad (1)$$

where b_{ci} is the bound coherent scattering length of the i^{th} atom of a molecule with n atoms. N_a is Avogadro's number, ρ_{mass} is the mass density of the material and M_R is its relative molecular mass.

For CPAM copolymers consisting of uncharged acrylamide (AM) and cationic dimethylaminoethylacrylate methyl chloride (DMA) monomers, ρ can be calculated from the individual ρ for AM and DMA, and their volume fractions (Φ) using equation (2):

$$\rho_{\text{CPAM}} = \rho_{\text{AM}} \times \Phi_{\text{AM}} + \rho_{\text{DMA}} \times (1 - \Phi_{\text{AM}}) \quad (2)$$

In this study, ρ_{AM} , ρ_{DMA} and the molecular volumes are calculated by assuming a density of 1.3 g/cm³ [31, 32]. SLDs of 1.76, 1.42 and 1.32 (10⁻⁶ Å⁻²), were calculated for CPAM with charge densities of 5, 40, and 50 wt%, respectively. These values were used for fitting neutron reflectometry data and calculating the properties of the CPAM layer at the interface.

Optimal fitting of the NR results with the model was achieved by assuming the proton-deuterium exchange [33] in the hydroxyl groups of the cellulose in D₂O [34] which corresponds to a cellulose density of 1.48 g/cm³. As the regenerated cellulose films are completely amorphous, we assumed full exchange would occur. The ρ value of deuterium exchanged cellulose (C₆H₇D₃O₅) is 3.39×10⁻⁶ Å⁻², which resulted in a better fitting with a

much lower χ^2 than using the value of $1.67 \times 10^{-6} \text{ \AA}^{-2}$ from the protonated cellulose ($\text{C}_6\text{H}_{10}\text{O}_5$), and the value of $3.39 \times 10^{-6} \text{ \AA}^{-2}$, was used to calculate the volume fraction of D_2O .

In addition to the thickness and roughness of the cellulose film, the volume fraction (Φ) of solvent (D_2O) in the layer can be determined from the calculated SLDs of the substances (cellulose or CPAM and D_2O) forming the layer. In Motofit, given ρ for a layer, then the solvent volume fraction is automatically calculated. As the model fitting is completed, all parameters (δ , σ , ρ , Φ) and chi squared (χ^2) are updated. A lower χ^2 indicates a minimisation of the differences between the measured data and the calculated fit.

The layer properties in D_2O studied by NR, with or without NaCl, are summarized in Table III. The average and 95% confidence interval is from three optimal fitting results. The adsorption thickness of CPAM-40% on silicon ($13 \pm 2 \text{ \AA}$) is thinner and smoother than on regenerated cellulose film ($43 \pm 4 \text{ \AA}$)-Figure 9. The surface layer density (SLD) for the D_2O /CPAM (40% charge)/cellulose/silicon interface is shown in Figure 9B.

Table III: CPAM adsorption at the solid/ D_2O interface was studied by the specular NR measurement. Thickness (δ), roughness (σ), and volume fraction (Φ) of D_2O in the layer were retrieved by fitting the NR curves. The absorbed amount (Γ) of CPAM was calculated with the absorbed layer δ and Φ . χ^2 indicates the quality of fitting, and the lower value of χ^2 indicate better fits from minimizing the differences between the theoretical and measured reflectivity curves. The reflectivity data were co-refined by at least two data sets where the solid substrate was exposed in D_2O without and with CPAM. $\rho_{\text{D}_2\text{O}} = 6.35 \times 10^{-6} \text{ \AA}^{-2}$. The 95% confidence in parenthesis is from three optimal fitting results.

Chapter 6

Solid interface	CPAM charge density (wt %)	χ^2	NaCl (mM)	Properties					
				Layer	δ (Å)	σ (Å)	Φ_{D20} (%)	Γ (mg/m ²)	Charge cover (μeq/m ²)
Cellulose	40	2.56	0	Cellulose	97 (10)	3 (1)	69 (5)		
				CPAM	43 (4)	7 (1)	96 (4)	2.3	2.3
			1 ^a	CPAM	20 (3)	2 (1)	95 (4)	1.3	1.3
		2.03	1 ^b	Cellulose	102 (9)	2 (1)	65 (4)		
				CPAM	89 (11)	9 (1)	97 (5)	3.5	3.5
	5	3.68	0	Cellulose	106 (11)	2 (1)	69 (4)		
				CPAM	10 (1)	8 (1)	82 (5)	2.4	0.3
	50	2.01	0	Cellulose ^c	68 (7)	4 (1)	97 (4)		
				CPAM ^d	156 (13)	38 (4)	6 (4)	201.8	274
				CPAM ^e	95 (10)	30 (6)	66 (4)	95.4	124
Si (SiO _x)	40	1.01	0	CPAM	13 (2)	1 (0)	32 (8)	12.8	12.8

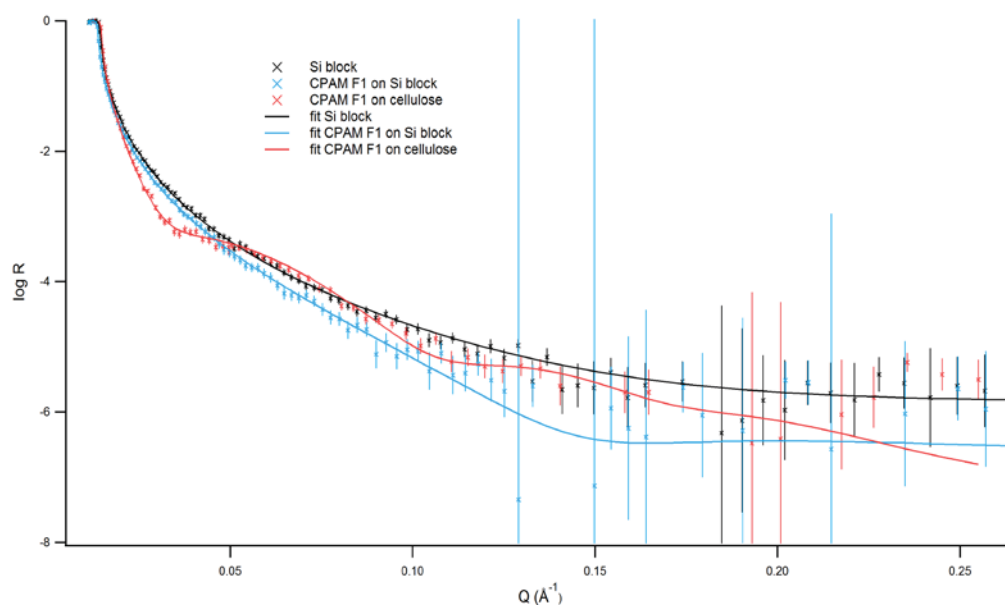
a: NaCl solution was added after CPAM adsorption.

b: CPAM was prepared in NaCl solution before adsorption.

c: The cellulose film is from 0.1 wt% CA solution

d: CPAM with 50% charge absorbed at the interface were divided into 2 layers to improve the fitting (decrease the χ^2).

e: The CPAM sublayer stretched out to D₂O.



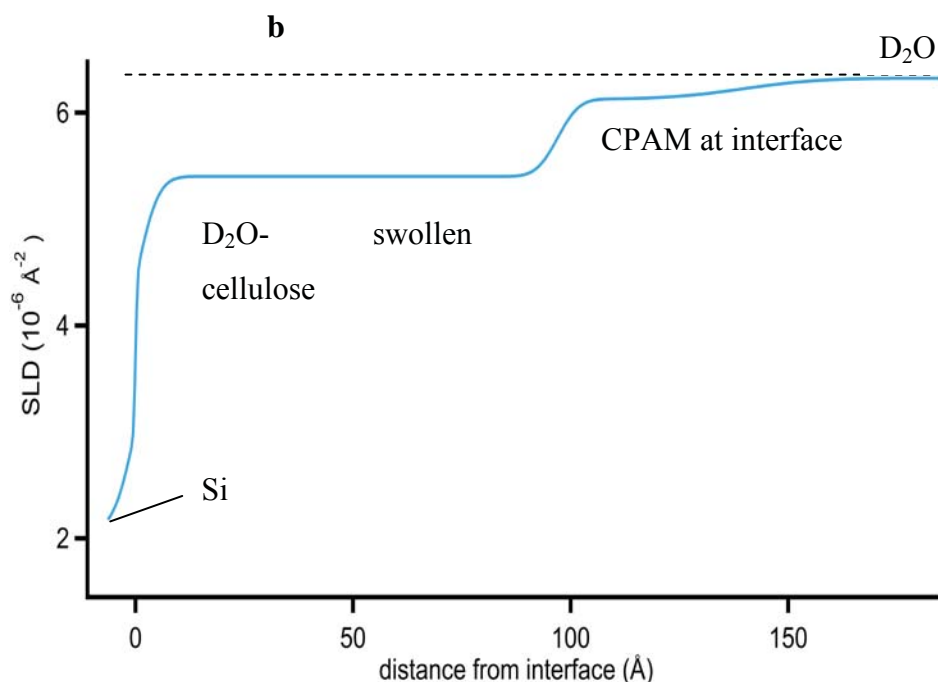


Figure 9: a) Neutron reflectivity from silicon surfaces with regenerated cellulose and CPAM adsorbed at two interfaces: Silicon with native oxide layer and cellulose film. b) SLD profile from simultaneous fits to the CPAM F1 on cellulose in part a.

During measurement, swelling of cellulose film was observed which increased film thickness (~ 100 Å); the volume fraction of D_2O in the film is 67%. The volume fraction of D_2O in the high charge adsorbed CPAM layer (40% charge) is 96%, higher than the 82% of the low charge CPAM (5% charge) - fitted by CPAM monolayer model. However, the layer thickness at the interface increased with higher charge density (Table III). The adsorption thickness of CPAM of charge density of 5% and 40% were 10 ± 1 Å and 43 ± 4 Å, respectively. The double-layer model improved the fitting (low χ^2) for the 50% CPAM absorbed, and its calculated thickness was much higher. The effect of CPAM charge density at constant molecular weight on the adsorption layer thickness at the cellulose- D_2O interface is shown in Figure 10. CPAM layer thickness increases with polymer charge density, while roughness remains constant.

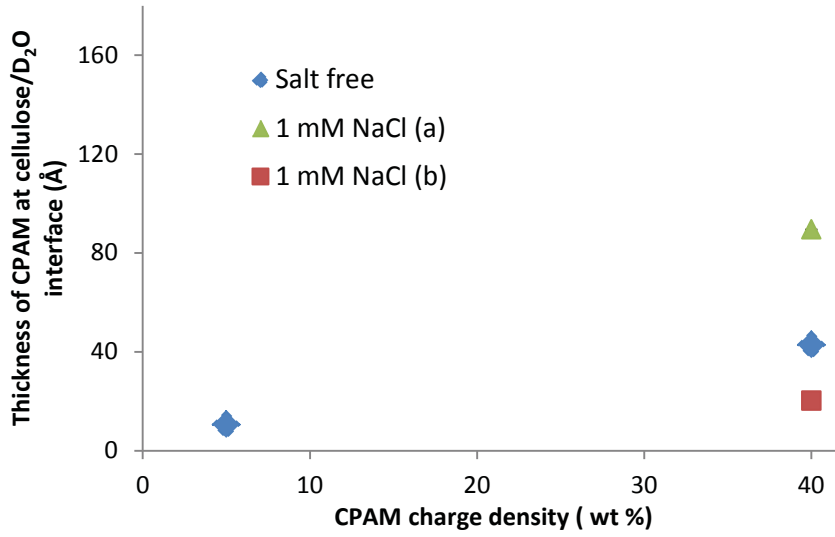


Figure 10: The thickness of CPAM ($M_w=13$ MDa) adsorbed at cellulose/ D_2O interface with and without NaCl. The data is presented in Table III.
a: F1 prepared in NaCl solution before adsorption.
b: NaCl solution was added after F1 adsorption.

The effect of 1mM NaCl on the CPAM adsorption layer thickness at the cellulose interface was studied in 2 modes. In the first, NaCl was added to D_2O after the CPAM had been adsorbed on cellulose; in the second, NaCl was introduced to the initial CPAM/ D_2O solution adsorbed on cellulose (Figure 10). Adding salt to a CPAM (40% charge) monolayer adsorbed on cellulose decreased both the polymer layer thickness and its roughness. For CPAM equilibrated in NaCl D_2O , the adsorption layer thickness on cellulose increased from 43 ± 4 Å to 89 ± 11 Å (Table III).

The amount of CPAM adsorbed at the cellulose interface (Γ in g/m^2) was approximated from the layer thickness and volume fraction of CPAM, using equation (3) [35]:

$$\Gamma = \frac{10^{20} M_R \Phi \delta}{N_a V} \quad (3)$$

Where M_R is the CPAM molecular weight; Φ is its volume fraction (CPAM) in the layer of thickness δ (Å); N_a is Avagadro's number and V is the molecular volume of CPAM (Å³). Φ and δ were fitted from neutron reflection curves. Without NaCl addition, the calculated CPAM specific adsorption capacity on cellulose (Γ) was comparable for both 5% and 40% charged CPAM (Table III). Realistic values of CPAM adsorption capacity

were determined for CPAM of 5% and 40% charge ($\Gamma = 1.3$ to 3.5 mg/m^2); however, the Γ values for CPAM 50% were unrealistically high.

6.5 Discussion

6.5.1 Smooth Cellulose films

Model cellulose films are convenient substrates for quantifying the morphology of adsorbed macromolecules and their interactions with surfaces, using sensitive characterization techniques such as X-ray/neutron reflectometry, ellipsometry, AFM, surface plasmon resonance (SPR), quartz crystal microbalance (QCM), X-ray photoelectron spectroscopy (XPS), wetting and the surface forces apparatus (SFA) [33, 36-39]. There are three main physical film attributes often required of a polymer film for advanced surface analysis: thickness, surface smoothness and uniformity, although each analytical technique has its own requirements. For example, reflectometry and SFA both require films with smooth surfaces and having constant thickness; SPR and QCM are restricted by film thickness, while AFM privileges high surface smoothness. This study investigates the adsorption layer thickness and uniformity of cationic polyacrylamides adsorbed on cellulose using neutron reflectometry. Cellulose films suitable to study interfacial phenomena have been explored with different methodologies such as spin coating, solution casting and Langmuir Blodgett [40, 41], as reviewed by Kontturi [42]. Cellulose films can either be deposited directly on a surface as cellulose nanocrystals [43] or as a cellulose solution [39], or indirectly via a cellulose derivative solution regenerated to cellulose in a subsequent step [26, 40]. The latter approach has produced the smoothest films and was selected in this study.

Spin coating has formed smooth and uniform cellulose films [24, 37]. The primary variables controlling the morphology and thickness (δ) of the film during coating include cellulose concentration, solvent and spin coating speed. In our preliminary experiments, the influence of these parameters was examined and the concentration of the cellulose acetate (CA) in solvent (acetone) was identified as the critical variable (Table II and Figure 3). Reducing the concentration of the cellulose in solution resulted in thinner and smoother cellulose films. The independent variables are the extent of molecular mobility during the time frame of film formation (which can be controlled by the spin coating

rotation speed and solvent evaporation rate) and the period of macromolecular mobility (as dictated by solution viscosity, polymer concentration and molecular weight). Spin coating produces some of the highest quality cellulose films due to increased molecular mobility and the higher time frame available to achieve a uniform polymer distribution on the surface. A quasi-molecularly smooth film with roughness of 7 ± 1 Å, and thickness of 40 ± 7 Å was achieved at a low cellulose solution concentration of 0.13 wt%; these films are suitable for neutron reflectometry.

The crystalline and amorphous regions of cellulose have different accessibility to solvent [44]. Therefore, films directly spun from a cellulose nanocrystal (CNC) aqueous dispersion were explored. Good CNC films were only prepared at high concentration (6.5 wt %); however, the surfaces were rough (57 ± 19 Å) likely due to a combination of poor packing and formation of aggregates. The nanocellulose films produced were too rough to serve as a suitable substrate to measure the CPAM adsorption layer thickness by neutron reflectometry. Smoothness might be improved by pre-treating the silicon wafer with a polyelectrolyte to enhance CNC adhesion [43].

The effect of regeneration time on the cellulose film properties was analyzed. The thickness of the CA film decreased rapidly with regeneration time in sodium methoxide to reach a plateau (Figure 4). The reaction clearly corrodes the surface in a non-uniform fashion as the length scale of the acetyl groups cleaved and replaced by much smaller hydroxyl groups is well below the nm scale measured by reflectometry and AFM. However, the inter- and intra-molecular hydrogen bonding network enables the film to become more compact, therefore forming a thinner and denser structure; heterogeneity in reaction would further contribute to roughness. The regeneration process produced a much rougher surface than the original CA film. This result contrasts with previous reports claiming that hydrolysing trimethylsilyl cellulose into cellulose results in smoother films [37, 40]. The rough surface caused initially by the cellulose acetate regeneration process (within 10-mins) corresponds to the regime of poor wettability identified with water contact angle greater than the $57.1\pm3.0^\circ$ for the CA film (Figure 5). We believe the change of roughness affects the wettability initially, as the conversion of acetyl groups into hydroxyl groups occurs at longer time frames (Figure 6).

6.5.2 CPAM adsorption at the cellulose/D₂O interface

Quasi-molecular smooth cellulose films regenerated on silicon blocks were used to measure, by neutron reflectometry, the effect of polyelectrolyte charge density and salt concentration on the cationic polyacrylamide (CPAM) layer thickness adsorbed at the solid-liquid interface (Table III, Figure 9 and 10).

6.5.2.1 Cellulose swells in D₂O

Two possibilities may occur when a dry cellulose film is exposed to liquid D₂O. In the first, the film remains unaffected by water and the thickness of the cellulose film in wet and dry states is identical. The second involves swelling of the cellulose film in water, as observed in situ from NR measurements. The swollen cellulose film is characterized by its water/D₂O content and its distribution profile through the film.

During the initial stage of swelling, water diffuses across the cellulose film in plane. This diffusion is controlled by film density and structure (porosity and defects), and a water gradient profile can be fitted from NR curves, which assumes the swollen film to consist of a series of hydrated layers (multilayers). Once water saturation of the cellulose has proceeded, the water distribution becomes fairly uniform throughout the film. As water penetration through an ultrathin film is very fast (seconds-minutes) and the total time of measurement long (6-14 hours of measurement per film), this study neglected any kinetic effects and assumes pseudo-equilibrium conditions to be achieved.

Once in contact with D₂O, the three labile protons of the hydroxyl groups of the D-glucose units (C₆H₁₀O₅) of amorphous cellulose rapidly exchange with deuterons from the solvent [33, 34]. Hence the ρ value of $3.39 \times 10^{-6} \text{ \AA}^{-2}$ was used for fitting cellulose films in D₂O, which corresponds to C₆H₇D₃O₅ after H-D exchange. As the regenerated cellulose films are completely amorphous, we assumed full exchange to proceed.

With one exception (50% charge CPAM adsorption spun from 0.1wt% CA solution), all the wet cellulose films were spun from 0.13 wt% CA solution and had a thickness and roughness of $\sim 100 \text{ \AA}$ and 3 \AA , respectively (in D₂O); this corresponds to an increased thickness by a factor of ~ 2.5 comparing to the dry cellulose films ($\delta = 40 \pm 7 \text{ \AA}$, $\sigma = 7 \pm 1 \text{ \AA}$). The volume fraction of D₂O in the cellulose layers ($\Phi_{\text{D}_2\text{O}}$) was calculated to be $67 \pm 2\%$, which lies between the findings of Cheng et al. ($59 \pm 1\%$) and those of Kontturi et al.

(86%). Thin hydrated cellulose films form hydrogels. Our measurements also noted the remarkable swelling ability of the cellulose layer while keeping a smooth outer interface.

6.5.2.2 CPAM absorbed at the cellulose/D₂O interface

CPAM was adsorbed under surface excess conditions to produce a full monolayer. CPAM molecular weight (13 MDa) and concentration in solution (0.1 mg/mL) were kept constant. The adsorption of polyelectrolyte is strongly affected by electrostatic interactions and the resulting polymer conformation is driven by the balance of surface-polymer interactions in competition with electrolyte [5, 8, 14-16]. The adsorption kinetics of CPAM onto cellulose fiber were reported to reach near-equilibrium within 30 mins [45]. In this study, CPAM solution was kept in contact with cellulose in a sample cell at least half an hour prior to the neutron reflectometry measurement to allow full polymer adsorption to proceed, but probably not full equilibrium relaxation to occur.

We assumed a single absorbed layer at the cellulose/D₂O interface for fitting unless the fitting quality is poor (chi squared is unacceptably high). Two cases were examined: the first one consisted of a solid CPAM layer with no water at the interface. This model was rejected as the very high chi squared (>10) indicated poor fitting/hypothesis. The second model represented an absorbed layer consisting of CPAM and D₂O. It was postulated that the mixed layer had a uniform composition [16, 46-48]. The effect of CPAM charge density on its adsorption layer thickness on the hydrated cellulose films is shown in Table III.

We selected CPAM of very high M_R (13 MDa) for this experiment to prevent polymer diffusion within the cellulose/D₂O layer. The thinness of the cellulose film combined with the high charge of the CPAM and the short duration of neutron reflection measurements (less than 3 hours), further contribute to retaining the adsorbed CPAM at the cellulose surface and prevent its miscibility with the cellulose-D₂O layer. However, it is of interest to consider the effect that CPAM diffusion/reptation into the swollen cellulose layer [49] might have. High molecular weight polyelectrolytes have been reported to be restricted to the external surface of the fibers [11]. Diffusion of cationic polyelectrolytes into cellulosic fibers have been studied by Horvath et al. [50]. High charge density polyelectrolytes were observed to diffuse on a time scale of months, whereas the diffusion of low charge density polyelectrolytes was measured on the order of hours. Additionally,

a significant change in the diffusion behaviour was only observed at high electrolyte concentrations (10^{-1} M NaHCO_3). The simulated SLDs of CPAM 40% and 5% charge adsorbed onto and uniformly mixed within the swollen cellulose layer, with and without deswelling (fixed at 25%), are shown in Figure 11. Best fit between the experiments and model was achieved by assuming segregation of CPAM on the cellulose surface, supporting our hypotheses and methodology. The two important variables affecting fitting are: 1) thickness of the layer and 2) SLD of the layers. This means that any swelling/deswelling and diffusion of the D_2O into the cellulose/CPAM layers are critical.

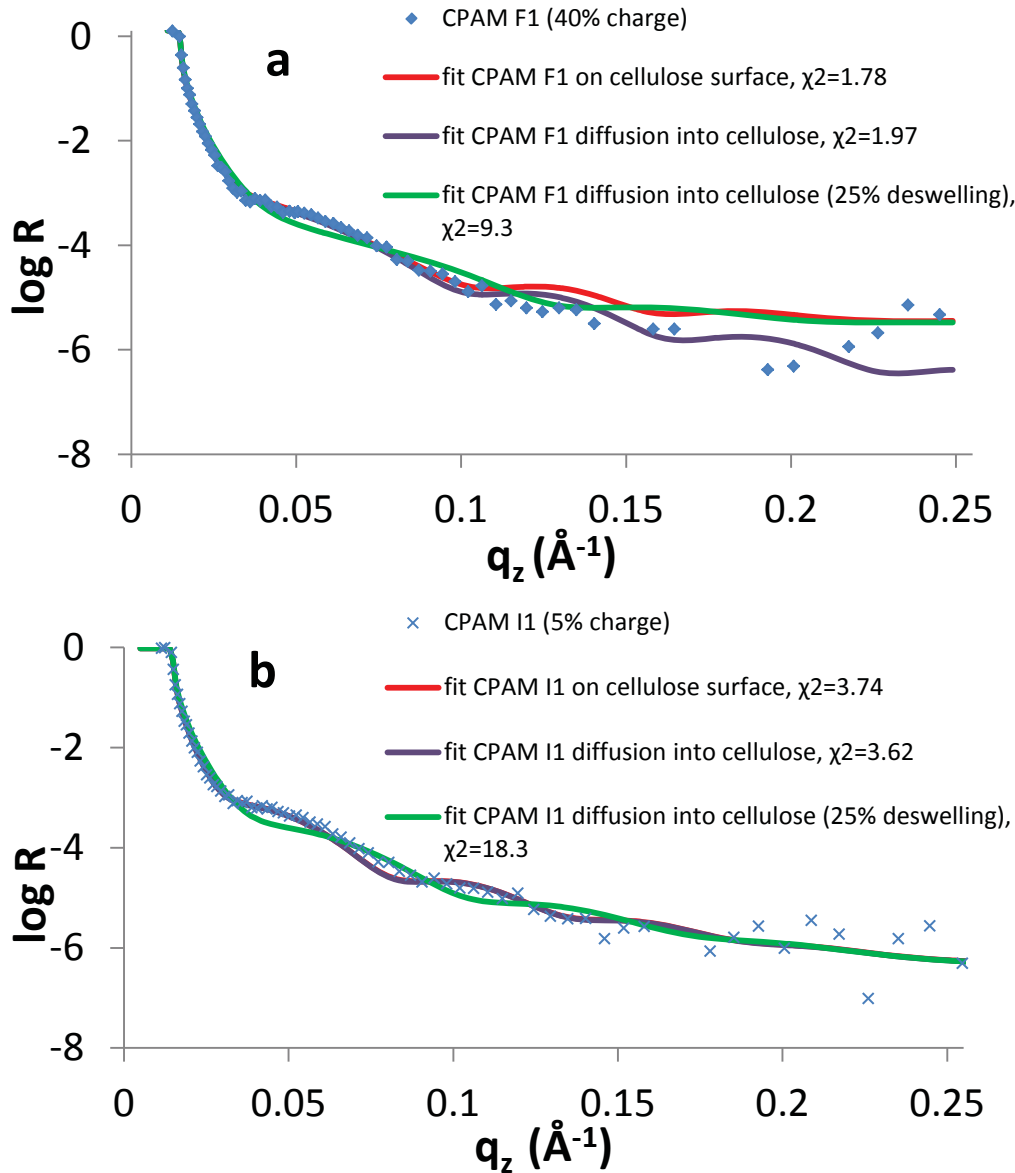


Figure 11: Model fitting for CPAM of a) 40 % and b) 5% charge density adsorption at 1) cellulose surface; 2) diffusion into cellulose layer without changing the cellulose swelling behaviour; 3) diffusion into

cellulose layer and the cellulose layer is deswelling 25%. χ^2 indicates the quality of fitting, and the lower value of χ^2 indicate better fits from minimizing the differences between the theoretical and measured reflectivity curves.

The CPAM of low charge density (5 %) was compared to the high charge density (40%) case. The layer absorbed at the interface was thinner and had a lower Φ_{D2O} . The value of Φ_{D2O} in the layer might depend on the hygroscopy of CPAM with different charge. However, the layer roughness (σ) and the calculated absorbed CPAM amount (Γ) are mostly independent of charge density (Table III). This observation might at first seem to contradict the work of Lindstrom and Soremark on the adsorption of CPAM on bleached sulphite pulp [9]; they found the adsorbed amount of CPAM decreased as the polymer charge density increased. However, there is a clear distinction between adsorbed polymer density (mg/m^2) and layer thickness (\AA). A thick adsorbed polymer layer can have a low adsorption density if its water content is high; this is illustrated in Figure 12.

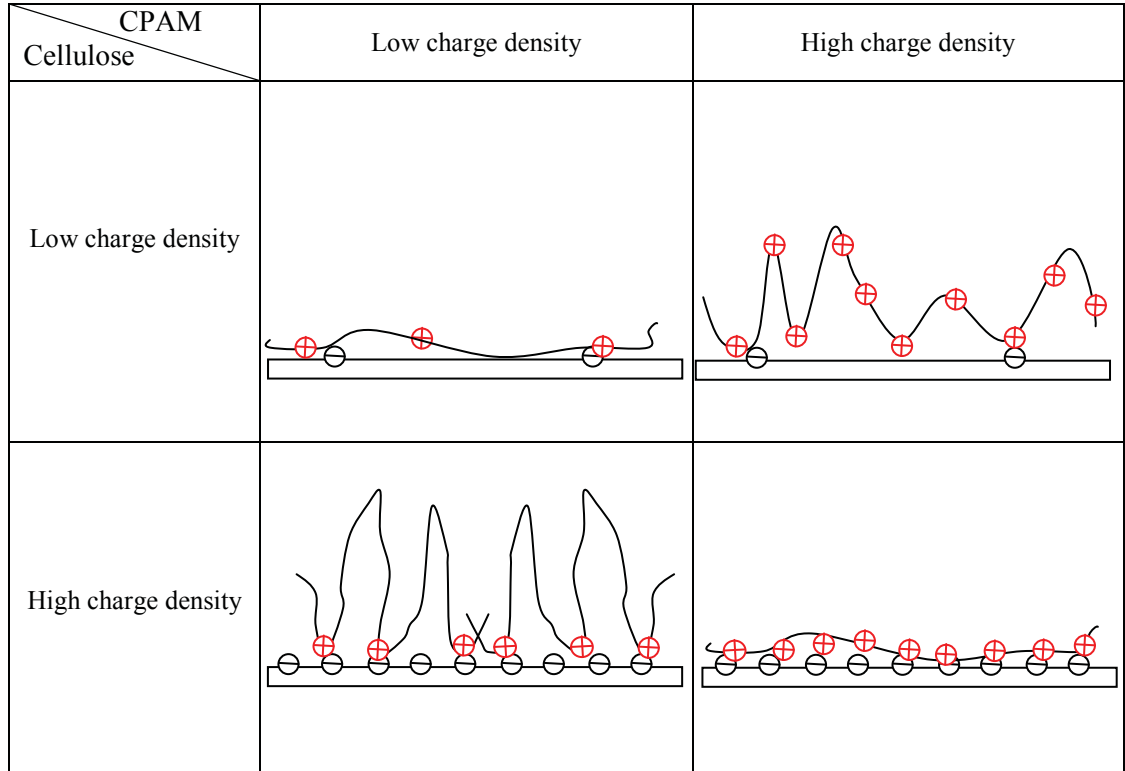


Figure 12: The proposed conformation of CPAM absorbed on the cellulose/water interface under different charge density conditions.

Polymer surface coverage (Γ) can be approximated from the CPAM measured thickness and volume fraction (Table III); calculating Γ is a good way to assess the results' validity. Realistic values of Γ are found for the adsorption of CPAM of 5% and 40% charge density onto cellulose; however, those of CPAM 50% charge are simply unrealistic ($\Gamma \geq 95 \text{ mg/m}^2$). The Γ calculated from Eq. (3) is very sensitive to the D_2O content; for CPAM 50% on cellulose, the very low D_2O content calculated completely skewed the results which is compensated by an unrealistically thick CPAM layer.

The CPAM equivalent charge coverage at the interface was further investigated. The calculated charge coverage ($\mu\text{eq/m}^2$) increases with CPAM charge density. This suggests that the charge of adsorbed CPAM does not stoichiometrically interact with that of the cellulose surface. The importance of surface chemistry and charge stoichiometry was examined by adsorbing 40% charge CPAM onto the more negatively charged silicon surface (with silicon oxide layer, S3 in Support information) [36, 39, 43, 45, 51]; a thinner CPAM layer was formed. Figure 12 schematically illustrates the effect of surface and CPAM charge density on the morphology and thickness of adsorbed polymer layers.

The configuration of polyelectrolyte adsorbed at the solid surface is often described by the “loops-trains-tails” model [5, 16]. The thickness of CPAM adsorbed at the cellulose interface is of the nanometer scale, an order of magnitude lower than its radius of gyration in solution. Wagberg proposed adsorption by charge stoichiometry between the CPAM and the cellulose surface [10]. Increased electrolyte concentration was reported to decrease the concentration of adsorbed “train” polyelectrolyte concentration [5, 16], therefore increasing the relative concentration of loops and tails, which increases polymer thickness (δ); polymer layer density can even decrease should desorption happen, though this is unlikely for high molecular weight polymers. The effect of salt is expected to be more important at low polymer adsorption density, although the effect of adsorption stoichiometry between the CPAM charges and the charges on the cellulose surface is clearly important [52, 53].

The role of ionic strength in CPAM adsorption at the cellulose- D_2O interface was investigated in two modes. Electrolyte in the form of 10^{-3} M NaCl was added either to the CPAM solution to be adsorbed or to the D_2O solution after CPAM adsorption had been

completed on cellulose. Salt did not affect Φ_{D_2O} in the absorbed layer in either mode; however, it changed the CPAM thickness. Once the CPAM adsorption was completed, addition of NaCl decreased layer thickness and roughness. This compressed CPAM conformation at the liquid-solid interface induced by electrolyte was previously reported [7]. In contrast, an increase in polymer adsorption thickness was measured by adsorbing a solution of CPAM equilibrated in NaCl. As cellulose charge is not expected to vary significantly from the addition of NaCl, CPAM adsorbed amount must be a function of ionic strength; this was previously reported by Peng et al [7]. The increase in ionic strength screens the CPAM charge, reducing the electrostatic attraction of the polymer for the cellulose surface and also the CPAM intra-molecular repulsions [16].

6.6 Conclusion

Thin and smooth cellulose films were prepared by spin coating either a nanocellulose crystal suspension or a cellulose acetate solution onto silicon surfaces and regenerating into cellulose by alkaline hydrolysis. These cellulose films were characterized by AFM, X-ray reflectometry, Raman spectroscopy and contact angle measurement. High molecular weight polyacrylamides (CPAM) were adsorbed from solution onto the cellulose surfaces under surface excess conditions to ensure full monolayer coverage. The CPAM adsorption thickness and roughness were measured by neutron reflectometry at the cellulose-D₂O interface. The effect of CPAM charge density and added NaCl (10⁻³ M) was quantified.

Thin cellulose films (40±7 Å) of roughness less than 10 Å were produced by spin coating a cellulose acetate-acetone solution and regenerating by alkaline hydrolysis. These films are ideal for reflectometry studies. Film smoothness was greatly improved by controlling the concentration of cellulose acetate (0.13 wt.%) and the hydrolysis time in sodium methoxide. Optimal model fitting demonstrates that high molecular weight CPAM adsorbs and remains at the hydrated cellulose-D₂O interface during the measurement. The charge of adsorbed CPAM does not stoichiometrically interact with that of the cellulose surface. These observations agree well with previous experimental findings [46, 50, 52].

The adsorption thickness (δ) formed by a 0.1 mg/mL solution of CPAM (40% charge, 13MD) at the solid-D₂O interface is 43±4 Å on cellulose and 13±2 Å on silicon. The

adsorption thickness is an order of magnitude smaller than the CPAM radius of gyration. At constant molecular weight, the thickness of the CPAM layer adsorbed on cellulose increases with polymer charge density (10 ± 1 Å at 5% and 43 ± 4 Å at 40%). Addition of 10^{-3} M NaCl decreased the thickness of CPAM layer already adsorbed on cellulose. However, the adsorption layer on cellulose of a CPAM solution equilibrated in 10^{-3} M NaCl is much thicker (89 ± 11 Å for 40% CPAM). For high molecular weight CPAMs of constant molecular weight adsorbed from solution under constant conditions, the adsorption layer can vary by 1 order of magnitude by controlling the variables affecting electrostatic forces. This finding confirms that polymer surface coverage is not the only important variable affecting colloid stability by polyelectrolyte as the bridging layer thickness can vary considerably [8, 17], and highlights the charge effect on polymer adsorption and conformation at solid surfaces and interfaces.

6.7 Acknowledgement

The financial contribution of Australian Research Council (LP0990526) is acknowledged. We thank ANSTO/ AINSE for the allocation of beam time (DB3363) and travel grants, and AQUA+TECH for providing the CPAM polymers.

ARC Linkage LP0989823 and Visy, Amcor, SCA, Norske Skog, Australian Paper, the Australian Pulp and Paper Institute and Monash University are all acknowledged.

6.8 References

1. Ngo, Y.H., D. Li, G.P. Simon, and G. Garnier, *Effect of cationic polyacrylamide dissolution on the adsorption state of gold nanoparticles on paper and their Surface Enhanced Raman Scattering properties*. Colloids and Surfaces a-Physicochemical and Engineering Aspects, 2013. **420**: p. 46-52.
2. Ngo, Y.H., D. Li, G.P. Simon, and G. Garnier, *Effect of cationic polyacrylamides on the aggregation and SERS performance of gold nanoparticles-treated paper*. Journal of Colloid and Interface Science, 2013. **392**: p. 237-246.
3. Wang, Y., W. Qi, R. Huang, R. Su, and Z. He, *Jet flow directed supramolecular self-assembly at aqueous liquid-liquid interface*. RSC Advances, 2014. **4**(30): p. 15340-15347.
4. Reye, J.T., K. Maxwell, S. Rao, J. Lu, and S. Banerjee, *Cationic polyacrylamides enhance rates of starch and cellulose saccharification*. Biotechnology letters, 2009. **31**(10): p. 1613-1616.
5. Fleer, G.J., M.A. Cohen Stuart, J.M.H.M. Scheutjens, T. Cosgrove, and B. Vincent, *Polymers at interfaces*. 1st ed 1998, London ; New York: Chapman & Hall. 495p.

6. Peng, P. and G. Garnier, *Effect of cationic polyacrylamide on precipitated calcium carbonate flocculation: Kinetics, charge density and ionic strength*. Colloids and Surfaces A: Physicochemical and Engineering Aspects, 2012. **408**(0): p. 32-39.
7. Peng, P. and G. Garnier, *Effect of Cationic Polyacrylamide Adsorption Kinetics and Ionic Strength on Precipitated Calcium Carbonate Flocculation*. Langmuir, 2010. **26**(22): p. 16949-16957.
8. Dobrynin, A.V. and M. Rubinstein, *Theory of polyelectrolytes in solutions and at surfaces*. Progress in Polymer Science, 2005. **30**(11): p. 1049-1118.
9. Lindstrom, T. and C. Soremark, *Adsorption of Cationic Polyacrylamides on Cellulose*. Journal of Colloid and Interface Science, 1976. **55**(2): p. 305-312.
10. Wågberg, L., L. Winter, L. Ödberg, and T. Lindström, *On the charge stoichiometry upon adsorption of a cationic polyelectrolyte on cellulosic materials*. Colloids and Surfaces, 1987. **27**(1-3): p. 163-173.
11. Wågberg, L. and R. Hägglund, *Kinetics of Polyelectrolyte Adsorption on Cellulosic Fibers*. Langmuir, 2001. **17**(4): p. 1096-1103.
12. Durand-Piana, G., F. Lafuma, and R. Audebert, *Flocculation and adsorption properties of cationic polyelectrolytes toward Na-montmorillonite dilute suspensions*. Journal of Colloid and Interface Science, 1987. **119**(2): p. 474-480.
13. Meadows, J., P.A. Williams, M.J. Garvey, R. Harrop, and G.O. Phillips, *Characterization of the adsorption-desorption behavior of hydrolyzed polyacrylamide*. Journal of Colloid and Interface Science, 1989. **132**(2): p. 319-328.
14. Tekin, N., Ö. Demirbaş, and M. Alkan, *Adsorption of cationic polyacrylamide onto kaolinite*. Microporous and Mesoporous Materials, 2005. **85**(3): p. 340-350.
15. Shubin, V., *Adsorption of Cationic Polyacrylamide onto Monodisperse Colloidal Silica from Aqueous Electrolyte Solutions*. Journal of Colloid and Interface Science, 1997. **191**(2): p. 372-377.
16. Shubin, V. and P. Linse, *Effect of Electrolytes on Adsorption of Cationic Polyacrylamide on Silica: Ellipsometric Study and Theoretical Modeling*. The Journal of Physical Chemistry, 1995. **99**(4): p. 1285-1291.
17. Solberg, D. and L. Wågberg, *Adsorption and flocculation behavior of cationic polyacrylamide and colloidal silica*. Colloids and Surfaces A: Physicochemical and Engineering Aspects, 2003. **219**(1-3): p. 161-172.
18. Scherer, J.R., G.F. Bailey, S. Kint, R. Young, D.P. Malladi, and B. Bolton, *Water in Polymer Membranes .4. Raman-Scattering from Cellulose-Acetate Films*. Journal of Physical Chemistry, 1985. **89**(2): p. 312-319.
19. Kirby, N.M., S.T. Mudie, A.M. Hawley, D.J. Cookson, H.D.T. Mertens, N. Cowieson, and V. Samardzic-Boban, *A low-background-intensity focusing small-angle X-ray scattering undulator beamline*. Journal of Applied Crystallography, 2013. **46**(6): p. 1670-1680.
20. Hammersley, A., *FIT2D V9. 129 Reference Manual V3. 1*. Inter Rep ESRF98HA01, ESRF, Grenoble, 1998.
21. James, M., A. Nelson, S.A. Holt, T. Saerbeck, W.A. Hamilton, and F. Klose, *The multipurpose time-of-flight neutron reflectometer "Platypus" at Australia's OPAL reactor*. Nuclear Instruments & Methods in Physics Research Section a-Accelerators Spectrometers Detectors and Associated Equipment, 2011. **632**(1): p. 112-123.
22. Nelson, A., *Co-refinement of multiple-contrast neutron/X-ray reflectivity data using MOTOFIT*. Journal of Applied Crystallography, 2006. **39**: p. 273-276.
23. Lefebvre, J. and D. Gray, *AFM of adsorbed polyelectrolytes on cellulose I surfaces spin-coated on silicon wafers*. Cellulose, 2005. **12**(2): p. 127-134.
24. Edgar, C. and D. Gray, *Smooth model cellulose I surfaces from nanocrystal suspensions*. Cellulose, 2003. **10**(4): p. 299-306.

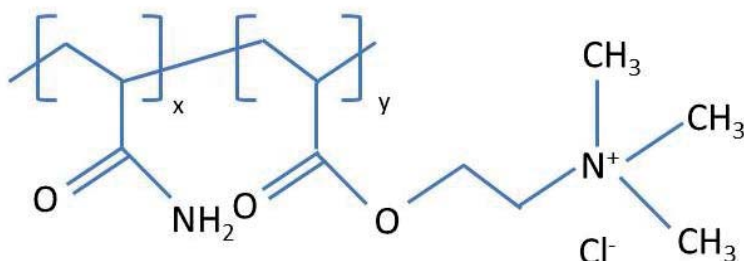
25. Van Oss, C.J., R.J. Good, and M.K. Chaudhury, *Additive and nonadditive surface tension components and the interpretation of contact angles*. Langmuir, 1988. **4**(4): p. 884-891.
26. Yu, L. and G. Garnier, *Mechanism of internal sizing with alkyl ketene dimers: The role of vapor deposition*. The fundamentals of papermaking materials, 1997. **2**: p. 1021.
27. Fink, H.P., D. Fanter, and B. Philipp, *Röntgen-Weitwinkeluntersuchungen zur übermolekularen Struktur beim Cellulose-I-II-Phasenübergang*. Acta Polymerica, 1985. **36**(1): p. 1-8.
28. Singh, M.A. and M.N. Groves, *Depth profiling of polymer films with grazing-incidence small-angle X-ray scattering*. Acta Crystallographica Section A, 2009. **65**(3): p. 190-201.
29. Kontturi, E., M. Suchy, P. Penttilä, B. Jean, K. Pirkkalainen, M. Torkkeli, and R. Serimaa, *Amorphous Characteristics of an Ultrathin Cellulose Film*. Biomacromolecules, 2011. **12**(3): p. 770-777.
30. Nevot, L. and P. Croce, *Characterization of Surfaces by Grazing X-Ray Reflection - Application to Study of Polishing of Some Silicate-Glasses*. Revue De Physique Appliquee, 1980. **15**(3): p. 761-779.
31. Scholtan, v.W., *Molekulargewichtsbestimmung von Polyacrylamid mittels der Ultrazentrifuge*. Die Makromolekulare Chemie, 1954. **14**(1): p. 169-178.
32. Mallam, S., F. Horkay, A.M. Hecht, and E. Geissler, *Scattering and swelling properties of inhomogeneous polyacrylamide gels*. Macromolecules, 1989. **22**(8): p. 3356-3361.
33. Cheng, G., Z.L. Liu, J.K. Murton, M. Jablin, M. Dubey, J. Majewski, C. Halbert, J. Browning, J. Ankner, B. Akgun, C. Wang, A.R. Esker, K.L. Sale, B.A. Simmons, and M.S. Kent, *Neutron Reflectometry and QCM-D Study of the Interaction of Cellulases with Films of Amorphous Cellulose*. Biomacromolecules, 2011. **12**(6): p. 2216-2224.
34. Hine, J. and C.H. Thomas, *The Rate of Deuterium Exchange between Ethanol and Water. A Reinvestigation*. Journal of the American Chemical Society, 1953. **75**(3): p. 739-740.
35. Su, T.J., J.R. Lu, R.K. Thomas, Z.F. Cui, and J. Penfold, *The Adsorption of Lysozyme at the Silica-Water Interface: A Neutron Reflection Study*. Journal of Colloid and Interface Science, 1998. **203**(2): p. 419-429.
36. Notley, S.M., B. Pettersson, and L. Wågberg, *Direct Measurement of Attractive van der Waals' Forces between Regenerated Cellulose Surfaces in an Aqueous Environment*. Journal of the American Chemical Society, 2004. **126**(43): p. 13930-13931.
37. Kontturi, E., P.C. Thune, and J.W. Niemantsverdriet, *Cellulose model surfaces-simplified preparation by spin coating and characterization by X-ray photoelectron spectroscopy, infrared spectroscopy, and atomic force microscopy*. Langmuir, 2003. **19**(14): p. 5735-5741.
38. Garnier, G., M. Bertin, and M. Smrckova, *Wetting Dynamics of Alkyl Ketene Dimer on Cellulosic Model Surfaces*. Langmuir, 1999. **15**(22): p. 7863-7869.
39. Eriksson, M., S.M. Notley, and L. Wågberg, *Cellulose Thin Films: Degree of Cellulose Ordering and Its Influence on Adhesion*. Biomacromolecules, 2007. **8**(3): p. 912-919.
40. Kontturi, E., P.C. Thune, and J.W. Niemantsverdriet, *Novel method for preparing cellulose model surfaces by spin coating*. Polymer, 2003. **44**(13): p. 3621-3625.
41. Aulin, C., S. Ahola, P. Josefsson, T. Nishino, Y. Hirose, M. Österberg, and L. Wågberg, *Nanoscale Cellulose Films with Different Crystallinities and Mesostructures—Their Surface Properties and Interaction with Water*. Langmuir, 2009. **25**(13): p. 7675-7685.
42. Kontturi, E., T. Tammelin, and M. Osterberg, *Cellulose - model films and the fundamental approach*. Chemical Society Reviews, 2006. **35**(12): p. 1287-1304.
43. Notley, S.M., M. Eriksson, L. Wågberg, S. Beck, and D.G. Gray, *Surface Forces Measurements of Spin-Coated Cellulose Thin Films with Different Crystallinity*. Langmuir, 2006. **22**(7): p. 3154-3160.
44. Ioelovich, M., *Accessibility and Crystallinity of Cellulose*. Bioresources, 2009. **4**(3): p. 1168-1177.

45. Tanaka, H., L. Ödberg, L. Wågberg, and T. Lindström, *Adsorption of cationic polyacrylamides onto monodisperse polystyrene latices and cellulose fiber: Effect of molecular weight and charge density of cationic polyacrylamides*. Journal of Colloid and Interface Science, 1990. **134**(1): p. 219-228.
46. Wågberg, L., *Polyelectrolyte adsorption onto cellulose fibres – A review*. Nordic Pulp & Paper Research Journal, 2000. **15**(5): p. 586-597
47. Ven, T.G.M.v.d., *A model for the adsorption of polyelectrolytes on pulp fibers: Relation between fiber structure and polyelectrolyte properties* Nordic Pulp & Paper Research Journal, 2000. **15**(5): p. 494-501.
48. Notley, S.M. and M. Norgren, *Adsorption of a Strong Polyelectrolyte To Model Lignin Surfaces*. Biomacromolecules, 2008. **9**(7): p. 2081-2086.
49. Wegner, G., V. Buchholz, L. Ödberg, and S. Stemme, *Regeneration, derivatization and utilization of cellulose in ultrathin films*. Advanced Materials, 1996. **8**(5): p. 399-402.
50. Horvath, A.T., A.E. Horvath, T. Lindström, and L. Wågberg, *Diffusion of Cationic Polyelectrolytes into Cellulosic Fibers*. Langmuir, 2008. **24**(19): p. 10797-10806.
51. Butt, H.-J., Karlheinz Graf, and M. Kappl., *Physics and Chemistry of Interfaces*, 2003, Wiley-VCH. p. 373p.
52. Winter, L., L. Wågberg, L. Ödberg, and T. Lindström, *Polyelectrolytes adsorbed on the surface of cellulosic materials*. Journal of Colloid and Interface Science, 1986. **111**(2): p. 537-543.
53. Wågberg, L., G. Pettersson, and S. Notley, *Adsorption of bilayers and multilayers of cationic and anionic co-polymers of acrylamide on silicon oxide*. Journal of Colloid and Interface Science, 2004. **274**(2): p. 480-488.

6.9 Supporting Information

S1: Theoretical estimation of the properties of CPAM

$$\frac{1}{2} \quad 1 \quad 1 \quad 1 \quad \frac{1}{2} = 4 \text{ C-C bonds}$$



Cationic dimethylaminoethylacrylate methyl chloride consists of acrylamide (AM) and dimethylaminoethylacrylate methyl chloride (DMA). Assume the density at 1.3 g/mL.

Molecular weight = 13MDa

$$\text{Monomer length, } b = 2 \times \sin \frac{109^\circ}{2} \times 1.54 \times 10^{-10} = 2.51 \times 10^{-10} \text{ m}$$

(C-C bond) (bond angle) (C-C bond length)

$$r_g = b \sqrt{\frac{N}{6}}$$

r_g = radius of gyration, b = monomer length, N = number of monomers

Estimation of end-to-end distance when the polymer is stretch out (chain length) = $b \times N$

CPAM	Charge density (wt %)	Charge (meq/g)	CPAM Mw (MDa)	AM Mw	DMA Mw	N of AM monomers	N of DMA monomers	Total N of monomers
E1	50	1.3	13	71.08	193.69	91446	33559	125005
F1	40	1				109736	26847	136583
I1	5	0.13				173748	3356	177104

	SLD ($\times 10^{-6} \text{ \AA}^{-2}$)	Molecular volume (\AA^3)
AM ($\text{C}_3\text{H}_5\text{NO}$)	1.81	90.79
DMA ($\text{C}_8\text{H}_{16}\text{NO}_2$)	0.71	202.11

S2: GIWAXS measurement of cellulose nanocrystals film

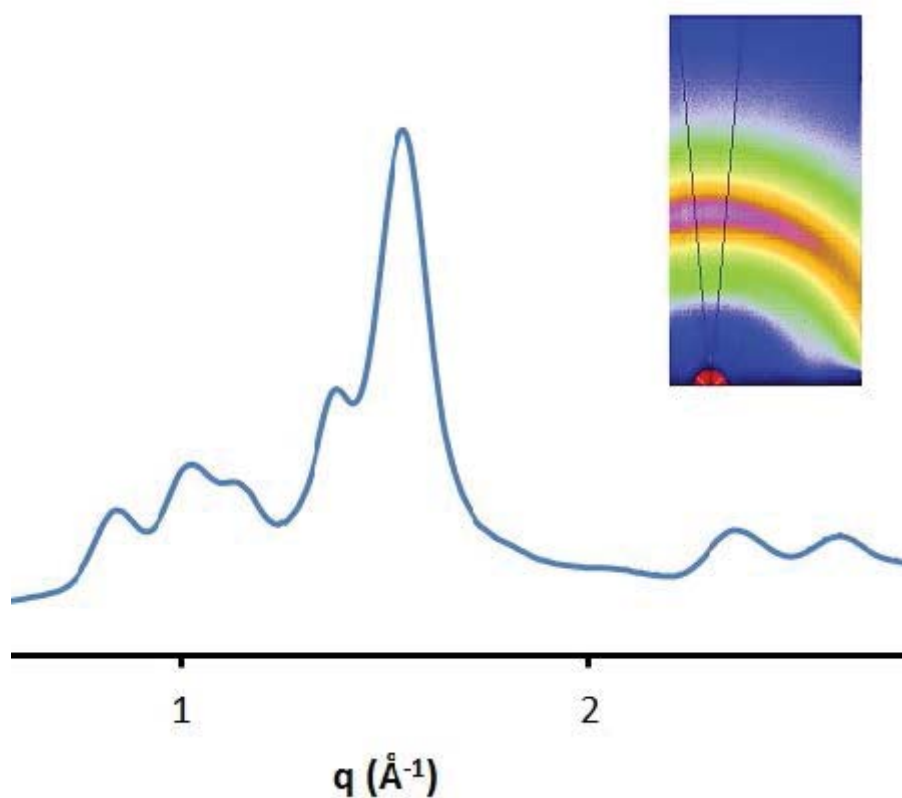


Figure A: GIWAXS profile in the specular direction from a cellulose nanocrystal film on quart substrate. The inset shows a typical GIWAXS image and cut, between two lines ($\pm 5^\circ$) emanating from beam centre, from 2D scattering pattern.

S3: Charge density of the regenerated cellulose film and silica surface

Surface potentials for cellulose surfaces have been measured in an elegant AFM experiment between a cellulose-coated probe sphere and flat surface by Notley *et al.*. Here we use their fitted surface potentials to calculate the equivalent surface charge density of the regenerated cellulose surface as a function of pH and NaCl concentration. Surface charge density Σ , was obtained from the surface potential ψ_0 , using the Grahame equation:

$$\Sigma = \sqrt{8c_0\epsilon\epsilon_0k_BT} \cdot \sinh\left(\frac{e\psi_0}{2k_BT}\right)$$

where c_0 is the bulk salt concentration, ϵ is the relative permittivity of the solution, ϵ_0 is the vacuum permittivities, k_B is Boltzmann's constant, T is the temperature and e is the fundamental charge. Under the conditions investigated, cellulose films have a moderately negative surface charge density ranging from 0.05 to 0.25 $\mu\text{C cm}^{-2}$ affected by NaCl concentration (pH was constant). Cellulose charge is much lower than that of silicon

Table A: Surface potentials from Notley *et al.* for cellulose surfaces at various pH and ionic strength conditions, and the corresponding calculated surface charge densities. The surface charge of silica was determined by titration from Tatiana *et al.*

c_0 (mM)	Substrate pH	Cellulose		Silica
		ψ_0 (mV)	Σ ($\mu\text{C cm}^{-2}$)	Σ ($\mu\text{C cm}^{-2}$)
0.1	3.5	-25	0.057	
	5.5	-40	0.091	
	8.5	-52	0.118	
1	3.5	-25	0.180	
	5.5	-30	0.215	1.220
	8.5	-39	0.280	3.530
10	3.5	-49	1.113	
	5.5	-44	0.999	1.340
	8.5	-50	1.135	6.230

Chapter 7

Preparation of smooth deuterated cellulose
films for visualisation of adsorbed
macromolecules

This page is intentionally blank

Declaration for Thesis Chapter 7

Declaration by candidate

In the case of Chapter 7, the nature and extent of my contribution to the work was the following:

Nature of contribution	Extent of contribution (%)
Initiation, key ideas, experimental and analysis works, development and writing up of paper	70

The following co-authors contributed to the work. If co-authors are students at Monash University, the extent of their contribution in percentage terms must be stated:

Name	Nature of contribution	Extent of contribution (%) for student co-authors only
Warwick Raverty	Advice on the preparation of deuterated cellulose derivatives, key ideas, reviewing and editing of the paper	External collaboration
Christopher J. Garvey	Initiation, key ideas, reviewing and editing of the paper	External collaboration
Peter Holden	Preparation of deuterated bacterial cellulose	External collaboration
Marie Gillon	Preparation of deuterated bacterial cellulose	External collaboration
Stephen Holt	conducting specular X ray reflectometry measurement and help on the data analysis	External collaboration
Warren Batchelor	Initiation, key ideas, reviewing and editing of the paper	Co-supervisor
Gil Garnier *	Initiation, key ideas, reviewing and editing of the paper	Supervisor

The undersigned hereby certify that the above declaration correctly reflects the nature and extent of the candidate's and co-authors' contributions to this work*.

Candidate's Signature		Date 2015-3-6.
Main Supervisor's Signature		Date

*Note: Where the responsible author is not the candidate's main supervisor, the main supervisor should consult with the responsible author to agree on the respective contributions of the authors.

This page is intentionally blank

Preparation of smooth deuterated cellulose films for visualisation of adsorbed macromolecules

Jieong Su¹, Warwick Raverty², Christopher J. Garvey³, Peter Holden³, Marie Gillon³,
Stephen Holt³, Warren Batchelor¹ and Gil Garnier^{1*}

¹BioPRIA- Bioresource Processing Research Institute of Australia,
Department of Chemical Engineering, Monash University

²Circa, Melbourne, Australia

³Australian Nuclear Science and Technology Organisation (ANSTO)

*For correspondence: [REDACTED]

Content

7.1	Abstract	207
7.2	Introduction	208
7.3	Materials and methods	211
7.3.1	Deuterated bacterial cellulose (DBC) yield and purification	212
7.3.2	Preparation of cellulose derivatives	212
7.3.3	(Deuterated) Cellulose film preparation	214
7.3.4	Physical Measurements	214
7.4	Results and discussion	215
7.4.1	Purification of DBC and determination of degree of deuteration.	218
7.4.2	Cellulose derivatives prepared in ILs and dissolution in solvents.	220
7.4.3	Deuterated cellulose film properties and perspectives	224
7.5	Conclusion	229
7.6	Acknowledgments	229
7.7	References	229

7.1 Abstract

An approach to prepare thin and smooth cellulose films for contrast variation neutron reflectivity is established in the study. Incorporation of varying degrees of deuteration into cellulose was achieved by growing *Gluconacetobacter xylinus* strain ATCC 53524 in deuterated glucose and deuterated glycerol carbon sources and using growth media

containing D₂O. The pattern of carbon source incorporation was characterised by mass spectrometry and is consistent with the biosynthesis of cellulose as characterized by ATR-FTIR. Derivatives of deuterated cellulose were prepared from acetylation or trimethylsilylation in ionic liquid (1-Butyl-3-methylimidazolium chloride), and then dissolved in solvents (acetone or toluene). The trimethylsilylation of deuterated cellulose allows high yield of product, and was used to prepare a toluene solution for spin-coating onto silicon substrates. The resultant film was hydrolysed back to deuterated cellulose in acid vapour, and then examined by specular X-ray reflection. The procedure established is of significant importance enabling preparation of a series of deuterated cellulose films with varying neutron scattering contrast which can be used to differentiate between cellulose and biomacromolecules when their interaction is studied by neutron reflectivity.

KEYWORDS

Deuteration; Cellulose; Solid-liquid interface; Adsorption; Reflectometry; Contrast; Biomolecules

7.2 Introduction

Cellulose is the most prevalent polymer. It is cheap, sustainable, hydrophilic, biodegradable, biocompatible and easy to functionalize thanks to its 6 hydroxyl groups per anhydrocellobiose monomer. Cellulose is an important commodity material with significant industrial applications in papermaking, textile and paints. It is also an emerging material for biodiagnostics and functional surfaces taking advantage of its regular polysaccharide surface and composition.

Bioactive papers have attracted wide interest to recognize or quantify biomolecules and chemical agents for environment and health applications [1, 2]. The interactions between the surface of the cellulose fibers and bio-macromolecules often play a critical role in the bioactive paper preparation and application. Based on the principle of red blood cells haemagglutination, blood typing has been successfully realized on paper substrate, where a specific antibody/antigen interaction occurs [3, 4]. Antibodies can be readily loaded on paper by spotting, printing or dip-coating from aqueous solution [5-7], and various paper-based systems have been designed to improve the accuracy of the tests, and different methods have been developed for better visible identification [8, 9].

The adsorption and desorption of antibodies at the cellulose/liquid interface governs many aspects that are critical for the formation and utilization of paper blood typing. However, experimentally derived information on the structure and density of absorbed antibodies at cellulose surfaces remains scarce. Paper webs have a complex three-dimension structure, and their varying characteristics such as porosity, thickness, and chemical composition make the analysis of adsorption and desorption of antibodies difficult. Hence, model cellulose films have been exploited as a platform to investigate the interfacial fundamentals [10-12].

Cellulose model films have been prepared mainly from nanocellulose or cellulose derivatives using two main approaches: Langmuir-Blodgett (LB) deposition and spin coating, these preparation techniques have been reviewed by Kontturi [13]. Native or functionalized films of regenerated and nanofibrillar cellulose, have been used to study the adsorption and chemical conjugation of antibodies, and the dynamic adsorption and features of the absorbed antibody have been characterized by quartz crystal microbalance with dissipation, atomic force microscopy and surface plasmon resonance [10, 12, 14]. Factors such as cationicity, ionic strength and pH of the solution were reported to control the antibody adsorption [11, 12]. Nevertheless, there is limited knowledge of antibodies conformation at the cellulose/water interface and the absorbed layer properties have not been readily examined by modern techniques.

Specular reflectivity is a non-intrusive technique for investigating the structure of thin films on the substrates where it may provide detailed compositional information in a direction normal to the interface in terms of a scattering length density (SLD) profile. Neutron reflectivity is particularly suited for the solid/liquid interface. The SLD profile represents a density of either electrons, in the case of x-ray reflectivity (XRR), or a nuclear property in the case of neutron reflectivity (NR). This real space compositional information is retrieved from reflectivity profiles using an SLD model to reproduce the reflectivity profile [15]. The information content of the experiment is poor, and so more than one possibility may exist for profiles to fit observed reflectivity data, particularly in the case of where more complex models are needed [16]. Contrast variation is particularly useful in bio-macromolecular science as hydrogen-deuterium substitution usually has a minimal effect on the sample offering superior visualisation between materials of similar

SLD [17] as well increasing the experimental information content [16]. In this study we explore through the production of smooth cellulosic with varying degrees of deuteration as a means of optimising the information content of the neutron reflectivity experiment in the particular case of thin cellulose films.

Due to the cost and complexity in the deuteration of biomacromolecules [18], a practical alternative is to prepare deuterated cellulose with varying SLD. By comparison to the cellulose from higher plants where the synthesis is achieved by membrane bound rosette complexes [19], the cellulose produced by *Gluconacetobacter xylinus* [20] (bacterial cellulose) exhibits many unique properties: it is synthesized extracellularly in large sheets of parallel and laterally hydrogen bonded [21] by a linear synthetic complex. The deuteration of high plant cellulose has been partially achieved [22], however higher degrees of deuteration and site specific incorporation of deuterium into bacterial cellulose has been reported [22-27]. These developments potentially enable continuous variation of the scattering length density of the deuterated cellulose, which in turn, permits optimal contrast conditions for the NR experiment.

Surface roughness represents an additional convolution to the SLD profile which may degrade the information content of the experiment. In addition to contrast variation, the smooth cellulose film is also critical for NR to investigate the adsorption and desorption behaviour at the solid/water interface. The flat surface could exclude the morphological factor (roughness) which affects the cellulose interaction with biomolecules. A straightforward method to prepare cellulose films is spin coating from (nano) cellulose aqueous dispersion or dissolution. The cellulose nanocrystal film is a good example [28] but it suffers from surface roughness which is greater than features than we wish to resolve at the interface [29]. However, this direct method is challenging for bacterial cellulose due to the fundamental differences in crystallite morphology. Another well-studied approach is to produce cellulose derivatives at first, followed by dissolution for spin coating, and then regenerate the films through hydrolysis [29].

In the terms of green chemistry, cellulose acetate and trimethylsilylated cellulose have been synthesized in ionic liquids with their solubilities in various solvents carefully examined [30-32]. In spin coating, the properties of solvents, type of cellulose derivatives, operating conditions and regeneration process greatly affect the smoothness

of the final cellulose film [33-35]. Previous research has been targeted towards the production of smooth protonated cellulose films [36]. The feasibility of preparing flat deuterated cellulose film by the same technique needs to be clarified. Particularly, the replacement of the protons in cellulose by deuterium, may result different inter- intra hydrogen bondings and interactions with the substrate. In this case, the morphology of deuterated cellulose film from spin coating may be dissimilar from that of the protonated film.

It is the objective of this study to prepare smooth cellulose model films with varying neutron scattering length densities (different deuteration level). This objective was achieved by growing cultures of *Gluconacetobacter xylinus* in media containing different carbon sources and varying amounts of D₂O and harvesting bacterial celluloses with different degree of deuteration that resulted. The deuterated bacterial celluloses (DBC) were then purified. There are no cellulose solvents having sufficient volatility to be suitable for spin coating and so a number of chemical derivatives of cellulose derivatives were prepared and these were dissolved in solvent for spin-coating. Finally, the contrast matching cellulose films were obtained by hydrolysis of the derivatised cellulose under mild conditions. The concept of contrast variation was explored by using the neutron reflectometry to investigate the structures of antibodies absorbed at the resulting cellulose-water interfaces.

7.3 Materials and methods

Micocrystalline cellulose (Avicel, PH 101) was purchased from FMC BioPolymer. 1-Butyl-3-methylimidazolium chloride (BMIM chloride, $\geq 98.0\%$, HPLC), cellulose acetate (relative molecular weight $\approx 29,000$ D, $\sim 40\%$ substitution of acetyl groups), acetic anhydride (99.5%), Pyridine (anhydrous, 99.8%), Hexamethyldisilazane (HMDS, ReagentPlus, 99.9%), chloroform (PCR Reagent, contains amylenes as stabilizer, $\geq 99\%$), toluene (anhydrous, 99.8%), acetone (AR, $\geq 99.5\%$) were all purchased from Sigma-Aldrich. Polished silicon wafers (50.8 mm diameter, 12 mm and 0.5 mm height, n-type Si:P, [100]) were bought from El-Cat Inc. The wafers were cleaned by soaking in a mixture of ammonium hydroxide, hydrogen peroxide and water (volume ratio=1:1:5) at 70 °C for 15 mins and used as substrates for spin coating.

7.3.1 Deuterated bacterial cellulose (DBC) yield and purification

The details and characterisation of bacterial cellulose pellicles using different (hydrogenated) carbon sources has been published elsewhere (Mikkelsen et al. 2009). Here we have produced bacterial cellulose pellicles from the *Gluconacetobacter xylinus* strain ATCC 53524 using deuterated glucose and deuterated glycerol. Bacteria were cultivated in Hestrin and Schramm (HS) media with either glucose or glycerol as the carbon source. The media consisted of 20 g/L carbon source, 5 g/L peptone, 5 g/L yeast extract, 2.7 g/L NaHPO₄ and 1.15 g/L of citric acid in light water initially for adaptation of the bacteria and thence in D₂O.

The pH of the media was adjusted to 5.0 at the start of growth. Cellulose pellicles were cultivated in the broth media by gradually increasing the deuteration level of the culture, rinsed with distilled water to remove excess media, and then immediately heated (90°C) in 0.1 M NaOH solution for 30 min to inactivate attached bacterial cells. After boiling, the pellicles were purified by extensive washing in distilled water at room temperature and centrifuged (5000 rpm, 10 mins) several times until the pH of the water reached 7. Small samples of DBC were collected before and after boiling and subjected to vacuum drying for 2 days for ATR-FTIR measurement. Oven-dried weights of the samples were also determined. The remaining wet DBC samples were dried by repeated exchange with 100% ethanol by placing the wet suspension in a 50mL tube for 10 mins with 100% ethanol (40 mL), and then centrifuging (5000 rpm, 10 mins). Removal of the aqueous ethanol supernatant and repetition of the process five times gave a suspension of DBC in ethanol that was essentially anhydrous. Finally, the excess ethanol was removed from the DBC by pressing against a nylon fabric mesh which was placed on top of a blotting paper. This DBC sample was used without further drying for preparing cellulose derivatives that could be dissolved in volatile solvents.

7.3.2 Preparation of cellulose derivatives

Before using protonated and deuterated bacterial cellulose (BC), microcrystalline cellulose (MCC) was used in preliminary experiments to evaluate and refine published techniques for preparing cellulose acetate and trimethylsilylated cellulose. Typical procedures were conducted as described below. It is worthwhile to point out the

dissolution of BC in BMIM chloride took longer than MCC due to their different molecular weight, crystallinity and structure.

Acetylation of cellulose: In a 50mL round bottomed flask under an air condenser with a dry nitrogen atmosphere 2 g of BMIM chloride and 0.1 g of Avicel were mixed and heated at 100 °C in a glycol bath under constant magnetic stirring until all of the cellulose had dissolved. The solution was then allowed to cool to room temperature. Acetic anhydride (1.0 mL) and then pyridine (1.0 mL) were added to the BMIM chloride solution which was then subjected to magnetic stirring for different periods (2, 4, 8 and 24 h) at 40 °C. The fully acetylated cellulose was regenerated by slowly adding distilled water (35 mL) down the air condenser while maintaining rapid magnetic stirring. The resulting suspension of white solid material was filtered, washed with distilled water, and dried for 24 hrs under vacuum (500 Pa) at room temperature. Heinze [37] has described in qualitative terms the solubilities of cellulose monoacetate, diacetate and triacetate derived from Avicel in various solvents. A sample of the dried solid thus obtained (0.1 g) was dispersed in acetone (20 g) by stirring overnight. The mixture was then centrifuged at 5000 rpm (10 mins) to remove any undissolved solid and then the acetone supernatant was distilled by rotary evaporator at 40 °C under vacuum (500 Pa) to enable determination of the amount of cellulose acetates that could be dissolved in acetone using this technique. The solid residue obtained after removal of the acetone supernatant was allowed to dry in air for 24 h and then dispersed in 10g chloroform at room temperature. The suspension was centrifuged to determine proportion of cellulose acetates that were soluble and insoluble in chloroform.

Trimethylsilylation of cellulose: BMIM chloride (10.0 g) was dried by placing it in a 25 mL single-necked round-bottomed flask and heating at 120 °C under vacuum (500 Pa) for 16 h. In order to minimise ingress of moisture, the flask was allowed to cool to room temperature and then fitted with a condenser, magnetic stir bar and silicone oil bubbler that enabled the BMIM chloride to be kept under an atmosphere of dry high purity nitrogen. Hexamethyl disilazane (2 mL) was added to the BMIM chloride and the mixture stirred overnight at 100 °C. The condenser and bubbler were removed, and then volatiles were removed by rotary evaporation under vacuum at 170 °C (3 h, 500 Pa).

A 25 mL three-necked, round-bottomed flask equipped with a reflux condenser and a magnetic stirring bar was charged with cellulose (0.1 g, 0.61 mmol equivalents) and

BMIM chloride (2.5 g dried as above). The mixture was stirred at 100 °C under vacuum (500 Pa). A clear solution of cellulose in the ionic liquid was obtained after 6 hrs. The flask was then equipped with a silicone bubbler and an inlet for dry nitrogen and was flushed with dry nitrogen for 30 min. Following dissolution of the cellulose, hexamethyl disilazane (1.8 g) was added and the mixture stirred at 100 °C for 2 hrs. Following this period, toluene (8 mL) was added and the mixture stirred at 100 °C for a further 16 hrs. At that point stirring was stopped and the solution allowed cooling to room temperature. The toluene phase was separated from the ionic liquid using a syringe and the ionic liquid was extracted twice with dry toluene (2 x 8 mL). The combined toluene fractions were reduced to a volume of 4 mL by rotary evaporation under vacuum (500 Pa). The product was precipitated by pouring the toluene solution into anhydrous methanol (50 mL). The product was isolated by filtration, washed three times with anhydrous methanol (3 x 5 mL) and dried at 60 °C, 5 Pa.

7.3.3 (Deuterated) Cellulose film preparation

Films of cellulose derivatives made from commercial cellulose acetate and DBC were prepared using the procedure described below. Solutions of cellulose acetate (CA) in acetone were prepared at different concentrations (0.13, 0.4 and 1 mg/mL). CA solution (2 mL) was placed on the cleaned silicon block and then spin-coated (Laurell Technologies Co., PA, model WS-650HZB-23NPPB-UD-3) at 4000 rpm for 30 seconds. After evaporation of acetone, the cellulose acetate film was hydrolysed to cellulose by soaking it in 0.5% sodium methoxide solution on methanol.

The trimethylsilyl cellulose (TMSC, 4 mg) was dissolved in toluene (0.4 mL) and the solution was placed on a cleaned silicon block and then spin-coated at 4000 rpm for 30 seconds. The TMSC films were hydrolysed to cellulose film by exposure to vapours above 1M aqueous HCl in a closed container for 30 mins.

7.3.4 Physical Measurements

Infrared spectra (IR) were obtained by the Fourier Transform method in attenuated total reflectance geometry (ATR-FTIR, Perkin-Elmer, Spectrum One with an STI “Thunderdome” ATR system). The spectra were the result of the accumulation of 64 scans, at a resolution of 4 cm⁻¹ in the range from 4,000 to 650 cm⁻¹.

X-ray reflectometry (XRR) measurements were performed at the Australian Nuclear Science and Technology Organization (ANSTO, Sydney, Australia). XRR was performed as a function of incident angle (θ) with a step size of 0.01° , measuring the specularly reflected beam as a function of the momentum change perpendicular to the surface ($q_z = 4\pi\sin\theta/\lambda$, where λ is the wavelength of the incident beam) [38]. The XRR measurements were performed in air on a Panalytical XPert Pro diffractometer operating with Cu tube to generate $\lambda=1.54 \text{ \AA}$ ($\text{CuK}\alpha 1$) radiation. The q -range corresponds to $0.007\text{-}0.718 \text{ \AA}^{-1}$. The Platypus reflectometer utilises both angular and wavelength dependence of the specularly reflected beam. The MOTOFIT [15] macro for Igor Pro 6.32A (Wavemetrics, Inc., Lake Oswego, USA) was used to model the XRR data.

7.4 Results and discussion

In many mammals, an antibody (Immunoglobulin, Ig), a Y-shaped protein, is produced by the immune system to identify and neutralize foreign objects. In humans, there are five isotypes of antibodies, within which the IgM a pentamer, and IgG a monomer, are commonly used in human blood typing. Recently, fundamentals and applications of paper diagnostics have been focussed on accurate, rapid and reliable blood typing. Further optimization of blood typing paper requires better understanding the interaction between antibodies and cellulose surface in terms of three aspects: 1) the conformation and morphology of antibodies on the cellulose surface, especially in aqueous media; 2) the relationship between the conformation of the antibodies in solution and at the cellulose/water interface, and 3) the effect of antibody conformation at the cellulose/water interface and macromolecule stability and surface functionality (Figure 1).

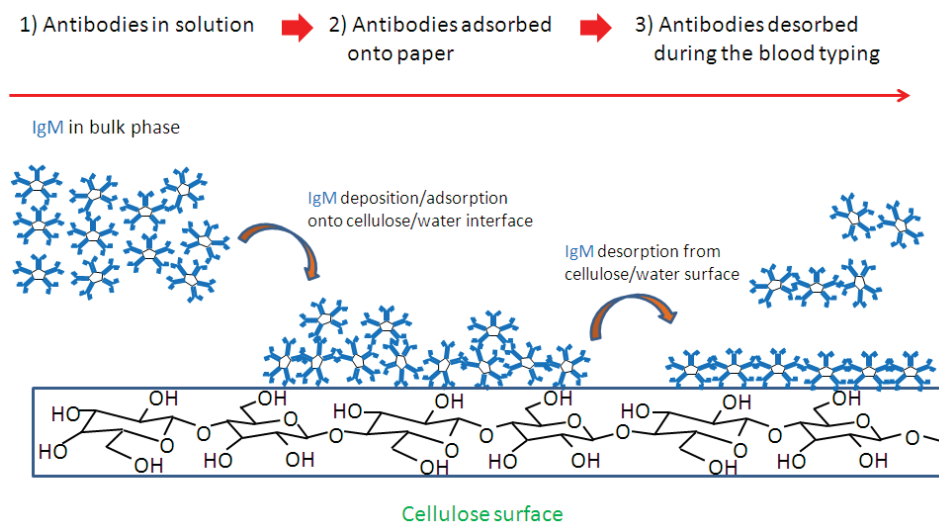


Figure 1: Schematic mechanism of blood typing paper on the cellulose interaction with antibodies (IgM).

Specular neutron reflection is a strong technique to directly investigate phenomena at the surface and solid/water interfaces [29, 39, 40], and this can be employed to monitor cellulose/biomacromolecules interfacial interaction in various conditions. In practice, the development of deuteration, either from water of solvation or from the macromolecule itself, is critical to reveal the structural information and their interaction with each other (Figure 2). When the water of solvation is replaced by heavy water, some of the protons of the macromolecule will be replaced by deuterium through exchange with the solvent, which following the principle that a proton bound to a carbon atom will not exchange, but that those bound to nitrogen and oxygen will exchange if they are accessible to the solvent [41, 42].

Although deuteration from $\text{H}_2\text{O}/\text{D}_2\text{O}$ mixture is relatively simple, the differentiation of neutron scattering length density (SLD) for the macromolecules is limited to a certain range. For example, SLD of protonated cellulose ($\text{C}_6\text{H}_{10}\text{O}_5$) with three labile protons is $1.73 \times 10^{-6} \text{ \AA}^{-2}$, and $3.39 \times 10^{-6} \text{ \AA}^{-2}$ for the full H-D exchanged cellulose ($\text{C}_6\text{H}_7\text{D}_3\text{O}_5$) (Figure 2). Another favourable approach to enhance the contrast is directly synthesizing the deuterated macromolecules. With regards to cellulose/biomacromolecules interaction, we target a routine which prepares cellulose with varying deuteration content, and then generate flat deuterated cellulose films for neutron reflection measurement.

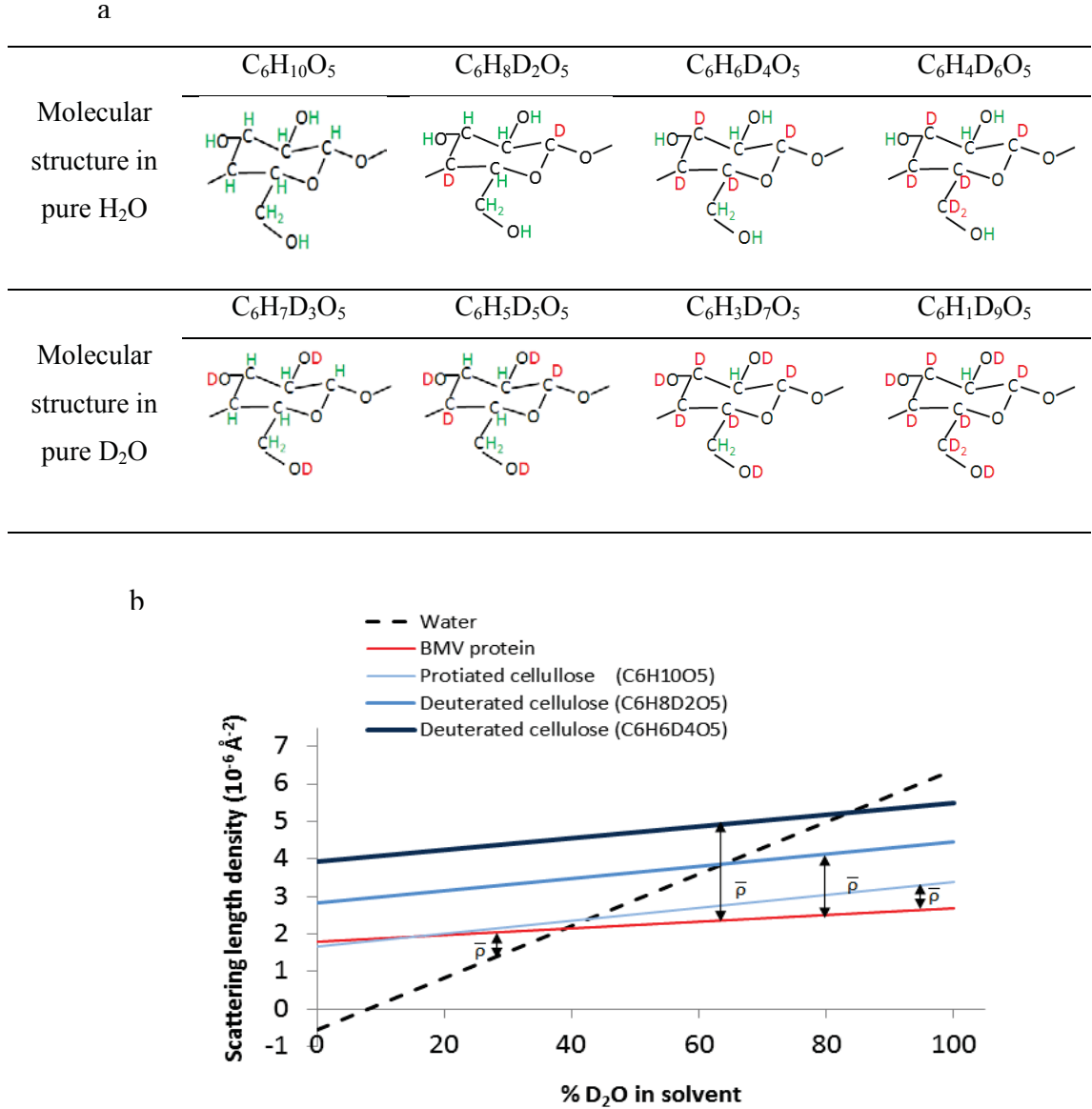


Figure 2: (a) Molecular structure of amorphous cellulose (three labile protons from hydroxyl groups) with different deuteration level when immerse in pure H_2O and D_2O . (b) Scattering length densities (SLDs) from BMV protein (ref.), protonated and deuterated cellulose (with three labile protons) as a function of D_2O content in the solvent. We assume that all labile protons (from hydroxyl groups) are exchanged in proportion with the D_2O content of the solvent. This figure depends on the value of the specific volume of the molecules used for the calculation. The crossing point of the water line with that of a molecule (protein and cellulose) is called the “matching point” or isopicnic point. $\bar{\rho}$ is called the contrast.

Biomass such as wood provides abundant resource for cellulose, and deuterated cellulose can be obtained by growing the plant in D_2O [43], and the deuterium incorporation recorded at 60%. Higher deuterium incorporation (>80%) were achieved in bacterial cellulose, reported by He and Bali [22, 23]. In this study, we explored the preparation of smooth cellulose film from deuterated bacterial cellulose, which can be used to study to the interaction with biomacromolecules such as antibodies by neutron reflectivity (Figure 3).

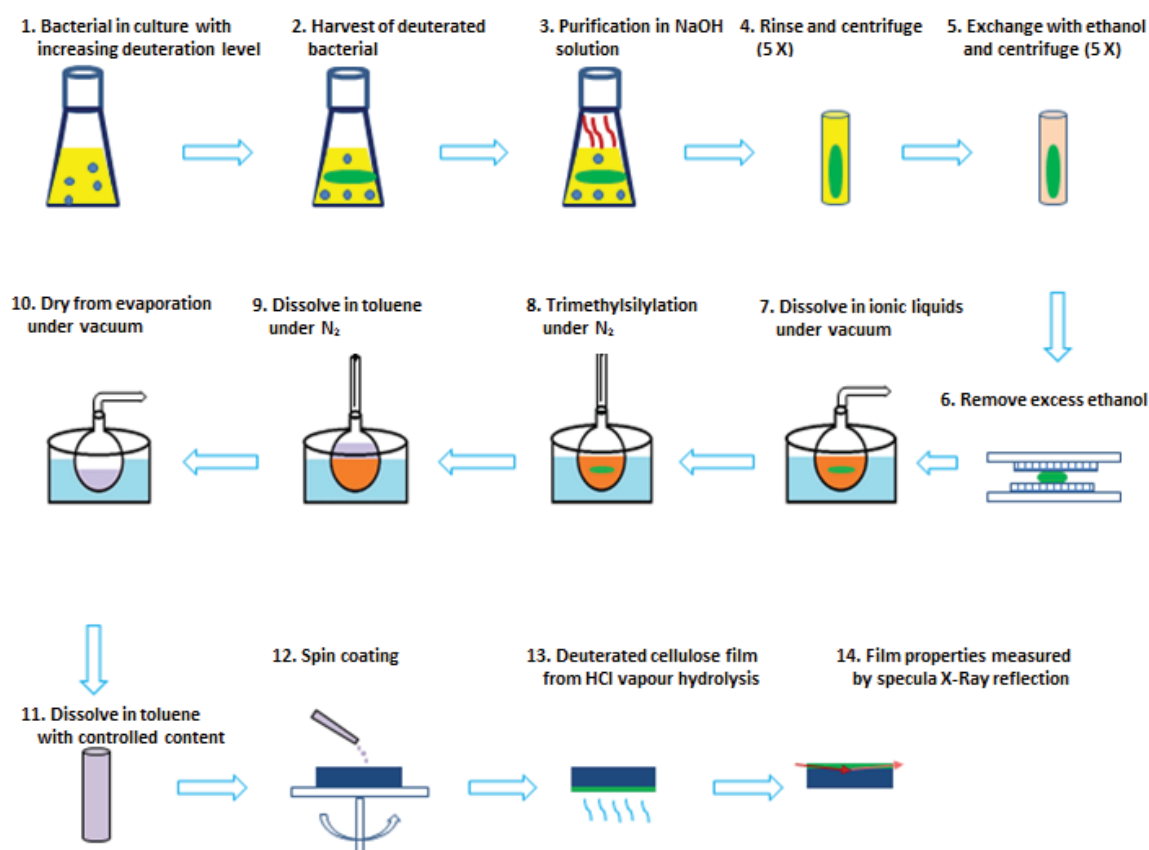


Figure 3: Schematic procedure to prepare cellulose films with contrast variation for neutron reflectometry

7.4.1 Purification of DBC and determination of degree of deuteration.

Strains of *Gluconacetobacter xylinus* are the most prolific in bacterial cellulose production, forming a pad or a membrane of cellulose called a pellicle on the surface of the culture medium. Unlike most plant-derived cellulose, the bacterial cellulose is not synthesized as a composite with other insoluble polymers (lignin, hemicelluloses) but is extruded into growth medium from where it can be isolated and purified readily. The

bacterial cells and debris were removed from the pellicles by soaking in NaOH solution [44], which was confirmed by the FTIR spectra (Figure 4) of deuterated bacterial cellulose (DBC) sample showing an absence of two signature bands of protein (amide I at $1,655\text{ cm}^{-1}$ and amide II at $1,545\text{ cm}^{-1}$) after the purification [45].

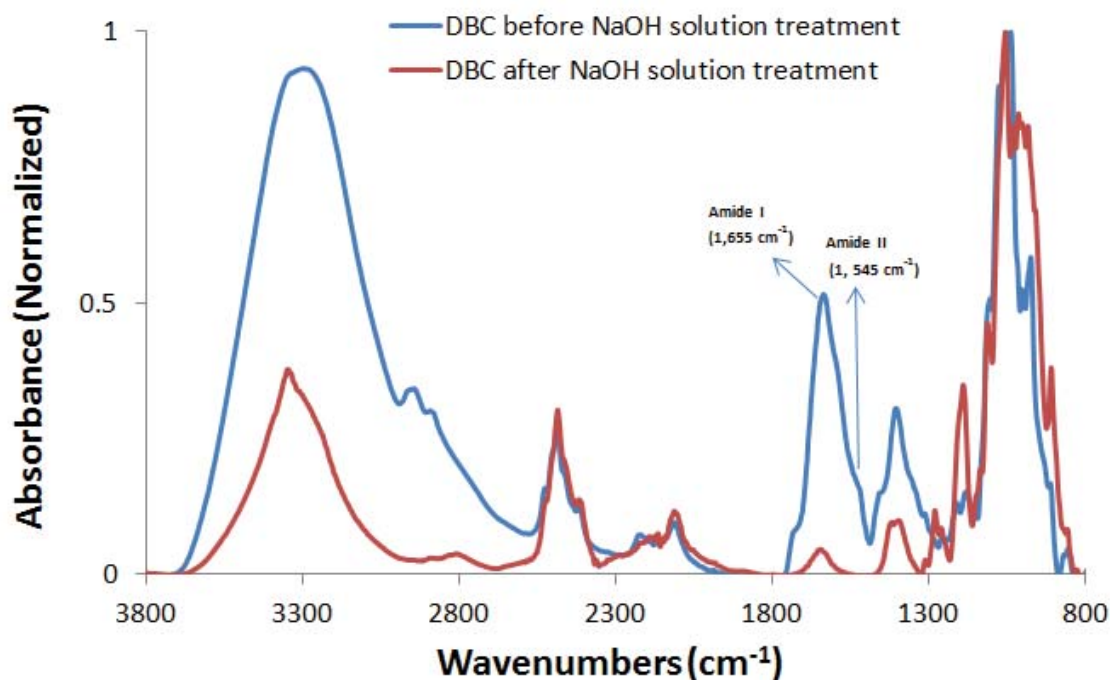


Figure 4: ATR-FTIR spectra of dried deuterated bacterial cellulose before and after NaOH treatment to remove protein and other cellular material. The spectrum has been normalized, for clarity of presentation.

The FTIR spectrum of DBC and protonated bacterial cellulose (PBC) as a reference was compared in Figure 5 and Table I. OH-stretching infrared bands are located at approximated $3,500$ and $3,300\text{ cm}^{-1}$ in the samples. The presence of OH stretching in DBC is attributed to the presence of hydration water at the surface of the cellulose [46]. The majority of the bands corresponding to the CH-stretching modes are located around $3,000\text{--}2,800\text{ cm}^{-1}$, and the expected absorption bands were observed in the PBC spectra (Figure 5). These bands were largely absent in the corresponding spectra of the DBC sample. Bands around $2,485\text{ cm}^{-1}$ and $2,100\text{ cm}^{-1}$, corresponding to O-D stretching and C-D stretching respectively, were recorded in DBC sample (Figure 5). These data provide strong evidence for incorporation of major proportions of deuterium in the DBC.

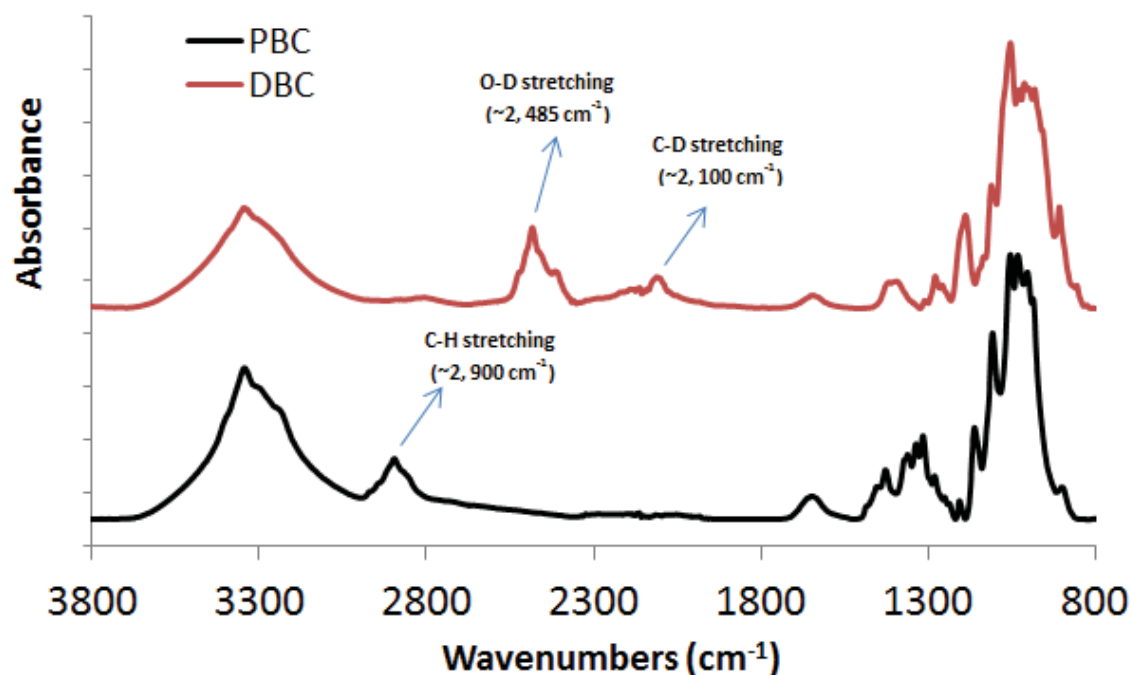


Figure 5: ATR-FTIR of bacterial cellulose with and without deuteration. The spectra are normalized and vertically offset, for clarity of presentation. The protonated bacterial cellulose (PBC) has been used as a reference.

Table I: Assignment of FTIR spectra of bacterial samples, and the ratio of absorbance of characteristic peaks from Figure 2.

Band assignments Wavenumber(cm ⁻¹)									
	O-H stretching	C-H stretching	C-H bending, deformation	O-H in plane bending	C-O stretching	C-O-C vibration	C-D stretching	O-D stretching	Associated Water
Protonated Bacterial Cellulose	3200-3480	2900	1454 1361 1315 1277	1208	1054	1108	-	-	1650
Deuterated Bacterial Cellulose	3337	2888 (weak)	1420 1308 1277 (weak)	1186	1054	1110	2100	2485	1648

7.4.2 Cellulose derivatives prepared in ILs and dissolution in solvents.

Nanocellulose has been used to prepared cellulose model films by spin coating. However, it has not been possible to achieve molecularly smooth film surfaces required for neutron reflectometry due to the morphology of nanocellulose and the packing capability of the silicon substrate [29], therefore more indirect methods have been developed in this study. The approach used has been to prepare cellulose derivatives (acetates and trimethylsilyl

derivatives) that can dissolve in volatile solvents, and then to spin coat a solution of the derivative on to a molecularly smooth silicon disc. Subsequent hydrolysis of the films under mild conditions gave molecularly smooth films of both protonated and deuterated celluloses suitable for analysis by neutron reflectance (NR) [39, 40]. Our initial attempts at using this approach used cellulose acetate (CA) made by homogenous reaction of cellulose dissolved in the ionic liquid, BMIM chloride with acetic anhydride and pyridine.

The solubility of cellulose acetate in solvents greatly depends on its degree of substitution. Cellulose triacetate (DS=3) is known to dissolve in chloroform, but is only sparingly soluble in acetone, whereas the diacetate (DS= 2) is soluble in acetone [30]. Acetone was chosen for spin coating in this study because of the lower toxicity compared to chloroform and the difficulty in avoiding inhalation of solvent vapours while spin coating. Cellulose diacetate with sufficient acetone solubility for spin coating is normally obtained from the triacetate by controlled hydrolysis [47]. The potential alternative of producing cellulose diacetate directly by controlled acetylation of cellulose was explored. In order to test this hypothesis, microcrystalline cellulose (MCC) was dissolved in 1-butyl-3-methylimidazolium chloride (BMIM chloride), and the acetylation was conducted in the presence of acetic acid and anhydrous pyridine within 24 h. As expected, the acetylation of the hydroxy groups was evidenced by a strong absorption in the FTIR spectrum of the crude product at $1,740\text{ cm}^{-1}$ (Figure 6), which is assigned to the symmetric stretching carbonyl group (C=O) in cellulose acetate [29].

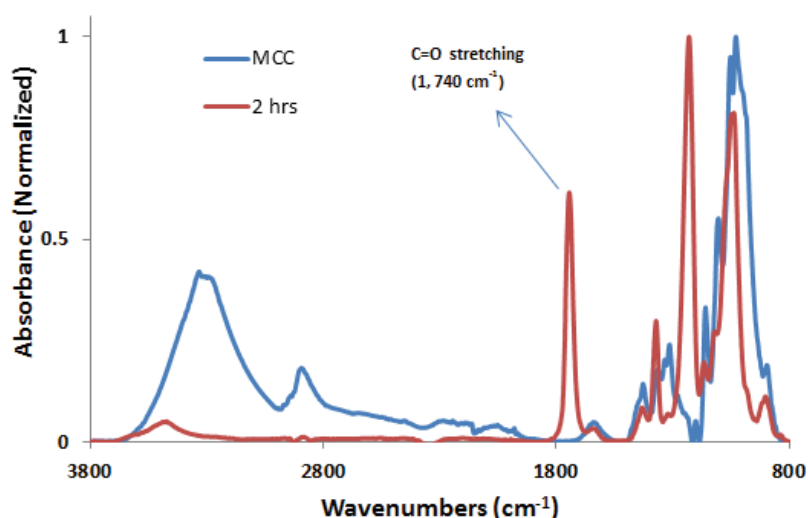


Figure 6: ATR-FTIR of cellulose derivatives from acetylation of microcrystalline cellulose (MCC) in ILs.

Table II: Solubility of cellulose derivatives from acetylation and trimethylsilylation. Complete solubility was confirmed by ensuring lack of any turbidity in the solution being observed when a red laser beam was shone through the solutions following centrifuging.

Notes: 1. Figures based on the total weights of acetylated products

2. Calculated from the ratio between toluene-soluble product and the expected theoretical yield of trimethylsilylated cellulose (DS=2.0)

Time of Acetylation (h)	Solubility in acetone	% cellulose soluble in acetone / % soluble in chloroform¹
2	Poor	10/26
2.5	High	46/48
3	Insoluble	0/100
24	Insoluble	0/100
Commercial cellulose acetate	High	100/0
Material for trimethylsilylation	Solubility in toluene	Percentage of cellulose can dissolved in toluene (%)²
Microcrystalline cellulose	High	81
Protonated Bacterial Cellulose	High	77
Deuterated Bacterial Cellulose	High	74

Cellulose acetate with a degree of substitution (DS) close to that of cellulose triacetate has been shown to form at room temperature within 24 hrs of reaction under similar reaction conditions (Table II). Because a significant yield product with a DS closer to 2, rather than 3 was required for spin coating, the yields and solubilities of products formed after different reaction times were studied. In all cases, crude acetylation products were dried as described above and the resulting solids were fractionated by mixing firstly with acetone and then with chloroform. The data obtained are shown in Table II. Under the reaction conditions described above, a DS close to 3 was obtained after no more than 3 hrs, because the entire product was soluble in chloroform. Following shorter reaction times, the amount of product found to be soluble in acetone (46 wt %) after 2.5 h was found to be higher than that obtained after 2.0 h (10 wt %). The crude product from the 2.5 h acetylation was however accompanied by a considerable amount of product (48 wt %) that is presumed to have a DS close to 3 because of its lack of solubility in acetone and its solubility in chloroform. Achieving an intermediate and uniform DS of all the cellulose molecules is difficult, resulting in partial solubilisation of the cellulose derivatives. This is the challenge of targeting cellulose diacetate to dissolve in acetone. It

is more practical to react cellulose to full substitution or to rely on a solvent effective above a minimal DS, such as trimethylsilyl cellulose dissolving in toluene for $DS > 2$.

Previous studies have demonstrated that the thickness and roughness of spin-coated films of cellulose esters are significantly influenced by: 1) the interaction energy between substrate and solvent and, 2) the solvent evaporation rate [33, 34, 48-51]. In general, films of cellulose esters prepared from solutions made from more volatile solvents yield rougher films. Because acetone evaporates quite rapidly under ambient conditions (vapour pressure = 24, 500 Pa at 20 °C), spin coating of cellulose derivatives from toluene (vapour pressure = 2,900 Pa at 20 °C) solution was also examined with the aim of producing even smoother films.

Trimethylsilylation of microcrystalline cellulose with hexamethyldisilazane (HMDS) in ionic liquids (ILs) has been investigated by Mormann et al who have reported that some of these derivatives are soluble in toluene [32]. These authors characterised the degree of silylation and molecular weights of the products made under a range of conditions using FTIR, NMR and gel-permeation chromatography (GPC). It was concluded that the yield of trimethylsilylation and degree of substitution (DS) were controlled primarily by four factors: 1) the solubility of HMDS in the IL used to dissolve the cellulose; 2) the ratio between the reactants used; 3) temperature and 4) reaction time. The authors found that trimethylsilylated cellulose is soluble in toluene when its DS is greater than 2 [32].

In the present study, the conditions used by Mormann et al were modified by increasing the HMDS /cellulose ratio. Under these modified conditions using MCC, the product obtained in 81 wt % yield showed similar solubility in toluene to some of the products described by Mormann (Table II). Having established suitable conditions for converting MCC into a toluene-soluble derivative, protonated and deuterated bacterial celluloses were also subjected to trimethylsilylation under the same conditions. Because bacterial cellulose is very difficult to dissolve in BMIM chloride once it has been dried from aqueous suspension, the bacterial celluloses were dried by exchanging the water with ethanol. Use of this technique preserved the porous fibrous web structure of the bacterial cellulose providing a much greater surface area for the solvent molecules to access. Yields of toluene soluble material from BC samples using this technique was found to be somewhat lower than yields obtained from dry MCC powder presumably because of

reaction of the reaction between hexamethyl disilazane and residual ethanol. Nevertheless, yields (0.5-1 %) of toluene soluble product were adequate to enable successful spin coating experiments.

7.4.3 Deuterated cellulose film properties and perspectives

Solutions from cellulose acetate (CA) in acetone and trimethylsilylated cellulose (TMSC) in toluene were compared for spin coating. It was found in our previous study that the regenerated film from CA became rougher on hydrolysis [29]. This increase in roughness is possibly caused by swelling of the film when completely immersed in ethanolic sodium methoxide solution and subsequent shrinkage of the cellulose on washing and drying. In contrast, the films made from TMSC became smoother during hydrolysis to cellulose in the vapour above 1 M aqueous HCl [33, 34]. This observation is possibly explained by the fact that neither the TMSC, nor the cellulose is swollen to the same extent by the water vapour containing and traces of HCl as the cellulose immersed in methanolic ethoxide. There is very little swelling and subsequent shrinkage, so the smoothness of the films is maintained and possibly enhanced by a small amount of shrinkage when the vapour is removed.

The inner structure of materials can be measured by small angle scattering (SAS) techniques due to their interaction of their electrons with X-rays, or their interactions of their nuclei with neutron beams. These interactions can be measured using scattering length density (SLD) profiles. Theoretical SLD (ρ) profiles for the materials can be calculated according to the following formula:

$$\rho = \frac{N_a \rho_{\text{mass}}}{M_R} \times \sum_{i=1}^n b_{ci} \quad (1)$$

In Equation (1), b_{ci} is the bound coherent scattering length of the i th atom of a molecule with n atoms (b_{ci} is different for X-ray to neutron beam). N_a is Avogadro's number, ρ_{mass} is the mass density of the material and M_R is its relative molecular mass. Theoretical neutron reflectivity curves of cellulose film with different SLD were plotted using the first order assumption that the thickness (200 Å) and roughness (4 Å) were the same for all films (Figure 7). The curve pattern is largely affected by the SLD, and the increasing SLD results the greater magnitude of the fringes.

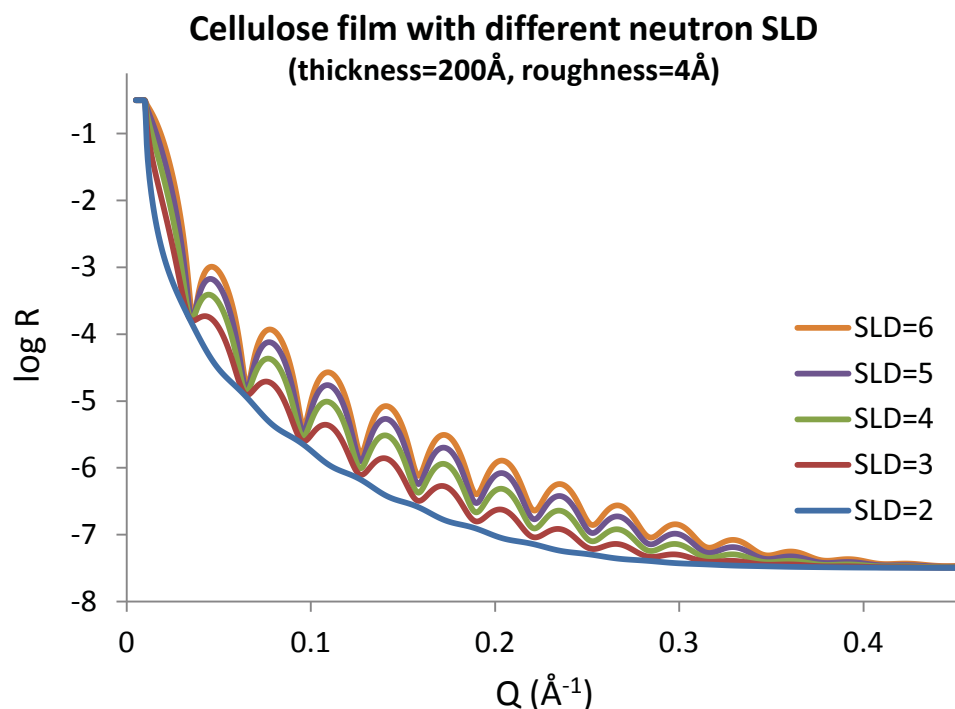


Figure 7: Theoretical NR curves for the cellulose films (air/solid interface, assume the thickness=200Å, roughness=4Å) with different SLD.

The SLD is directly related to the atomic composition and the density. Theoretical value of SLD of cellulose with different deuteration level as a function of D₂O content in the solvent was plotted in Figure 2. The density is affected by the crystallinity of the cellulose in the film [52] because the density of amorphous cellulose ranges from 1.26 to 1.50 g/cm³, whereas the density of crystalline cellulose is ~1.6 g/cm³. The SLD value of protonated cellulose (C₆H₁₀O₅) films with a density of 1.48 gcm⁻³ increases from $1.73 \times 10^{-6} \text{ Å}^{-2}$ up to $7.02 \times 10^{-6} \text{ Å}^{-2}$, in the case of the most highly deuterated cellulose. This feature can be utilized to investigate the biomacromolecules, such as antibodies, absorbed at cellulose interfaces. In cases where the SLD of layers are close to each other, interfacial properties become indistinguishable, whereas changing the SLD of the cellulose layer by use of deuterated cellulose opens up the opportunity to gain much better contrast between the SLD of the cellulose and that of the antibody, or other protein. When water/biomolecule/cellulose interfacial phenomena is studied by neutron reflection measurement, the contrast variation can be engineered either by alteration of % D₂O in water or by deuteration of cellulose, as deuteration of biomolecules is much more technically difficult. Cellulose (C₆H₁₀O₅) has 10 protons per anhydroglucose monomer (Figure 2a); 3 of those are from hydroxyl groups which are labile and readily

exchangeable with solution, and 7 are part of the carbon backbone and not labile. That means that chemical derivatization with a deuterated substituent or exchange in D_2O can bring the D content to 30%, which would result in a SLD of around $3.4 \times 10^{-6} \text{ \AA}^{-2}$ (Figure 2b), providing only a moderate contrast with (bio)polymers (Figure 2b). Maximum contrast requires deuteration of the non-exchangeable protons on the cellulose backbone, this engineering of the cellulose match point provides for clear contrast with the biomacromolecules (protein, enzyme), thereby enabling clear observation of the interaction with cellulose.

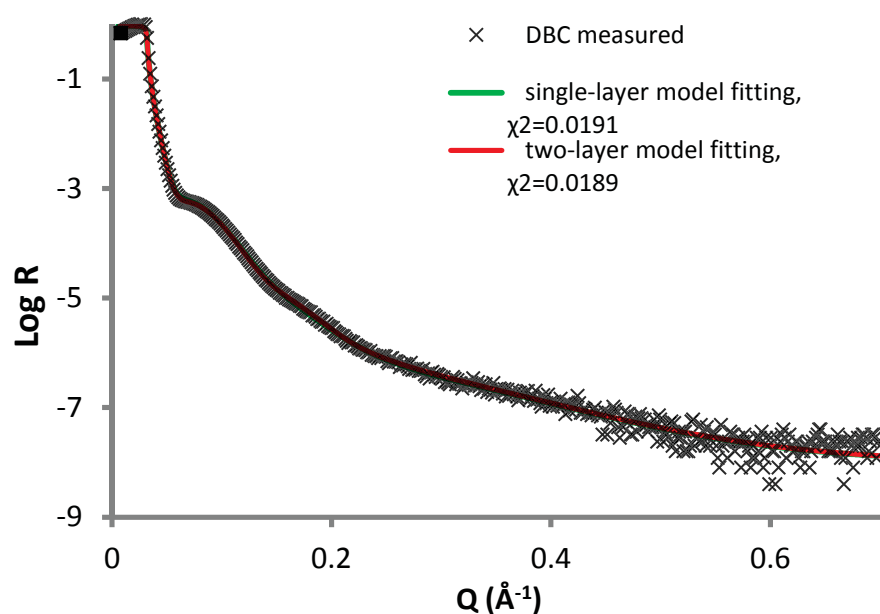


Figure 8: Specular X-ray reflection measurement of deuterated cellulose film and fitting results from two models: single-layer and two-layer.

The variables affecting properties of regenerated cellulose film from spin coating are not only dictated by cellulose derivatives solution (solvent, concentration) and substrate used, but also spinning (speed, period) and regeneration process [33, 35, 48, 53]. Deuterated cellulose films prepared from their trimethylsilylated derivatives (TMSD) were analysed by X-ray reflectivity, to which the same principles apply in the case of SAS. Specular X-ray reflection measurement of deuterated cellulose film regenerating from TMSD (0.8 wt% in toluene) was plotted in Figure 8, and the experimental data is fitted by two models: 1) single-layer model where we assume the TMSD layer is fully hydrolysed back into deuterated cellulose film. 2) Multilayer-model under the circumstance where the film

is not homogenous due to incomplete regeneration (as unknown hydrolysis kinetics). These models provide different SLD profiles of layers perpendicular to the substrate (Figure 9).

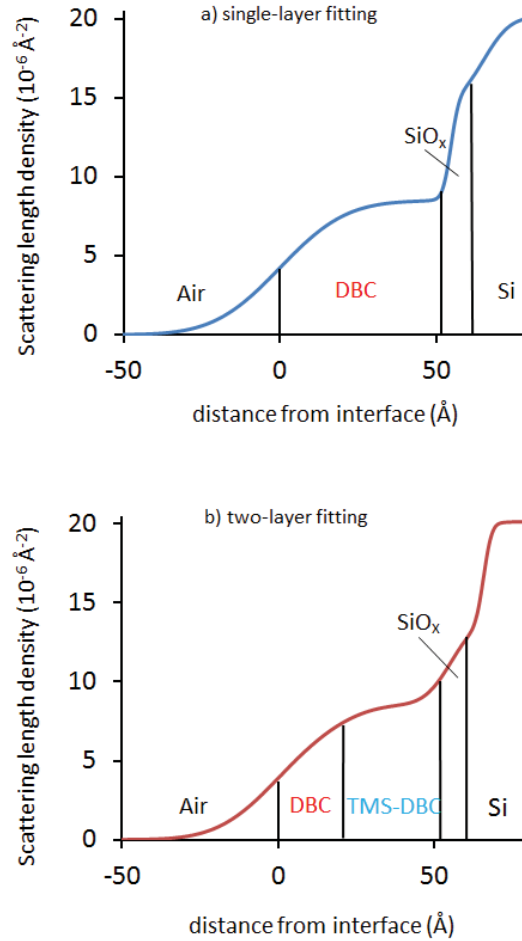


Figure 9: SLD profile from simultaneous fits to deuterated cellulose film on silicon block: a) single-layer model. b) two-layer model.

Properties on thickness (δ), roughness (σ) and SLD of each layer from fitting were shown in Table III. The fitting quality can be evaluated by χ^2 , and the lower value of χ^2 indicates better fits from minimizing the differences between the theoretical and measured reflectivity curves. In the case of single-layer modelling with a slightly lower fitting quality ($\chi^2=0.0191$), where the roughness (σ) of deuterated cellulose layer is 16.6(0.8) Å, which are comparable to 15.3(1.2) Å from two-layer modelling (deuterated cellulose and its derivatives, $\chi^2=0.0189$). The film is thinner but relatively rougher comparing to those regenerated from trimethylsilylated cellulose (protonated, $\delta=78$ Å, $\sigma=8$ Å) [54]. Two possibilities account for this: 1) the hydrogen bondings within deuterated cellulose are

different from that in protonated cellulose [55]. 2) The spin-coating and regeneration process need to be optimized for deuterated cellulose. In addition, the estimated SLD from the deuterated cellulose layer is lower than the theoretical values (Table IV). This probably suggests the film is not fully dense, and contain voids rather than water (X-ray $SLD_{\text{water}}=9.45 \times 10^{-6} \text{ \AA}^{-2}$).

Table III: Deuterated cellulose film on silicon block studied by specular X-ray reflection measurement. Thickness (δ), roughness (σ) and scattering length density (SLD) of the layer were retrieved by fitting the experimental data. χ^2 indicates the quality of fitting, and the lower value of χ^2 indicates better fits from minimizing the differences between the theoretical and measured reflectivity curves. χ^2 , δ , σ and SLD from the best fitting. The 95% confidence in the parenthesis is from three optimal fitting results.

Model	χ^2	Layer	Properties		
			δ (Å)	σ (Å)	SLD (10^{-6} \AA^{-2})
single-layer	0.0191	Deuterated Cellulose	54.6 (0.3)	16.6 (0.8)	8.49 (0.03)
		SiO _x	10.4 (0.1)	2.0 (0.1)	14.61 (0.02)
two-layer	0.0189	Deuterated Cellulose	23.1 (0.1)	15.3 (1.2)	7.79 (0.04)
		Trimethylsilylated deuterated cellulose	32.3 (0.2)	9.5 (1.6)	8.57 (0.03)
		SiO _x	10.3 (0.1)	6.78 (0.8)	14.02 (0.05)

Table IV: X-Ray Scattering length density ($\times 10^{-6} \text{ \AA}^{-2}$) of amorphous cellulose at different level of deuteration and density.

Density (g/cm ³)	1.48	1.30	1.26
Cellulose			
C ₆ H ₁₀ O ₅ (Protonated)	13.38	11.75	11.39
C ₆ H ₉ DO ₅	13.30	11.68	11.32
C ₆ H ₈ D ₂ O ₅	13.22	11.61	11.25
C ₆ H ₇ D ₃ O ₅	13.13	11.54	11.18
C ₆ H ₆ D ₄ O ₅	13.05	11.47	11.11
C ₆ H ₅ D ₅ O ₅	12.98	11.40	11.05
C ₆ H ₄ D ₆ O ₅	12.90	11.33	10.98
C ₆ H ₃ D ₇ O ₅	12.82	11.26	10.91

7.5 Conclusion

Preparation of thin and smooth deuterated cellulose film with contrast variation for neutron reflectometry is investigated in the study. Incorporation of deuterium into cellulose is successfully obtained from bacterial cellulose at first. This is achieved by growing *Gluconacetobacter xylinus* strain ATCC 53524 in deuterated glucose and deuterated glycerol, and deuteration of cellulose was confirmed by ATR-FTIR. Afterwards, two strategies are compared to synthesize cellulose derivatives which can dissolve in solvents (acetone and toluene) for spin coating: either acetylation or trimethylsilylation in ionic liquid (1-Butyl-3-methylimidazolium chloride). The trimethylsilylation of deuterated cellulose allows high yield of product, and is used to prepare toluene solution for spin-coating onto silicon substrate. The resultant thin film is hydrolysed back to deuterated cellulose in HCl vapour, and then examined by specular X-ray reflection measurement. The established approach is of significant importance to prepare a series of deuterated cellulose films with varying neutron scattering contrast, and used to investigate the interaction between cellulose and biomacromolecules by neutron reflectivity.

7.6 Acknowledgments

Funding was provided by ARC LP09990526. Many thanks to ANSTO and AINSE for beam time and travel grants, respectively.

7.7 References

1. Ngo, Y.H., D. Li, G.P. Simon, and G. Garnier, *Paper surfaces functionalized by nanoparticles*. Advances in Colloid and Interface Science, 2011. **163**(1): p. 23-38.
2. Then Whui, L. and G. Garnier, *Paper diagnostics in biomedicine*, in *Reviews in Analytical Chemistry* 2013. p. 269.
3. Khan, M.S., G. Thouas, W. Shen, G. Whyte, and G. Garnier, *Paper Diagnostic for Instantaneous Blood Typing*. Analytical Chemistry, 2010. **82**(10): p. 4158-4164.
4. Al-Tamimi, M., W. Shen, R. Zeineddine, H. Tran, and G. Garnier, *Validation of Paper-Based Assay for Rapid Blood Typing*. Analytical Chemistry, 2012. **84**(3): p. 1661-1668.
5. Jarujamrus, P., J.F. Tian, X. Li, A. Siripinyanond, J. Shiowatana, and W. Shen, *Mechanisms of red blood cells agglutination in antibody-treated paper*. Analyst, 2012. **137**(9): p. 2205-2210.
6. Li, M.S., W.L. Then, L.Z. Li, and W. Shen, *Paper-based device for rapid typing of secondary human blood groups*. Analytical and Bioanalytical Chemistry, 2014. **406**(3): p. 669-677.

7. Then, W.L., M. Li, H. McLiesh, W. Shen, and G. Garnier, *The detection of blood group phenotypes using paper diagnostics*. Vox Sanguinis, 2014: p. n/a-n/a.
8. Su, J.L., M. Al-Tamimi, and G. Garnier, *Engineering paper as a substrate for blood typing bio-diagnostics*. Cellulose, 2012. **19**(5): p. 1749-1758.
9. Li, M.S., J.F. Tian, M. Al-Tamimi, and W. Shen, *Paper-Based Blood Typing Device That Reports Patient's Blood Type "in Writing"*. Angewandte Chemie-International Edition, 2012. **51**(22): p. 5497-5501.
10. Orelma, H., I. Filpponen, L.S. Johansson, M. Osterberg, O.J. Rojas, and J. Laine, *Surface Functionalized Nanofibrillar Cellulose (NFC) Film as a Platform for Immunoassays and Diagnostics*. Biointerphases, 2012. **7**(1-4).
11. Orelma, H., L.S. Johansson, I. Filpponen, O.J. Rojas, and J. Laine, *Generic Method for Attaching Biomolecules via Avidin-Biotin Complexes Immobilized on Films of Regenerated and Nanofibrillar Cellulose*. Biomacromolecules, 2012. **13**(9): p. 2802-2810.
12. Orelma, H., T. Teerinen, L.S. Johansson, S. Holappa, and J. Laine, *CMC-modified cellulose biointerface for antibody conjugation*. Biomacromolecules, 2012. **13**(4): p. 1051-8.
13. Kontturi, E., T. Tammelin, and M. Osterberg, *Cellulose - model films and the fundamental approach*. Chemical Society Reviews, 2006. **35**(12): p. 1287-1304.
14. Orelma, H., I. Filpponen, L.S. Johansson, J. Laine, and O.J. Rojas, *Modification of Cellulose Films by Adsorption of CMC and Chitosan for Controlled Attachment of Biomolecules*. Biomacromolecules, 2011. **12**(12): p. 4311-4318.
15. Nelson, A., *Co-refinement of multiple-contrast neutron/X-ray reflectivity data using MOTOFIT*. Journal of Applied Crystallography, 2006. **39**: p. 273-276.
16. Gutberlet, T. and M. Lösche, *Complex Biomimetic Structures at Fluid Surfaces and Solid-Liquid Interfaces*, in *Neutron Scattering in Biology* 2006, Springer Berlin Heidelberg. p. 283-306.
17. Svergun, D.I., M.H. Koch, P.A. Timmins, and R.P. May, *Small Angle X-Ray and Neutron Scattering from Solutions of Biological Macromolecules*. Vol. 19. 2013: Oxford University Press.
18. Leiting, B., F. Marsilio, and J.F. O'Connell, *Predictable deuteration of recombinant proteins expressed in Escherichia coli*. Analytical Biochemistry, 1998. **265**(2): p. 351-355.
19. Doblin, M.S., I. Kurek, D. Jacob-Wilk, and D.P. Delmer, *Cellulose biosynthesis in plants: from genes to rosettes*. Plant and Cell Physiology, 2002. **43**(12): p. 1407-1420.
20. Hestrin, S. and M. Schramm, *SYNTHESIS OF CELLULOSE BY ACETOBACTER-XYLINUM .2. PREPARATION OF FREEZE-DRIED CELLS CAPABLE OF POLYMERIZING GLUCOSE TO CELLULOSE*. Biochemical Journal, 1954. **58**(2): p. 345-352.
21. Ohad, I., S. Hestrin, and D. Danon, *SYNTHESIS OF CELLULOSE BY ACETOBACTER XYLINUM .5. ULTRASTRUCTURE OF POLYMER*. Journal of Cell Biology, 1962. **12**(1): p. 31-&.
22. Bali, G., M.B. Foston, H.M. O'Neill, B.R. Evans, J.H. He, and A.J. Ragauskas, *The effect of deuteration on the structure of bacterial cellulose*. Carbohydrate Research, 2013. **374**: p. 82-88.
23. He, J.H., S.V. Pingali, S.P.S. Chundawat, A. Pack, A.D. Jones, P. Langan, B.H. Davison, V. Urban, B. Evans, and H. O'Neill, *Controlled incorporation of deuterium into bacterial cellulose*. Cellulose, 2014. **21**(2): p. 927-936.
24. Chumpitazi-Hermoza, B.F., D. Gagnaire, and F.R. Taravel, *Bacterial biosynthesis of cellulose from d-glucose or glycerol precursors labelled with deuterium*. Carbohydrate Polymers, 1983. **3**(1): p. 1-12.
25. Chumpitazihermoza, B., D. Gagnaire, and F.R. Taravel, *BIOSYNTHESIS OF BACTERIAL CELLULOSE FROM GLYCEROL SELECTIVELY DEUTERATED IN 1, 2 OR 3 POSITION - STUDY BY NUCLEAR MAGNETIC-RESONANCE*. Biopolymers, 1978. **17**(10): p. 2361-2372.

26. Gagnaire, D. and F.R. Taravel, *BIOSYNTHESIS OF BACTERIAL CELLULOSE FROM GLUCOSE SELECTIVELY DEUTERATED IN POSITION 6 - NMR-STUDY*. FEBS letters, 1975. **60**(2): p. 317-321.
27. Barnoud, F., D. Gagnaire, L. Odier, and Vincendo.M, *BIOSYNTHESIS OF DEUTERATED BACTERIAL CELLULOSE - NMR STUDY ON LEVELS OF INCORPORATION AND LOCALIZATION OF DEUTERIUM*. Biopolymers, 1971. **10**(11): p. 2269-8.
28. Edgar, C.D. and D.G. Gray, *Smooth model cellulose I surfaces from nanocrystal suspensions*. Cellulose, 2003. **10**(4): p. 299-306.
29. Su, J., C.J. Garvey, S. Holt, R.F. Tabor, B. Winther-Jensen, W. Batchelor, and G. Garnier, *Adsorption of cationic polyacrylamide at the cellulose-liquid interface: a neutron reflectometry study*. Journal of Colloid and Interface Science, 2015(0).
30. Kamide, K., K. Okajima, K. Kowsaka, and T. Matsui, *Solubility of Cellulose-Acetate Prepared by Different Methods and Its Correlations with Average Acetyl Group Distribution on Glucopyranose Units*. Polymer Journal, 1987. **19**(12): p. 1405-1412.
31. Qu, C., T. Kishimoto, M. Kishino, M. Hamada, and N. Nakajima, *Heteronuclear Single-Quantum Coherence Nuclear Magnetic Resonance (HSQC NMR) Characterization of Acetylated Fir (Abies sachalinensis MAST) Wood Regenerated from Ionic Liquid*. Journal of Agricultural and Food Chemistry, 2011. **59**(10): p. 5382-5389.
32. Mormann, W. and M. Wezstein, *Trimethylsilylation of Cellulose in Ionic Liquids*. Macromolecular Bioscience, 2009. **9**(4): p. 369-375.
33. Kontturi, E., P.C. Thune, and J.W. Niemantsverdriet, *Novel method for preparing cellulose model surfaces by spin coating*. Polymer, 2003. **44**(13): p. 3621-3625.
34. Kontturi, E., P.C. Thune, and J.W. Niemantsverdriet, *Cellulose model surfaces-simplified preparation by spin coating and characterization by X-ray photoelectron spectroscopy, infrared spectroscopy, and atomic force microscopy*. Langmuir, 2003. **19**(14): p. 5735-5741.
35. Kontturi, E., L.S. Johansson, K.S. Kontturi, P. Ahonen, P.C. Thune, and J. Laine, *Cellulose nanocrystal submonolayers by spin coating*. Langmuir, 2007. **23**(19): p. 9674-9680.
36. Su, J., C.J. Garvey, S. Holt, R.F. Tabor, B. Winther-Jensen, W. Batchelor, and G. Garnier, *Adsorption of cationic polyacrylamide at the cellulose-liquid interface: A neutron reflectometry study*. Journal of Colloid and Interface Science, 2015. **448**(0): p. 88-99.
37. Heinze, T., K. Schwikal, and S. Barthel, *Ionic Liquids as Reaction Medium in Cellulose Functionalization*. Macromolecular Bioscience, 2005. **5**(6): p. 520-525.
38. Nelson, A., *Co-refinement of multiple-contrast neutron/X-ray reflectivity data using MOTOFIT*. Journal of Applied Crystallography, 2006. **39**(2): p. 273-276.
39. Cheng, G., Z.L. Liu, J.K. Murton, M. Jablin, M. Dubey, J. Majewski, C. Halbert, J. Browning, J. Ankner, B. Akgun, C. Wang, A.R. Esker, K.L. Sale, B.A. Simmons, and M.S. Kent, *Neutron Reflectometry and QCM-D Study of the Interaction of Celluloses with Films of Amorphous Cellulose*. Biomacromolecules, 2011. **12**(6): p. 2216-2224.
40. Kontturi, E., M. Suchy, P. Penttila, B. Jean, K. Pirkkalainen, M. Torkkeli, and R. Serimaa, *Amorphous Characteristics of an Ultrathin Cellulose Film*. Biomacromolecules, 2011. **12**(3): p. 770-777.
41. Campbell, S., M.T. Rodgers, E.M. Marzluff, and J.L. Beauchamp, *Deuterium exchange reactions as a probe of biomolecule structure. Fundamental studies of gas phase H/D exchange reactions of protonated glycine oligomers with D2O, CD3OD, CD3CO2D, and ND3*. Journal of the American Chemical Society, 1995. **117**(51): p. 12840-12854.
42. Jacrot, B., *Study of Biological Structures by Neutron-Scattering from Solution*. Reports on Progress in Physics, 1976. **39**(10): p. 911-953.
43. Evans, B.R., G. Bali, D.T. Reeves, H.M. O'Neill, Q.N. Sun, R. Shah, and A.J. Ragauskas, *Effect of D2O on Growth Properties and Chemical Structure of Annual Ryegrass (Lolium multiflorum)*. Journal of Agricultural and Food Chemistry, 2014. **62**(12): p. 2595-2604.

44. Mikkelsen, D., B.M. Flanagan, G.A. Dykes, and M.J. Gidley, *Influence of different carbon sources on bacterial cellulose production by Gluconacetobacter xylinus strain ATCC 53524*. Journal of Applied Microbiology, 2009. **107**(2): p. 576-583.
45. Giordano, M., M. Kansiz, P. Heraud, J. Beardall, B. Wood, and D. McNaughton, *Fourier transform infrared spectroscopy as a novel tool to investigate changes in intracellular macromolecular pools in the marine microalga Chaetoceros muellerii (Bacillariophyceae)*. Journal of Phycology, 2001. **37**(2): p. 271-279.
46. Kim, D.Y., Y. Nishiyama, and S. Kuga, *Surface acetylation of bacterial cellulose*. Cellulose, 2002. **9**(3-4): p. 361-367.
47. Yarsley, V.E., *Cellulosic plastics : cellulose acetate, cellulose ethers, regenerated cellulose, cellulose nitrate* 1964, London: Iliffe for the Plastics Institute. 220 p.
48. Blachechen, L.S., M.A. Souza, and D.F.S. Petri, *Effect of humidity and solvent vapor phase on cellulose esters films*. Cellulose, 2012. **19**(2): p. 443-457.
49. Park, M.S., W. Joo, and J.K. Kim, *Porous structures of polymer films prepared by spin coating with mixed solvents under humid condition*. Langmuir, 2006. **22**(10): p. 4594-4598.
50. Skrobis, K.J., D.D. Denton, and A.V. Skrobis, *Effect of Early Solvent Evaporation on the Mechanism of the Spin-Coating of Polymeric Solutions*. Polymer Engineering and Science, 1990. **30**(3): p. 193-196.
51. Sukanek, P.C., *Dependence of Film Thickness on Speed in Spin Coating*. Journal of the Electrochemical Society, 1991. **138**(6): p. 1712-1719.
52. Zugenmaier, P. and SpringerLink (Online service), *Crystalline cellulose and cellulose derivatives characterization and structures*, in *Springer series in wood science*, 2008, Springer,: Berlin ; New York. p. 1 online resource (x, 285 p).
53. Sannino, A., S. Pappada, L. Giotta, L. Valli, and A. Maffezzoli, *Spin coating cellulose derivatives on quartz crystal microbalance plates to obtain hydrogel-based fast sensors and actuators*. Journal of Applied Polymer Science, 2007. **106**(5): p. 3040-3050.
54. Schaub, M., G. Wenz, G. Wegner, A. Stein, and D. Klemm, *Ultrathin Films of Cellulose on Silicon-Wafers*. Advanced Materials, 1993. **5**(12): p. 919-922.
55. Hofstetter, K., B. Hinterstoisser, and L. Salmen, *Moisture uptake in native cellulose - the roles of different hydrogen bonds: a dynamic FT-IR study using Deuterium exchange*. Cellulose, 2006. **13**(2): p. 131-145.

Chapter 8

Conclusion

This page is intentionally blank

In recent years, a large number of different paper diagnostic devices (PADs) have been fabricated, applied and investigated in fields ranging from biomedical diagnostics to environmental monitoring. Deficiencies in Sensitivity, Selectivity, Simplicity and Strength (collectively referred to as 4S) still limit commercialisation of PADs. It has been shown that novel strategies based on investigation of structure-property relationships of paper composites and interfacial phenomenon at cellulose surfaces can be used to reduce many of these deficiencies.

Based on the results presented in Chapter 2 it is concluded that, for hardwood pulps, the highest wet to dry strength ratio was obtained at 10 mg addition of PAE to each gram of pulp. Further enhancement of wet tensile strength at 10 mg/g PAE was achieved at NaCl and CaCl_2 concentration of 10 mM, while higher salt additions weakened the paper. This phenomenon can be explained in terms of ionic strength affecting the conformation of the polymer and its adsorption density onto fibres. Ion type and concentration in the papermaking process water influence strength development in different ways –namely by screening electrostatic interaction and ion exchanging with the pulp fibers which affecting the polymer coil morphology in solution and upon adsorption. It is possible to evaluate paper repulpability behaviour in quantitative terms using the new laboratory method that has been developed in this study based on energy consumption by the disintegrator. The repulpability of PAE-strengthened paper reveals a direct link between wet strength and recyclability. The stronger the paper is in a wet state, the more energy it requires for repulping into a usable fiber furnish.

On the **mesoscale**, the strength and porosities of paper composites can be engineered by use of PAE polymers. On a microscale and nanoscales, the cellulose additives with length scales ranging from the nanometer to the micrometer can be used to control properties of paper composites. It was found that cellulose micro-particles (CMPs), produced by cryogenic milling softwood fiber, act as mechanical debonding agents, and decrease the density of the composite resulting in improved paper bulk an porosity but reduced performance of paper as strength decreases. In contrast to CMPs, MFC produced by ball milling that have a higher aspect ratio and smaller size than CMPs significantly improve paper composite strength and decrease its porosity, yielding a denser structure which gives better performance as higher uniformity and strength. The addition of MFC

combined with polyamideamine-epichlorohydrin (PAE) can increase both dry and wet strength of cellulosic materials equivalently by an order of magnitude. Their different stress-strain curves measured under wet conditions suggest two different mechanisms of strength development: MFC-fiber entanglement and fiber-fiber contact reinforcement.

Compared to addition of untethered MFC, refining hardwood fibers can produce tethered MFC that provide equivalent improved strength properties and significant drainage benefits. Furthermore, significant benefits in paper formation uniformity can be achieved. At constant dry strength, composites made with refined fibers had higher density and lower wet strength than those made by blending MFC. The addition of tethered MFC, to pulp fibers combined with polyamideamine-epichlorohydrin (PAE) can also increase the dry strength and wet strength of cellulosic materials by an order of magnitude under appropriate conditions. Air permeability of these composites decreases by up to 4 orders of magnitude with MFC addition, opening new avenues to engineer PADs with controlled porosity. Novel applications in packaging where gas permeativity and sustainability are critical, such as in food are also promising.

In Chapter 5 the data generated demonstrate that the performance of PADs used to type human red blood cells (RBCs) can be correlated quantitatively with the macroscale structure and properties of the paper substrate. Image analysis can be used to distinguish unequivocally between antibody agglutinated (specific) and non-agglutinated (non-specific) RBCs on both commercial and laboratory produced papers under appropriately controlled conditions. Paper blood typing performance decreases in an almost linear manner with paper density, thickness and is inversely proportionally with paper pore size. The type of fibres in the substrate plays a minor role in governing performance of the PAD in this application. Porous cellulose webs modified with cationic polyelectrolyte can further optimize blood typing analysis.

Based on the results presented in Chapter 6, **nanoscale** thin cellulose films (40 ± 7 Å) of roughness less than 10 Å can be formed successfully as model cellulose surfaces. Such films can be produced by spin coating a cellulose acetate-acetone solution onto a smooth flat silicon disc and regenerating the cellulose by alkaline hydrolysis. Film smoothness

can be greatly improved by controlling the concentration of cellulose acetate and the hydrolysis time in methanolic sodium methoxide.

In order to clearly investigate the biomolecules adsorption on cellulose using specular neutron reflectometry, necessary levels of contrast variation in the film can be achieved by spin coating a solution of trimethylsilylated deuterated cellulose in toluene onto a smooth flat silicon disc and then hydrolysing the silyl ether with aqueous hydrogen chloride vapour to regenerate cellulose. Deuterium can be successfully incorporated into bacterial cellulose by growing *Gluconacetobacter xylinus* - strain ATCC 53524 in deuterated glucose and deuterated glycerol solution. 2) Trimethylsilylation of the deuterated bacterial cellulose can be achieved in high yield using ionic liquid as a solvent. The yields of solvent soluble cellulose derivative obtained by this method are much better than those obtained by partial acetylation. These thin and quasi-molecularly smooth cellulose films can find application in any advanced surface characterization technique including AFM, QCM, SFA and ellipsometry.

Characterization of nanoscale cationic polyelectrolyte layers adsorbed at cellulose/water interfaces can be achieved in situ using specular neutron reflectometry. High molecular weight (13MD) polyacrylamide (CPAM) polyelectrolytes of varying charge densities can be used for this purpose. The thickness of CPAM (40% charge) layers at a solid-D₂O interface is 43 ± 4 Å on cellulose and 13 ± 2 Å on silicon. The adsorption thickness is an order of magnitude smaller than the CPAM radius of gyration. The thickness of the CPAM layer adsorbed on cellulose increases with polymer charge density (10 ± 1 Å at 5% and 43 ± 4 Å at 40%). Addition of 10^{-3} M NaCl decreases the thickness of a CPAM layer already adsorbed on cellulose. However, the thickness of an adsorbed layer on cellulose of CPAM deposited from a solution equilibrated in 10^{-3} M NaCl is much higher (89 ± 11 Å for 40% CPAM). The results highlight the charge effect on cationic polyelectrolyte adsorption and conformation at cellulose surfaces and interfaces.

The information generated in this study validate the initial hypothesis that study of cellulose interactions with cationic polyelectrolytes can be used to engineering paper strength, structure and surface properties such that their potential for use in paper-based bio-analytical devices (PADs) is considerably enhanced. By carefully interpreting and

reconciling the results from nanoscale, mesoscale and macroscale studies of papers engineered using cationic polyelectrolytes, low-cost, recyclable substrates with high wet strength, controlled structure and surface properties can be developed and optimized, with benefits to use of paper in current and future bio-diagnostics. Many new applications also emerge in food packaging, where the controlled gas permeability and recycling are critical.

APPENDIX

Papers Included in Each Chapter in Their Published Format

PAPER STRENGTH DEVELOPMENT AND RECYCLABILITY WITH POLYAMIDEAMINE-EPICHLOROHYDRIN (PAE)

Jielong Su,^a Wade K. J. Mosse,^a Scot Sharman,^a Warren Batchelor,^a and Gil Garnier^{a,*}

The tensile strength behavior and recyclability of the paper prepared with the addition of polyamideamine-epichlorohydrin (PAE) were investigated. The dry and wet tensile strengths obtained with different PAE dosage were measured. The highest wet-to-dry strength ratio of 35% was obtained at 10 mg/g; above this addition level wet strength dropped slightly and then remained constant. The repulpability of strengthened paper was correlated directly with wet strength. The effect of electrolyte on tensile strength was also quantified by varying sodium chloride and calcium chloride concentration in the furnish stock. Without PAE, high salt concentrations (100 mM) reduced the tensile strength by 15-20%. At constant PAE addition level of 10 mg/g, low levels of salt addition (of either 10 mM NaCl or 10 mM CaCl₂) slightly improved the strength; paper strength decreased at high salts concentrations. The cation valency and concentration in the process water were important variables which affected the efficiency of PAE. These results present the significance of developing sustainable wet strength agents that can be applied in demanding salty conditions while maintaining the product recyclability.

Keywords: Strength; Repulpability; Polyamideamine-epichlorohydrin (PAE); Recyclability; Paper; Wet-strength

Contact information: a: BioPRIA, Australian Pulp and Paper Institute, Department of Chemical Engineering, Monash University, Wellington Road, Clayton, VIC 3800, Australia.

* Corresponding author: gil.garnier@monash.edu

INTRODUCTION

Strength distribution across paper is ensured by the multiple fibre-fibre bonds and controlled by the bonding area, the adhesion strength, and the fibre strength and size distribution. The Page equation describes the tensile failure of paper in terms of some of these critical variables (Page 1969). The strength of dry and wet paper is crucial to many applications, especially in packaging and tissue products. It has long been established that the tensile strength of paper is directly affected by the swelling behavior of the fibres interacting with water (Rowland Stanley 1977). The strength is controlled by fibre-to-fibre interactions that are developed during the process of paper formation, consolidation, and drying. In dry paper, hydrogen bonding is the dominant adhesive force and only acts over very short distances. As the bonds are water sensitive, the penetration of water into the dry paper matrix leads to a rapid weakening of fibre-to-fibre bonding and a concurrent loss in paper strength (Gardner et al. 2008). To lessen the reduction of paper strength upon contact with water, reactive water-soluble polymers such as polyamide-

amine-epichlorohydrin (PAE) are commonly used to improve the bonding between fibres, which constitutes the weak link in wet paper (Davison 1972).

The generally accepted mechanism of wet-strength development by PAE in paper is through the establishment of chemical bonds at fibre-fibre contacts. The process involves two steps: retention of the polymer and development of bonds. The main variables affecting PAE efficiency include its azetidinium concentration, the type of fibres, and the drying conditions (Obokata et al. 2002; Saito and Isogai 2005). Carboxyl groups, which significantly affect both PAE retention and reactivity, can be introduced to fibres by kraft pulping and through the bleaching process. When adding PAE to a slurry of cellulosic fibres, adsorption is driven by the electrostatic attraction between the anionic carboxylated groups on the fibre surface and the cationic azetidinium groups of the polymer (Espy and Rave 1988; Obokata and Isogai 2007). After PAE adhesion to cellulosic fibres, the curing process facilitates the formation of bonds between fibres. These bonds are covalent between the carboxyl groups of cellulose or hemicelluloses and the polymer's azetidinium group, resulting in inter-fibre bonds that are not water-soluble (Devore and Fischer 1993; Espy 1995). Therefore, special techniques such as a combination of mechanical energy and oxidizing agents are required for successful repulping (Chan 1994; Espy and Geist 1993).

While the fundamentals of PAE resin strength development mechanism are relatively well understood, the effects of PAE addition on recycling are more obscure. This is especially the case for optimizing water and fibre recycling for sustainability. The direct implications are the necessity to form paper with a furnish having very high salt concentration and the ability to fully and easily repulp PAE-made fibre products to insure full recycling. Indeed, many packaging grades are exclusively made of recycled fibres. In these circumstances, the addition of PAE is expected to fulfill two contradictory requirements. On one hand PAE is requested to provide permanent and strong fibre-fibre bonds; on the other hand, the resulting strengthened paper must remain fully recyclable. Very little quantitative information is available in this realm. It is the objective of this study to quantify the behavior of PAE from the modern perspective of sustainable papermaking.

The first part of this study quantifies the effect of PAE on paper strength development and repulpability. A new methodology was developed to quantify recycling. The second part investigated the effect of salt valency and concentration on paper strength with and without PAE. This study aims at quantifying the potential and limitations of reinforced strength agents in the context of sustainable papermaking.

EXPERIMENTAL

Materials

The commercial PAE (WSR 557 HP) was provided by Nuplex Industries (Australia) Pty Ltd (12.5% w/w solid content solution); PAE solutions were diluted with deionised water prior to each experiment. Analytical grade sodium chloride (NaCl) and calcium chloride (CaCl₂) were purchased from Sigma-Aldrich (Australia). Bleached

eucalyptus kraft pulp was obtained from the dry lap sheet (NIST Standard reference material 8946).

Methods

Handsheets preparation

Cellulose handsheets were prepared according to the Australian/New Zealand Standard Method 203s. Basically, the dry pulp was thoroughly wetted by soaking in deionized water for about 12 hours. The pulp was transferred to a disintegrator (Model MKIIC, Messmer Instruments Ltd), diluted to 2 L with deionized water, and disintegrated for 75,000 propeller revolutions. Prior to handsheet forming, the PAE solution was added to the pulp slurry in either salt-free or salt-containing conditions and stirred for 5 min. The pH of the pulp slurry mixture was non-adjusted, and the value was about 5. The addition quantity of PAE was based on oven dry grammage of 60 g/m². After manual couching and wet-pressing at 0.4 MPa for about 15 seconds, the sheets were cured in a drum-dryer at 100 °C for 10 min, in order to activate the bonds between the PAE and the cellulose surface.

Formation test

The handsheet uniformity was measured with the Paper Perfect Formation Tester (Op Test Equipment Inc, Canada). The tester classifies formation quality in 10 formation components over a specific range and produces the formation value. The relative formation value (RFV) of each component relates to selected reference sheet (without PAE). RFV values less than 1 means that the formation quality of the tested paper is worse than the formation quality of the reference paper.

Tensile strength test

The sheets were equilibrated at 23°C and 50% relative humidity for at least 24 hours before wet and dry tensile testing based on the Australian/New Zealand Standard Methods 448s and 437s. The test strip was slightly bent and the middle part touched to the surface of the deionised water for 2 seconds. The wetted length is about 25 mm. The width of sample strips was 15 mm and test span was 100 mm. An Instron tensile tester (Instron 5566) was used to record maximum tensile force with constant rate of elongation at 10 mm/min. The tensile index for each sample was calculated as tensile strength (expressed in newtons per metre) divided by basis weight (grams per square meter). The mean value was obtained from seven valid tests and the error bars in figures indicated the 95% confidence interval. T-Test was used to determine statistical significance of data.

Evaluation of recyclability of strengthened sheets

The laboratory disintegrator (Model MKIIC, Messmer Instruments Ltd) was used for evaluating the recyclability of the sheets. A 1.2 g handsheet was torn into small pieces of about 1 cm², added to 2 L deionised water, and disintegrated immediately for 3000 revolutions at room temperature (operation time of 1 minute). After repulping, the slurry from the disintegrated handsheet was screened in a fibre classifier (Brecht & Holl type, model BIH-6/12) for 20 min through a 0.2 mm slot screen at a water flow rate of 2.5 L/minute. The rejects (fraction that did not pass the screen) were collected, dried at 105

°C for 4 hours and weighed. Repulping and classification were performed at ambient temperature in triplicate and the average was reported.

The repulpability index (R.I.) was defined as:

$$R.I. = \frac{\text{mass of dry sheet} - \text{mass of dry rejects}}{\text{mass of dry sheet}} \times 100 \quad (1)$$

The index represents the percentage of fibres satisfactorily repulped and recovered. A higher value of R.I. indicates easier recycling process of the sheet.

RESULTS AND DISCUSSION

Effect of PAE Concentration on Paper Strength

Paper without PAE retained less than 10% of its original strength (dry) when wetted. Figure 1 shows that wet over dry strength ratio increased significantly to 28% at a PAE concentration of 5 mg/g (mg PAE per g oven dry cellulose fibre), to reach a maximum ratio of 33% at 10 mg/g. The ratio leveled off thereafter, at least to a PAE concentration up to 50 mg/g.

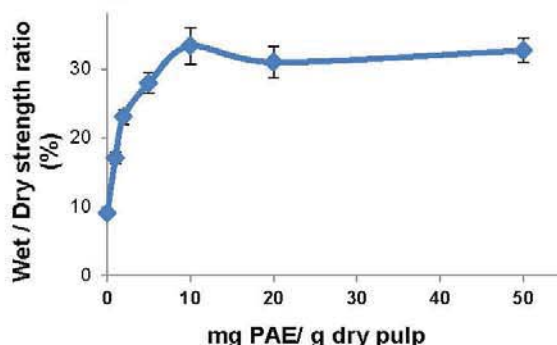


Figure 1. Effect of PAE dosage on the wet and dry strength ratio

The paper wet and dry tensile index both changed non-linearly with the addition of PAE (Fig. 2). At low PAE dosages, the fibre's surface was unsaturated and all polymer adsorbed onto the fibres. Paper strength increased with polymer addition in this regime. The wet tensile index (W.T.I.) increased with PAE addition up to 10 mg/g, to reach a maximum of 4.6 ± 0.1 Nm/g; this was about four times the strength of the reference sheet. The W.T.I. reduced to 4.2 ± 0.1 Nm/g at a PAE dosage of 20 mg/g and leveled off until 50 mg/g. The wet strength improvement is attributed to co-crosslinking with ester bonds forming between pulp carboxyl groups and PAE azetidinium groups. The decrease in paper strength at high PAE concentration could be attributed to homo-crosslinking of PAE, which was very sensitive to water and is weaker than the co-crosslinking involving PAE and fibres (Bates 1969; Espy and Rave 1988).

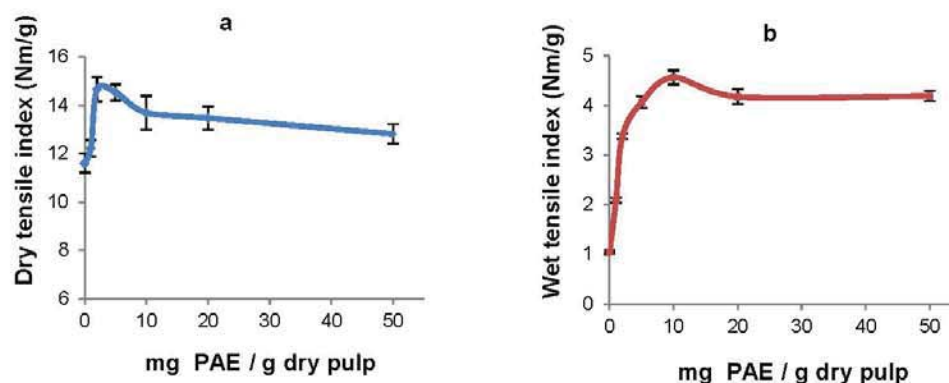


Figure 2. Effect of PAE concentration on the dry tensile index (a) and wet tensile index (b) of papersheets

In contrast to wet strength, the maximum dry tensile index of 14.7 ± 0.5 Nm/g was achieved at 2 mg/g; at higher dosages there was a gradual decline in dry tensile index. Paper formation worsened upon PAE addition, especially at larger inspection sizes (Fig. 3). This was probably related to the high cationic charge and the medium molecular weight of PAE, promoting strong fibre flocculation. Therefore PAE has two antagonistic effects on paper strength. The first is a beneficial increase in fibre-fibre bond strength promoted by covalent bonds; the second is a detrimental effect of impaired formation caused by increased fibre flocculation. At low doses of PAE, the covalent bonding properties of the additive were dominant, and paper strength improved. As polymer addition increased further, fibre flocculation induced by PAE becomes significant and counteracted the strength improvement.

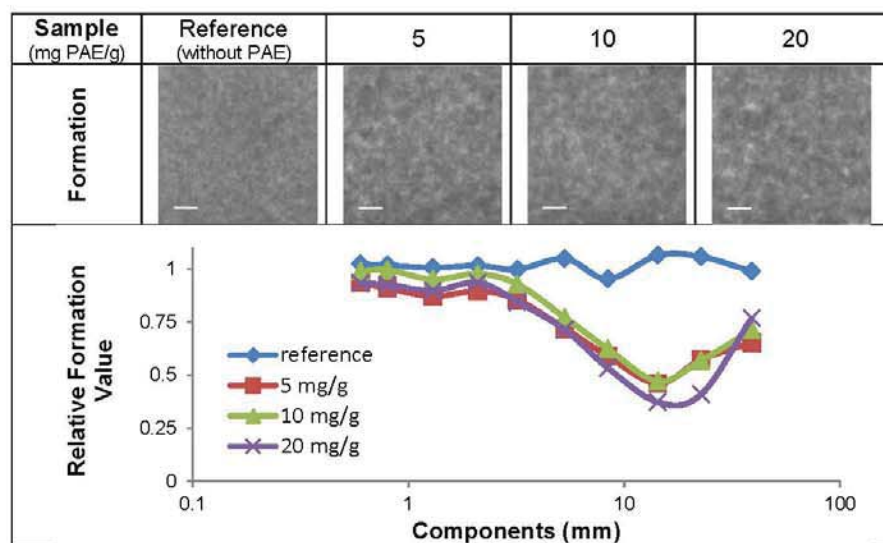


Figure 3. Formation of paper sheets with different PAE dosage (scale bar equals 1 centimeter).

Recyclability of PAE Strengthened Paper

As there is no widely accepted standard test method to evaluate the recyclability of paper; each organization is left to define its own method. Repulping is the process in which paper is recycled into fibres capable of being used again in papermaking. This is achieved by subjecting a paper slurry to mechanical forces; chemical and bleaching aids are sometimes also used. In this study, a method initially developed by a paper company was modified to rate the sheet recyclability under constant operating parameters.

The effect of PAE concentration on repulpability is shown in Fig. 4. The paper's repulpability decreased in a non-linear fashion with increasing PAE concentration. A repulpability index (R.I.) of 100% for the control sheet indicated that the original sheet was totally recyclable under the experimental conditions. When the control paper sheet was wetted in recycling conditions, the hydrogen bonds between fibres were rapidly disrupted by the competing water molecules, leading to much weaker inter-fibre bonding. Under these circumstances, the paper sheet was very easy to break down into individual fibres upon a short exposure to mechanical shear force.

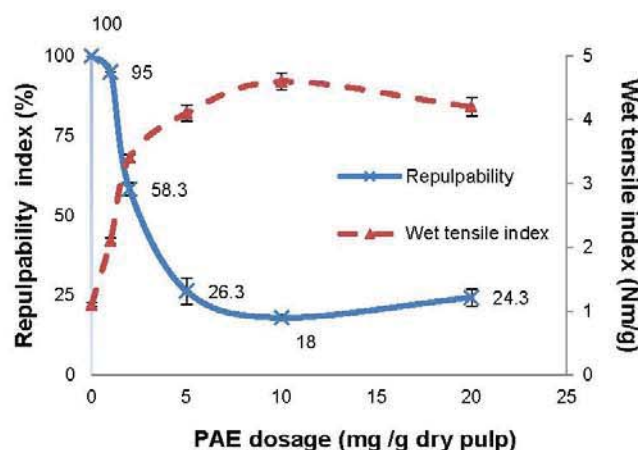


Figure 4. Effect on PAE concentration on repulpability index (solid line) and wet tensile index (dashed line)

Adding PAE increased inter-fibre bonding, thus inhibiting network breakdown and adversely affecting the recycling. The addition of 1 mg PAE /g fibre doubled the wet tensile index to 2.1 Nm/g, and the R.I. decreased to 95%, meaning that a small amount of rejects were left on the screen at end of processing. As the polymer dosage was increased to 2 mg PAE/g fibre, W.T.I. rose to 3.4 Nm/g and the R.I. value dropped sharply to 58%. By further increasing PAE dosage, the R.I. continued to decrease. The sheet was most difficult to repulp at a PAE dosage of 10 mg/g, the PAE concentration at which the greatest wet tensile index was observed. It was notable that paper sheets exhibited similar repulpability at PAE dosages of 5 mg/g and 20 mg/g, where the W.T.I. was very similar.

There was obviously a strong correlation between the paper wet-strength and its repulpability; this relationship was plotted in Fig. 5 in terms of W.T.I and R.I. The relationship was seen to be linear for the samples tested. The initial paper sample with no

PAE was excluded from the line, as there are no covalent bonds formed. No paper repulpability was extrapolated to occur at wet strength higher than 5 Nm/g, using the current method. The slope of the line was expected to vary as a function of the ratio of bond strength/mechanical shear; the wet-strength polymer chemical composition, the repulping configuration, and the power would be important variables. Bennington et al. (1998) applied a more mechanical analysis to the repulpability process. The proposed model described the repulping process at a pulp mass concentration no less than 1%, and concluded that the rate of defibrization depends on the amount of contact between the rotor and the suspension, the force imparted by the rotor, and the paper strength. In comparison with Bennington's work, the relationship curve from this study was achieved at a much lower fibre concentration (about 0.06%) and constant recycling time.

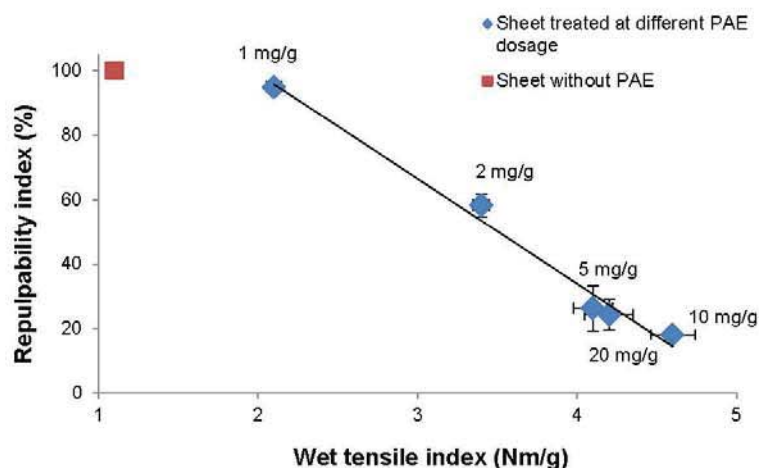


Figure 5. Plot of repulpability index versus wet tensile index obtained from sheets strengthened by PAE and a reference without PAE. Data in Fig. 4 were used to calculate the treadline.

Effect of Electrolyte on Paper Strength

From the standpoint of paper physics, the formation and consolidation of paper structure may be altered by the presence of salt (Scallan 1979). Figure 6 presents the weakening of both dry and wet paper without PAE, which was observed when formed with high salt concentration (100mM of NaCl or CaCl₂) in pulp slurry. Dry tensile index declined from 10.7 Nm/g to 8.9 Nm/g with NaCl addition and to 9.1 Nm/g with CaCl₂ addition (Fig 6a). This can be attributed to three factors: reduced inter-fibre strength, reduced pore radius, and increased moisture content. The joint strength that holds fibres together is dependent on ionic strength. A decreased joint strength is expected as salt is added (Torgnysdotter and Wagberg 2004). Also the average pore radii of fibre was reported to decrease at high concentration (100 mM NaCl), and it was suggested that the smaller pores result in a lower molecular contact area between the fibres, reducing the joint strength (Andreasson et al. 2005; Forsstrom et al. 2005). Salts are known to affect paper hygroscopy. In this study, the moisture content of paper sheets upon equilibrium in

a 50% RH environment was 5.5%, 6.3%, and 6.7% respectively for salt-free, NaCl, and CaCl_2 (100mM).

The wet tensile index of paper without PAE was reduced by 17% and 20% with NaCl and CaCl_2 respectively (Fig. 6b). The cellulose fibre surface can be regarded as a hydrogel when saturated in water. The decrease of salt-induced fibre swelling can be caused by an osmotic pressure differential resulting from a difference in concentration of mobile ions between the interior of the gel and the exterior solution (Grignon and Scallan 1980; Lindström 1992). A previous study presented evidence that fibre entanglements and friction are two important mechanisms controlling for the strength of wet paper (Tejado and van de Ven 2010). For this reason, the lower degree of swelling of fibres in saline environment may create a smaller friction area (Fig. 7), resulting in a paper web of lower wet strength.

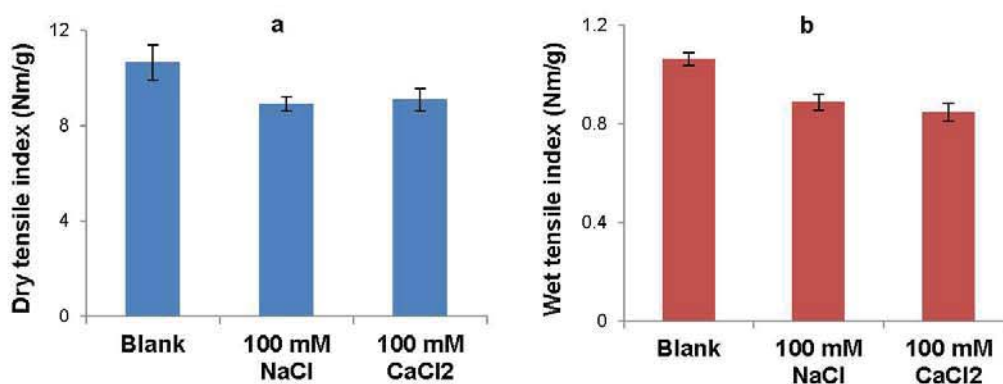


Figure 6. Effect of salt concentration in stock on paper strength (without PAE addition). a) Dry strength, b) Wet strength

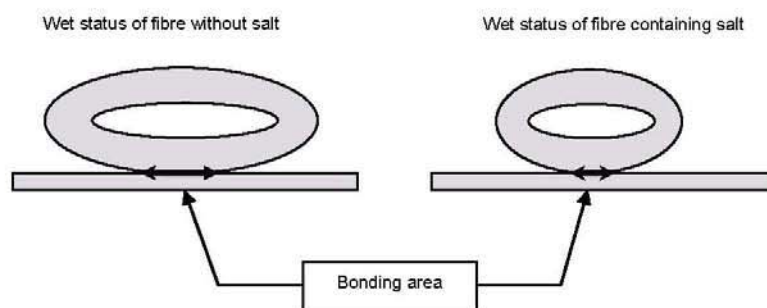


Figure 7. Schematic illustration of salt effect on fibres dimension/swelling and bonding area. The geometry is not drawn to scale.

Salt also influences the strength of PAE-strengthened sheets. Figures 8 and 9 show the effect of the NaCl and CaCl_2 concentration, respectively, on wet and dry paper strength using a PAE dosage of 10 mg/g. The paper wet strength slightly increased at the low concentration of 10 mM, both for NaCl and CaCl_2 . Polyelectrolyte adsorption onto

surfaces was previously investigated both in model surface and cellulosic fibre (Bates 1969; Enarsson and Wagberg 2008; Solberg and Wagberg 2003), and a maximum in the saturation adsorption of cationic polymer was found at a low NaCl concentration of 10 mM. The increase of strength may be linked to a larger amount of PAE adsorbed on fibres in the presence of salt. A small amount of salt may shield the repulsion between the positively charged groups on the PAE chain and allow the macromolecule to coil up into a tighter, less extended conformation which, in turn, enables the PAE chain attach to the fibres more densely and increase the probability of the azetidinium groups forming covalent bonds with fibres. This mechanism is schematically illustrated in Fig. 10.

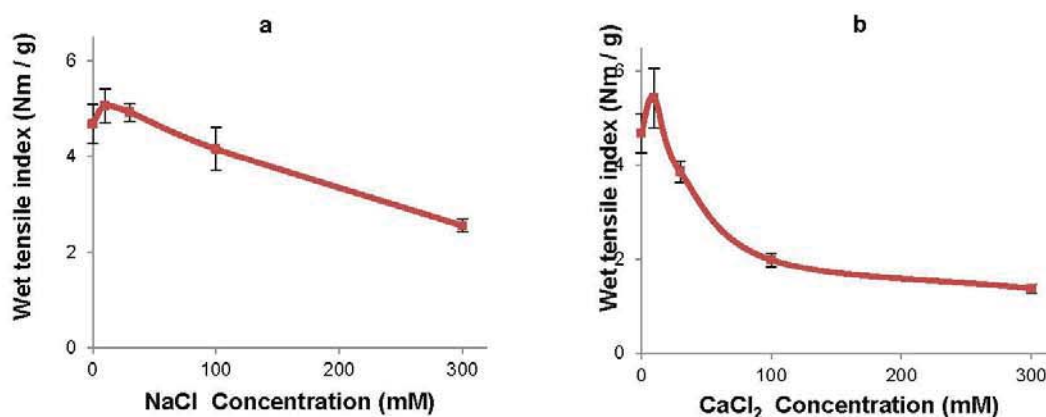


Figure 8. Dry tensile index as a function of (a) NaCl and (b) CaCl₂ concentration at constant addition level of 10 mg PAE /g dry pulp

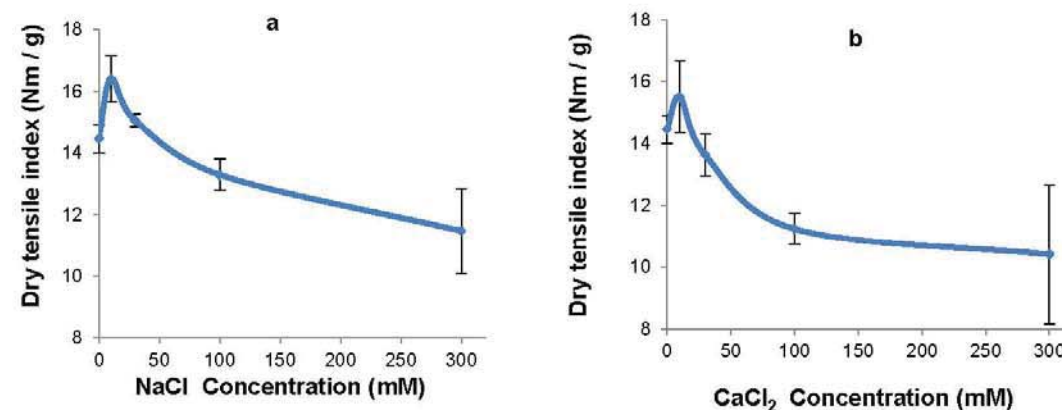


Figure 9. Wet tensile index as a function of (a) NaCl and (b) CaCl₂ concentration at a constant addition level of 10 mg PAE /g dry pulp

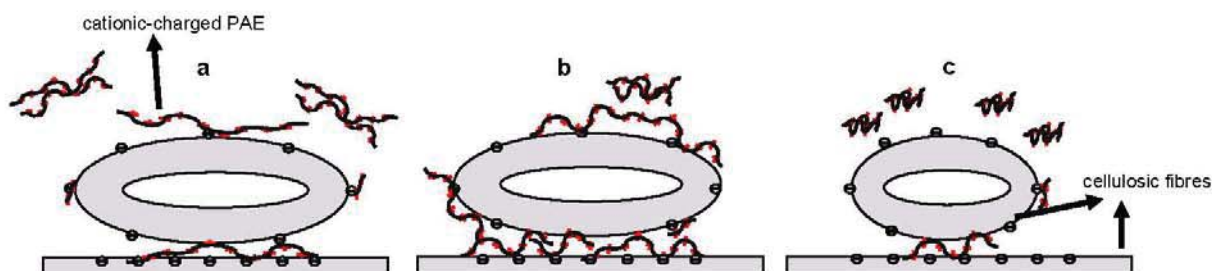


Figure 10. Schematic representation of possible mechanism for cationic-charged PAE being adsorbed to cellulosic fibres in different salt concentrations (a) without salt, (b) Low salt concentration, (c) High salt concentration. The figure is not drawn to scale.

Although the paper's tensile index increased at low salt concentration, for concentrations of 30 mM and above, the strength of the paper sheet declined as increasing salt addition screened the electrostatic interaction required for high polymer adsorption (Enarsson and Wagberg 2009). From the perspective of polymer retention, the adsorbed amount of PAE decreases when salts are added (Strazdins 1974). Considering ion exchange between inorganic cations (Na^+ , Ca^{2+}) and polycations from the dissociation of PAE in solution, the high ionic strength significantly affects the PAE adsorption behavior because the increase in the number of small cationic counterions would interfere with the process (Ampulski and Neal 1989). Ca^{2+} ions decreased PAE efficiency more than Na^+ did. Ca^{2+} can not only better compete for the fibres carboxyl sites but also decrease the anionicity of fibres, therefore inhibiting PAE retention

CONCLUSIONS

1. The ability of polyamideamine-epichlorohydrin (PAE) to improve paper tensile strength was investigated by preparing handsheets with bleached eucalyptus kraft pulp. The maximum enhancement of dry and wet strength properties was achieved at different PAE addition levels; the highest wet to dry strength ratio was obtained at 10 mg/g. Above this addition level, the wet strength falls slightly and then remains constant. Fibre flocculation and poor formation of the paper sheets induced by the cationic polymer were observed during the sheet forming process, which explains why higher PAE doses did not improve tensile strength. The repulpability of PAE-strengthened paper revealed a direct link between wet strength and recyclability. The stronger the paper was in a wet state, the harder it became to repulp, being quantified at the same disintegrator energy.
2. The tensile properties of paper formed in various salt-containing environments with and without PAE were examined. In the absence of PAE, both dry and wet paper strength was decreased at high salt concentration. The strength of sheets reinforced by PAE was also affected by the salt concentration in papermaking stock. At PAE dosage of 10 mg/g, low salt (NaCl and CaCl_2) concentration at 10

mM enhanced the strength of paper while higher salt addition weakened the paper; this can be explained in terms of ionic strength affecting the polymer's conformation and their adsorption density onto fibres. Ion type and concentration in the papermaking process water influenced the strength development in different manners. Experimental results in this study show the need for new wet strength agents that can be applied in demanding salty conditions while maintaining the product recyclability.

ACKNOWLEDGMENTS

The financial contribution of Australian Research Council (LP0990526), Visy and Nopco paper technology is acknowledged.

REFERENCES CITED

- Ampulski, R. S., and Neal, C. W. (1989). "The effect of inorganic ions on the adsorption and ion exchange of Kymene 557H by bleached northern softwood kraft pulp," *Nordic Pulp and Paper Research Journal* 04(2), 155-163.
- Andreasson, B., Forsstrom, J., and Wagberg, L. (2005). "Determination of fibre pore structure: influence of salt, pH and conventional wet strength resins," *Cellulose*, 12(3), 253-265.
- Bates, N. A. (1969). "Polyamide-epichlorohydrin wet-strength resin. 2. A study of mechanism of wet-strength development in paper," *Tappi* 52(6), 1162-1169.
- Bates, N. A. (1969). "Polyamide-epichlorohydrin wet-strength resin. I. Retention by pulp," *Tappi* 52(6), 1157-1161.
- Bennington, C. P. J., Sui, O. S., and Smith, J. D. (1998). "The effect of mechanical action on waste paper defibering and ink removal in repulping operations," *Journal of Pulp and Paper Science* 24(11), 341-348.
- Chan, L. L. (1994). *Wet-strength Resins and their Application*, TAPPI Press, Atlanta, Ga.
- Davison, R. W. (1972). "Weak link in paper dry strength," *Tappi* 55(4), 567-573.
- Devore, D. I., and Fischer, S. A. (1993). "Wet-strength mechanism of polyaminoamide-epichlorohydrin resins," *Tappi Journal* 76(8), 121-128.
- Enarsson, L. E., and Wagberg, L. (2008). "Adsorption kinetics of cationic polyelectrolytes studied with stagnation point adsorption reflectometry and quartz crystal microgravimetry," *Langmuir* 24(14), 7329-7337.
- Enarsson, L. E., and Wagberg, L. (2009). "Polyelectrolyte adsorption on thin cellulose films studied with reflectometry and quartz crystal microgravimetry with dissipation," *Biomacromolecules* 10(1), 134-141.
- Espy, H. H. (1995). "The mechanism of wet-strength development in paper - A review," *Tappi Journal* 78(4), 90-99.
- Espy, H. H., and Geist, G. W. (1993). "Persulfates as repulping reagents for neutral alkaline wet-strength broke," *Tappi Journal* 76(2), 139-142.

- Espy, H. H., and Rave, T. W. (1988). "The mechanism of wet-strength development by alkaline-curing amino polymer-epichlorohydrin resins," *Tappi Journal* 71(5), 133-137.
- Forsstrom, J., Andreasson, B., and Wagberg, L. (2005). "Influence of pore structure and water retaining ability of fibres on the strength of papers from unbleached kraft fibres," *Nordic Pulp and Paper Research Journal* 20(2), 176-185.
- Gardner, D. J., Oporto, G. S., Mills, R., and Samir, M. A. S. A. (2008). "Adhesion and surface issues in cellulose and nanocellulose," *Journal of Adhesion Science and Technology* 22(5-6), 545-567.
- Grignon, J., and Scallan, A. M. (1980). "Effect of pH and neutral salts upon the swelling of cellulose gels," *Journal of Applied Polymer Science* 25(12), 2829-2843.
- Lindström, T. (1992). "Chemical factors affecting the behaviour of fibres during papermaking," *Nordic Pulp and Paper Research Journal* 7(4), 181-192.
- Obokata, T., and Isogai, A. (2007). "The mechanism of wet-strength development of cellulose sheets prepared with polyamideamine-epichlorohydrin (PAE) resin," *Colloids and Surfaces a-Physicochemical and Engineering Aspects* 302(1-3), 525-531.
- Obokata, T., Isogai, A., and Onabe, F. (2002). "Studies on the mechanism of wet strength development," *Emerging Technologies of Pulping and Papermaking*, 613-617.
- Page, D. H. (1969). "A theory for tensile strength of paper," *Tappi* 52(4), 674-681.
- Rowland Stanley, P. (1977). "Cellulose: Pores, internal surfaces, and the water interface," *Textile and Paper Chemistry and Technology*, American Chemical Society, 20-45.
- Saito, T., and Isogai, A. (2005). "A novel method to improve wet strength of paper," *Tappi Journal* 4(3), 3-8.
- Scallan, A. M., and Grignon, J. (1979). "The effect of cations on pulp and paper properties," *Svensk Papperstidning* 82, 40-47.
- Solberg, D., and Wagberg, L. (2003). "Adsorption and flocculation behavior of cationic polyacrylamide and colloidal silica," *Colloids and Surfaces A - Physicochemical and Engineering Aspects* 219(1-3), 161-172.
- Strazdins, E. (1974). "Surface chemical aspects of polymer retention," *Tappi* 57(12), 76-80.
- Tejado, A., and van de Ven, T. G. M. (2010). "Why does paper get stronger as it dries?" *Materials Today* 13(9), 42-49.
- Torgnysdotter, A., and Wagberg, L. (2004). "Influence of electrostatic interactions on fibre/fibre joint and paper strength," *Nordic Pulp and Paper Research Journal* 19(4), 440-447.

Article submitted: October 30, 2011; Peer review completed: December 19, 2011;

Revised version received and accepted: January 9, 2011; Published: January 12, 2011.

Paper engineered with cellulosic additives: effect of length scale

Jielong Su · Liyuan Zhang · Warren Batchelor · Gil Garnier

Received: 28 January 2014 / Accepted: 9 May 2014 / Published online: 22 May 2014
© Her Majesty the Queen in Right of Australia as represented by the Monash University 2014

Abstract Composites of cellulose fibers were made with paper-making technology. Two types of microfibrillated cellulose (MFC), obtained by with either homogenization or ball milling, were blended with hardwood fibers to give composites having high strength and low air permeability. The strengthening effects of the MFCs were compared with strengthening by cellulose microparticles (CMPs) made by cryogenic milling, with and without polyamideamine-epichlorohydrin addition. The MFC from homogenization was fully retained on the fiber web due to a broad size distribution; in contrast, the retention ratio for MFC produced by ball milling was lower than 50 % because of its smaller particle size. The small size caused the resulting paper to display a more compact and denser structure. The main distinction between the papers made with the two types of MFC was the elongation at break under wet conditions, suggesting that they reinforce the paper in different ways. On the other hand, CMPs act as mechanical debonders and could find application in tissue paper, increasing paper bulk and decreasing the density and thus improve tissue softness.

Keywords MFC · Polymer · Paper · Composite · Permeability · Strength

Introduction

Papers of engineered structure and surface properties are drawing strong interest as a substitute for traditional applications, such as packaging and tissue, and also for novel uses including clear films and bio-diagnostics. Microfibrillated cellulose (MFC) of nano-scale diameter and micro-scale length shows high potential for paper engineering. Its advantages include: abundant natural resources for preparation, the controlled dimensions, being biocompatible and biodegradable. Novel MFC products including composites and films have been prepared (Siro and Plackett 2010; Klemm et al. 2011; Koga et al. 2013). The preparation efficiency and properties of the products were directly determined by the dimension of the MFC. However, little is known on the effect of the dimension for nano and micro cellulose used as an additive on the properties and structure of paper composites.

Many approaches have been explored to produce films and composites with MFC. The common one is by filtration of a MFC suspension. Mechanical strength, surface smoothness and transparency of the films typically all increase as the dimension of the MFC fibers decreases, while the porosity and gas

J. Su · L. Zhang · W. Batchelor · G. Garnier (✉)
Department of Chemical Engineering, Bioprocessing
Research Institute of Australia (BioPRIA), Monash
University, Clayton, Australia

permeability decrease (Aulin et al. 2010; Zhang et al. 2012). However, the continuous films made by MFC suspension present some serious drawbacks such as low tear strength and poor dimensional stability. A major issue for the preparation is a very slow drainage of water, typical of small, high surface area and electrically charged colloids. Another is cost as MFC materials remain much more expensive than pulp fibers.

A strategy to alleviate these problems is to make paper composites using MFC as additives and relying on the flexible and readily available paper technology. Minimizing the amount of MFC, while maximizing their retention and performance are keys for commercialization. Several studies have demonstrated the process and material benefits of adding MFC to pulp fiber suspension, especially in conjunction with a reactive-cationic polymer, such as polyamideamine-epichlorohydrin (PAE) (Ahola et al. 2008). The novel properties achieved for these composites paper: smoothness and mechanical properties under wet and dry conditions were shown to significantly increase; paper gas permeability decrease and suspension drainage was little affected. Nonetheless, there is a poor understanding on the effect of MFC dimension and structure on these paper composites.

In this work, we investigated two types of MFC, produced either by homogenization or by ball milling. This study aims at quantifying the effect of MFC dimension on the paper composite properties. MFC is used as additive with or without a polymeric wet strength additive (PAE). The performance of MFC is also compared to cellulose micro-particles (CMPs) from cryogenic milling. All additives are used in the hardwood pulp slurry by direct adsorption onto pulp fibers prior to drainage and web consolidation using the paper making process. It is our objective to develop high performance-low cost paper composites and to better understand the role played by the MFC in terms of surface, colloid and material science.

Experimental method

Materials

Commercial MFC was denoted as MFC1 and supplied never dried at a 25 % solid content by Daicel chemical Industries Ltd., Japan (Celish KY-100s). MFC1 is made from pure cellulose fibers through high pressure

Table 1 Dimension properties of cellulosic fibers used in this work

Sample	Mean diameter (μm)	Aspect ratio	Mean length (μm)
Hardwood fibers	10	65	650
Softwood fibers (Varanasi et al. 2012)	28	72	2,000 ^a
MFC1 (Varanasi et al. 2012)	0.073	153	11.2
MFC2 (Zhang et al. 2012)	0.032	146	4.7
Cellulose microparticles (CMPs)	10	–	–

^a From estimation

homogenization. Their diameters range from 10 nm to several microns. The dimension of the fibers is summarized in Table 1. This information was used to calculate their surface area. The charge density of MFC1 is 1.1×10^{-2} μeq/g determined by streaming current titration with poly-diallyldimethylammonium chloride (poly-DADMAC). The titration was performed with a Mutek PCD-02 particle charge detector (BTG Instruments, Germany) and polyDADMAC of average molecular weight of 400,000–500,000 was purchased from Aldrich. The endpoint of the titration was determined by the signal (mV) reaching zero.

Northern softwood bleached kraft pulp (National Institute of Standards and Technology, reference material 8495) was used for preparing cellulose microparticles (CMPs) by cryogenic milling and MFC by ball milling, which was denoted as MFC2.

MFC2 were fabricated by ball milling in water, and received in the form of an aqueous dispersion. Specifically, MFC2 were prepared in a SPEX 8000 M shaker mill. Firstly, cellulose pulp sheet (NIST reference material 8495) was torn into 5 × 5 cm pieces and soaked in deionised water overnight to prepare a 1 wt% solid suspension. The wet cellulose pieces were then shredded using a conventional kitchen blender. Then 20 g of 1 wt% cellulose pulp suspension, 45 g of cerium-doped Zirconium balls (0.5 mm in diameter) and 20 mL of deionised water were placed in a 70 mL polypropylene container using ball mill for 60 min. The final suspension was filtered using a polyester mesh (opening size 125 micron) to remove the zirconium balls and any larger remaining fibres. Full information is provided elsewhere by Zhang et al. (2010).

CMPs were obtained from cryogenic milling (SPEX SamplePrep 6870 Large Freezer Mill). The

preparation was conducted by immersing the steel sample vial in liquid nitrogen, and the air dried softwood pulp of 1 g in the vial was milled for 100 min through the action of the impactor under the influence of an alternating magnetic field.

The reference sheet with target oven dry (o.d.) basis weight of 60 g eucalyptus kraft hardwood fiber/m², was made from the National Institute of Standards and Technology (NIST) reference material 8496 (Bleached eucalyptus kraft pulp). The charge density of NIST 8496 is 1.54 µeq/g determined by poly-DADMAC titration. The commercial PAE (WSR 557 HP) with an average molecular mass of 500,000 was supplied by Nuplex Industries (Australia) Pty Ltd., (12.5 % w/w solid content solution). PAE solutions were diluted prior to use for each experiment. Unless specified, deionized water was used in the experiments.

Methods

Handsheets preparation

Cellulose handsheets were made using a standard British hand sheet maker according to the Australian/New Zealand Standard Method 203s. Basically, 24 g o.d. lap sheet was torn to small pieces and thoroughly wetted by soaking in deionized water for about 12 h, then transferred to a disintegrator (Model MKIIC, Messmer Instruments Ltd.,). By diluting to 2 L with deionized water and disintegrating for 75,000 propeller revolutions, the pulp stock was prepared for further use. The cellulose additives (CMPs, MFC1 and MFC2) were used in the form of aqueous dispersions, which were directly added into pulp slurry or mixed with PAE solution together prior to adding into the pulp. The resulting furnish was stirred for 5 min prior to hand-sheet forming. The dewatering time was measured as the time taken to remove all free water from the wet fiber web, starting from when drainage commenced.

The pH of the pulp slurry mixture was about 5 and was not adjusted. The addition of 10 mg PAE/g

hardwood fiber was based on the target o.d. basis weight of 60 g eucalyptus kraft hardwood fiber/m². After manual couching and wet-pressing at 0.4 MPa for about 15 s, the sheets were cured in a drum-dryer at 100 °C for 10 min, in order to activate reactive bonds between the PAE and the cellulose surface.

Cellulosic fiber and paper properties

Scanning electron micrographs (SEMs) of MFC (MFC1 and MFC2) and engineered paper were obtained using a JEOL 7001 FEG system operating at 5 kV and 180 pA. A drop of diluted MFC dispersion was placed on a silicon wafer, air dried and then platinum coated. The paper composites were also platinum coated prior to SEM imaging. 0.02 g CMPs was dispersed in 10 mL of deionised water, casted on a conductive carbon adhesive tab and air dried prior to platinum coating. Their images were analyzed by Phenom Pro desktop SEM.

Streaming current titration used series of aqueous suspensions consisting of MFC1, MFC2 and eucalyptus kraft hardwood fibers (1 % w/v solid) respectively, and PAE solutions prepared at 10 mg/mL. Suitable amounts of PAE solution (no more than 1 mL in total) were added to fiber samples of 100 mL and stirred for 2 min. Finally, a 10 mL sample was withdrawn and the streaming current titration measured with a Müttek PCD-03 pH particle charge detector (BTG Instruments, Germany).

The retention of cellulose additive was calculated as the ratio of the weight of additive retained in the sheet to the amount of additive used. This was estimated following equation (1). The dosage of additive was kept constant at 100 mg/g hardwood fiber. The target grammage of the control sheet (without additive) is 60 g hardwood fiber/m² (oven-dried). The sheet weight was measured using a balance (METTLER TOLEDO, model AB304-S) with readability of 0.1 mg. The average was measured from seven replicates.

$$\text{Retention ratio (\%)} = \frac{\text{average o.d. weight of sheet with additive} - \text{average o.d. weight of sheet without additive}}{\text{weight of additive used}} \times 100 \quad (1)$$

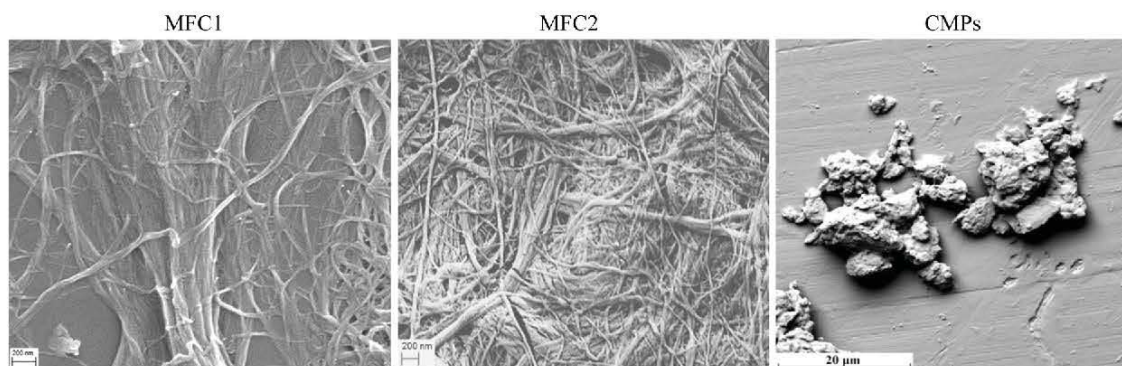


Fig. 1 SEM micrographs of cellulosic additives applied to engineer the paper

The paper basis weight and thickness were measured from ten replicates according to Australian/New Zealand Standard Methods 426s and 208s. The basis weight of the paper, divided by its thickness was used to calculate the apparent sheet density. Air resistance was assessed by air permeance tester (type 977102, Lorentzen and Wettre, Sweden) according to Australian/New Zealand Standard Method 420s. Both sides of the seven replicates were measured and the results were valued at the unit of Gurley second/100 mL.

The sheets were equilibrated at 23 °C and 50 % relative humidity for at least 24 h before wet and dry tensile tests based on the Australian/New Zealand Standard Methods 448s and 437s. For wet tests, the test paper strip was slightly bent and the middle part touched to the surface of the deionised water for 2 s. The wetted length is about 25 mm. The width of sample strips were 15 mm and test span was 100 mm. An Instron tensile tester (Instron 5566) was used to record maximum tensile force with constant rate of elongation at 10 mm/min. The tensile index for each sample was calculated as tensile strength (expressed in N/m) divided by basis weight (g/square meter). The mean value was obtained from seven valid tests and the error bars in the figures indicate the 95 % CI. *t* Test was used to determine statistical significance of data. The typical stress–strain curve selected for analysis was that from the paper strip having the closest tensile index to the mean value of the series samples.

Results

The morphologies of the two MFCs and CMPs were compared on Fig. 1. MFC1 and MFC2 maintained

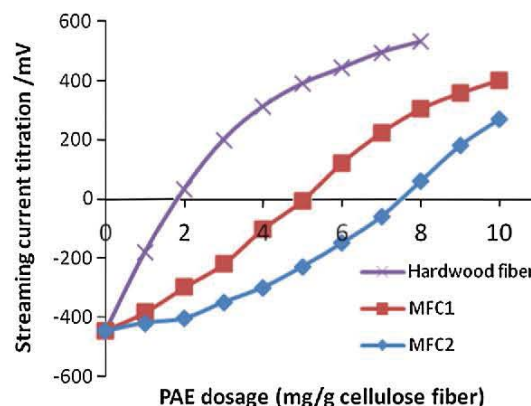


Fig. 2 Streaming current titration measured for the cellulosic products with increasing PAE addition. Lines shown are to guide the eye

fibrillar shape after mechanical treatment, and displayed a higher aspect ratio than hardwood and softwood fibers (Table 1). The mean length of MFC1 (11.2 μm) was close to the mean diameter of the hardwood fibers (10 μm) used for the control paper. CMPs of irregular shape and short aspect ratio were produced by cryogenic milling. Their size ranged from 5 to 15 μm with mean diameter of 10 μm .

Figure 2 shows the streaming current titration of the hardwood pulp and the two nano-sized cellulose additives (MFC1 and MFC2), measured by varying the amounts of PAE. Titration of fiber suspension with PAE first neutralized and then reversed the net charge of the fiber samples. The hardwood pulp reached neutral charge close to 2 mg/g addition level, while MFC1 reached neutral charge at an addition level of approximately 5 mg/g, and a PAE dose at 7.5 mg/g neutralized the charge of MFC2 (Fig. 2). Once the

Table 2 Paper formation, stress–strain at break and elastic modulus affected by addition of 100 mg cellulosic additives/g hardwood fiber with and without PAE

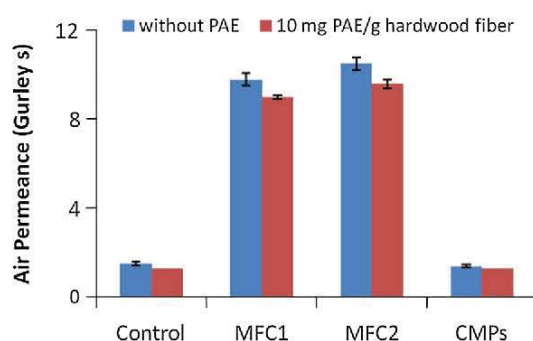
	Without PAE				10 mg PAE/g pulp			
	Control	MFC1	MFC2	CMPs	Control	MFC1	MFC2	CMPs
Relative retention (%)		100 (0)	46.5 (4.1)	71 (3.4)		100 (0)	67.8 (3.8)	88 (4.7)
Dewatering time (s)	<1	1	2	<1	<1	1	2	<1
Thickness (μm)	136 (3)	141 (3)	147 (9)	166 (4)	142 (6)	138 (3)	138 (4)	176 (4)
Apparent density(kg/m^3)	461 (19)	495 (15)	446 (40)	405 (19)	449 (29)	513 (21)	497 (28)	395 (21)
Stress at break-dry (Mpa)	5.2 (0.2)	10.4 (0.6)	12.4 (0.4)	3.4 (0.2)	6.0 (0.5)	15.7 (0.8)	17.1 (0.4)	5.2 (0.3)
Stress at break-wet (Mpa)	0.49 (0.06)	0.68 (0.03)	0.83 (0.04)	0.33 (0.03)	1.72 (0.13)	5.28 (0.3)	4.44 (0.38)	1.71 (0.08)
Strain at break-dry (%)	1.2 (0.2)	2.1 (0.2)	1.7 (0.3)	1.5 (0.3)	1.1 (0.2)	2.4 (0.3)	2.4 (0.3)	1.2 (0.2)
Strain at break-wet (%)	4.0 (0.5)	4.2 (0.3)	1.8 (0.3)	3.1 (0.4)	3.5 (0.4)	5.3 (0.2)	2.1 (0.2)	4.2 (0.4)
Elastic modulus-dry (GPa)	0.7 (0.07)	1.2 (0.11)	1.4 (0.13)	0.5 (0.02)	0.8 (0.08)	1.5 (0.05)	1.5 (0.1)	0.7 (0.07)
Elastic modulus-wet (GPa)	0.05 (0.01)	0.08 (0.02)	0.13 (0.02)	0.05 (0.01)	0.1 (0.02)	0.2 (0.03)	0.4 (0.03)	0.1 (0.03)

The target oven-dry grammage for the control sheet is 60 gsm. 95 % CIs from ten measurements indicated in parenthesis

cellulose additives (100 mg/g hardwood fiber) were blended with PAE (10 mg/g hardwood fiber), their negatively charged surface was reversed to positive, which resulted in the increased retention of MFC2 and CMPs to 67.8 and 88 % on the paper web, respectively. However, the dewatering for sheet forming, resultant paper thickness and apparent density were only marginally affected.

A series of paper was built with wet-end addition of two types of MFC and CMPs, respectively, at a constant concentration of 100 mg/g pulp. In the absence of PAE, the addition of 100 mg MFC1/g pulp resulted in full retention in the papersheet web. In contrast, sheets made with MFC2 and CMPs had retentions of 47 and 71 %, respectively (Table 2). During wet web forming, the addition of MFC2 increased the dewatering time to 2 s. Increased paper thickness up to $166 \pm 4 \mu\text{m}$ and reduced apparent density of $405 \pm 19 \text{ kg}/\text{m}^3$ were recorded with the addition of 100 mg CMPs/g pulp.

Paper air permeability was recorded from Gurley measurement (Fig. 3). Higher air permeability is measured for the control ($1.5 \pm 0.1 \text{ s}$) and paper with CMPs ($1.4 \pm 0.1 \text{ s}$). The addition of MFC1 and MFC2 at 100 mg/g hardwood fiber dosage into paper critically reduced permeability to 9.8 ± 0.3 and $10.5 \pm 0.3 \text{ s}$. No obvious change in the air permeance resulted simply with PAE addition. The morphology and surface structure of paper made with MFC2 additives are significantly different from those of the other fibrous composites (Fig. 4). Paper with MFC2 displays a much smoother surface and more compact

**Fig. 3** Air permeability of paper by addition of 100 mg modified fibers/g hardwood pulp, without PAE and 10 mg PAE/g hardwood pulp

configuration. In contrast, the web structure of the control and the paper embedded with CMPs are porous.

Without PAE treatment, MFC1 and MFC2 at dosage of 100 mg/g hardwood fiber considerably increased paper dry strength to 21 ± 1 and $28 \pm 1 \text{ Nm}/\text{g}$, respectively (Fig. 5). Comparing with the control (dry tensile of $11.3 \pm 0.5 \text{ Nm}/\text{g}$), the addition of CMPs significantly weakened the paper strength to $8.4 \pm 0.5 \text{ Nm}/\text{g}$. Once water penetrated the fiber web, the control paper lost most of its strength to $1.1 \pm 0.1 \text{ Nm}/\text{g}$ (Fig. 6). In comparison, paper with MFC2 and MFC1 reached wet tensile index of 1.9 ± 0.1 and $1.4 \pm 0.1 \text{ Nm}/\text{g}$, respectively.

Addition of PAE (10 mg/g hardwood fiber) to the pulp slurry substantially improved wet strength of the control up to $3.8 \pm 0.3 \text{ Nm}/\text{g}$. Combining PAE with the addition of MFC1 or MFC2 to the fiber suspension

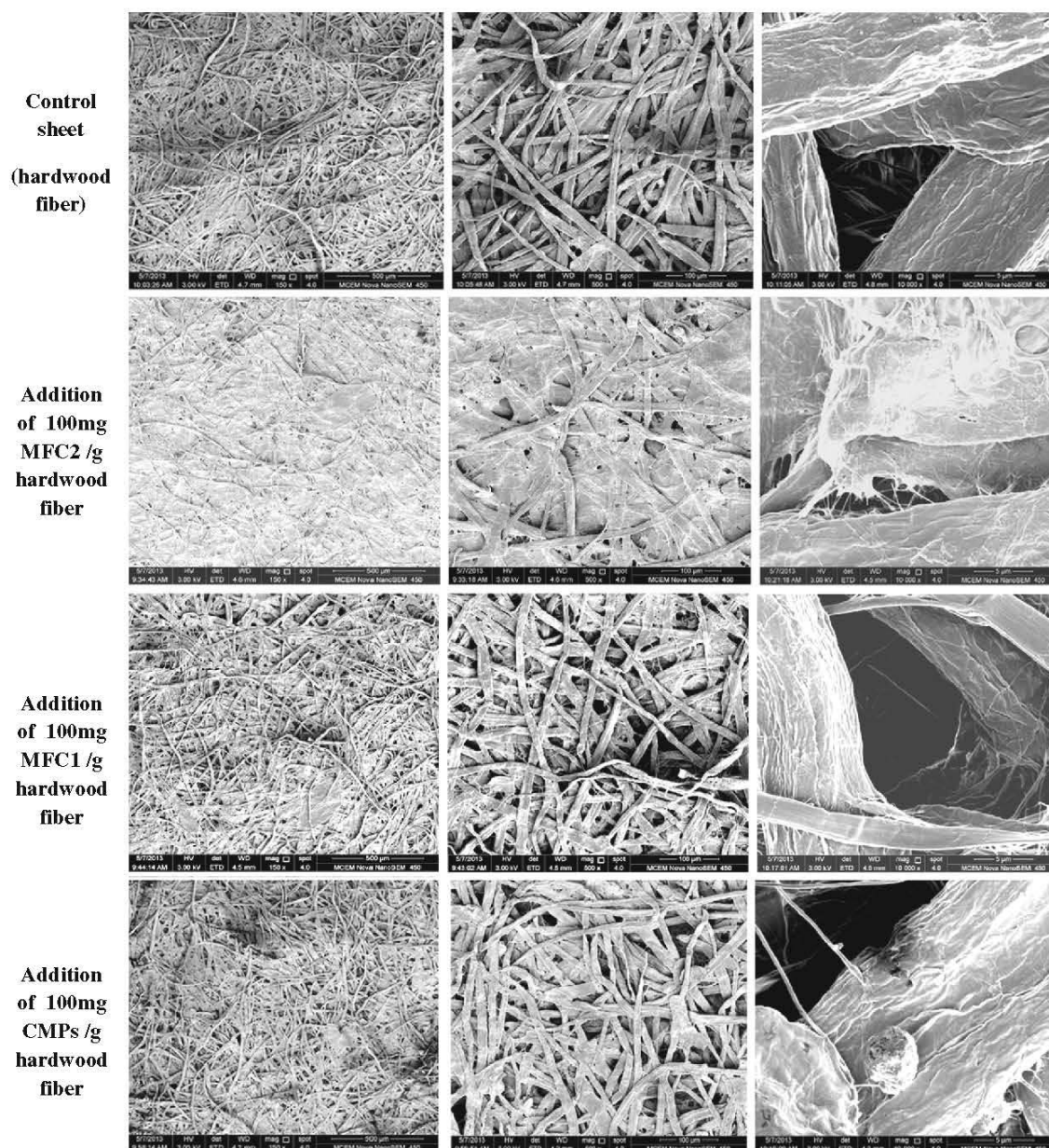


Fig. 4 Morphologies of paper engineered by cellulosic additives, examined by SEM of three different magnification ($\times 150$, $\times 500$, $\times 10,000$). The bar represents a length of 500, 100 and 5 μm

resulted in considerable synergy both for dry and wet strengthening (Figs. 5, 6). Dry tensile indices were drastically increased to $34.4 \pm 0.9 \text{ Nm/g}$ for MFC2/PAE composite and $30.6 \pm 1.6 \text{ Nm/g}$ for MFC1/PAE composite, and the corresponding wet tensile indices were 8.9 ± 0.8 and $10.3 \pm 0.6 \text{ Nm/g}$, respectively.

The stress-strain curve of paper was modified differently by the various cellulose additives (Figs. 7, 8). Elongation of dry paper at failure was prolonged by the addition of MFC1 and MFC2; however, the wet strain at failure was noticeably decreased by MFC2. Dry paper with MFC2/PAE and MFC1/PAE

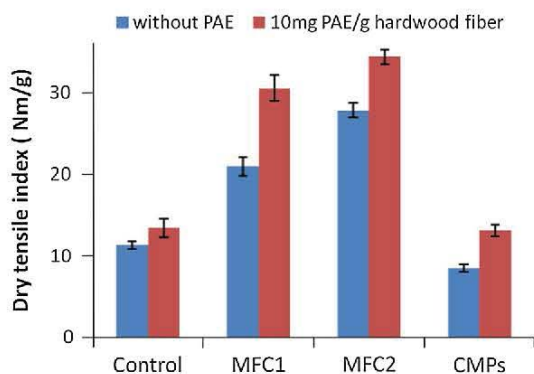


Fig. 5 Dry tensile index of paper. (blue) Without PAE and (red) with PAE (10 mg/g hardwood fiber) treatment. MFC1, MFC2 and CMPs were added at 100 mg/g hardwood fiber. (Color figure online)

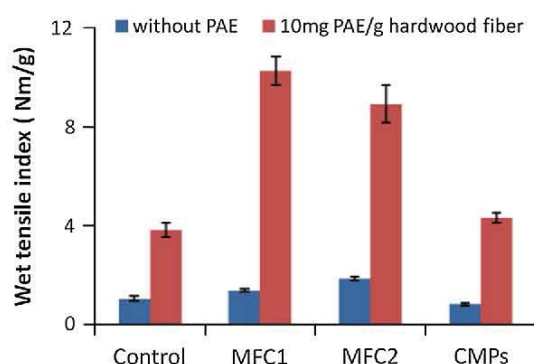


Fig. 6 Wet tensile index of paper. (blue) Without PAE and (red) with PAE (10 mg/g hardwood fiber) treatment. MFC1, MFC2 and CMPs were added at 100 mg/g hardwood fiber. (Color figure online)

composites stretched in a quite similar way, and both papers exhibit high value of elastic modulus (Table 2). Interestingly, in wet conditions, the stress–strain plots of PAE-strengthened paper became linear, and the highest elastic modulus was recorded for paper with MFC2/PAE composite (Table 2).

Discussion

Effect of cellulosic additives on the paper processing

During mechanical processing, morphology and dimension of cellulose fibers are greatly modified by

external forces (Fig. 1; Table 1). Under the strong shearing force generated between the milling balls, MFC2 are disintegrated from the bundles of cellulose fibrils of the softwood fiber. By comparison, MFC1 was prepared through microfibrillation of cellulose fibers by a high pressure homogenizer. As the average length of MFC is difficult to measure directly, the aspect ratio and average diameter of the samples are employed to estimate their length. From sedimentation experiments, both MFC1 and MFC2 were found to possess aspect ratio close to 150, higher than the aspect ratio of 72 for softwood fibers (Varanasi et al. 2013). SEM images analyzed by ImageJ showed MFC2 diameters were more uniformly distributed than MFC1 and were smaller with a size of 32 nm (Varanasi et al. 2012). However, the CMPs made from cryogenic milling cellulose fibers consist mostly of irregularly shaped particles of low aspect ratio, which act as debonder in paper by increasing thickness and decreasing its apparent density.

The drainage time of papermaking was reported to be proportional to the MFC ratio in the stock (Taipale et al. 2010; Su et al. 2013). Bonding of the fibrous network is drastically affected by MFC addition, which also increases shrinkage during drying (Maninen et al. 2011). In this study, the drainage time was very short: <3 s for all handsheets. An increase in drainage resistance was observed for the fiber suspension with the addition of MFC (Table 2). This reflects the combined effect of high aspect ratio MFC and low density/deformable fiber flocs, which increase the surface area and contribute to reducing the pore size of the filter mat on the wire. This later mechanism is further supported by the drainage rate remaining constant while MFC2 retention increases when PAE is used; this is likely caused by coagulation of MFCs (Table 2).

The efficiency of fibers/additives retaining in the paper is important for the papermaking process. The cellulose fiber diameter distributions and aspect ratio are reported to play critical roles during sheet formation (Zhang et al. 2012). The MFC1 has a slightly higher aspect ratio and an average fiber length of 11.2 μm , which is a dimension similar to the diameter of the hardwood fibers. Hence, the MFC1 is more likely to form physical entanglements than the shorter MFC2 or the CMPs of lower aspect ratio. In comparison to MFC2 and CMPs, MFC1 has a broader size distribution, and mixed with nanofibers, larger fibers

Fig. 7 Stress–strain curve of dry paper. **a** Without PAE and **b** with PAE (10 mg/g hardwood fiber) treatment

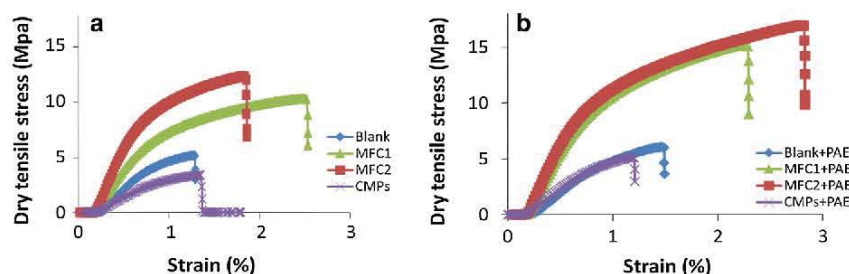
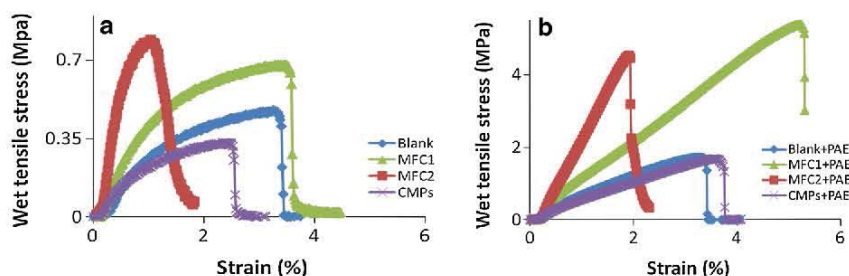


Fig. 8 Stress–strain curve of wet paper. **a** Without PAE and **b** with PAE (10 mg/g hardwood fiber) treatment



and particles (Varanasi and Batchelor 2013). These features explain their full retention on paper without need for a retention aid.

The addition of a cationic polymer to an anionic fiber suspension modifies the interaction between cellulose surfaces via electrostatic force, polymer bridging and steric repulsion; these interaction forces cause dramatic changes in yield stress, floc strength and network strength of the fiber suspension (Mosse et al. 2012). Two stages were proposed for the adsorption of PAE onto fibers: an initial fast dynamic adsorption (seconds–minutes) and a slow approach to equilibrium (hours–days) (Yoon 2006). In this study, the surface area of 1 g hardwood fibers (close to 1 m²) would be fully covered with 10 mg PAE while their surface charge was neutralized at 1.8 mg PAE (Fig. 2). 1 g MFC1 and MFC2 have much larger surface area (36.5 and 83.3 m², respectively), and their charge reversals occur at higher PAE amount (5 and 7.5 mg) in spite of their lower surface charge density. There are two possibilities for this observation. The first is the negative charge on the MFC surface being neutralized by cationic PAE addition. Another is the adjacent fibers being bridged by PAE to form relatively strong flocs.

Polymer assisted fiber flocculation is a major factor governing the retention of a fiber suspension. The addition of 10 mg PAE reversed the anionic surface of

1 g MFC fibers (MFC1 and MFC2) to cationic (Fig. 2), which promotes the electrostatic interactions with the hardwood fibers. The addition of PAE/cellulosic additives can have three main influences: (1) coagulate cellulosic additives into bigger “fine like” structures, (2) co-flocculate fibers with PAE mixture and (3) modify floc properties (density/compressibility and size). In this case, MFC2 and CMPs were flocculated into bigger and denser flocs (Su et al. 2012), resulting in the increased retention observed in paper web. The optimization of cationic-polymer assisted flocculation can efficiently improve the retention of cellulosic additives.

Structure and air permeability of paper

Paper properties are greatly affected by the 3-D fibers distribution and porous web structure. Fluid and gas transportation in the fiber network closely relates to the porosity, the ratio of void volume and total volume of paper (Jackson and James 1986; Niskanen 1998), which can be estimated from paper density. In this study, air permeability of paper is not affected by the addition of 100 mg CMPs/g hardwood fiber, but the lower apparent density was recorded. It is anticipated that some fiber–fiber joints were replaced by loose fiber–CMPs contact, thus creating weak bonds and more voids in the fiber web. In contrast, the addition of

MFC drastically decreased air permeability of the paper composites. These results suggest changes in the paper structure: increasing pore tortuosity, decreasing pore area and pore connectivity. This effect is better visualized with the surface morphology illustrated by SEM (Fig. 4).

In previous work, air permeance of paper composites was correlated with its drainage period (Su et al. 2013); the time needed for air to diffuse through the dry substrate plane was found proportional to the time required for dewatering pulp fibers into a web; the current study is in good agreement with these previous observations. The air permeability for MFC2 paper composite was lower than that from MFC1, considering a lower retention amount of MFC2 at a given dose of 100 mg/g pulp (Fig. 3; Table 2). This result is consistent with the less porous surface morphology observed by scanning electron microscopy (Fig. 4). The compact structure of MFC2 composite suggested their greater resistance to air flow from that of porous paper.

Strength of paper

In preliminary experiments, low addition level (<2 wt% of pulp fiber) of MFC was explored for paper composites. However, there were no significant strength improvements. This is probably due to a low retention of MFC within the fiber web. By increasing the MFC addition up to 100 mg/g fiber, paper displayed higher wet and dry tensile indices without using polymer additives (Figs. 5, 6). Unlike paper made with CMPs, MFC additives not only improved the paper dry strength, but also promoted wet strength. This property allows the fiber web to better retain strength under high moisture or wet conditions. Taking retention amount into account, paper with MFC2 is much stronger than that made with MFC1 (Table 2; Fig. 5). This can be explained by two reasons. The first is the addition of MFC2 allows more hydrogen bonding by increasing fiber–fiber contacts. When the paper is wetted, MFC2 causes considerable internal friction, which resists the relative motion of the fibers and results in greater wet strength (Tejado and van de Ven 2010). The second is the lower coarseness of MFC2. The tensile strength of wet web is expected to be inversely proportional to the square of fiber coarseness (Seth 1995).

Interaction between fibers and polymer greatly affect viscoelasticity and water plasticization of cellulosic composites (Myllytie et al. 2010). Once water penetrates into the cellulosic web, the hydrogen bonding between fibers decreases, leading to a loss of strength (Gardner et al. 2008). Crosslinking cellulose with the cationic thermal reactive PAE improves bonding properties, upon drying, against moisture change by creating a network of covalent bonds which restrict fibers swelling (Espy 1995; Obokata and Isogai 2007, 2009). Interestingly with PAE, the strength development from MFC2 was quite similar to that of MFC1 sheets (Figs. 5, 6), even with the increased retention of MFC2. Two reasons could account for this observation. First, the surface charge of MFC2 could have been modified upon adsorption of the cationic PAE; MFC2 reoriented during web forming and fibril entanglement would be reduced. Second, wet strength development may be dominated by building up of the covalent bonds network between the fibers and PAE upon drying, which counteracts the influence of MFC2 on fiber friction. For paper made with CMPs, the addition of PAE offset the debonding and improved the strength, but without changing the bulk and thickness of the web. These features may find application such as mechanical debonder in tissue making. Traditional tissue making usually combines softeners, typically a cationic surfactant, with wet and dry strength agents, such as PAE and carboxymethyl cellulose (CMC). CMPs could provide a non-chemical alternative to cationic surfactants to improve paper bulk, should softness not be affected.

The stress–strain curve of a fiber network indicates the elastic and viscoelastic nature of paper; a linear stress–strain plot suggests that PAE enhances the elasticity of paper. Comparing with the control, both dry MFC1 and MFC2 composites with and without PAE stretched longer at break, and demonstrated higher Young's modulus due to the strong affinity of fibrils bonded to each other (Fig. 7). When paper was wetted, the saturated fibers displayed gel-like behaviour, which may account for the extended strain observed (Saarikoski et al. 2012). MFC2 composite presents a unique lower strain at failure and a much higher Young's modulus, indicating a brittle material (Fig. 8).

The difference of wet elongation between MFC1 and MFC2 composites probably indicates two mechanisms of strengthening (Fig. 9). The first is

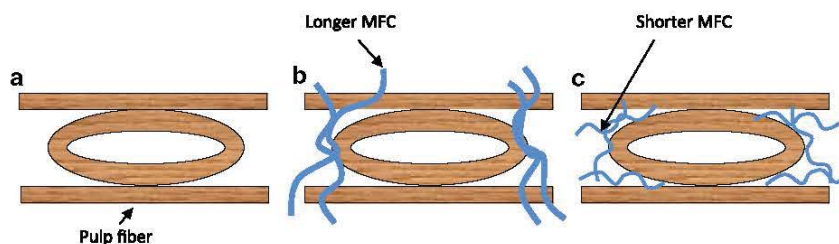


Fig. 9 Proposed mechanisms for paper web reinforcement. **a** Hardwood fiber web, **b** the addition of MFC, whose mean length is close to the value of hardwood fiber diameter, **c** the addition of MFC, whose mean length is lower than the value of hardwood fiber diameter

dominated by MFC-fiber entanglement, where MFC length is greater than the fiber diameter, and MFC acts as a bridge to bond the neighbouring fibers. As load is applied to the wet web, the structure deformation mainly relies on MFC entanglements around the fiber joints, explaining the extended failure behaviour. Secondly, in the case of MFC length shorter than fiber diameter, fiber-fiber contact reinforcement controls the strength improvement. When wetted, the MFCs on the fiber surface swell, which causes an initial separation of the fiber web. This would explain the deformation of the web observed at a short strain.

Conclusion

Cellulosic fiber web of increased strength and reduced air permeability were produced using the papermaking technology with cellulose additives of length scale ranging from the nano-meter to the micro-meter. MFC achieved by ball milling and CMPs developed by cryogenic milling softwood fiber were compared to commercial MFC produced from homogenization. The effect of blending two MFCs and CMPs with hardwood fibers on the paper properties was investigated in terms of nano/micro cellulose dimension. CMPs act as mechanical debonder and may find application in tissue making to increase paper bulk and decrease the substrate density, thus improving softness. In contrast to CMPs, MFC having a higher aspect ratio and smaller size significantly improved paper composite strength and decreased its porosity, yielding a denser structure. The retention of MFC was high even without polymeric retention aid thanks to their broad size distribution.

The addition of MFC combined with PAE can increase both dry and wet strength of cellulosic materials equivalently by an order of magnitude.

Their different stress-strain curves in wet condition suggest two different mechanisms of strength development: MFC-fiber entanglement and fiber-fiber contact reinforcement. Strong and low permeability paper with cellulosic nano-additives can be produced with a standard paper machine. These composites offer unique possibilities in packaging, tissue and light weight materials.

Acknowledgments The financial contribution of Australian Research Council (LP0990526), Visy and Nopco paper technology is acknowledged. Thank to Dr. W.K.J. Mosse, P. Chandran and I. Stopka for the cellulose micro-particles, Professor X. Wang and Associate Professor T. Tsuzuki from Deakin University for providing cellulose nanofibrils, and S. Sharman, S. Varanasi, S. Narayanan and H. Chiam for technical help.

References

- Ahola S, Osterberg M, Laine J (2008) Cellulose nanofibrils-adsorption with poly(amideamine) epichlorohydrin studied by QCM-D and application as a paper strength additive. *Cellulose* 15(2):303–314. doi:10.1007/s10570-007-9167-3
- Aulin C, Gallstedt M, Lindstrom T (2010) Oxygen and oil barrier properties of microfibrillated cellulose films and coatings. *Cellulose* 17(3):559–574. doi:10.1007/s10570-009-9393-y
- Espy HH (1995) The mechanism of wet-strength development in paper—a review. *Tappi J* 78(4):90–99
- Gardner DJ, Oporto GS, Mills R, Samir MASA (2008) Adhesion and surface issues in cellulose and nanocellulose. *J Adhes Sci Technol* 22(5–6):545–567. doi:10.1163/156856108x295509
- Jackson GW, James DF (1986) The permeability of fibrous porous-media. *Can J Chem Eng* 64(3):364–374
- Klemm D, Kramer F, Moritz S, Lindstrom T, Ankerfors M, Gray D, Dorris A (2011) Nanocelluloses: a new family of nature-based materials. *Angew Chem Int Ed* 50(24):5438–5466. doi:10.1002/anie.201001273
- Koga H, Saito T, Kitaoka T, Nogi M, Suganuma K, Isogai A (2013) Transparent, conductive, and printable composites consisting of TEMPO-oxidized nanocellulose and carbon

- nanotube. *Biomacromolecules* 14(4):1160–1165. doi:10.1021/Bm400075f
- Manninen M, Kajanto I, Happonen J, Paltakari J (2011) The effect of microfibrillated cellulose addition on drying shrinkage and dimensional stability of wood-free paper. *Nord Pulp Pap Res J* 26(3):297–305
- Mosse WKJ, Boger DV, Simon GP, Garnier G (2012) Effect of cationic polyacrylamides on the interactions between cellulose fibers. *Langmuir* 28(7):3641–3649. doi:10.1021/La2049579
- Myllytie P, Salmen L, Haimi E, Laine J (2010) Viscoelasticity and water plasticization of polymer–cellulose composite films and paper sheets. *Cellulose* 17(2):375–385. doi:10.1007/s10570-009-9376-z
- Niskanen K (1998) Papermaking science and technology: paper physics, Book 16. Fapet Oy, Helsinki
- Obokata T, Isogai A (2007) The mechanism of wet-strength development of cellulose sheets prepared with polyamideamine-epichlorohydrin (PAE) resin. *Colloid Surf A* 302(1–3):525–531. doi:10.1016/j.colsurfa.2007.03.025
- Obokata T, Isogai A (2009) Wet-strength development of cellulose sheets prepared with polyamideamine-epichlorohydrin (PAE) resin by physical interactions. *Nord Pulp Pap Res J* 24(2):135–140
- Saarikoski E, Saarinen T, Salmela J, Seppala J (2012) Flocculated flow of microfibrillated cellulose water suspensions: an imaging approach for characterisation of rheological behaviour. *Cellulose* 19(3):647–659. doi:10.1007/s10570-012-9661-0
- Seth RS (1995) The effect of fiber length and coarseness on the tensile-strength of wet webs—a statistical geometry explanation. *Tappi J* 78(3):99–102
- Siro I, Plackett D (2010) Microfibrillated cellulose and new nanocomposite materials: a review. *Cellulose* 17(3):459–494. doi:10.1007/s10570-010-9405-y
- Su JL, Mosse WKJ, Sharman S, Batchelor W, Garnier G (2012) Paper strength development and recyclability with polyamideamine-epichlorohydrin (PAE). *Bioresources* 7(1):913–924
- Su JL, Mosse WKJ, Sharman S, Batchelor WJ, Garnier G (2013) Effect of tethered and free microfibrillated cellulose (MFC) on the properties of paper composites. *Cellulose* 20(4):1925–1935. doi:10.1007/s10570-013-9955-x
- Taipale T, Osterberg M, Nykanen A, Ruokolainen J, Laine J (2010) Effect of microfibrillated cellulose and fines on the drainage of kraft pulp suspension and paper strength. *Cellulose* 17(5):1005–1020. doi:10.1007/s10570-010-9431-9
- Tejado A, van de Ven TGM (2010) Why does paper get stronger as it dries? *Mater Today* 13(9):42–49
- Varanasi S, Batchelor WJ (2013) Rapid preparation of cellulose nanofibre sheet. *Cellulose* 20(1):211–215. doi:10.1007/s10570-012-9794-1
- Varanasi S, Chiam HH, Batchelor W (2012) Application and interpretation of zero and short-span testing on nanofibre sheet materials. *Nord Pulp Pap Res J* 27(2):343–351. doi:10.3183/Npprj-2012-27-02-P343-351
- Varanasi S, He RL, Batchelor W (2013) Estimation of cellulose nanofibre aspect ratio from measurements of fibre suspension gel point. *Cellulose* 20(4):1885–1896. doi:10.1007/s10570-013-9972-9
- Yoon SH (2006) Adsorption kinetics of polyamide-epichlorohydrin on cellulosic fibres suspended in aqueous solution. *J Ind Eng Chem* 12(6):877–881
- Zhang LY, Tsuzuki T, Wang XG (2010) Preparation and characterization on cellulose nanofiber film. *Mater Sci Forum* 654–656:1760–1763. doi:10.4028/www.scientific.net/MSF.654-656.1760
- Zhang LY, Batchelor W, Varanasi S, Tsuzuki T, Wang XG (2012) Effect of cellulose nanofiber dimensions on sheet forming through filtration. *Cellulose* 19(2):561–574. doi:10.1007/s10570-011-9641-9

Effect of tethered and free microfibrillated cellulose (MFC) on the properties of paper composites

Jielong Su · Wade K. J. Mosse · Scot Sharman ·
Warren J. Batchelor · Gil Garnier

Received: 27 January 2013 / Accepted: 14 May 2013 / Published online: 28 May 2013
© Her Majesty the Queen in Right of Australia 2013

Abstract High strength and low gas permeability cellulosic composites were produced using the paper-making technology with a commercial microfibrillated cellulose (MFC). The effect of blending MFC with hardwood fibers was compared to the direct refining of the fibers with and without polyamideamine-epichlorohydrin (PAE) addition. The addition of MFC, free or tethered, to pulp fibers combined with PAE can increase the dry strength and wet strength of cellulosic materials by an order of magnitude. Air permeability of the composites decreases by up to orders four of magnitude with MFC addition. The hypothesis that refining wood fibers can produce tethered MFC which provides equivalent strength properties but significant drainage benefits was proven. Furthermore, major benefits in paper formation uniformity (fiber distribution homogeneity) were achieved with refined fibers.

Keywords Microfibrillated cellulose (MFC) · Paper · Polyamideamine-epichlorohydrin (PAE) · Refining · Hardwood fibers · Composites · Tethered microfibrils

Introduction

Microfibrillated cellulose (MFC), made by a mechanical (Nakagaito and Yano 2004; Iwamoto et al. 2007; Saito et al. 2007), acid hydrolysis (Saïd Azizi Samir et al. 2004) or enzymatic process (Janardhnan and Sain 2006; Henriksson et al. 2007), have shown strong potential in developing novel paper products and renewable composites of unique properties. Some of the MFC composites attributes include high mechanical properties and gas barrier ability, biodegradability and transparency. MFC fibres are interesting as they combine nanoscale diameter (5–50 nm) with micron-scale length (1–1,000 µm) (Dufresne et al. 2000; Nakagaito et al. 2005; Leitner et al. 2007). The polyanhydroglucosidic backbone of MFC is capable of strong hydrogen bonding (3 OH/unit) and of adsorbing in a closed packing configuration onto another cellulose surface. MFC has good potential for industrial deployment thanks to the wide availability of cellulosic raw material, the increased production capacity worldwide, and the continuously improving process, which have all contributed to a price steadily decreasing toward the rank of commodity chemical intermediate.

Composites made of MFC using the papermaking process have already been investigated (Ahola et al. 2008; Eriksen et al. 2008; Taipale et al. 2010; Sehaqui et al. 2010). MFC has been either blended with pulp fibers or used as a pure suspension, with and without polymeric strength agents. MFC composites with high

J. Su · W. K. J. Mosse · S. Sharman ·
W. J. Batchelor · G. Garnier (✉)
Department of Chemical Engineering, BioPRIA,
Australian Pulp and Paper Institute, Monash University,
Clayton, VIC 3800, Australia

tensile strength have been achieved, with properties depending on material and preparation procedure (Siro and Plackett 2010; Klemm et al. 2011). However, studies have consistently reported a very slow drainage rate incompatible with the current papermaking process. Another promising avenue investigated has been the coating of MFC onto paper for improved strength, printability and selective barrier properties (Aulin et al. 2010). While composites of significant properties have been achieved, two main issues have arisen. The first is again a very slow drainage, and the second is the loss of gas barrier and strength properties under conditions of high humidity moisture/or wet conditions (Syverud and Stenius 2009; Taipale et al. 2010; Miura and Kitaoka 2011; Varanasi et al. 2012).

The drainage of papermaking is governed by factors such as pH, ionic strength, type of the cationic polyelectrolyte and fiber dimensions. As the surface area of the fiber increases with the reciprocal of the diameter of the average fiber, and the drainage resistance is inversely proportional to the square of the specific surface area (Hubbe and Heitmann 2007), the drainage rate is expected to drop at a faster than linear rate with the content of MFC in the furnish. Fiber refining is a current practice in papermaking to increase fiber–fiber bonding through defibrillation of the external surface and increase flexibility of the fiber. Tethered cellulose microfibrils have been observed on the surface of refined pulp in many studies (Chakraborty et al. 2005; Janardhnan and Sain 2006; Mao et al. 2009). Tethered microfibrils are defined as the fibrils delaminated from the outer layers of the fiber that remain attached by a segment or an extremity. Drainage rate is known from experimental practice to drop at a slower than linear rate upon fiber refining (Cole et al. 2008). We raise the hypothesis that refining creates MFC tethered onto the surface of the fiber able to provide equivalent strength but at a drainage benefit compared to MFC addition which tend to block flow through the wet web. The objective of this study is to probe this hypothesis in the context of high performance cellulosic composites.

In this study, we compare the performance of tethered and free microfibrillated cellulose in paper composites made by standard papermaking technique. Tethered MFC was generated by refining hardwood fibers to different extents. MFC-pulp paper composites were prepared from blending fibers using the

regular paper process. The effect of polyamideamine-epichlorohydrin (PAE), a typical wet strength polymer, on the MFC composites was also investigated. The study aims at producing high performance cellulosic composites from the paper process and at better understanding the strength development mechanism of MFC-polymer-fiber composites.

Experimental method

Materials

The commercial polyamideamine-epichlorohydrin (PAE) was provided by Nopco Paper Technology Pty Ltd, Australia (33 % w/w solid content solution); PAE solutions were diluted with deionised water prior to each experiment. Bleached eucalyptus kraft pulp was obtained from the dry lap sheet (National Institute of Standards & Technology, Standard reference material 8,496). Commercially available MFC (free MFC) was purchased from Daicel Chemical Industries Ltd, Japan. This material was made from pure cellulose fibers mechanically treated in a high pressure homogenizer, and was supplied never dried at a 25 % solid content. The average length of MFC is 0.5–0.6 mm, fiber diameter range from 10 nm to several microns. The MFC was characterized as mean diameter of 73 nm and aspect ratio of 147 in previous work (Varanasi et al. 2012). The properties of the MFC used in this study were compared with typical primary and secondary fines from bleached hardwood kraft pulp in Table 1.

Refining of the fibers and preparation of cellulosic composites

30 g (oven dry weight) NIST 8,496 was soaked in 2 L deionized water overnight and then disintegrated for 75,000 revolutions. The obtained pulp slurry was concentrated into 10 % solid consistency by filtration through woven stainless steel wire (mesh aperture of 125 μm). When refined pulp was required, the pulp was refined at different revolutions (500, 1,000, 2,000, 5,000 and 10,000) by PFI mill (HAM-JERN, Hamar, Norway) at a load of $1.77 \text{ N}\cdot\text{mm}^{-1}$.

Cellulosic composites were prepared according to the Australian/New Zealand Standard Method 203 s. The dry pulp was thoroughly wetted by soaking in

Table 1 Properties of MFC, primary and secondary fines

Material	Origin	Dimension	Appearance	References
MFC	Micro-fibrillated from high refined pure cellulosic fiber	11 μm in length, and 0.073 μm in width	Fibrillar	Varanasi et al. (2012, 2013)
Primary fines	Originally presented in bleached hardwood kraft pulp	50–92 μm in length, and 14–30 μm in width	Blocky, rectangular	Cole et al. (2008), Chen et al. (2009)
Secondary fines	Refined from fines-free bleached hardwood kraft pulp	121–179 μm in length, and 9–18 μm in width	Slender, transparent	

deionized water overnight. The pulp was transferred to a disintegrator (Model MKIIIIC, Messmer Instruments Ltd), diluted to 2 L with deionized water, and disintegrated for 75,000 propeller revolutions. The pulp was blended with commercial MFC at different ratios (5, 10, 25, 50, 75 weight %). The prepared pulp-MFC mixture or refined pulps (1.2 g oven dry) in 3 L deionized water were used to construct the composites by handsheet machine (Mavis Engineering Limited, United Kingdom). The forming process is automatically controlled and the drainage time was recorded from 7 replicates. In order to decrease the drainage time for preparation of pure MFC substrate, water jet vacuum attached to the sheet machine was used. Deionized water was used for pulp slurry preparation and also for sheet forming. No salt was added to achieve a specified ionic strength.

The PAE solution was added to the fiber stock slurry and stirred for 10 min. The pH of the pulp slurry mixture was about six, and no adjustment was made. The quantity of PAE added was based on target oven dry basis weight of 60 g/m². After couching and wet-pressing at 0.4 MPa by sheet press (Type 5–1, AB Lorentzen & Wettre) for 7 min, the cellulose composite sheets were placed between two blotting papers, followed by a 10-min drum-dryer (Type MR-3, Japo Co., Ltd) treatment at 100 °C; this was to activate the bonds between the PAE and the cellulose surface.

Characterization of the composites

Freeness of the pulp was tested according to Australian/New Zealand Standard Methods 1301.206 s: 2002. The thickness and apparent density were measured according to Australian/New Zealand Standard Methods 426 and 208 s. Air resistance was assessed by air permeance tester (Type 977102, Lorentzen & Wettre, Sweden) according to Australian/New Zealand

Standard Method 420 s. Both sides of the seven replicates were measured and the results were determined in Gurley seconds.

The composite uniformity was measured by the paper perfect formation tester (Op Test Equipment Inc, Canada). The tester classifies formation quality in 10 formation components over a specific range and produces the formation value. The relative formation value (RFV) of each component relates to selected reference sheet (without PAE). RFV values less than 1 means that the formation quality of the tested paper is worse than the formation quality of the reference paper. Scanning electron micrographs (SEM) were obtained using a JEOL 7001 FEG system operating at 5 kV and 180 pA.

The sheets were equilibrated at 23 °C and 50 % relative humidity for at least 24 h before wet and dry tensile testing based on the Australian/New Zealand Standard Methods 448 and 437 s. For wet strength measurement, the strips were totally immersed in deionized water for 1 min, then the excess water was removed from the test piece by a blotter. The width of sample strips was 15 mm and test span was 100 mm. An Instron tensile tester (Instron 5,566) was used to record maximum tensile force with constant rate of elongation at 10 mm/min. The tensile index for each sample was calculated as tensile strength (expressed in Nm⁻¹) divided by basis weight (gm⁻²). The mean value was obtained from seven valid tests and the error bars in figures indicate the 95 % CI. Student's *t* test was used to determine statistical significance of data.

Results

MFC composites and refined fiber sheet

Paper handsheets were constructed from pure MFC and hardwood fibers, used as control, and were tested

in tension; their properties are listed in Table 2. Dry and wet paper made from 100 % MFC was 6 and 14 times stronger, respectively, than the control paper made from the hardwood fibers. The elongation at break of MFC paper was also higher than the control: dry strain was twice as high and wet strength three-fold higher. MFC composites are stronger than the control paper for three reasons. First, MFC has a much higher aspect ratio than eucalyptus fibers (140 vs. 60). Second, sheet density is higher for MFC composites, which means more contacts than at lower density, producing a structure more efficient mechanically. Third, hardwood fibers are dried once; without refining, it will have a low bonding potential, producing weak sheet. MFC samples are never-dried which should make a stronger sheet. MFC paper had extremely low permeability compared to the control hardwood fiber paper. The Gurley air permeability test used measures the time required for air, at a given pressure, to pass through a unit area. However, the time required for dewatering the MFC suspension into a paper sheet was also very high (about 15 min) and a dense fibrous structure was obtained. Paper entirely made of MFC cannot practically be drained; it is of interest to investigate whether blending MFC with Hardwood fibers can produce high strength composites that can be drained on a paper machine. An alternative to MFC addition is to refine fibers to increase their fibrillation, thus producing tethered micro-fibrils. Tethered cellulose microfibrils are defined as the fibrils delaminated from the outer layers of the fiber that remain connected by a segment or an extremity.

The morphology of microfibrillated fibers (MFC) and tethered fibers obtained from refining are compared on Fig. 1. The tethered fibrils on the refined fibers enable binding with the surrounding fibers (Fig. 1).

Increasing the MFC ratio in the fiber mixture and using highly refined fibers are two techniques that increase paper density and strength. Two series of paper were prepared and their strength-density relationships are presented in Fig. 2. The first series consisted of papers made from fiber blends varying the ratio of MFC/unrefined hardwood fibers; the second was achieved by refining hardwood fibers to different extent. The dry tensile indices improved with increased paper density. The strength-density relationship of papers made from MFC and refined fibers paper were both increased up to a density of 625 kg/m³, with the MFC composites having a constant slope; strength develops faster than linearly for refined papers of higher density.

The morphology and surface structure of composites made from 75 % MFC are significantly different from those prepared with highly refined hardwood fibers (10,000-revs) even though both composites have similar strength (Fig. 3). MFC (75 %) composites have a smoother surface and are more compact than papers made from refined fibers. This might be related to the higher shrinkage of paper made of 75 % MFC upon drying; the mean diameter of the handsheet was 155 ± 2.7 mm, compared to 159 ± 0.5 mm for the reference made from 100 % unrefined hardwood fiber.

The uniformity of paper formation was quantified at different length scales and analyzed with the relative

Table 2 Properties of 100 % MFC, unrefined and refined hardwood (HW) handsheets (basis weight of 60 g/m²)

	Tensile index (Nm/g)		Strain at break (%)		Thickness (μm)	Air permeability (Gurley s)	Apparent density (kg/m ³)	Freeness (ml)
	Dry	Wet	Dry	Wet				
MFC	69.5 ± 5.4	13.6 ± 2.5	3.3 ± 1	11.8 ± 1.2	95 ± 1	42,300 ± 562	660 ± 30	–
Unrefined HW	11.1 ± 0.8	1.0 ± 0.1	1.3 ± 0.2	3.4 ± 0.3	127 ± 1	1.4 ± 0.1	461 ± 18	520
500-rev refined HW	17.4 ± 2.6	1.0 ± 0.1	1.4 ± 0.1	3.4 ± 0.4	122 ± 3	1.7 ± 0.2	493 ± 15	520
1,000-rev refined HW	16.9 ± 1.0	1.0 ± 0.1	1.8 ± 0.2	4.3 ± 0.4	105 ± 2	1.8 ± 0.3	535 ± 14	510
2,000-rev refined HW	34.0 ± 4.0	1.3 ± 0.1	3.3 ± 0.4	4.6 ± 0.8	105 ± 2	5.5 ± 1.8	582 ± 12	436
5,000-rev refined HW	40.4 ± 3.6	1.4 ± 0.1	4.3 ± 0.6	4.2 ± 0.7	102 ± 1	18.3 ± 1.9	613 ± 9	343
10,000-rev refined HW	56.8 ± 5.4	1.8 ± 0.1	5.8 ± 0.4	4.0 ± 0.5	97 ± 1	52.2 ± 3.2	620 ± 9	198

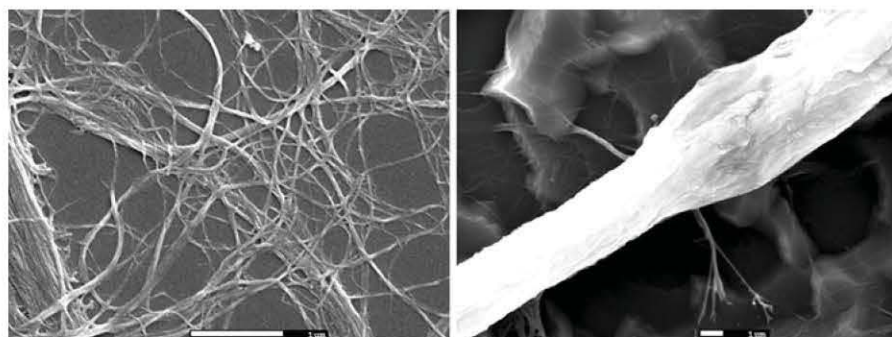


Fig. 1 SEM micrographs of (*left*) free MFC from the commercial product and (*right*) tethered MFC on refined fibers (10,000-revolutions)

values defined by comparing the sample with a control (Fig. 4). Composite formation uniformity worsened upon MFC addition, especially at the larger inspection sizes around 5 mm corresponding to fiber flocs (Fig. 4). In contrast, papers made from refined fibers had improved uniformity of formation at all inspection ranges (0.1–30 mm). The air permeability-density relationship of the MFC and refined fibers composites was compared (Fig. 5). At a given density, the permeability of papers made from refined fibers was much higher than those containing MFC (lower Gurley values). Air permeability decreased dramatically as the content of MFC increased (Fig. 5); by contrast, only a slight decline in air permeability was recorded for the webs made of refined fibers.

The relationship of wet-dry strength for composites made from MFC and for sheet of refined fibers is

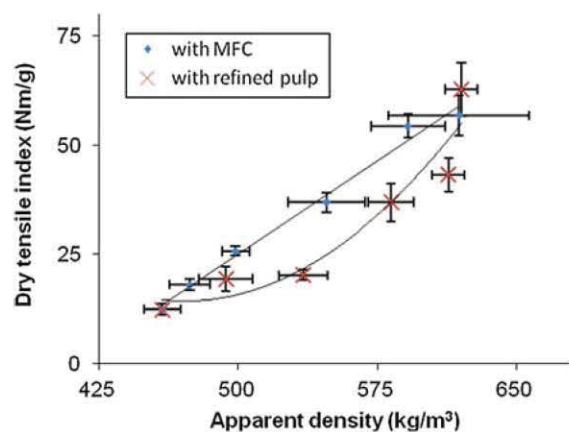


Fig. 2 Relationship between dry tensile index and apparent density for composites made from unrefined hardwood fiber-MFC mixtures and refined hardwood fibers

presented in Fig. 6; it is linear for composite made of refined pulps and exponential for MFC composites. Refining fibers significantly improved the dry tensile index, from 11 ± 1 to 63 ± 6 Nm/g, for fibers heavily refined (10,000 revolutions). Refining did not enhance wet tensile to any large extent; a maximum wet strength of 2 ± 0.1 Nm/g was reached compared with 1 ± 0.1 Nm/g for the control. The addition of MFC steadily increased composite strength. The slope of strength development from composites with MFC was higher than that made with refined fibers, indicating that MFC provided significant fibers entanglement frictions in the web. The wet tensile index increased sharply when the MFC ratio rose above 50 %. The MFC not only affected the tensile index but also the strain behavior of the papers. Wet composites made of 75 % MFC had higher strain at break than those made from refined fibers (10,000-revs). However, the dry strain of 75 % MFC paper was lower (Fig. 7).

Polyamideamide-epichlorohydrin (PAE) as additive in cellulose composites

Polyamideamide-epichlorohydrin (PAE) was adsorbed from solution onto the fibers prior to papermaking for composites made of MFC and refined fibers. Two PAE concentrations were investigated: 2 mg/g and 10 mg/g; 2 mg/g corresponds to the theoretical polymer half surface coverage for normal pulp fibers (unrefined) and 10 mg/g is the PAE concentration for maximum wet strength for sheets made of hardwood kraft fibers (Su et al. 2012). PAE addition considerably influenced the dewatering time and air permeability for composites with MFC concentration higher than 10 % (Table 3). Increased drainage time and reduced

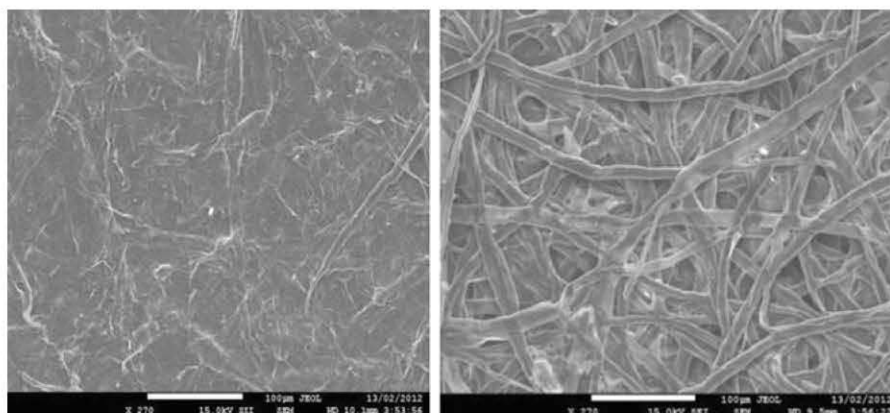


Fig. 3 SEM micrographs of composites made with (left) 75 % MFC and (right) refined fiber (10,000-revolutions)

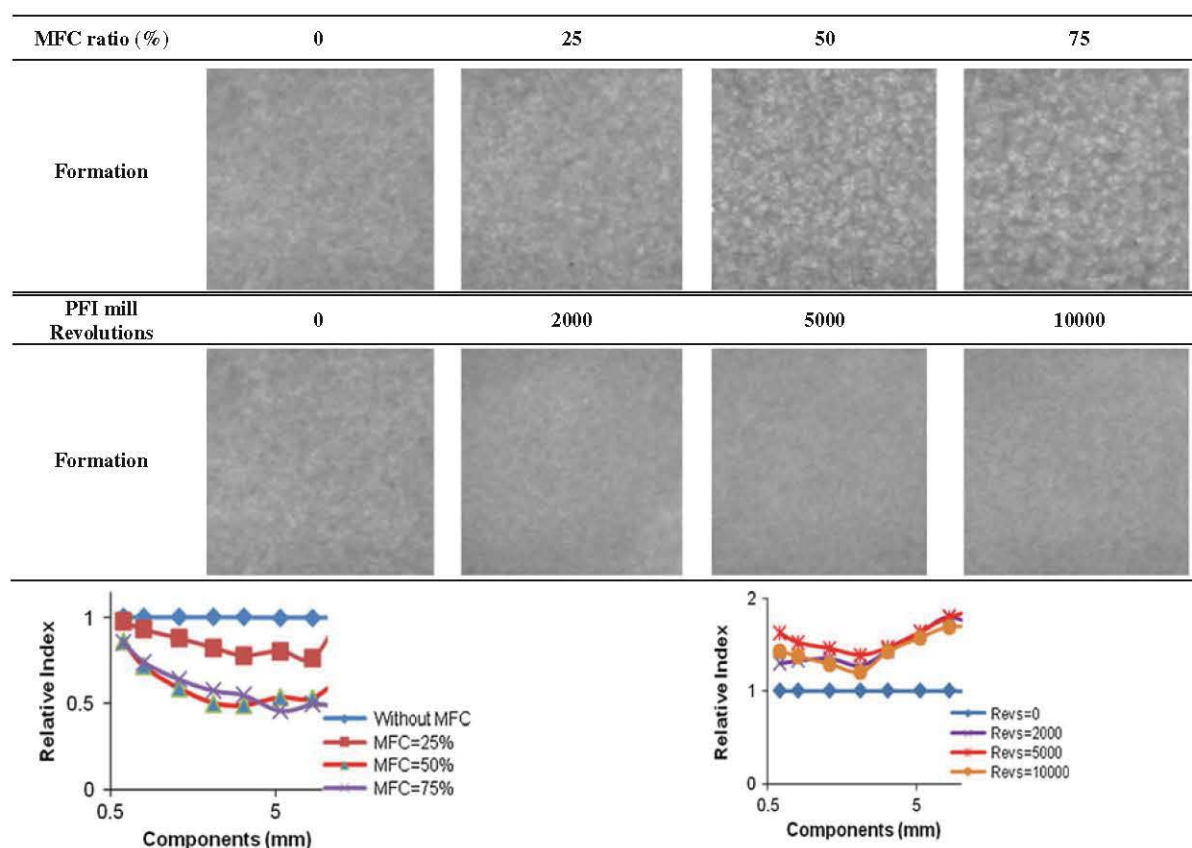


Fig. 4 Formation of the composites prepared from MFC and refined fibers. Each image is recorded from the area of 6.75 cm × 6.75 cm

composites air permeability were measured with increasing MFC concentration and at 2 mg/g PAE, where the drainage time for paper made with 25 and 50 % MFC were 21 ± 3 and 209 ± 16 s, respectively. Interestingly, less time of dewatering and

increased air permeability of all MFC composites was achieved at 10 mg PAE/g.

The composites dry-wet strength relationships were evaluated with 2 and 10 mg/g for composites made of MFC and refined fibers (Fig. 8). With refined fibers

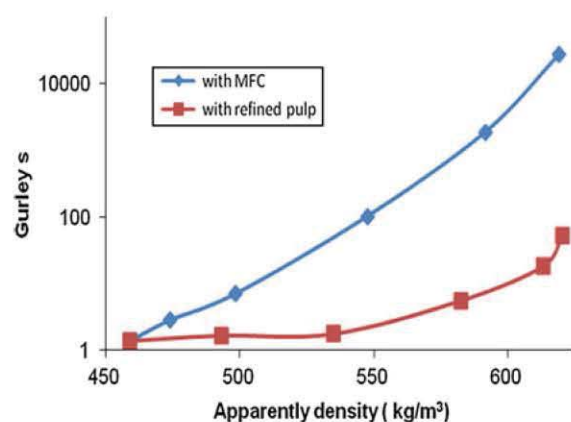


Fig. 5 Air permeability-density relationship for composites made of MFC and refined fibers (No PAE addition)

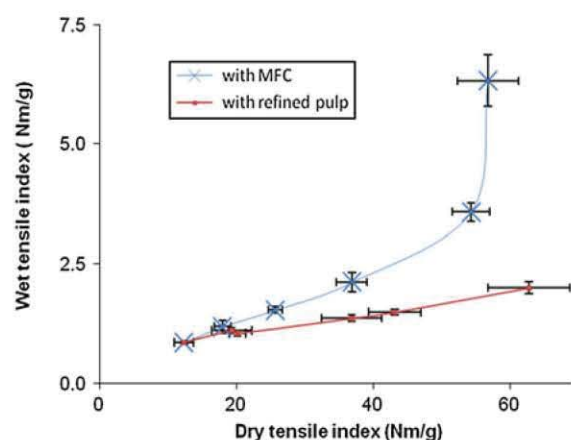


Fig. 6 Wet tensile-dry tensile relationship for composites made of MFC and refined fibers (No PAE addition)

and MFC composites, dry strength increased linearly with wet strength, the slope of which was a function of the PAE concentration. The addition of 2 and 10 mg PAE/g substantially improved the composites wet strength and increased the wet over dry strength ratio from 10 to 30 %.

The effect of refining the hardwood fiber fraction on the MFC composites strength properties was investigated. A series of composites were constructed by blending fibers at different MFC/hardwood fiber ratios, with either unrefined or refined (10,000 revs) fibers. These composites were tested for mechanical properties—wet and dry (Fig. 9). Without PAE, increasing the ratio of MFC increased strength in all instances. Adding PAE to refined fibers is especially efficient at increasing composite wet-strength. Composites of

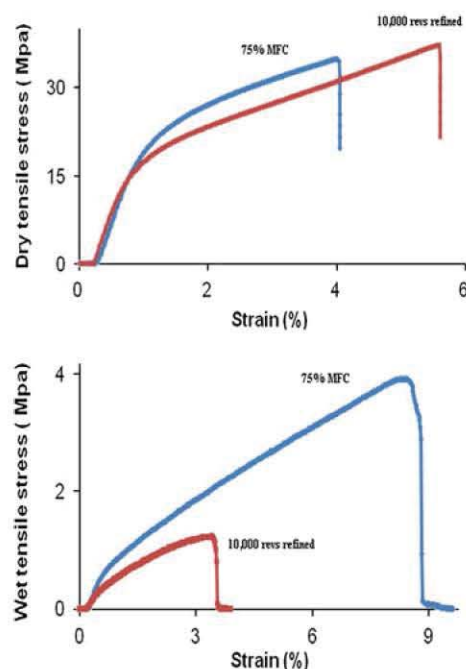


Fig. 7 Stress-strain curves of (upper) the dry and (bottom) wet composites prepared by 75 % MFC and fibers refined at 10,000 revolutions

high and similar wet and dry strength can be achieved by adding PAE to composites made of highly refined (10,000 revs) hardwood fibers and MFC.

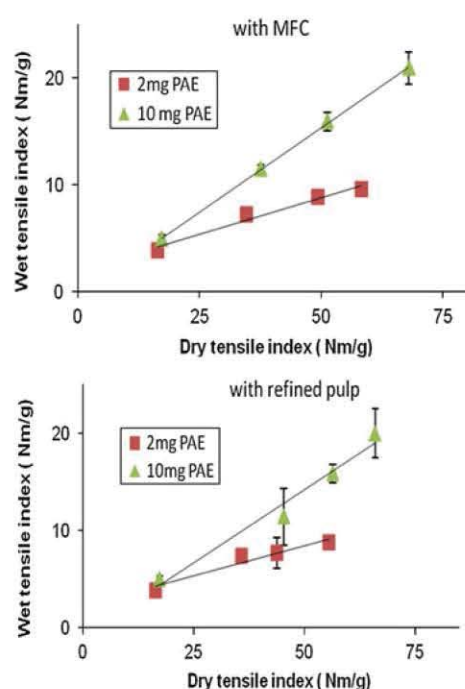
Discussion

Effect of MFC on composites process

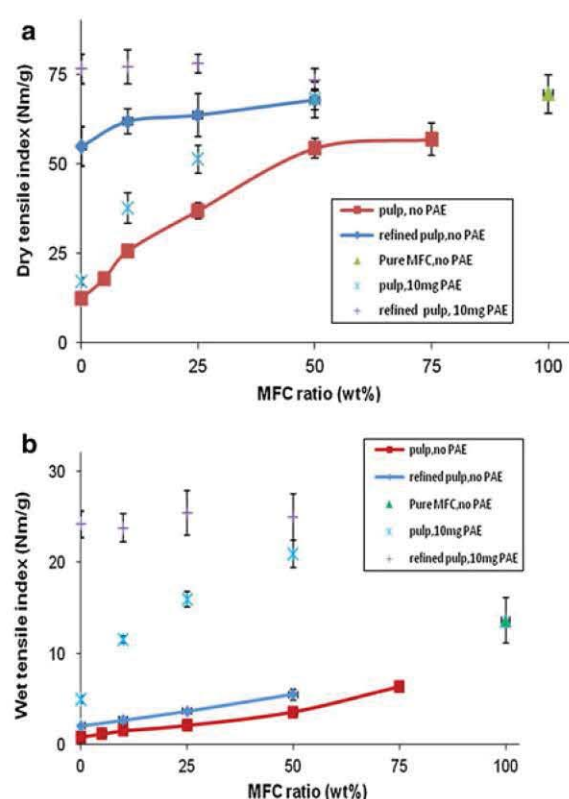
During refining, the long round cellulose fibers are transformed into collapsed, flexible and flat strips with various levels of surface fibrillation. Meanwhile, some of the primary wall or secondary wall layers are delaminated and become detached from the fibers. More fines are also generated (Karademir and Imamoglu 2007). The contribution of the fines to dewatering increased in inverse proportion to particle size and with increasing surface area (Chen et al. 2009). In this study, the drainage time was less than three seconds for all handsheets; their fibers were refined to different extents. The size of the paper remained stable upon unrestrained drying. On the contrary, the MFC content in the pulp slurry significantly affected the dewatering time (Table 3) and the dimensional stability of the paper.

Table 3 Effect of PAE on drainage for (upper) MFC composites preparation and (bottom) air permeability of the composites

Drainage time (sec) PAE dosage (mg/g)	MFC ratio (wt%) in unrefined pulp						MFC ratio (wt%) in 10,000-rev refined pulp		
	0	5	10	25	50	75	10	25	50
0	<3	<3	<3	14 ± 0.5	131 ± 8	322 ± 37	8 ± 3	57 ± 14	349 ± 59
2	<3	<3	<3	21 ± 3	209 ± 16	–	–	–	–
10	<3	<3	<3	11 ± 1	100 ± 9	–	6 ± 1	34 ± 2	180 ± 28
Air permeability (Gurley s) PAE dosage (mg/g)	MFC ratio (wt%) in unrefined pulp					Revolutions for refined pulp			
	0	10	25	50		500	2,000	5,000	
0		1.4 ± 0.1	7.1 ± 0.2	103.4 ± 7.6	1905 ± 385	1.7 ± 0.2	5.5 ± 1.8	18.3 ± 1.9	
2		1.5 ± 0.2	13.7 ± 1.3	161.1 ± 4.9	2656 ± 55	2.5 ± 0.2	4.1 ± 0.4	10.2 ± 1.2	
10		1.3 ± 0	5.7 ± 0.8	60.9 ± 4.1	1279 ± 39	1.6 ± 0.1	2.9 ± 0.2	5.6 ± 0.8	

**Fig. 8** Effect of PAE addition on wet-dry tensile relationship of composites prepared from (upper) MFC and (bottom) refined fibers

Many methods have been explored to prepare composites made of MFC substrates (Sehaqui et al. 2010; Siro and Plackett 2010). The major process consists of dispersing MFC in water and draining using the papermaking process. To achieve a high solid content before pressing and drying, vacuum assisted filtration is commonly used to drain the MFC suspension. Filtration times are very high with

**Fig. 9** a Dry tensile and b wet tensile properties of composites prepared by MFC-fibers and MFC-refined fibers mixture

drainage times more than half an hour long commonly reported, depending on the final basis weight of the product (Sehaqui et al. 2010). This is simply impractical for commercial scaling. Unlike the dimension of traditional fines (Table 1), the MFC shows higher

aspect ratio (147) and appears to be mainly from the whole of the fiber. The drainage time of our study was proportional to the MFC ratio above 25 %, in absence of PAE. This finding is in accordance with literature for MFC (below 10 %) monitored by dynamic drainage analyzer (Taipale et al. 2010; Varanasi and Batchelor 2013). Bonding of the fibrous network is drastically affected by MFC addition, which also increases drying shrinkage (Manninen et al. 2011).

Polymer assisted fiber flocculation is a critical factor governing the drainage of a fiber suspension. The cationic water-soluble polymer also strongly influences the rheological properties of fibrous suspensions. The polymer modifies the interaction between cellulose surfaces via electrostatic force, polymer bridging and steric repulsion. Increasing the PAE concentration to a MFC/fiber fibrous suspension has three main effects: (1) coagulate MFC into bigger “fine like” structures, (2) co-flocculate fibers with MFC and (3) modify floc properties (density/compressibility and size). In this study, the increasing drainage resistance observed for the fiber suspension with 2 mg PAE/g could indicate the combined effect of free MFC and low density/deformable fiber flocs which can contribute to blocking the wire upon deposition (Table 3). At higher PAE dose (10 mg/g), most fibers and MFC were flocculated into bigger and especially denser flocs (Su et al. 2012), resulting in a fast drainage. The optimization of polymer assisted flocculation can improve paper drainage.

Structure and air permeability of MFC composites

Paper properties are greatly affected by the three-dimensional fibers distribution. Fibers of a nanoscale diameter combined with micron to millimeter length could easily be formed into paper sheets (Zhang et al. 2012). The uniformity of the composites was analyzed by transmitted light (Fig. 4). The uniformity deteriorated significantly upon MFC addition. However, refining maintained and even improved formation uniformity. Refining has a combined effect of producing fines and increasing fibers flexibility (Li et al. 2011); this could explain the improved uniformity from 2,000 revs-refined fibers. However, little additional improvement was observed upon further refining.

Refining fibers did not decrease permeability of composite to a large extent. However, the addition of

MFC drastically decreased air permeability of composites by increasing pore tortuosity and decreasing pore area and pore connectivity. MFC films were reported to have similar oxygen transmission rate as common synthetic polymers (Syverud and Stenius 2009). Fluid and gas transportation in the fiber network closely relates to the porosity, the ratio of void volume and total volume of paper (Jackson and James 1986; Niskanen et al. 1998), which can be estimated from density. The air permeability for MFC composites is much lower than those from refined fibers, even at comparable densities (Fig. 5). This trend is more obvious at high MFC content, complying with the less porous surface morphology observed by microscopy (Fig. 3). The compact structure of MFC composites suggested their distinctive barrier behavior from that of porous paper.

With PAE addition, the air permeance of MFC-containing composites was modified. Air permeance correlated with drainage time (Table 3); the longer the time required for dewatering pulp fibers into a web, the longer the period needed for air to diffuse through the dry substrate plane. Although dewatering time reflects the resistance in the dynamic process of wet web forming, it may also indicate the extent of fiber flocculation and substrate structure.

Strength of MFC composites

Microfibrillated cellulose papers displayed excellent wet and dry tensile indices (Table 2) and a higher wet to dry strength ratio (15 %) than paper (below 10 %) without polymer additives. Unlike paper made of highly refined fibers, increasing the MFC content not only improved the paper dry strength, but considerably promoted wet strength (Fig. 6). This property could enable the MFC-made composites to better retain strength under high moisture or wet conditions. An hypothesis is that the larger amount of MFC in the paper web allows more fibers entanglements, and increases inner friction area between fibers, thus leading to greater wet strength (Tejado and van de Ven 2010). Another reason is that the much higher aspect ratio of MFC (140) than hardwood fiber (60) produces stronger sheets, as predicted by theory. The dry elongation of MFC and highly-refined fibers composites were similar (Fig. 7). Once water penetrates into the cellulosic web, the hydrogen bonding between fibers weakens rapidly (Gardner et al. 2008),

leading to a loss in strength and strain of paper from refined pulp (10000 revs). Conversely, the wet MFC composite demonstrates higher strain at break than the dry. The gel-like behavior of swollen MFC may account for the extended strain observed (Saarikoski et al. 2012).

Viscoelasticity and water plasticization of cellulosic composites are greatly affected by the interaction with polymers (Myllytie et al. 2010). Improved bonding properties against moisture change can be achieved by crosslinking cellulose with cationic-charged, thermal reactive PAE upon drying (Espy 1995; Obokata and Isogai 2007, 2009). With PAE, the strength development from MFC composites was similar to that of refined fibers sheets (Fig. 8). Two reasons could account for this observation. First, the surface charge of free MFC could have been modified upon cationic PAE adsorption; reorientation of the MFC which occurs during web forming and fiber entanglement would be reduced. Second, wet strength development may be dominated by building up of covalent bonds between the fibers and PAE upon drying, which diminishes the influence of MFC on fiber friction.

Microfibrillated cellulose blending with unrefined fibers and 10,000-revs refined fibers was compared to better understand the role of MFC in strength development (Fig. 9). Without PAE, the addition of MFC into unrefined fibers radically increases the relative bonded area and fibers entanglements, resulting in stronger papers. In contrast, the dry strength of composites from the mixture of refined fibers and MFC presented little change despite varying MFC content. This suggests similar MFC and refined fibers bond strength; paper made with 10,000-revs refined fibers (tethered MFC) and pure MFC substrate had comparable dry strength (Fig. 9a). Yet the mechanism of strength development must be somewhat different as composites made of refined fibers lose much more strength when wet. Refined fibers might allow more hydrogen bonds, and thus closer cellulose–cellulose contacts than MFC addition.

Conclusion

Novel cellulosic composites of high strength and low gas permeability were produced using the papermaking technology with microfibrillated cellulose (MFC).

The effect of blending MFC with hardwood fibers was compared with the refining of the hardwood fibers on the paper composite properties. The hypothesis that refining wood fibers can produce tethered MFC which provide equivalent strength properties but significant drainage benefits was proven. Furthermore, significant benefits in paper formation uniformity (fiber distribution homogeneity) were achieved.

At constant dry strength, composites made with refined fibers had higher density and lower wet strength than those made by blending MFC. This might suggest a higher contribution of hydrogen bonding. The addition of MFC, free or tethered, to pulp fibers combined with polyamideamine-epichlorohydrin (PAE) can increase the dry strength and wet strength of cellulosic materials by an order of magnitude. Air permeability of the composites decreases by up to four orders of magnitude with MFC addition, opening new avenues for packaging for food and novel applications.

Acknowledgments The financial contribution of Australian Research Council (LP0990526), Visy and Nopco paper technology is acknowledged. The authors would like to thank Misses Sigappi Narayanan and Hui Hui Chiam for experimental assistance, and Mr Swambabu Varanasi for SEM expertise.

References

- Ahola S, Osterberg M, Laine J (2008) Cellulose nanofibrils-adsorption with poly (amideamine) epichlorohydrin studied by QCM-D and application as a paper strength additive. *Cellulose* 15(2):303–314
- Aulin C, Gällstedt M, Lindström T (2010) Oxygen and oil barrier properties of microfibrillated cellulose films and coatings. *Cellulose* 17(3):559–574
- Chakraborty A, Sain M, Kortschot M (2005) Cellulose microfibrils: a novel method of preparation using high shear refining and cryocrushing. *Holzforschung* 59(1):102–107
- Chen H, Park A, Heitmann JA, Hubbe MA (2009) Importance of cellulosic fines relative to the dewatering rates of fiber suspensions. *Ind Eng Chem Res* 48(20):9106–9112
- Cole CA, Hubbe MA, Heitmann JA (2008) Water release from fractionated stock suspensions. Part 1—effects of the amounts and types of fiber fines. *Tappi J* 7(7):28–32
- Dufresne A, Dupeyre D, Vignon MR (2000) Cellulose microfibrils from potato tuber cells: processing and characterization of starch–cellulose microfibril composites. *J Appl Polym Sci* 76(14):2080–2092
- Eriksen O, Syverud K, Gregersen O (2008) The use of microfibrillated cellulose produced from kraft pulp as strength enhancer in TMP paper. *Nord Pulp Pap Res J* 23(3):299–304
- Espy HH (1995) The mechanism of wet-strength development in paper—a review. *Tappi J* 78(4):90–99

- Gardner DJ, Oporto GS, Mills R, Samir MASA (2008) Adhesion and surface issues in cellulose and nanocellulose. *J Adhes Sci Technol* 22(5–6):545–567
- Henriksson M, Henriksson G, Berglund LA, Lindstrom T (2007) An environmentally friendly method for enzyme-assisted preparation of microfibrillated cellulose (MFC) nanofibers. *Eur Polym J* 43(8):3434–3441
- Hubbe MA, Heitmann JA (2007) Review of factors affecting the release of water from cellulosic fibers during paper manufacture. *Bioresources* 2(3):500–533
- Iwamoto S, Nakagaito AN, Yano H (2007) Nano-fibrillation of pulp fibers for the processing of transparent nanocomposites. *Appl Phys A* 89(2):461–466
- Jackson GW, James DF (1986) The permeability of fibrous porous-media. *Can J Chem Eng* 64(3):364–374
- Janardhanan S, Sain MM (2006) Isolation of cellulose microfibrils—an enzymatic approach. *Bioresources* 1(2):176–188
- Karademir A, Imamoglu S (2007) Effects of dry strength resin and surfactant addition on the paper made from pulps with different freeness level. *J Appl Sci* 7(4):484–488
- Klemm D, Kramer F, Moritz S, Lindstrom T, Ankerfors M, Gray D, Dorris A (2011) Nanocelluloses: a new family of nature-based materials. *Angew Chem Int Edit* 50(24):5438–5466
- Leitner J, Hinterstoisser B, Wastyn M, Keckes J, Gindl W (2007) Sugar beet cellulose nanofibril-reinforced composites. *Cellulose* 14(5):419–425
- Li B, Li HM, Zha QQ, Bandekar R, Alsagoff A, Ni YH (2011) Review: effects of wood quality and refining process on tmp pulp and paper quality. *Bioresources* 6(3):3569–3584
- Manninen M, Kajanto I, Happonen J, Paltakari J (2011) The effect of microfibrillated cellulose addition on drying shrinkage and dimensional stability of wood-free paper. *Nord Pulp Pap Res J* 26(3):297
- Mao JL, Kadla JF, Kerekes RJ (2009) Retaining surface fibrillation of wet-beaten wood pulp in the dry state. *Tappi J* 8(7):25–30
- Miura S, Kitaoka T (2011) In situ synthesis of gold nanoparticles on zinc oxides preloaded into a cellulosic paper matrix for catalytic applications. *Bioresources* 6(4):11
- Myllytie P, Salmen L, Haimi E, Laine J (2010) Viscoelasticity and water plasticization of polymer-cellulose composite films and paper sheets. *Cellulose* 17(2):375–385
- Nakagaito AN, Yano H (2004) The effect of morphological changes from pulp fiber towards nano-scale fibrillated cellulose on the mechanical properties of high-strength plant fiber based composites. *Appl Phys A* 78(4):547–552
- Nakagaito AN, Iwamoto S, Yano H (2005) Bacterial cellulose: the ultimate nano-scalar cellulose morphology for the production of high-strength composites. *Appl Phys A* 80(1):93–97
- Niskanen K, Suomen Paperi-insinöörien Yhdistys (1998) Technical association of the pulp and paper industry. Paper physics. Papermaking science and technology, vol book 16. Published in cooperation with the Finnish Paper Engineers' Association and TAPPI, Helsinki; Atlanta
- Obokata T, Isogai A (2007) The mechanism of wet-strength development of cellulose sheets prepared with polyamideamine-epichlorohydrin (PAE) resin. *Colloid Surface A* 302(1–3):525–531
- Obokata T, Isogai A (2009) Wet-strength development of cellulose sheets prepared with polyamideamine-epichlorohydrin (PAE) resin by physical interactions. *Nord Pulp Pap Res J* 24(2):135–140
- Saarikoski E, Saarinen T, Salmela J, Seppälä J (2012) Flocculated flow of microfibrillated cellulose water suspensions: an imaging approach for characterisation of rheological behaviour. *Cellulose* 19(3):647–659
- Said Azizi Samir MA, Alloin F, Paillet M, Dufresne A (2004) Tangling effect in fibrillated cellulose reinforced nanocomposites. *Macromolecules* 37(11):4313–4316
- Saito T, Kimura S, Nishiyama Y, Isogai A (2007) Cellulose nanofibers prepared by TEMPO-mediated oxidation of native cellulose. *Biomacromolecules* 8(8):2485–2491
- Sehaqui H, Liu AD, Zhou Q, Berglund LA (2010) Fast preparation procedure for large, flat cellulose and cellulose/inorganic nanopaper structures. *Biomacromolecules* 11(9):2195–2198
- Siro I, Plackett D (2010) Microfibrillated cellulose and new nanocomposite materials: a review. *Cellulose* 17(3):459–494
- Su J, Mosse WKJ, Sharman S, Batchelor W, Garnier G (2012) Paper strength development and recyclability with polyamineamine-epichlorohydrin (PAE). *Bioresources* 7(1):913–924
- Syverud K, Stenius P (2009) Strength and barrier properties of MFC films. *Cellulose* 16(1):75–85
- Taipale T, Osterberg M, Nykanen A, Ruokolainen J, Laine J (2010) Effect of microfibrillated cellulose and fines on the drainage of kraft pulp suspension and paper strength. *Cellulose* 17(5):1005–1020
- Tejado A, van de Ven TGM (2010) Why does paper get stronger as it dries? *Mater Today* 13(9):42–49
- Varanasi S, Batchelor W (2013) Rapid preparation of cellulose nanofibre sheet. *Cellulose* 20(1):211–215
- Varanasi S, Chiam HH, Batchelor W (2012) Application and interpretation of zero and short-span testing on nanofibre sheet materials. *Nord Pulp Pap Res J* 28(2):343–351
- Zhang LY, Batchelor W, Varanasi S, Tsuzuki T, Wang XG (2012) Effect of cellulose nanofiber dimensions on sheet forming through filtration. *Cellulose* 19(2):561–574

Engineering paper as a substrate for blood typing bio-diagnostics

Jielong Su · Mohammad Al-Tamimi ·
Gil Garnier

Received: 14 May 2012 / Accepted: 12 July 2012 / Published online: 25 July 2012
© Springer Science+Business Media B.V. 2012

Abstract The effect of paper structure on blood typing visualization was quantified and analyzed to engineer low-cost diagnostics. Commercial and experimental papers varying in fibre composition, basis weight, density and porosity were investigated for their ability to separate agglutinated (blood interacted with specific antibodies) from non-agglutinated (blood interacted with non-specific antibodies) red blood cells (RBCs). Antibodies solutions and blood samples were sequentially absorbed on paper, allowed to interact, eluded with a saline solution, and the intensity of the remaining blood spot was quantified by image analysis. The efficiency and clarity of RBC separation was quantified with the relative intensity (R.I.) index defined as the intensity ratio of the non-specific test over the specific system; the lower the R.I., the better is the separation between a positive from a negative test. Thick and dense papers are improper for blood typing as they retain indiscriminately both agglutinated and non-agglutinated RBCs. Thin and porous papers provided the best performance. The R.I. index (the lower the better) increased fairly linearly with paper density and thickness but inversely proportionally with paper pore size. The type of fibres played a minor role. The paper structure is critical in the design of blood typing assay.

However, it is only one element of the diagnostic system to engineer with the interactions RBC-antibody-paper.

Keywords Paper · Structure · Blood typing · Bioassay · Diagnostics · Antibody · Red blood cell (RBC)

Introduction

Low cost cellulosic blood typing biodiagnostic based on paper and cotton thread have shown great potential for direct medical analysis and reporting. Accurate assessment of blood group is essential for the safe blood transfusion and transplantation medicine (Daniels and Reid 2010). Blood group is determined by the presence or absence of certain antigens on red blood cells (RBCs) (Daniels and Bromilow 2010; Malomgre and Neumeister 2009). Over 300 different antigens have been identified on RBCs and classified into more than 30 different blood groups, among them the typing ABO and Rhesus D (RhD) blood groups are by far the most important (Daniels and Bromilow 2010; Daniels et al. 2009). Every year about 75 million units of blood are collected before a life saving procedure (Klein et al. 2007). The identification of ABO and RhD blood group for both blood recipient and donor is essential to prevent incompatible blood transfusion that can lead to fatal haemolytic transfusion reaction (Daniels and Reid 2010; Daniels and Bromilow 2010).

J. Su · M. Al-Tamimi · G. Garnier (✉)
Department of Chemical Engineering, BioPRIA,
Australian Pulp and Paper Institute, Monash University,
Clayton, VIC 3800, Australia

Human blood groups can be identified from the principles of RBCs agglutination using specific antibodies raised against different RBCs antigens. Agglutinated RBCs can be detected using different assays with reliable sensitivity and specificity rate, including the traditional tube test, microplate and solid phase assays, gel column agglutination and affinity column technology (Malomgre and Neumeister 2009; Beck et al. 1986; Lapierre et al. 1990; Harmening 1999; Knight and deSilva 1996; Anstee 2009; Harmening 1999). Recently, advanced methods for blood groups identification using gene sequencing and flow cytometry-based assays have been reported (Roback et al. 2003; Anstee 2009; Petrik 2001). These assays require special laboratory instruments operated by trained laboratory personal which increases the relative cost and test reporting time for these assays (Beck et al. 1986; Lapierre et al. 1990; Harmening 1999). Few point-of-care assays can be done without laboratory equipment or blood collection. These assays are associated with higher rate of errors leading to erroneous transfusion (Eldon 1956; Plapp et al. 1986; Blakeley et al. 1990; Giebel et al. 2008; Bienek and Charlton 2011; Giebel et al. 2008; Ingrand et al. 1998; Dujardin et al. 2000; Ahrens et al. 2005; Migeot et al. 2002). Development of simple, rapid and reliable blood grouping assays would be of great value for pre-transfusion compatibility checks and in situations where there is no access to laboratory facilities such as in rural areas and in military applications.

In biodiagnostic for blood typing application, the paper or cotton thread substrates serves three purposes. The first is the driving force to transport by capillarity the blood sample to be analyzed—and reactants if required. The second is to separate the stable RBCs from the agglutinated RBCs by a combination of filtration, size exclusion and chromatography. The third is the simple and direct communication of results. The paper surface and bulk structure and the interactions between paper–antibody–antigen at the liquid–solid interface were previously observed to play critical roles in these three steps (Khan et al. 2010; Al-Tamimi et al. 2012; Jarujamrus et al. 2012). However, there has been no systematic study on the effect of paper structure on blood typing analysis.

This study investigates the effect of paper structure for paper-based diagnostics for blood typing applications. Antibodies solutions and blood samples were sequentially adsorbed on the different papers, allowed

to rest (30 s) before being eluted with a 0.9 % saline solution. The papers were dried and the level of RBCs separation was quantified by image analysis. Two types of paper were tested: commercial papers including filter papers, towel and blotting paper, and experimental papers made in our laboratory. The effect of paper basis weight, porosity, density and fibre composition on RBCs separation for specific and non-specific antibody-antigen interactions was analyzed for blood typing applications.

Experimental

Blood and antibodies

Antibodies against RBC antigens approved for human blood grouping including Anti-A IgM antibodies (clone 51000), Anti-B IgM antibodies (clone 10091) and Anti-D IgM antibodies (clones MS 201) were obtained from Lateral Grifols, Australia. Blood group was identified by a diagnostic laboratory using the standard diagnostic assay (Lateral Grifols, Australia). Blood samples were stored at 4 °C and tested within 7 days of collection. Analytical grades of NaCl, were purchased from Sigma-Aldrich, USA.

Paper

The standard Drink Coster blotting paper 280 gm⁻² was from Fibrosystem AB, Sweden. Whatman filter paper (#1, 3, 4, 5, and 113) were purchased from Whatman International Ltd, England. Filter #2883 was purchased from Adalab Scientific, Australia. Towel tissue (Kleenex) manufactured by Kimberly-Clark, Australia was also purchased. The particle retention size of filters was provided by the manufacturers.

Long and short fibres were obtained from disintegration of NIST standard reference material 8495 (Northern Softwood Bleached Kraft Pulp) and 8496 (Eucalyptus Hardwood Bleached Kraft Pulp), respectively. The moving belt sheet former was used to prepare square (22 × 22 cm²) paper. The basis weight and thickness were measured from ten replicates according to Australian/New Zealand Standard Methods 426 s and 208 s. Capillary rise was determined by Klemm method based on ISO 8787:1986. Basically, papers were cut into 15 ± 1 mm × 220 mm strips, which were suspended vertically with their lower end

immersed in water. The capillary rise in 10 min was measured. The result was the mean value from three measurements.

Methods

Agglutinated RBCs fixation on paper

Assessment of red colour optical density of blood spotted over specific and non-specific antibodies and subjected to chromatographic elution was essentially performed as previously described (Al-Tamimi et al. 2012). Briefly, Fresh 10 μ L droplets of Anti-A, Anti-B and Anti-D antibody solutions were spotted at 2 cm from the lower edge of blotting, filter or towel tissue and experimental paper strips, followed by the addition of 3 μ L of blood to the center of each antibody spot and allowed to interact for 30 s. The paper strip was then suspended vertically with an extremity dipping (about 1 cm) in a 0.9 % NaCl buffer contained in a thin film chromatography tank for 10 min. The paper was left to dry at room temperature for another 10 min and a digital picture was recorded using a standard Epson scanner. The intensity of the blood spot after elution was quantified by measuring the mean optical density of the red colour using ImageJ software (National Institute of Health).

Statistical analysis

The optical density of the red colour of blood spot after chromatographic elution was reported as mean \pm standard deviation (SD). Unpaired two-tailed *t* test was used to compare the mean optical density of blood collected from different donors spotted over specific versus non-specific antibodies, while one way ANOVA test was applied to compare the mean optical density in more than two groups. Statistical analysis was performed using GraphPad Prism (version 5) software with *P* < 0.05 considered significant.

Results

A series of commercial and experimental papers were tested for their ability to separate antibody agglutinated from non-agglutinated blood using a standard technique relying on saline elution and image analysis.

The efficiency and clarity of separation was quantified with the relative intensity (R.I.) index defined as the intensity ratio of the non-specific test over the specific system; the lower the R.I., the better is the separation between a positive from a negative test. The commercial papers selected included a low density towel, a series of filter papers of different pores size and blotting paper. Experimental papers varying in fibre composition (softwood, hardwood) and basis weight were also tested.

Agglutinated blood fixation on different papers

The effect of paper structure on the chromatographic elution of antibody agglutinated and non-agglutinated blood was investigated as technique to identify blood typing (Table 1). A specific and an unspecific droplet of antibody solution were deposited on two different paper strips. A blood droplet of donors with different blood groups (A, B, AB, O, RhD+ and RhD-) was immediately spotted on paper over the typing antibody ring, allowed to interact 30 s before the end of the paper strip was contacted with a saline solution and chromatographically eluted for 10 min. The paper was dried, scanned and the colour intensity of the residual blood droplets was measured by image analysis. The optical density of at least eight replicates was plotted for the filter, blotting & towel and experimental papers in Fig. 1. A representative picture of a typical eluded drop of blood group A spotted over specific Anti-A and non-specific Anti-B antibody with different paper substrates is also included in Fig. 1. Agglutinated blood, consisting of blood spotted over specific antibodies including blood group A with Anti-A, blood group B with Anti-B, and blood group D with Anti-D, showed a strong fixation on all papers with little variations among the different types of paper. Paper structure had an important effect on the fixation of non-agglutinated blood, which is the blood spotted on a non-specific antibody. For robust blood typing testing, it is critical to avoid any overlap between a specific and an unspecific test, and to maximize their difference in optical density; a low relative index is desired.

The intensity of unspecific and specific blood tests of six filter papers varying in particle size retention was compared (Fig. 1a). Good separation between the specific and non-specific tests was achieved with only three filters grades (2883, 113 and 4). Blotting paper

Table 1 Paper properties

Properties	Paper							
	Blotting	Grade 5	Grade 3	Grade 1	Grade 4	Grade 113	Grade 2883	Towel tissue
Basis weight (g/m ²)	267	96	91	89	94	113	135	28
Thickness (μm)	458 (21)	209 (3)	221 (7)	202 (6)	214 (2)	396 (10)	430 (16)	111 (2)
Apparent density (kg/m ³)	582	460	411	439	439	332	315	253
Particle retention size (μm)		2.5	6	11	22.5	30	40	

Properties	Paper					
	Long fibre			Short fibre		
	High	Medium	Low	High	Medium	Low
Basis weight (g/m ²)	71	52	25	76	48	24
Thickness (μm)	127 (8)	108 (10)	74 (11)	192 (10)	125 (9)	81 (5)
Apparent density (kg/m ³)	559	479	336	396	386	294

The top section presents the commercial papers, the bottom the experimental papers. Standard deviation from 10 measurements indicated in parenthesis

provided poor intensity differences between specific and non-specific tests, while towel paper yielded near perfect results, with the RBC of non-specific tests almost completely eluding from paper (Fig. 1b).

Papers of different basis weights but similar structures were prepared in our laboratory with long (softwood) and short (hardwood) fibres. The orientation of the fibres in paper was kept random to avoid any isotropic effects leading to preferential wicking. These experimental papers were tested for blood typing using the standard technique developed and the optical density from agglutinated and non-agglutinated blood after elution is shown in Fig. 1c. Paper basis weight and the type of fibres had very little impact on optical density of the blood dot after saline elution for agglutinated blood (specific) (Table 2). However, the mean optical density of blood spotted to non-specific antibodies after elution was significantly lower for low grammage papers (long fibres 23 ± 6 , $P < 0.001$ and short fibres 41 ± 9 , $P < 0.001$) and towel paper (46 ± 8 , $P < 0.001$). There were no overlaps between optical densities for agglutinated and non-agglutinated blood with low grammage papers and the towel.

Optimizing paper properties for blood typing

Six filter papers of particle size retention ranging from 2.5 to 40 μm were tested for the relative intensity ratio of their unspecific over specific tests (Fig. 2). The size

data were provided by the suppliers and the particle retention was rated at 98 % efficiency. For filter papers of low particle size retention (lower than 25 μm), the relative intensities remain high (R.I. > 0.75) and decrease slowly with particle retention size. This means the agglutinated and non-agglutinated blood samples were very difficult to distinguish after elution. The relative intensity of blood test decreases steadily, but much faster, for filter papers having a retention size higher than 25 μm. The most porous filter paper tested, grade 2883 with the size of 40 μm, had the best relative intensity at around 0.5.

The relationship between R.I. and paper thickness of all papers tested for blood typing was investigated (Fig. 3). In general, the thinner substrates have a lower R.I. Thick papers (over 200 μm) retain both individual and aggregated RBC and do not segregate well a positive test from a negative. For thin papers (up to 200 μm) the R.I. linearly increases with the web thickness up to R.I. = 0.75 both for long and short fibres papers, forming a master curve. The blotting paper 458 μm thick reached R.I. of 0.88, similar to that of filter grade 5 (thickness of 209 μm). However, two thicker filter papers (#113 with 396 μm and #2883 with 430 μm) demonstrated relatively lower R.I. than those of the other thin filters. These two grades are modified with wet strength polymers.

For papers made from a given fibre, the R.I. increased linearly with the paper apparent density

Fig. 1 Optical density from blood typing on different papers. **a** Filter papers. **b** Blotting and Kleenex towel papers. **c** Experimental papers made from long and short fibres (average \pm standard deviation of at least five measurements)

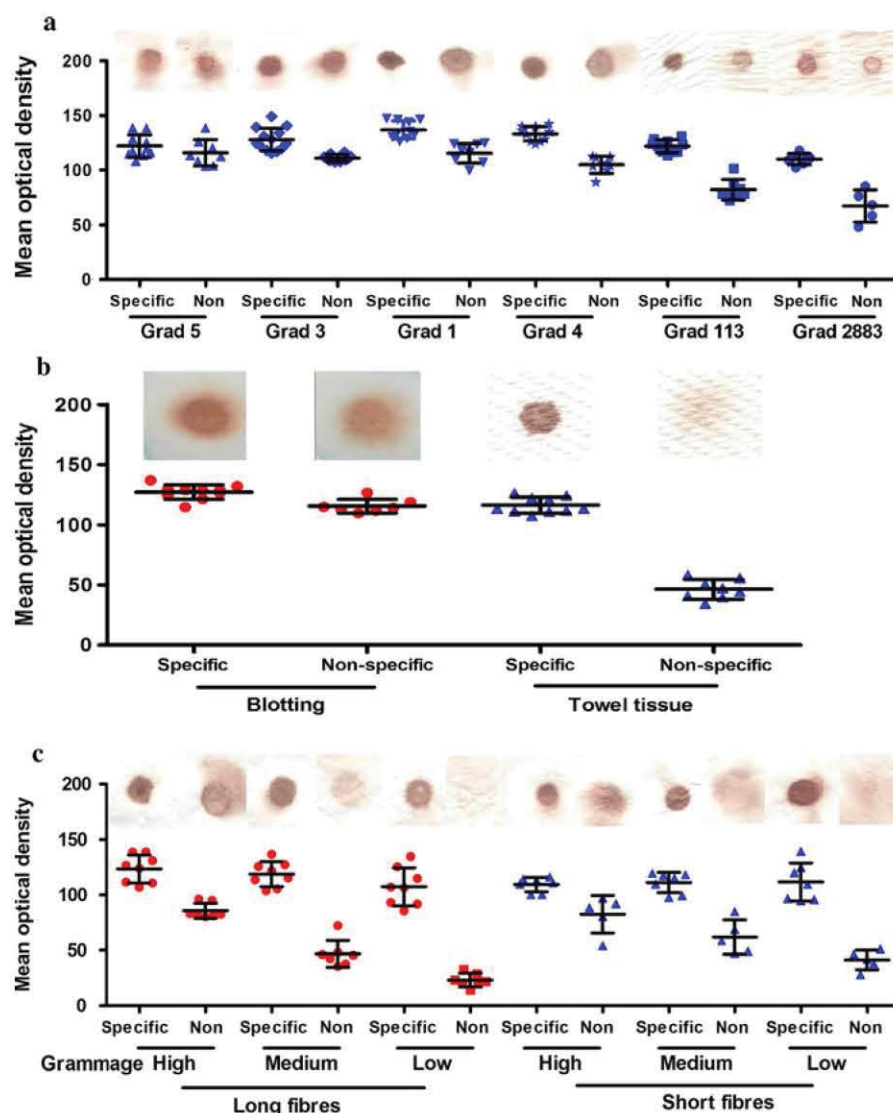


Table 2 Optical density for blood spotted on specific antibodies and non-specific antibodies fixed in different paper substrates (average \pm standard deviation). Standard deviation is from eight measurements

Paper substrate	Optical density for blood spotted on specific antibodies	Optical density for blood spotted on non-specific antibodies	<i>P</i> value ¹
Long fibres, 25 g/m ²	107 \pm 17	23 \pm 6	0.0001
Short fibres, 24 g/m ²	112 \pm 17	41 \pm 9	0.0001
Towel tissue	116 \pm 7	46 \pm 8	0.0001
	<i>P</i> value ² = 0.41	<i>P</i> value ² < 0.0001	

P value¹ is from unpaired two-tailed *t* test. *P* value² is from one way ANOVA. *P* value < 0.05 considered significant

(Fig. 4); papers from each type of fibre yielded a separate curve. The R.I. from long fibres webs gradually raised with density (up to 559 kg/m³). The

minimum R.I. was obtained at 0.19 for a web of long fibres with a density of 336 kg/m³, higher than the density of the towel (253 kg/m³). By comparison with

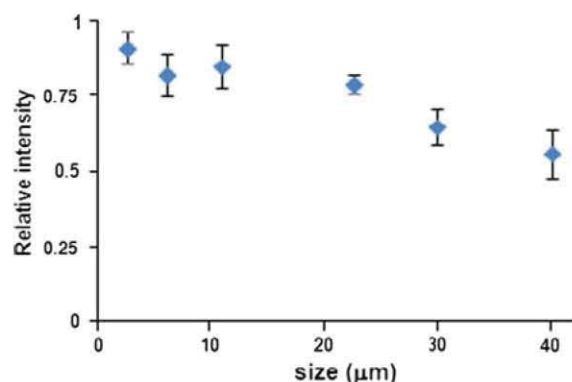
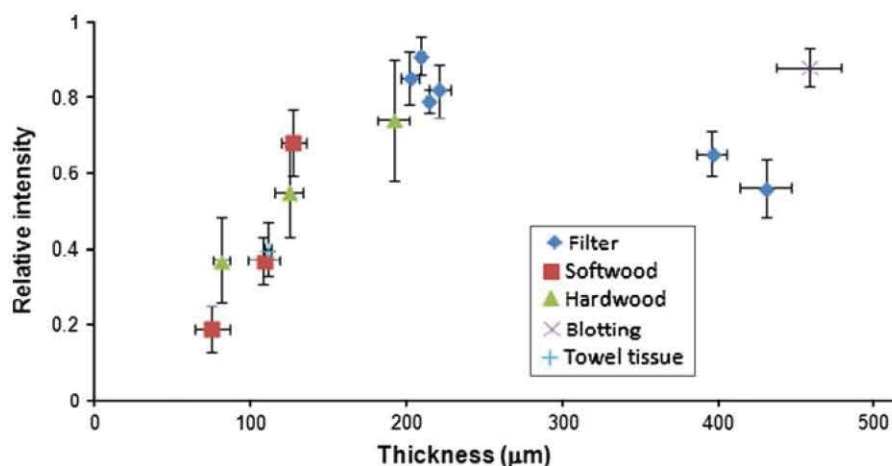


Fig. 2 Relationship between blood relative intensity index and particle retention size for different filter papers. The error bars represent the standard deviation from eight measurements

long fibre papers, the R.I. of short fibres papers increased only slightly for basis weight ranging from 48 to 76 g/m². Filters with density above 500 kg/m³ had high and similar comparable R.I. (0.8–0.9) which characterizes poor blood typing. Filter papers with wet-strength additives had lower R.I. with decreased density.

Paper capillary provides the driving force for elution during blood typing. The capillary rises of water were quantified for the different papers (Fig. 5). The blotting paper displayed the lowest rise (60 mm) and the towel tissue the highest (104 mm). The experimental papers made from short fibres rose to 97 mm for medium basis weight (48 g/m²), and 102 mm for the high basis weight (76 g/m²). Papers made from long fibres exhibited a lower trend: 82 mm rise for 71 g/m² and 98 mm for 25 g/m².

Fig. 3 Relationship between blood relative intensity index and paper thickness. The horizontal error bars represent the standard deviation from 10 measurements. The vertical error bars represent the standard deviation from eight measurements



Discussion

Measuring the intensity of a blood dot eluted by a saline solution is a convenient and reproducible way to measure the effect of paper structure on blood typing; it is not necessary the preferred embodiment of a commercial paper blood typing diagnostic. The length of the eluted blood can be measured, or better, the test results can directly be printed (Li et al. 2012). This section analyses the role of paper structure on blood typing and the interactions paper–blood–antibody in the context of low cost bio-diagnostics. Specificity is insured by the interaction of the RBC antigen with specific monoclonal antigens triggering blood agglutination.

Paper serves two major functions in blood typing analysis. The first is blood transport, the second is blood separation. Blood transport occurs mostly by wicking along the fibre's long axis and through the inter-fibre spaces (Khan et al. 2010). The driving force is capillarity driven by the difference in surface energy between the fluid and the solid. Wicking can be simply described by the liquid flow in a capillary. A velocity (V) for a liquid of viscosity η and surface tension γ flowing in a capillary of radius r and length l can be calculated by the Lucas-Washburn equation (Cecil and Andreoli 1993):

$$V = \frac{\gamma r \cos \theta_E}{8\eta l} \quad (1)$$

where θ_E is the equilibrium contact angle, which is a function of chemistry of the liquid, solid surfaces and pore wall geometry (Borch 2002; Cassie and Baxter 1944). Red blood cell agglutination has two direct effects: a drastic increase in red cell blood viscosity (η)

Fig. 4 Relationship between blood relative intensity index and paper apparent density. The horizontal error bars represent the standard deviation from 10 measurements. The vertical error bars represent the standard deviation from eight measurements. Lines are shown to guide the eye

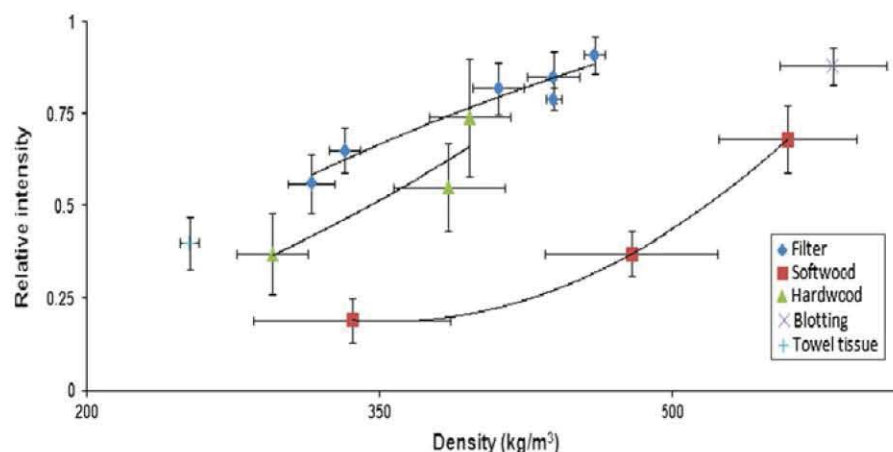
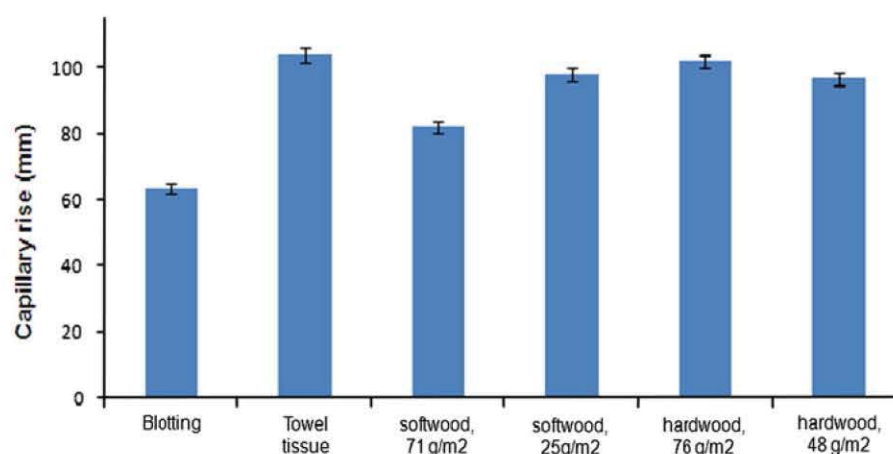


Fig. 5 Capillary rise of different paper for blood typing. The error bars represent the standard deviation from three measurements



and the reduction of paper capillary (r); both effects decrease the wicking velocity of the RBCs according to Eq. 1.

There are a few length scales of interest in paper for blood typing diagnostics. The concept is to agglutinate RBC through specific antibody interaction and to rely on paper for a clear cut segregation between the RBC as aggregates from the stable RBC colloids to communicate typing. It is critical to avoid any overlap between specific interaction and non-specific interaction. Normal RBCs have a diameter ranging from 6 to 8 μm , which is close to the diameter of a eucalyptus (hardwood) fibre (10 μm), and roughly a third of the diameter of a pine radiate (softwood) fibre (30 μm). The hardwood and softwood fibres have lengths of 0.8 and 2 mm, respectively; surface roughness is in the order of the micron (Niskanen et al. 1998). The typing antibodies causing RBC agglutination are

immunoglobulin M (IgM) with diameters of 11 and 40 nm for the individual molecule and the pentamer assembly, respectively (Abe et al. 2008, 2010; Di Risio and Yan 2010).

Blood separation occurs by a combination of filtration, surface roughness elution and chromatography. For filtration, no significance difference in separation between specific and unspecific tests was recorded for filter papers having a retention size lower than 25 μm . The most porous filter paper tested, with the size of 40 μm , had the best relative intensity of 0.5, meaning that unspecific tests had half the density of RBC of specific test, after elution. Proper dimension of pores are required to immobilize the agglutinated RBCs passing through the cellulose web while allowing the non-agglutinated RBCs to wash away with the solution. The larger pore sizes are likely to enable a better discrimination between the agglutinated from

the non-agglutinated RBCs (Figs. 1a, 2). We also noticed that the mean optical density from agglutinated blood spots decreased on filter 113 and 2883 (Fig. 1a); this suggests that the average substrate pore size (30 and 40 μm , respectively) is only slightly larger than the average RBC diameter; otherwise the agglutinated RBCs would not be sufficiently retained by the substrate. The pore size of the substrate can be designed to optimize the sensitivity and specificity of the test.

The thickness of the substrate is another factor influencing the clarity of blood typing. When antibody solutions were spotted onto different papers, the antibody molecules could either wick and spread over the in-plane surface or penetrate deeper into the thickness of the substrates. We hypothesize that a gradient of antibody concentration was developed along the thickness (z direction) of the substrate. The relationship thickness–R.I. generally reveals that thinner substrates provide more sensitive blood type detection (Fig. 3). However, there are exceptions. The thick filters 113 and 2883 showed better performance of blood grouping than the other filters; we believe this was caused by the wet strength polymer, which improved the amount of antibody adsorption on the surface without affecting the antibody activity (Pelton 2009; Wang et al. 2010).

The interaction between a specific antibody with RBCs results in their agglutination. On paper, the antibody can adsorb onto the surface of the fibres and immobilize RBCs through specific antibody-antigen reaction. Once wetted, the antibody, only help by physisorption on paper, can also desorb and diffuse into the blood sample to induce further agglutination of the RBC. This is achieved either by bridging RBCs onto the adsorbed RBC layers on the surface of the cellulose fibre or by the formation of agglutinated RBC particles in the blood sample bulk (Jarujamrus et al. 2012; Khan et al. 2010).

The mechanism of interaction between antibody, RBCs and paper to test blood typing is schematically illustrated in Fig. 6. The ideal substrate should have a porous structure, where the deposited antibodies could easily interact with specific RBCs while nonspecific RBCs can be easily washed away by solution. This ability may be partially estimated with the apparent density of the substrate. In most cases, low density (high porosity) substrates implied less resistance for mass transportation, thus leading to a clear

identification of RBCs (Fig. 4). However, the results were obviously affected by the type of fibres, which all possess different surface properties (Krueger and Hodgson 1995).

Blood transportation mostly occurs through the interfibre spaces driven by the capillary forces. The capillary rises of water in vertical strips of different substrates were compared using the Klemm method, which is similar to the blood type test studied. A high capillary rise indicates a superior driving force of the fluid into paper; its link to substrate potential for blood typing applications is neither direct nor obvious, and deserves further attention. For paper made of long fibres, blotting and towel tissue, a correlation between water rise distance and R.I. of blood typing can be observed by combining Figs. 1 and 5; higher water rise distance corresponded to lower R.I. in blood typing. However, papers made from short fibres provide exceptions which emphasize that interactions between fibres, RBCs and antibody must be considered. The paper structure certainly affects blood typing; however, it is only one element of the diagnostic system.

Conclusion

The effect of paper structure on blood typing visualization was quantified and analyzed in the context of low-cost diagnostics. A series of commercial and experimental papers varying in fibre composition, basis weight, density and porosity was investigated for their ability to separate antibody agglutinated (specific) from non-agglutinated (non-specific) RBCs. Antibodies solutions and blood samples were sequentially absorbed on paper, allowed to interact, eluted with a saline solution, and the intensity of the remaining blood spot was quantified by image analysis. The efficiency and clarity of RBC separation was quantified with the R.I. index defined as the intensity ratio of the non-specific test over the specific system; the lower the R.I., the better is the separation between a positive from a negative test.

The interaction between a specific antibody with blood results in the agglutination of the RBCs; the RBCs remain as stable colloids when interacting with their non-specific antibodies. Agglutinated blood remains on paper upon elution with a saline solution disrupting the electrostatic interactions, while the RBCs of non-agglutinated blood simply wash away.

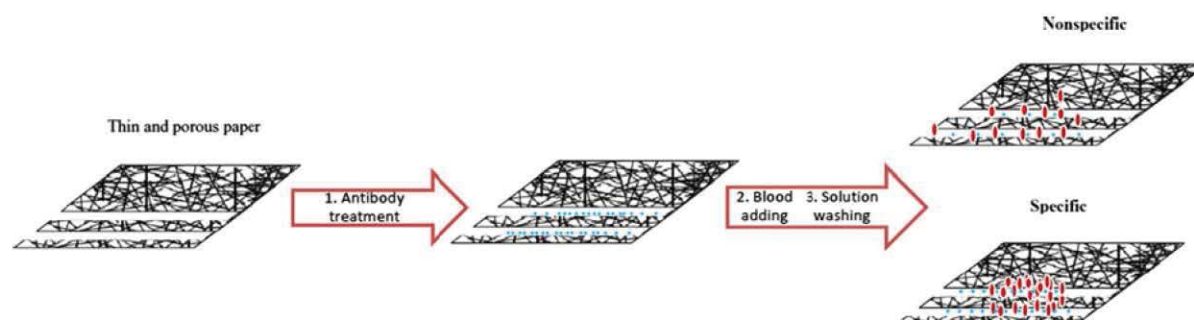


Fig. 6 Schematic mechanistic diagram for the effect of paper structure during the blood typing process. Comparison of specific and unspecific test over the thin/porous papers

This provides the basis for a diagnostic with direct visualization of the cells.

Paper serves three purposes in blood typing diagnostics. The first is to provide, by capillarity, the driving force for the transport of the blood sample and the elution of the saline solution to wash away the non-agglutinated RBCs. The second is to clearly segregate the elution of the agglutinated RBCs (fixed) from that of the non-agglutinated (washed away); this is achieved by a combination of chromatography, surface size exclusion and filtration mechanisms. The third is to directly and visually communicate blood typing results.

Blood typing was best achieved with the low basis weight papers made from softwood fibers. This paper provided a better separation (lower relative intensity) than the commercial towel tissue used in our previous work. Thick and dense papers are improper for blood typing as they tend to retain indiscriminately both stable RBCs (non-specific) and aggregated RBCs (specific). Thin and porous papers provided the best performance. The relative intensity index (the lower the better) increased fairly linearly with paper density, thickness and inversely proportionally with paper pore size. The type of fibres played a minor role. Porous cellulose webs modified with cationic polymers could further optimize blood typing analysis. The paper structure is critical in the design of blood typing assay. However, it is only one element of the diagnostic system that must be engineered along with the control of the multiple interactions of the RBC-antibody-paper system.

Acknowledgments Many thanks to Assoc./Prof W. Shen for discussion, and to ARK linkage grants LP0989823 and LP110200973 for funding.

References

- Abe K, Suzuki K, Citterio D (2008) Inkjet-printed microfluidic multianalyte chemical sensing paper. *Anal Chem* 80(18):6928–6934. doi:10.1021/Ac800604v
- Abe K, Kotera K, Suzuki K, Citterio D (2010) Inkjet-printed paperfluidic immuno-chemical sensing device. *Anal Bioanal Chem* 398(2):885–893
- Ahrens N, Pruss A, Kiesewetter H, Salama A (2005) Failure of bedside ABO testing is still the most common cause of incorrect blood transfusion in the Barcode era. *Transfus Apher Sci* 33(1):25–29. doi:10.1016/j.transci.2005.04.006
- Al-Tamimi M, Shen W, Zeineddine R, Tran H, Garnier G (2012) Validation of paper-based assay for rapid blood typing. *Anal Chem* 84(3):1661–1668. doi:10.1021/Ac202948t
- Anstee DJ (2009) Red cell genotyping and the future of pretransfusion testing. *Blood* 114(2):248–256. doi:10.1182/blood-2008-11-146860
- Beck ML, Plapp FV, Sinor LT, Rachel JM (1986) Solid-phase techniques in blood-transfusion serology. *Crit Rev Cl Lab Sci* 22(4):317–342
- Bienek DR, Charlton DG (2011) Accuracy of user-friendly blood typing kits tested under simulated military field conditions. *Mil Med* 176(4):454–460
- Blakeley D, Tolliday B, Colaco C, Roser B (1990) Dry instant blood typing plate for bedside use. *Lancet* 336(8719): 854–855
- Borch J (2002) Handbook of physical testing of paper, 2nd edn. Marcel Dekker, New York
- Cassie ABD, Baxter S (1944) Wettability of porous surfaces. *T Faraday Soc* 40:0546–0550
- Cecil RL, Andreoli TE (1993) Cecil essentials of medicine, 3rd edn. Saunders, Philadelphia
- Daniels G, Bromilow I (2010) Essential guide to blood groups, 2nd edn. Wiley-Blackwell, Chichester
- Daniels G, Reid ME (2010) Blood groups: the past 50 years. *Transfusion* 50(2):281–289. doi:10.1111/j.1537-2995.2009.02456.x
- Daniels G, Castilho L, Flegel WA, Fletcher A, Garratty G, Levene C, Lomas-Francis C, Moulds JM, Moulds JJ, Olsson ML, Overbeeke M, Poole J, Reid ME, Rouger P, van der Schoot E, Scott M, Sistonen P, Smart E, Storry JR, Tani Y, Yu LC, Wendel S, Westhoff C, Yahalom V, Zelinski T (2009) International society of blood transfusion

- committee on terminology for red blood cell surface antigens: Macao report. *Vox Sang* 96(2):153–156. doi:10.1111/j.1423-0410.2008.01133.x
- Di Risio S, Yan N (2010) Bioactive paper through inkjet printing. *J Adhes Sci Technol* 24(3):661–684. doi:10.1163/016942409x12561252292387
- Dujardin PP, Salmi LR, Ingrand P (2000) Errors in interpreting the pretransfusion bedside compatibility test—an experimental study. *Vox Sang* 78(1):37–43
- Eldon K (1956) Experience with ABO and Rh blood-grouping cards (Eldon Cards). *Brit Med J* 2(Nov 24):1218–1220
- Giebel F, Picker SM, Gathof BS (2008) Evaluation of four bedside test systems for card performance, handling and safety. *Transfus Med Hemoth* 35(1):33–36. doi:10.1159/000111385
- Harmening D (1999) Modern blood banking and transfusion practices, 4th edn. F. A. Davis, Philadelphia
- Ingrand P, Surer-Pierres N, Houssay D, Salmi LR (1998) Reliability of the pretransfusion bedside compatibility test: association with transfusion practice and training. *Transfusion* 38(11–12):1030–1036
- Jarujamrus P, Tian J, Li X, Siripinyanond A, Shiowatana J, Shen W (2012) Mechanisms of red blood cells agglutination in antibody-treated paper. *Analyst* 137(9):2205–2210
- Khan MS, Thouas G, Shen W, Whyte G, Garnier G (2010) Paper diagnostic for instantaneous blood typing. *Anal Chem* 82(10):4158–4164. doi:10.1021/Ac100341n
- Klein HG, Spahn DR, Carson JL (2007) Transfusion medicine 1—red blood cell transfusion in clinical practice. *Lancet* 370(9585):415–426
- Knight RC, deSilva M (1996) New technologies for red-cell serology. *Blood Rev* 10(2):101–110
- Krueger JJ, Hodgson KT (1995) The relationship between single-fibre contact-angle and sizing performance. *Tappi J* 78(2):154–161
- Lapierre Y, Rigal D, Adam J, Josef D, Meyer F, Greber S, Drot C (1990) The gel test—a new way to detect red-cell antigen-antibody reactions. *Transfusion* 30(2):109–113
- Li M, Tian J, Al-Tamimi M, Shen W (2012) Paper-based blood typing device that reports patient's blood type “in Writing”. *Angew Chem Inter Edn*. doi:10.1002/anie.201201822
- Malomgre W, Neumeister B (2009) Recent and future trends in blood group typing. *Anal Bioanal Chem* 393(5):1443–1451. doi:10.1007/s00216-008-2411-3
- Migeot V, Ingrand I, Salmi LR, Ingrand P (2002) Reliability of bedside ABO testing before transfusion. *Transfusion* 42(10):1348–1355
- Niskanen K, Suomen Paperi-insinöörien Yhdistys., Technical Association of the Pulp and Paper Industry. (1998) Paper physics. Papermaking science and technology, vol book 16. Published in cooperation with the Finnish Paper Engineers' Association and TAPPI, Helsinki, Atlanta
- Pelton R (2009) Bioactive paper provides a low-cost platform for diagnostics. *TrAC, Trends Anal Chem* 28(8):925–942. doi:10.1016/j.trac.2009.05.005
- Petrik J (2001) Microarray technology: the future of blood testing? *Vox Sang* 80(1):1–11
- Plapp FV, Rachel JM, Sinor LT (1986) Dipsticks for determining ABO blood-groups. *Lancet* 1(8496):1465–1466
- Roback JD, Barclay S, Hillyer CD (2003) An automatable format for accurate immunohematology testing by flow cytometry. *Transfusion* 43(7):918–927
- Wang J, Pelton R, Veldhuis LJ, MacKenzie CR, Hall JC, Filipe CDM (2010) Wet-strength resins and surface properties affect paper-based antibody assays. *Appita J* 63(1):32–36



Adsorption of cationic polyacrylamide at the cellulose–liquid interface: A neutron reflectometry study



Jielong Su^a, Christopher J. Garvey^d, Stephen Holt^d, Rico F. Tabor^c, Bjorn Winther-Jensen^b, Warren Batchelor^a, Gil Garnier^{a,*}

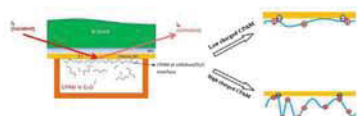
^a BioPRIA-Bioresource Processing Research Institute of Australia, Department of Chemical Engineering, Monash University, Australia

^b Department of Material Engineering, Monash University, Australia

^c School of Chemistry, Monash University, Australia

^d Australian Nuclear Science and Technology Organisation (ANSTO), Australia

GRAPHICAL ABSTRACT



ARTICLE INFO

Article history:

Received 3 November 2014

Accepted 3 February 2015

Available online 10 February 2015

Keywords:

Cellulose

CPAM

Polymer layer

Solid–liquid interface

Reflectometry

Polyelectrolyte

Adsorption

ABSTRACT

The layer thickness and density of high molecular weight cationic polyacrylamide (CPAM) adsorbed at the cellulose–water interface was quantified by neutron reflectometry. The thickness of a full monolayer of CPAM of constant molecular weight (13 MD) but different charge densities, adsorbed with or without NaCl (10^{-3} M), was studied. Thin cellulose films (40 ± 7 Å) of roughness <10 Å were produced by spin coating a cellulose acetate–acetone solution and regenerating by alkaline hydrolysis. Film smoothness was greatly improved by controlling the concentration of cellulose acetate (0.13 wt%) and the hydrolysis time in sodium methoxide. The adsorption thickness of CPAM (40% charge 13 MD) at the solid–D₂O interface was 43 ± 4 Å on cellulose and 13 ± 2 Å on silicon, an order of magnitude smaller than the CPAM radius of gyration. At constant molecular weight, the thickness of the CPAM layer adsorbed on cellulose increases with polymer charge density (10 ± 1 Å at 5%). Addition of 10^{-3} M NaCl decreased the thickness of CPAM layer already adsorbed on cellulose. However, the adsorption layer on cellulose of a CPAM solution equilibrated in 10^{-3} M NaCl is much thicker (89 ± 11 Å for 40% CPAM). For high molecular weight CPAMs adsorbed from solution under constant conditions, the adsorption layer can be varied by 1 order of magnitude via control of the variables affecting electrostatic intra- and inter-polymer chain interactions.

Crown Copyright © 2015 Published by Elsevier Inc. All rights reserved.

1. Introduction

Polyelectrolytes are widely used in industrial and research settings to control the stability of colloids and the interaction properties of surfaces. In papermaking, polyelectrolytes are commonly used as retention aids for process colloids (filler and fines) and as

drainage additives. In wastewater treatment, polyelectrolytes coagulate dissolved solids, suspended matter and control the flocculation of sludge; in mining and oil industries, polyelectrolytes improve recovery through selective adsorption. Recent research applications of polyelectrolytes include the retention of enzymes, antibodies and nanoparticles on surfaces for paper bionanotechnology [1,2], the development of functional materials, and control of biomolecule activity [3,4].

* Corresponding author.

Cationic polyacrylamides copolymers (CPAMs) are among the most commonly used polyelectrolytes and are important for industry, because of their efficiency, low cost and availability in a wide range of polymer compositions and structures. CPAM is commercially available with molecular weight and charge densities up to 15 MD and 100%, respectively. The linear charge density of CPAM is defined as the percentage of monomers bearing a formal charge, typically a quaternary amine. However, in spite of their economic and technological importance, the adsorption behavior of CPAM and the effect of the adsorbed layer morphology on the dynamic stability of colloids are still poorly quantified and understood [5–7], where separate trials are usually needed for each application.

Typically, a polyelectrolyte is adsorbed from solution onto a surface and remains at the liquid–solid interface. The variables affecting the morphology of the adsorbed layer are dictated by the polymer (composition, charge, molecular weight), its affinity for the solvent and surface (Flory–Huggins factor χ), the concentration at which it is adsorbed, solvent properties (temperature, pH, salt concentration and type), surface coverage and kinetics. The theory predicting the basic behavior of polyelectrolytes in solutions and at interfaces is a topic of active research, and can be expressed mathematically as reviewed by Dobrynin and Rubinstein [8] and Fleer et al. [5]; however, the practical behavior is not well characterized. For polyelectrolytes adsorbed at the interface, Dobrynin and Rubinstein [8] identified 2 regimes. At lower surface charge densities, polyelectrolytes adsorb as two-dimensional layers. For this regime, the balance of the electrostatic attraction between the polymer and charged surface and the electrostatic repulsion between the adsorbed chains control the adsorbed morphology. At high surface charge densities, polyelectrolytes adsorb as three dimensional chains with electrostatic attractions governing the phenomenon [8].

Experimental information on the structure and thickness of adsorbed polyelectrolyte layers remains scarce [5]. The structural features of polyelectrolytes adsorbed at the solid–liquid interface have been quantified by ellipsometry, neutron reflectometry, atomic force microscopy and the surface forces apparatus. Three key issues remain poorly understood: (1) the morphology of polymers on surfaces, (2) the link between the morphology of the polymer in solution and at the solid–liquid interface, especially under the kinetically controlled conditions used in industry, and (3) the effect of polymer morphology at the solid–liquid interface and colloid stability/surface functionality. This study focuses on the first issue with a special emphasis on CPAM adsorbed onto cellulosic surfaces. Cellulose is an important surface for paper diagnostics in which polyelectrolytes can be used to retain biomolecules (antibodies, enzymes, cell) and nanoparticles used to amplify signal. The CPAM–cellulose interaction also plays an important role in industrial processes such as papermaking, painting and coating.

Lindstrom and Soremark measured the adsorption and surface coverage of CPAM on cellulose fibers under the high shear conditions relevant to papermaking [9]. The variables investigated were CPAM charge density, molecular weight and concentration as well as the ionic strength and temperature of the solution. The quantity of polymer adsorbed on fibers was calculated from the CPAM concentration measured in the supernatant by refractive index. An increase in CPAM molecular weight and charge density was found to decrease the amount of CPAM adsorbed on cellulose fibers [9]. The charge stoichiometry was found to be a governing factor [10]. Wagberg et al. also measured the kinetics of polyelectrolyte adsorption on cellulosic fibers, finding a strong correlation with key polymer properties (MW, charge, concentration) [11].

The hydrodynamic thickness (δ) of cationic polyacrylamides on silica is reported to increase as an increasing amount of polymer is adsorbed (Γ) until a plateau is reached. Small cations

compete with polymer for surface adsorption and decrease both δ and Γ [5,12], which represents the typical behavior of electro-sorption of weakly charged polymer chains. A different behavior was reported for hydrolysed polyacrylamides on cationic polystyrene latex with the amount of polymer adsorbed and its layer thickness both increasing with the ionic strength of the solution [13]. This was apparently due to non-electrostatic affinity of the polymer for the surface [5,13], in contrast to the observation that electrolytes strongly affect electrostatically-driven CPAM adsorption [6,7,14–16]. Shubin and Linse reported yet a different behavior for the adsorption of CPAM on silica in which Γ and δ both decreased as a function of the electrolyte concentration. Moreover, Γ was a function of the type of cation, while δ was mostly independent of this [16]. This was explained by the change in the ratio of adsorbed polymer trains-ends and loops. By competing for the surface, the cations dislodged or prevented trains of polymer from effectively adsorbing on the surface, resulting in a lower adsorbed amount but an increased layer thickness. Solberg and Wagberg reported a similar behavior for the adsorption of CPAM on silica as a function of NaCl concentration using ellipsometry [17].

These previous studies highlight the complex and poorly understood effect of surface chemistry, polymer charge, molecular weight and concentration as well as salt concentration on the morphology of adsorbed polymer. Little is known about the effect of the surface crystallinity, swelling and porosity on the adsorption morphology of polyelectrolyte. Cellulose is the ideal surface to investigate these important variables.

It is the objective of this study to quantify the layer thickness of high molecular weight cationic polyacrylamide (CPAM) adsorbed at the cellulose–water interface using a well-defined system. The thickness of CPAM of different charge densities, but constant molecular weight (13MD) adsorbed with or without NaCl (10^{-3} M), was measured by neutron reflectometry on smooth cellulose films under conditions of full surface coverage. Smooth cellulose films were prepared by spin coating either a nanocellulose crystal suspension or a cellulose acetate solution subsequently regenerated into cellulose by alkaline hydrolysis. The cellulose films were fully characterized and their smoothness and chemical homogeneity were optimized for neutron reflectometry characterization of their interfaces. In this study, we aim at quantifying how the interaction between cellulose and CPAM can affect the adsorbed polymer morphology, with a view to better understanding the surface interactions involved.

2. Experimental section

2.1. Materials

Cellulose acetate ($M_n \sim 29,000$, acetyl groups substitution $\sim 40\%$), sodium methoxide (purum, $\geq 97.0\%$), methanol (anhydrous, 99.8%) and sodium chloride were purchased from Sigma–Aldrich. Cellulose nanocrystals were graciously provided by U.S. Department of Agriculture in dry powder form. The cationic polyacrylamides (CPAMs) were kindly supplied by AQUA + TECH (Switzerland) and used as received. The specific polymer formulations were copolymers of uncharged acrylamide with cationic dimethylaminoethylacrylate methyl chloride (Table 1 and Fig. 1a). The charge of CPAM was determined by polyelectrolyte titration from sodium poly(ethylenesulfonate) (Pes-Na, 0.001 N, BTG Australia). Polished silicon blocks (50.8 mm diameter, 12 mm and 0.5 mm height, n-type Si:P, [100], El-Cat, Inc. US.) were cleaned for 20 min by UV ozonolysis (UVO cleaner®, model 144AX), and used as substrates for spin coating.

Table 1

The estimated properties of copolymer CPAM consisting of uncharged acrylamide (AM) and cationic dimethylaminoethylacrylate methyl chloride (DMA) monomers, with different charge density but constant molecular weight of 13 MDa (Supporting Information). Φ and ρ present the volume fraction and neutron scattering length density, respectively.

CPAM	Charge density (wt%)	Molar ratio (AM:DMA)	Φ_{AM} in CPAM (%)	ρ_{CPAM} ($\times 10^{-6} \text{ \AA}^{-3}$)	Radius of gyration (nm)	Chain length (μm)
E1	50	2.7	55.0	1.32	18.1	31.3
F1	40	4.1	64.7	1.42	18.9	34.2
I1	5	51.8	95.9	1.76	21.5	44.4

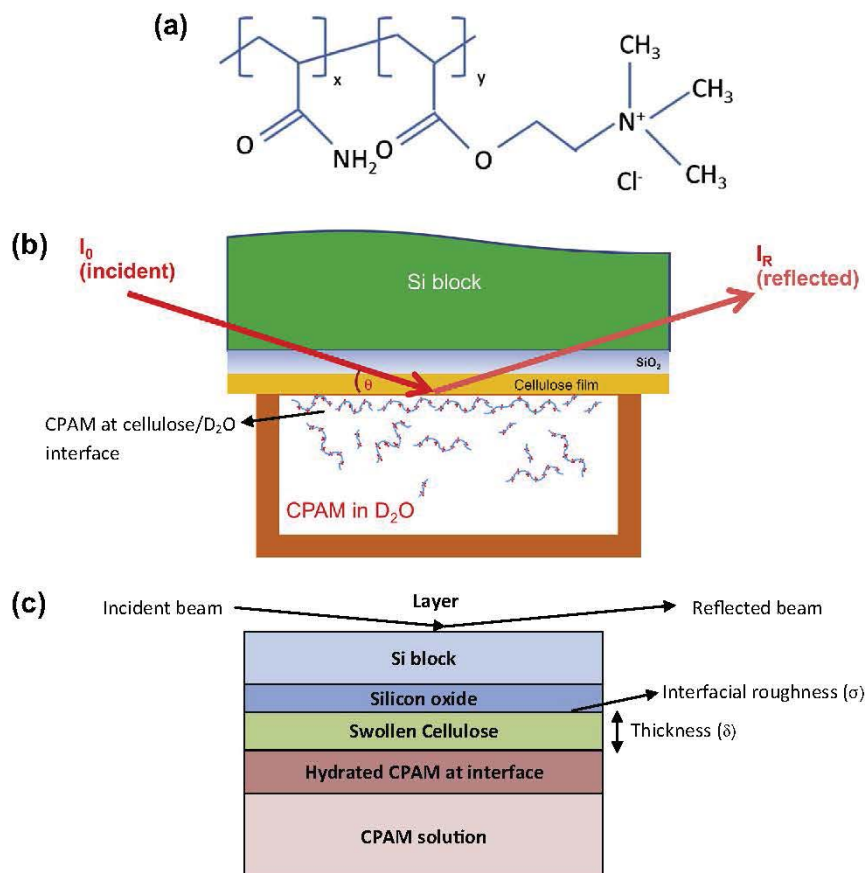


Fig. 1. (a) Molecular structure of CPAM. (b) Configuration of neutron reflectivity measurement for CPAM absorption at the solid/liquid interface. (c) Neutron Reflection from a stratified medium.

2.2. Methods

2.2.1. Film preparation

Cellulose acetate (CA) was dissolved in acetone at different concentrations. A 4 mL aliquot of CA solution was placed on the cleaned silicon block and then spin coated (Laurell Technologies Co., PA, model WS400B-6NPP-LITE) at 4000 rpm for 30 s. After evaporation of acetone, the cellulose acetate film was hydrolysed to cellulose by soaking it in 0.5% sodium methoxide. The hydrolysis of acetate into hydroxyl was followed using Raman spectroscopy. The CH₃ band around 1375 cm⁻¹, CH₂ band around 1430 cm⁻¹, CH band from 2900 to 3000 cm⁻¹ and C=O band from 1730 to 1760 cm⁻¹ were monitored [18]. The regenerated cellulose film was washed with deionised water, methanol, and then air dried.

Raman spectra were recorded with a Jobin Yvon T64000 Raman microscope utilizing a 488 nm incident laser with 0.07 mW power at the laser head and a 5% neutral density filter placed between the

laser and the instrument. A contact angle measurement system (OCA-230, DataPhysics, Germany) was used to measure water contact angles. To quantify the water contact angle, a water drop of 4 μL was placed on the sample and the "Ellipse Fitting" method was used to calculate the contact angle.

2.2.2. Crystallinity by X-ray scattering

Grazing incidence wide angle X-ray scattering (GIWAXS) measurements were performed on the SAXS/WAXS beam line [19] at the Australian Synchrotron on regenerated cellulose samples on a quartz microscope slide as a substrate. GIWAXS patterns were accumulated on a Dectris Pilatus 1 M detector (DECTRIS Ltd, Switzerland) using 11 keV X-rays and sample to detector distance of 315 mm in grazing incidence geometry. The angle of incidence for GIWAXS measurements were 0.1°, 0.3° and 0.5°. Each GIWAXS image consisted of a composite of 3 images combined to cover the gaps between the modules of Pilatus detector. The 2-dimensional

images were processed into the intensity *versus* scattering vector q using the program Fit2D [20] accounting for the scattering geometry described above, after subtraction of a background (the GIWAXS scattering from a bare quartz slide). A cut, $\pm 5^\circ$, was taken in the specular direction to assess the order of the cellulose chains in the thin film.

2.2.3. AFM

Atomic force microscopy images were obtained in AC mode (intermittent contact) using a JPK Nanowizard 3 AFM. The instrument is equipped with capacitive sensors to ensure accurate reporting of height, z , and x – y lateral distances. Cantilevers used were Bruker NCHV model ‘tapping’ mode levers, with nominal resonant frequencies of 340 kHz and spring constants of 20–80 N/m respectively. Imaging was performed with a set-point force of <1 nN. In post-processing, images were ‘flattened’ only by the subtraction of a linear equation from each scan line in the JPK image analysis software; no further manipulations were performed. Height images convert the lateral (z) scale to a colour for ease of presentation. Phase images do the same for the phase information obtained during imaging, *i.e.* the phase difference between the fixed end of the cantilever (driven by the AC piezo) and the free end with the tip where deflection is measured. This phase difference provides information on the way the energy is dissipated by the sample, and can indicate materials with different surface mechanical properties, such as crystalline *versus* amorphous regions.

2.2.4. X-ray and neutron reflectometry

X-ray Reflectometry Measurements (XRR) and Neutron Reflectometry (NR) were performed at the Australian Nuclear Science and Technology Organization (ANSTO), Lucas Heights, Australia. XRR and NR measurements were made as a function of incident angle (θ), measuring the specularly reflected beam as a function of the momentum change perpendicular to the surface ($q_z = 4\pi \sin \theta / \lambda$, where λ is wavelength of incident beam). The XRR measurements were performed in air on a Panalytical XPert Pro diffractometer operating with Cu K α 1 ($\lambda = 1.54056$ Å) radiation using X-rays from a (45 kV) tube source. The q -range corresponds to 0.007 – 0.718 Å $^{-1}$ and the step size in θ used was 0.01° .

The Platypus time-of-flight neutron reflectometer (ANSTO, Lucas Heights) [21], was used to probe interfacial thickness and density of the CPAM layer in the direction normal to the substrate surface. The reflectometer is on the cold guide CG3 at the OPAL 20 MW research reactor.

Stock CPAM solutions were prepared by first dissolving CPAM at 1 g/L in D $_2$ O for 24 h under strong mixing; this solution was then diluted to 0.1 mg/mL in D $_2$ O, with and without NaCl addition, and stirred for at least 12 h to ensure proper dissolution of the polymer. For the Neutron reflectometry (NR) measurement, a silicon block (50.8 mm diameter, 12 mm height) coated with regenerated cellulose was fitted in a solid–liquid cell (Fig. 1b). 5 mL of CPAM/D $_2$ O solution was slowly flowed through the cell ($d = 40.5$ mm, $z = 0.5$ mm, $V = 0.64$ mL) which was then closed for measurements. The neutron beam impinged onto the film/water interface by penetrating through the silicon block. Neutron reflectometry (NR) data were collected for a series of conditions where the film was first exposed to pure D $_2$ O, followed by CPAM in D $_2$ O. Cellulose films were swollen in D $_2$ O. The measurements of CPAM adsorption were performed at 20 °C after at least half an hour further equilibration. Using two angles of incidence, 0.9° and 3.5° , a q -range of ~ 0.010 – 0.265 Å $^{-1}$ was achieved in this work. The MOTOFIT macro for Igor Pro 6.32A (Wavemetrics, Inc., Lake Oswego, USA) was used to model the XRR and NR data [22] in terms of a minimum of layers of defined thickness, scattering

length density (chemical and isotopic composition and density) and roughness between the layers.

3. Results

Smooth cellulose films were spin coated on silicon wafer and quartz surfaces and characterized by X-ray reflectometry, AFM, contact angle measurement, and Raman spectroscopy. CPAM was adsorbed from solution onto the cellulose and silicon surfaces, and the thickness of the polymer layer at the solid–liquid layer was measured by neutron reflectometry. The effect of the CPAM charge density and solution ionic strength on the thickness of the CPAM adsorption layer was investigated. The influence of the control variables within the spin coating and cellulose regeneration processes on the cellulose film properties was first studied. Cellulose films were then prepared under the conditions providing optimal smoothness, and these films used as substrates for the CPAM adsorption study.

3.1. Cellulose film preparation and properties

Thin and smooth cellulose films of roughness (variability) lower than the length scale of the adsorbed CPAM layer thickness to be measured (nm range) are required in order to obtain meaningful reflectometry data. A cellulose film roughness lower than 10 Å was targeted. Two types of cellulose films were made by spin coating: cellulose nanocrystals and regenerated cellulose films. Cellulose nanocrystals films form a mostly crystalline surface that does not swell in water; films of regenerated cellulose are expected to be mostly amorphous and show significant swelling in water.

The dry cellulose nanocrystal (CNC) film spin coated on silicon wafers displayed characteristic non-uniform interference colours (Fig. 2). The small dark blue spots resulted from large CNC aggregates. The colour surrounding the spots faded out along the radial direction, which represents rough surface coverage. The colour blue of the CNC film is caused by its thickness and also by colour interference reflected by the heterogeneously distributed CNC [23]. The radial arrangement of nanocrystals on the wafer (Fig. 2) is similar to that reported on glass and mica [24]. A 57 ± 19 Å roughness was measured by X-ray reflectometry (Table 2).

The preparation of regenerated cellulose films was more reproducible than the CNC film. Spin coating a 2.5 wt% cellulose acetate in acetone solution onto silicon wafers produced regenerated cellulose films 471 ± 96 Å thick, which is greater than the 133 ± 57 Å of CNC films made from a 6.5 wt% aqueous dispersion. We assumed the presence of a surface oxide layer on the silicon block; the

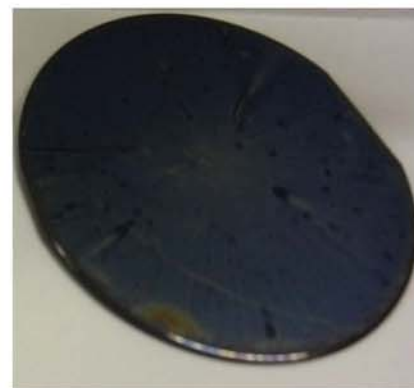


Fig. 2. Appearance of cellulose films made from cellulose nanocrystals aqueous dispersion (6.5 wt%) on silicon wafer (diameter = 50.8 mm).

Table 2

Properties of cellulose films spin-coating from different raw materials. The thickness and roughness were measured by X-ray reflectometry. The average value and 95% confidence interval were from five samples.

Raw material	Concentration (wt%)	Thickness (Å)	Roughness (Å)	Appearance	Reproducibility
Cellulose acetate solution (acetone)	2.5	471 ± 96	28 ± 11	Dark blue	Good
	0.4	127 ± 26	19 ± 3	Transparent	
	0.13	40 ± 7	7 ± 1	Transparent	
Cellulose nanocrystals aqueous dispersion	6.5	133 ± 57	57 ± 19	Blue	Poor

roughness and thickness of the silicon oxide layer were 0.2 Å and 4 Å, respectively. However, these regenerated cellulose films were very smooth with a roughness of 28 ± 11 Å, significantly smoother than the CNC films (57 ± 19 Å). Decreasing the cellulose acetate concentration produced thinner and smoother cellulose films (Table 3 and Fig. 3). The thinnest (40 ± 7 Å) and smoothest (roughness of 7 ± 1 Å) cellulose film was achieved at the lowest cellulose acetate concentration of 0.13 wt%, which was selected to prepare all the regenerated films for the neutron reflectometry study.

Cellulose films can be regenerated from acetate cellulose through hydrolysis with a strong base such as sodium methoxide. Most previous studies have used equilibrium conditions to ensure full hydrolysis into cellulose. However, few studies have analyzed the impact the regeneration process might have on the cellulose film quality. As part of this study we addressed two questions: (1) what is the effect of regeneration on film thickness and smoothness? and (2) what is the minimum hydrolysis time required to ensure full conversion of the acetate groups into hydroxyls? The effect of regeneration time was studied to optimize the quality of the cellulose films.

The cellulose acetate film thickness of 64 ± 5 Å and roughness of 3 ± 1 Å were measured by X-ray reflectometry (Fig. 4A). After 10 mins regeneration by soaking in a sodium methoxide solution, the film thickness was reduced to 40 ± 7 Å, and the roughness considerably increased to 12 Å. As the regeneration period further increased, the film thickness became constant, but the roughness slightly decreased with time (Fig. 4B).

The effect of regeneration time on the surface chemical composition of the cellulosic film was characterized by measuring the equilibrium contact angle formed by water droplets on the surfaces. The contact angle of water on the original cellulose acetate film was $57.1 \pm 3.0^\circ$, characteristic of a moderately wettable surface and in good agreement with literature [25]. After only 1 min of regeneration, the water contact angle of the cellulosic film sharply increased to $76.4 \pm 2.0^\circ$; this was followed by a steady decrease to $31.1 \pm 2.8^\circ$ after 60 mins regeneration (Fig. 5). The contact angle of water on the cellulosic film did not significantly change thereafter. The chemical composition of the cellulosic films was also analyzed by Raman spectroscopy (Fig. 6). After 12 h regeneration, decrease of C=O band around 1750 cm^{-1} , CH₃ band around 1375 cm^{-1} , CH₂ band around 1430 cm^{-1} and band of C–H stretching vibration at $2930\text{--}2960 \text{ cm}^{-1}$ were confirmed by Raman spectroscopy [18]. This indicates completion of the hydrolysis of acetate into hydroxyl [26].

The morphology of the three types of cellulosic films spin coated on quartz (cellulose acetate, regenerated cellulose and cellulose nanocrystals) was analyzed by AFM (Fig. 7) in intermittent contact mode. Root-mean-square (RMS) roughness values across a $1 \mu\text{m}^2$ area were: 3.5 nm (CNC), 1.1 nm (regenerated cellulose acetate), and 1.6 nm (cellulose acetate). The length scale of heterogeneity varies among the 3 surfaces, and in the case of CNC films corresponds to the size of the CNC crystals. Phase information from measurements of the CNC films also revealed preferential orientation of the crystals induced by spin coating.

The major feature of the specular cut of GIWAXS 2d data images (Fig. 8) is a very broad peak centred at 1.44 Å^{-1} . The feature does not change in shape with increasing incident angle but shifts to slightly higher q values with increasing incident angle. This is the correct value for the position of the amorphous halo. The most intense reflections of cellulose II occur at $q = 1.5 \text{ Å}^{-1}$, there is no evidence of cellulose II diffraction peaks [27]. Within the range of depths probed by the evanescent X-ray beam [28], the cellulose film is completely and homogeneously amorphous. GIWAXS measurement of the cellulose nanocrystal film revealed high crystallinity (Fig. S2, Supplementary information).

3.2. Cationic polyacrylamide (CPAM) adsorbed at the D₂O/solid interface

CPAM was adsorbed from solution onto smooth regenerated cellulose films, and the thickness of the polymer layer at the liquid–solid interface was measured by neutron reflectometry. This was achieved under conditions of CPAM surface excess expected to produce a full polymer monolayer, and polymer concentration and molecular weight were kept constant at 0.1 mg/mL and 13 MD, respectively. From the CPAM charge density and molecular weight (13 MDa), the radius of gyration (R_g), end-to-end distance and scattering length density (SLD) of the polymers were calculated (Table 1 & Fig. S1, supporting information).

Specular neutron reflectometry data were fitted using the solvent penetration mode in Motofit, with the Abeles Formalism to fit multiple contrast neutron and X-ray reflectometry data. The measured reflectivity depends on the variation in the scattering length density (SLD) profile, $(\rho(z))$ perpendicular to the interface. The interfacial structure was approximated by a slab model with layers of thickness (δ), roughness (σ), SLD (ρ) and volume fraction (Φ) of solvent.

Motofit minimises the difference between the theoretical and measured reflectivity curves, by changing the parameters (δ , σ , ρ , Φ) that describe each layer (Fig. 1c). As the thickness of the thin film is well-defined and its roughness is low, the NR spectra of thin films display oscillations (Kiessig fringes) which are directly related to the total thickness of the multilayer film [29]. Roughness is implemented in terms of an error function [30] and defined as the standard deviation of the erf function. The scattering length density profile SLD (ρ) of the materials forming the layers is calculated with:

$$\rho = \frac{N_a \rho_{\text{mass}}}{M_R} \times \sum_{i=1}^n b_{\text{ci}} \quad (1)$$

where b_{ci} is the bound coherent scattering length of the i th atom of a molecule with n atoms. N_a is Avogadro's number, ρ_{mass} is the mass density of the material and M_R is its relative molecular mass.

For CPAM copolymers consisting of uncharged acrylamide (AM) and cationic dimethylaminoethylacrylate methyl chloride (DMA) monomers, ρ can be calculated from the individual ρ for AM and DMA, and their volume fractions (Φ) using Eq. (2):

Table 3

CPAM adsorption at the solid/D₂O interface was studied by the specular NR measurement. Thickness (δ), roughness (σ), and volume fraction (Φ) of D₂O in the layer were retrieved by fitting the NR curves. The absorbed amount (Γ) of CPAM was calculated with the absorbed layer δ and Φ . χ^2 indicates the quality of fitting, and the lower value of χ^2 indicate better fits from minimizing the differences between the theoretical and measured reflectivity curves. The reflectivity data were co-refined by at least two data sets where the solid substrate was exposed in D₂O without and with CPAM. $\rho_{D_2O} = 6.35 \times 10^{-6} \text{ Å}^{-2}$. The 95% confidence in parenthesis is from three optimal fitting results.

Solid interface	CPAM charge density (wt%)	χ^2	NaCl (mM)	Properties				
				Layer	δ (Å)	σ (Å)	Φ_{D_2O} (%)	Γ (mg/m ²)
Cellulose	40	2.56	0	Cellulose	97 (10)	3 (1)	69 (5)	
				CPAM	43 (4)	7 (1)	96 (4)	2.3
		2.03	1 ^a	CPAM	20 (3)	2 (1)	95 (4)	1.3
				Cellulose	102 (9)	2 (1)	65 (4)	
	5	3.68	0	CPAM	89 (11)	9 (1)	97 (5)	3.5
				Cellulose	106 (11)	2 (1)	69 (4)	
	50	2.01	0	CPAM	10 (1)	8 (1)	82 (5)	2.4
				Cellulose ^c	68 (7)	4 (1)	97 (4)	
		2.01	0	CPAM ^d	156 (13)	38 (4)	6 (4)	201.8
				CPAM ^e	95 (10)	30 (6)	66 (4)	95.4
Si (SiO ₂)	40	1.01	0	CPAM	13 (2)	1 (0)	32 (8)	12.8
				CPAM	13 (2)	1 (0)	32 (8)	12.8

^a NaCl solution was added after CPAM adsorption.

^b CPAM was prepared in NaCl solution before adsorption.

^c The cellulose film is from 0.1 wt% CA solution.

^d CPAM with 50% charge absorbed at the interface were divided into 2 layers to improve the fitting (decrease the χ^2).

^e The CPAM sublayer stretched out to D₂O.

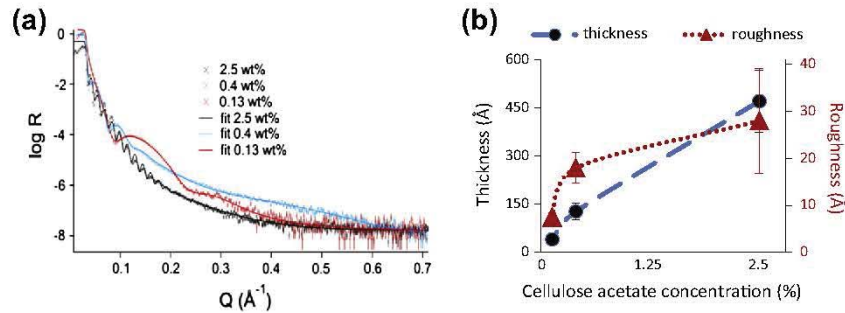


Fig. 3. (a) X-ray reflectometry of the regenerated cellulose films from different cellulose acetate solutions (in acetone). (b) Effect of cellulose acetate concentrations on regenerated films thickness and roughness (Lines shown are to guide the eye).

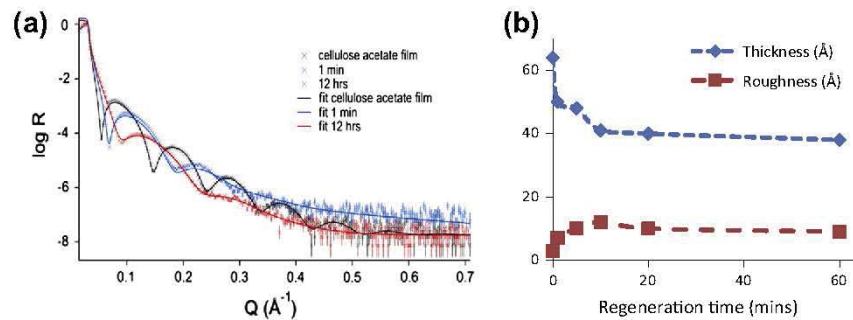


Fig. 4. (a) X-ray reflectometry of cellulose acetate film from cellulose acetate solution (0.13 wt% in acetone) and cellulose films after 1 min and 12 h regeneration. (b) The effect of regeneration time on the thickness and roughness of the film (Lines shown are to guide the eye).

$$\rho_{CPAM} = \rho_{AM} \times \Phi_{AM} + \rho_{DMA}^*(1 - \Phi_{AM}) \quad (2)$$

In this study, ρ_{AM} , ρ_{DMA} and the molecular volumes are calculated by assuming a density of 1.3 g/cm³ [31,32]. SLDs of 1.76, 1.42 and 1.32 (10^{-6} Å^{-2}), were calculated for CPAM with charge densities of 5, 40, and 50 wt%, respectively. These values were used for fitting neutron reflectometry data and calculating the properties of the CPAM layer at the interface.

Optimal fitting of the NR results with the model was achieved by assuming the proton-deuterium exchange [33] in the hydroxyl groups of the cellulose in D₂O [34] which corresponds to a cellulose density of 1.48 g/cm³. As the regenerated cellulose films are completely amorphous, we assumed full exchange would occur. The ρ value of deuterium exchanged cellulose (C₆H₇D₃O₅) is $3.39 \times 10^{-6} \text{ Å}^{-2}$, which resulted in a better fitting with a much lower χ^2 than using the value of $1.67 \times 10^{-6} \text{ Å}^{-2}$ from the

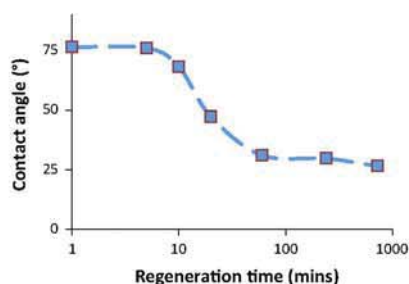


Fig. 5. Contact angle (CA) profile for the cellulose (acetate) films after different regeneration time (CA of cellulose acetate film was measured as $57.1 \pm 3.0^\circ$).

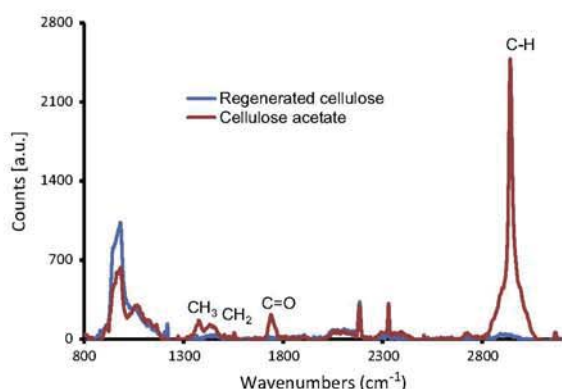


Fig. 6. Raman spectra of cellulose acetate film (spin coating from 2.5% solution) and after 12 h regeneration time. The important peaks are labelled.

protonated cellulose ($C_6H_{10}O_5$), and the value of $3.39 \times 10^{-6} \text{ \AA}^{-2}$, was used to calculate the volume fraction of D_2O .

In addition to the thickness and roughness of the cellulose film, the volume fraction (Φ) of solvent (D_2O) in the layer can be determined from the calculated SLDs of the substances (cellulose or CPAM and D_2O) forming the layer. In Motofit, given ρ for a layer, then the solvent volume fraction is automatically calculated. As the model fitting is completed, all parameters (δ , σ , ρ , Φ) and chi squared (χ^2) are updated. A lower χ^2 indicates a minimisation of the differences between the measured data and the calculated fit.

The layer properties in D_2O studied by NR, with or without NaCl, are summarized in Table 3. The average and 95% confidence interval is from three optimal fitting results. The adsorption thickness of CPAM-40% on silicon ($13 \pm 2 \text{ \AA}$) is thinner and smoother than on regenerated cellulose film ($43 \pm 4 \text{ \AA}$) Fig. 9. The surface layer density (SLD) for the D_2O /CPAM (40% charge)/cellulose/silicon interface is shown in Fig. 9B.

During measurement, swelling of cellulose film was observed which increased film thickness ($\sim 100 \text{ \AA}$); the volume fraction of D_2O in the film is 67%. The volume fraction of D_2O in the high charge adsorbed CPAM layer (40% charge) is 96%, higher than the 82% of the low charge CPAM (5% charge) – fitted by CPAM monolayer model. However, the layer thickness at the interface increased with higher charge density (Table 3). The adsorption thickness of CPAM of charge density of 5% and 40% were $10 \pm 1 \text{ \AA}$ and $43 \pm 4 \text{ \AA}$, respectively. The double-layer model improved the fitting (low χ^2) for the 50% CPAM absorbed, and its calculated thickness was much higher. The effect of CPAM charge density at constant molecular weight on the adsorption layer thickness at the cellulose- D_2O interface is shown in Fig. 10. CPAM layer thick-

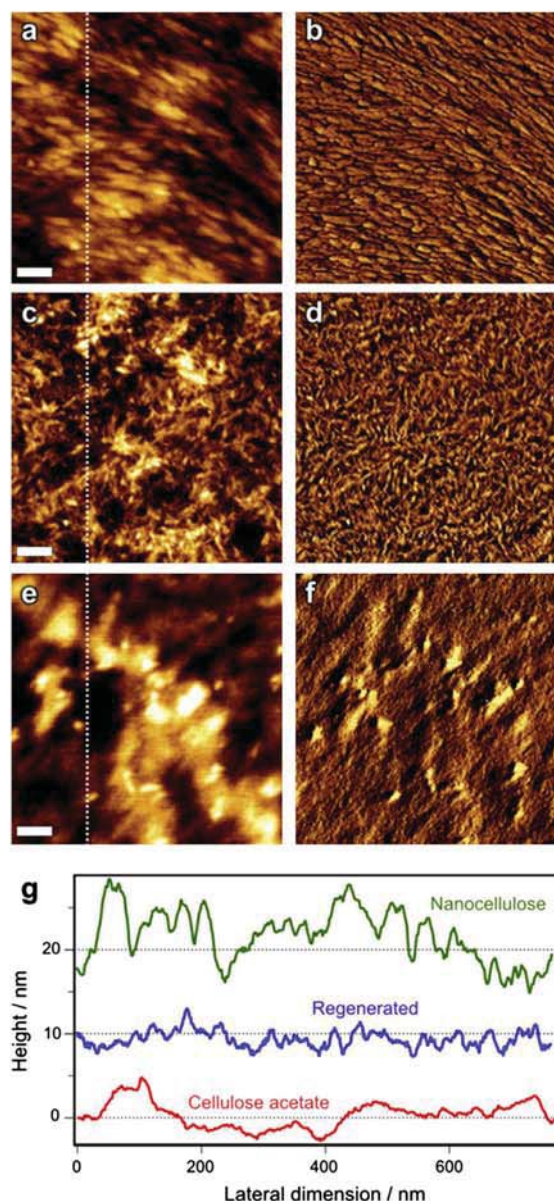


Fig. 7. AFM images and extracted parameters from nanocellulose (a and b), regenerated cellulose acetate (c and d) and pure cellulose acetate (e and f) films. In each case, the left-hand pane (a, c, e) shows height information (wherein the height scale is defined by the line profile in (g) and the right hand pane (b, d, f) shows the phase information. The scale bars represent 100 nm. Line profiles of selected cross-sections are shown in (g), representing the sectional heights defined by the dotted lines in (a, c, e). The two uppermost traces are vertically offset by 10 and 20 nm as indicated by their 'zero' lines, for clarity of presentation.

ness increases with polymer charge density, while roughness remains constant.

The effect of 1 mM NaCl on the CPAM adsorption layer thickness at the cellulose interface was studied in 2 modes. In the first, NaCl was added to D_2O after the CPAM had been adsorbed on cellulose; in the second, NaCl was introduced to the initial CPAM/ D_2O solution adsorbed on cellulose (Fig. 10). Adding salt to a CPAM (40% charge) monolayer adsorbed on cellulose decreased both the polymer layer thickness and its roughness. For CPAM

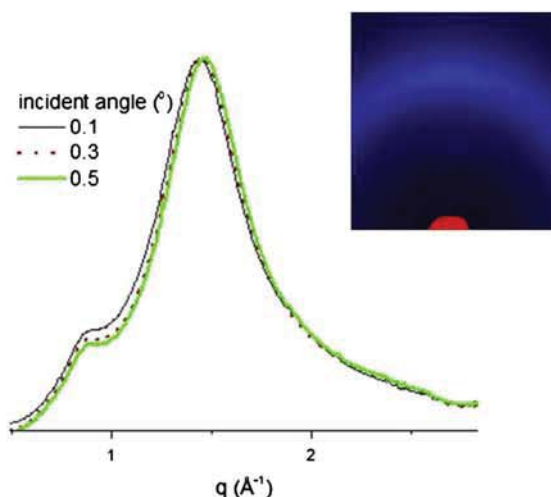


Fig. 8. Peak intensity normalized GIWAXS profiles in the specular direction from a regenerated cellulose film on quartz substrate as a function of incident angle. The inset shows a typical GIWAXS image. The beam stop is masked by red. (For interpretation of the references to colour in this figure legend, the reader is referred to the web version of this article.)

equilibrated in NaCl D₂O, the adsorption layer thickness on cellulose increased from 43 ± 4 Å to 89 ± 11 Å (Table 3).

The amount of CPAM absorbed at the cellulose interface (Γ in g/m²) was approximated from the layer thickness and volume fraction of CPAM, using Eq. (3) [35]:

$$\Gamma = \frac{10^{20} M_R \phi \delta}{N_a V} \quad (3)$$

where M_R is the CPAM molecular weight; ϕ is its volume fraction (CPAM) in the layer of thickness δ (Å); N_a is Avagadro's number and V is the molecular volume of CPAM (Å³). ϕ and δ were fitted from neutron reflection curves. Without NaCl addition, the calculated CPAM specific adsorption capacity on cellulose (Γ) was comparable for both 5% and 40% charged CPAM (Table 3). Realistic values of CPAM adsorption capacity were determined for CPAM of 5% and 40% charge ($\Gamma = 1.3$ – 3.5 mg/m²); however, the Γ values for CPAM 50% were unrealistically high.

4. Discussion

4.1. Smooth cellulose films

Model cellulose films are convenient substrates for quantifying the morphology of adsorbed macromolecules and their

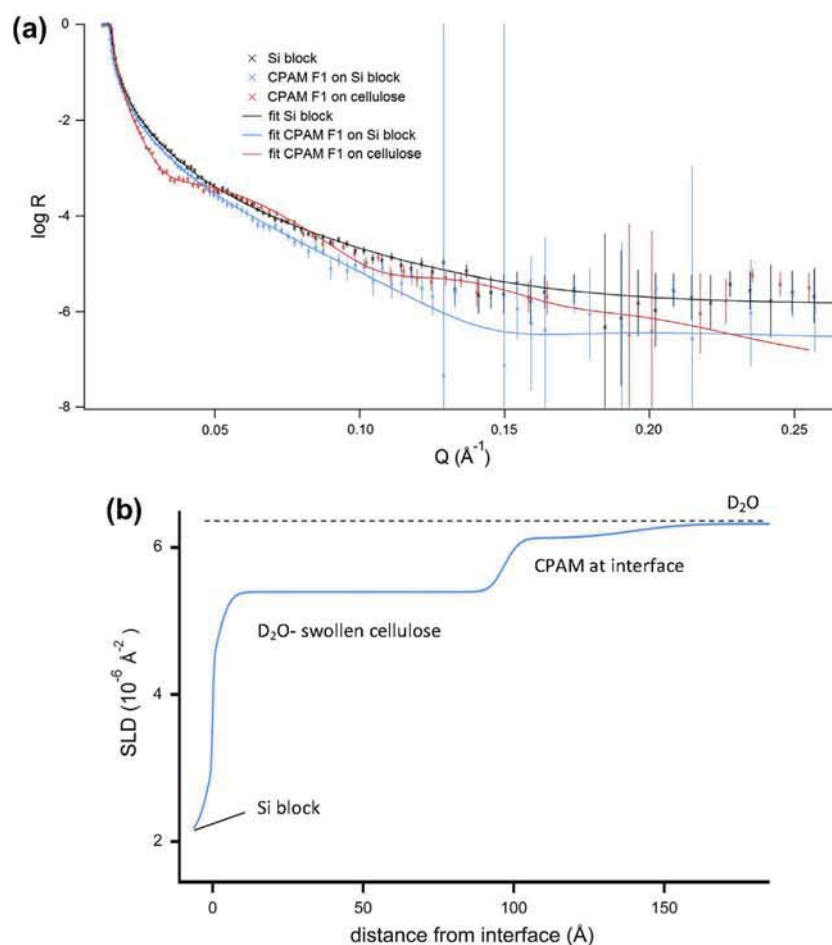


Fig. 9. (a) Neutron reflectivity from silicon surfaces with regenerated cellulose and CPAM absorbed at two interfaces: Silicon with native oxide layer and cellulose film. (b) SLD profile from simultaneous fits to the CPAM F1 on cellulose in part a.

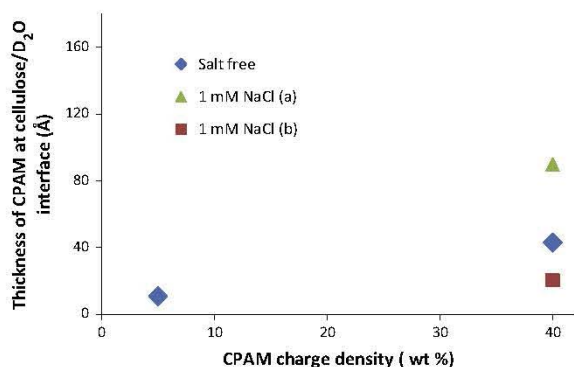


Fig. 10. The thickness of CPAM (Mw = 13 MDa) adsorbed at cellulose/D₂O interface with and without NaCl. The data is presented in Table 3. (a) F1 prepared in NaCl solution before adsorption. (b) NaCl solution was added after F1 adsorption.

interactions with surfaces, using sensitive characterization techniques such as X-ray/neutron reflectometry, ellipsometry, AFM, surface plasmon resonance (SPR), quartz crystal microbalance (QCM), X-ray photoelectron spectroscopy (XPS), wetting and the surface forces apparatus (SFA) [33,36–39]. There are three main physical film attributes often required of a polymer film for advanced surface analysis: thickness, surface smoothness and uniformity, although each analytical technique has its own requirements. For example, reflectometry and SFA both require films with smooth surfaces and having constant thickness; SPR and QCM are restricted by film thickness, while AFM privileges high surface smoothness. This study investigates the adsorption layer thickness and uniformity of cationic polyacrylamides adsorbed on cellulose using neutron reflectometry. Cellulose films suitable to study interfacial phenomena have been explored with different methodologies such as spin coating, solution casting and Langmuir Blodgett [40,41], as reviewed by Kontturi [42]. Cellulose films can either be deposited directly on a surface as cellulose nanocrystals [43] or as a cellulose solution [39], or indirectly via a cellulose derivative solution regenerated to cellulose in a subsequent step [26,40]. The latter approach has produced the smoothest films and was selected in this study.

Spin coating has formed smooth and uniform cellulose films [24,37]. The primary variables controlling the morphology and thickness (δ) of the film during coating include cellulose concentration, solvent and spin coating speed. In our preliminary experiments, the influence of these parameters was examined and the concentration of the cellulose acetate (CA) in solvent (acetone) was identified as the critical variable (Table 2 and Fig. 3). Reducing the concentration of the cellulose in solution resulted in thinner and smoother cellulose films. The independent variables are the extent of molecular mobility during the time frame of film formation (which can be controlled by the spin coating rotation speed and solvent evaporation rate) and the period of macromolecular mobility (as dictated by solution viscosity, polymer concentration and molecular weight). Spin coating produces some of the highest quality cellulose films due to increased molecular mobility and the higher time frame available to achieve a uniform polymer distribution on the surface. A quasi-molecularly smooth film with roughness of 7 ± 1 Å, and thickness of 40 ± 7 Å was achieved at a low cellulose solution concentration of 0.13 wt%; these films are suitable for neutron reflectometry.

The crystalline and amorphous regions of cellulose have different accessibility to solvent [44]. Therefore, films directly spun from a cellulose nanocrystal (CNC) aqueous dispersion were explored. Good CNC films were only prepared at high concentration

(6.5 wt%); however, the surfaces were rough (57 ± 19 Å) likely due to a combination of poor packing and formation of aggregates. The nanocellulose films produced were too rough to serve as a suitable substrate to measure the CPAM adsorption layer thickness by neutron reflectometry. Smoothness might be improved by pre-treating the silicon wafer with a polyelectrolyte to enhance CNC adhesion [43].

The effect of regeneration time on the cellulose film properties was analyzed. The thickness of the CA film decreased rapidly with regeneration time in sodium methoxide to reach a plateau (Fig. 4). The reaction clearly corrodes the surface in a non-uniform fashion as the length scale of the acetyl groups cleaved and replaced by much smaller hydroxyl groups is well below the nm scale measured by reflectometry and AFM. However, the inter- and intra-molecular hydrogen bonding network enables the film to become more compact, therefore forming a thinner and denser structure; heterogeneity in reaction would further contribute to roughness. The regeneration process produced a much rougher surface than the original CA film. This result contrasts with previous reports claiming that hydrolysing trimethylsilyl cellulose into cellulose results in smoother films [37,40]. The rough surface caused initially by the cellulose acetate regeneration process (within 10-mins) corresponds to the regime of poor wettability identified with water contact angle greater than the $57.1 \pm 3.0^\circ$ for the CA film (Fig. 5). We believe the change of roughness affects the wettability initially, as the conversion of acetyl groups into hydroxyl groups occurs at longer time frames (Fig. 6).

4.2. CPAM adsorption at the cellulose/D₂O interface

Quasi-molecular smooth cellulose films regenerated on silicon blocks were used to measure, by neutron reflectometry, the effect of polyelectrolyte charge density and salt concentration on the cationic polyacrylamide (CPAM) layer thickness adsorbed at the solid–liquid interface (Table 3, Figs. 9 and 10).

4.2.1. Cellulose swells in D₂O

Two possibilities may occur when a dry cellulose film is exposed to liquid D₂O. In the first, the film remains unaffected by water and the thickness of the cellulose film in wet and dry states is identical. The second involves swelling of the cellulose film in water, as observed in situ from NR measurements. The swollen cellulose film is characterized by its water/D₂O content and its distribution profile through the film.

During the initial stage of swelling, water diffuses across the cellulose film in plane. This diffusion is controlled by film density and structure (porosity and defects), and a water gradient profile can be fitted from NR curves, which assumes the swollen film to consist of a series of hydrated layers (multilayers). Once water saturation of the cellulose has proceeded, the water distribution becomes fairly uniform throughout the film. As water penetration through an ultrathin film is very fast (seconds–minutes) and the total time of measurement long (6–14 h of measurement per film), this study neglected any kinetic effects and assumes pseudo-equilibrium conditions to be achieved.

Once in contact with D₂O, the three labile protons of the hydroxyl groups of the D-glucose units (C₆H₁₀O₅) of amorphous cellulose rapidly exchange with deuterons from the solvent [33,34]. Hence the ρ value of 3.39×10^{-6} Å⁻² was used for fitting cellulose films in D₂O, which corresponds to C₆H₇D₃O₅ after H–D exchange. As the regenerated cellulose films are completely amorphous, we assumed full exchange to proceed.

With one exception (50% charge CPAM adsorption spun from 0.1 wt% CA solution), all the wet cellulose films were spun from 0.13 wt% CA solution and had a thickness and roughness of ~ 100 Å and 3 Å, respectively (in D₂O); this corresponds to an

increased thickness by a factor of ~ 2.5 comparing to the dry cellulose films ($\delta = 40 \pm 7$ Å, $\sigma = 7 \pm 1$ Å). The volume fraction of D_2O in the cellulose layers (Φ_{D2O}) was calculated to be $67 \pm 2\%$, which lies between the findings of Cheng et al. ($59 \pm 1\%$) and those of Kontturi et al. (86%). Thin hydrated cellulose films form hydrogels. Our measurements also noted the remarkable swelling ability of the cellulose layer while keeping a smooth outer interface.

4.2.2. CPAM adsorbed at the cellulose/ D_2O interface

CPAM was adsorbed under surface excess conditions to produce a full monolayer. CPAM molecular weight (13 MDa) and concentration in solution (0.1 mg/mL) were kept constant. The adsorption of polyelectrolyte is strongly affected by electrostatic interactions and the resulting polymer conformation is driven by the balance of surface-polymer interactions in competition with electrolyte [5,8,14–16]. The adsorption kinetics of CPAM onto cellulose fiber were reported to reach near-equilibrium within 30 mins [45]. In this study, CPAM solution was kept in contact with cellulose in a sample cell at least half an hour prior to the neutron reflectometry measurement to allow full polymer adsorption to proceed, but probably not full equilibrium relaxation to occur.

We assumed a single adsorbed layer at the cellulose/ D_2O interface for fitting unless the fitting quality is poor (chi squared is unacceptably high). Two cases were examined: the first one consisted of a solid CPAM layer with no water at the interface. This model was rejected as the very high chi squared (>10) indicated poor fitting/hypothesis. The second model represented an adsorbed layer consisting of CPAM and D_2O . It was postulated that the mixed layer had a uniform composition [16,46–48]. The effect of CPAM charge density on its adsorption layer thickness on the hydrated cellulose films is shown in Table 3.

We selected CPAM of very high M_R (13 MDa) for this experiment to prevent polymer diffusion within the cellulose/ D_2O layer. The thinness of the cellulose film combined with the high charge of the CPAM and the short duration of neutron reflection measurements (less than 3 h), further contribute to retaining the adsorbed CPAM at the cellulose surface and prevent its miscibility with the cellulose– D_2O layer. However, it is of interest to consider the effect that CPAM diffusion/reptation into the swollen cellulose layer [49] might have. High molecular weight polyelectrolytes have been reported to be restricted to the external surface of the fibers [11]. Diffusion of cationic polyelectrolytes into cellulosic fibers have been studied by Horvath et al. [50]. High charge density polyelectrolytes were observed to diffuse on a time scale of months, whereas the diffusion of low charge density polyelectrolytes was measured on the order of hours. Additionally, a significant change in the diffusion behavior was only observed at high electrolyte concentrations (10^{-1} M $NaHCO_3$). The simulated SLDs of CPAM 40% and 5% charge adsorbed onto and uniformly mixed within the swollen cellulose layer, with and without deswelling (fixed at 25%), are shown in Fig. 11. Best fit between the experiments and model was achieved by assuming segregation of CPAM on the cellulose surface, supporting our hypotheses and methodology. The two important variables affecting fitting are: (1) thickness of the layer and (2) SLD of the layers. This means that any swelling/deswelling and diffusion of the D_2O into the cellulose/CPAM layers are critical.

The CPAM of low charge density (5%) was compared to the high charge density (40%) case. The layer adsorbed at the interface was thinner and had a lower Φ_{D2O} . The value of Φ_{D2O} in the layer might depend on the hygroscopy of CPAM with different charge. However, the layer roughness (σ) and the calculated adsorbed CPAM amount (Γ) are mostly independent of charge density (Table 3). This observation might at first seem to contradict the work of Lindstrom and Soremark on the adsorption of CPAM on bleached sulphite pulp [9]; they found the adsorbed amount of CPAM

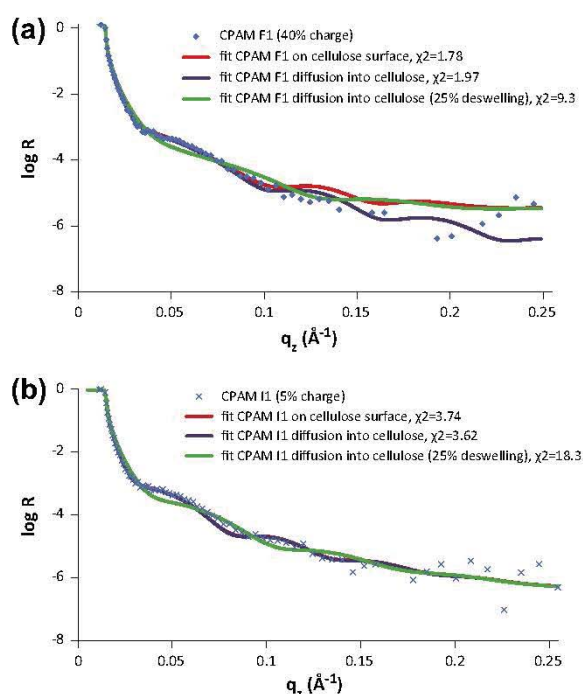


Fig. 11. Model fitting for CPAM of (a) 40% and (b) 5% charge density adsorption at (1) cellulose surface; (2) diffusion into cellulose layer without changing the cellulose swelling behavior; (3) diffusion into cellulose layer and the cellulose layer is deswelling 25%. χ^2 indicates the quality of fitting, and the lower value of χ^2 indicate better fits from minimizing the differences between the theoretical and measured reflectivity curves.

decreased as the polymer charge density increased. However, there is a clear distinction between adsorbed polymer density (mg/m^2) and layer thickness (Å). A thick adsorbed polymer layer can have a low adsorption density if its water content is high; this is illustrated in Fig. 12.

Polymer surface coverage (Γ) can be approximated from the CPAM measured thickness and volume fraction (Table 3); calculating Γ is a good way to assess the results' validity. Realistic values of Γ are found for the adsorption of CPAM of 5% and 40% charge density onto cellulose; however, those of CPAM 50% charge are simply unrealistic ($\Gamma \geq 95$ mg/m^2). The Γ calculated from Eq. (3) is very sensitive to the D_2O content; for CPAM 50% on cellulose, the very low D_2O content calculated completely skewed the results which is compensated by an unrealistically thick CPAM layer.

The CPAM equivalent charge coverage at the interface was further investigated. The calculated charge coverage ($\mu eq/m^2$) increases with CPAM charge density. This suggests that the charge of adsorbed CPAM does not stoichiometrically interact with that of the cellulose surface. The importance of surface chemistry and charge stoichiometry was examined by adsorbing 40% charge CPAM onto the more negatively charged silicon surface (with silicon oxide layer, S3 in Support information) [36,39,43,45,51]; a thinner CPAM layer was formed. Fig. 12 schematically illustrates the effect of surface and CPAM charge density on the morphology and thickness of adsorbed polymer layers.

The configuration of polyelectrolyte adsorbed at the solid surface is often described by the “loops-trains-tails” model [5,16]. The thickness of CPAM adsorbed at the cellulose interface is of the nanometer scale, an order of magnitude lower than its radius of gyration in solution. Wagberg proposed adsorption by charge stoichiometry between the CPAM and the cellulose surface [10].

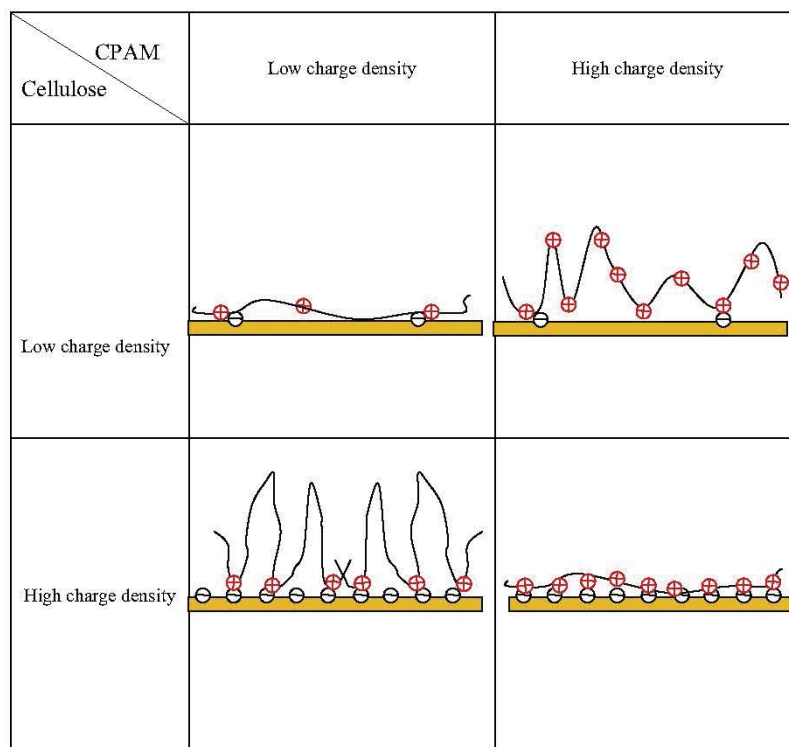


Fig. 12. The proposed conformation of CPAM adsorbed on the cellulose/water interface under different charge density conditions.

Increased electrolyte concentration was reported to decrease the concentration of adsorbed “train” polyelectrolyte concentration [5,16], therefore increasing the relative concentration of loops and tails, which increases polymer thickness (δ); polymer layer density can even decrease should desorption happen, though this is unlikely for high molecular weight polymers. The effect of salt is expected to be more important at low polymer adsorption density, although the effect of adsorption stoichiometry between the CPAM charges and the charges on the cellulose surface is clearly important [52,53].

The role of ionic strength in CPAM adsorption at the cellulose–D₂O interface was investigated in two modes. Electrolyte in the form of 10^{-3} M NaCl was added either to the CPAM solution to be adsorbed, or to the D₂O solution after CPAM adsorption had been completed on cellulose. Salt did not affect Φ_{D2O} in the adsorbed layer in either mode; however, it changed the CPAM thickness. Once the CPAM adsorption was completed, addition of NaCl decreased layer thickness and roughness. This compressed CPAM conformation at the liquid–solid interface induced by electrolyte was previously reported [7]. In contrast, an increase in polymer adsorption thickness was measured by adsorbing a solution of CPAM equilibrated in NaCl. As cellulose charge is not expected to vary significantly from the addition of NaCl, CPAM adsorbed amount must be a function of ionic strength; this was previously reported by Peng et al. [7]. The increase in ionic strength screens the CPAM charge, reducing the electrostatic attraction of the polymer for the cellulose surface and also the CPAM intra-molecular repulsions [16].

5. Conclusion

Thin and smooth cellulose films were prepared by spin coating either a nanocellulose crystal suspension or a cellulose acetate

solution onto silicon surfaces and regenerating into cellulose by alkaline hydrolysis. These cellulose films were characterized by AFM, X-ray reflectometry, Raman spectroscopy and contact angle measurement. High molecular weight polyacrylamides (CPAM) were adsorbed from solution onto the cellulose surfaces under surface excess conditions to ensure full monolayer coverage. The CPAM adsorption thickness and roughness were measured by neutron reflectometry at the cellulose–D₂O interface. The effect of CPAM charge density and added NaCl (10^{-3} M) was quantified.

Thin cellulose films (40 ± 7 Å) of roughness less than 10 Å were produced by spin coating a cellulose acetate–acetone solution and regenerating by alkaline hydrolysis. These films are ideal for reflectometry studies. Film smoothness was greatly improved by controlling the concentration of cellulose acetate (0.13 wt.%) and the hydrolysis time in sodium methoxide. Optimal model fitting demonstrates that high molecular weight CPAM adsorbs and remains at the hydrated cellulose–D₂O interface during the measurement. The charge of adsorbed CPAM does not stoichiometrically interact with that of the cellulose surface. These observations agree well with previous experimental findings [46,50,52].

The adsorption thickness (δ) formed by a 0.1 mg/mL solution of CPAM (40% charge, 13 MD) at the solid–D₂O interface is 43 ± 4 Å on cellulose and 13 ± 2 Å on silicon. The adsorption thickness is an order of magnitude smaller than the CPAM radius of gyration. At constant molecular weight, the thickness of the CPAM layer adsorbed on cellulose increases with polymer charge density (10 ± 1 Å at 5% and 43 ± 4 Å at 40%). Addition of 10^{-3} M NaCl decreased the thickness of CPAM layer already adsorbed on cellulose. However, the adsorption layer on cellulose of a CPAM solution equilibrated in 10^{-3} M NaCl is much thicker (89 ± 11 Å for 40% CPAM). For high molecular weight CPAMs of constant molecular weight adsorbed from solution under constant conditions, the adsorption layer can vary by 1 order of magnitude by controlling

the variables affecting electrostatic forces. This finding confirms that polymer surface coverage is not the only important variable affecting colloid stability by polyelectrolyte as the bridging layer thickness can vary considerably [8,17], and highlights the charge effect on polymer adsorption and conformation at solid surfaces and interfaces.

Acknowledgments

The financial contribution of Australian Research Council (LP0990526) is acknowledged. We thank ANSTO/AINSE for the allocation of beam time (DB3363) and travel grants, and AQUA + TECH for providing the CPAM polymers.

Appendix A. Supplementary material

Supplementary data associated with this article can be found, in the online version, at <http://dx.doi.org/10.1016/j.jcis.2015.02.008>.

References

- [1] Y.H. Ngo, D. Li, G.P. Simon, G. Garnier, *Colloid. Surface A* 420 (2013) 46.
- [2] Y.H. Ngo, D. Li, G.P. Simon, G. Garnier, *J. Colloid. Interf. Sci.* 392 (2013) 237.
- [3] Y. Wang, W. Qi, R. Huang, R. Su, Z. He, *RSC Advances* 4 (2014) 15340.
- [4] J.T. Reye, K. Maxwell, S. Rao, J. Lu, S. Banerjee, *Biotechnol. Lett.* 31 (2009) 1613.
- [5] G.J. Fleer, M.A. Cohen Stuart, J.M.H.M. Scheutjens, T. Cosgrove, B. Vincent, *Polymers at Interfaces*, 1st ed., Chapman & Hall, London, New York, 1998.
- [6] P. Peng, G. Garnier, *Colloids Surfaces A: Physicochem. Eng. Aspects* 408 (2012) 32.
- [7] P. Peng, G. Garnier, *Langmuir* 26 (2010) 16949.
- [8] A.V. Dobrynin, M. Rubinstein, *Progress Polym. Sci.* 30 (2005) 1049.
- [9] T. Lindström, C. Soremark, *J. Colloid. Interf. Sci.* 55 (1976) 305.
- [10] L. Wågberg, L. Winter, L. Ödberg, T. Lindström, *Colloid. Surface* 27 (1987) 163.
- [11] L. Wågberg, R. Häggglund, *Langmuir* 17 (2001) 1096.
- [12] G. Durand-Piana, F. Lafuma, R. Audebert, *J. Colloid. Interf. Sci.* 119 (1987) 474.
- [13] J. Meadows, P.A. Williams, M.J. Garvey, R. Harrop, G.O. Phillips, *J. Colloid. Interf. Sci.* 132 (1989) 319.
- [14] N. Tekin, Ö. Demirbaş, M. Alkan, *Microporous Mesoporous Mater.* 85 (2005) 340.
- [15] V. Shubin, *J. Colloid. Interf. Sci.* 191 (1997) 372.
- [16] V. Shubin, P. Linse, *J. Phys. Chem.* 99 (1995) 1285.
- [17] D. Solberg, L. Wågberg, *Colloid. Surfaces A: Physicochem. Eng. Aspects* 219 (2003) 161.
- [18] J.R. Scherer, G.F. Bailey, S. Kint, R. Young, D.P. Malladi, B. Bolton, *J. Phys. Chem.-Us* 89 (1985) 312.
- [19] N.M. Kirby, S.T. Mudie, A.M. Hawley, D.J. Cookson, H.D.T. Mertens, N. Cowieson, V. Samardzic-Boban, *J. Appl. Crystallogr.* 46 (2013) 1670.
- [20] A. Hammersley, *Inter Rep ESRF98HA01*, ESRF, Grenoble, 1998.
- [21] M. James, A. Nelson, S.A. Holt, T. Saerbeck, W.A. Hamilton, F. Klose, *Nucl. Instrum. Meth. A* 632 (2011) 112.
- [22] A. Nelson, *J. Appl. Crystallogr.* 39 (2006) 273.
- [23] J. Lefebvre, D. Gray, *Cellulose* 12 (2005) 127.
- [24] C. Edgar, D. Gray, *Cellulose* 10 (2003) 299.
- [25] C.J. Van Oss, R.J. Good, M.K. Chaudhury, *Langmuir* 4 (1988) 884.
- [26] L. Yu, G. Garnier, *Fundam. Papermak. Mater.* 2 (1997) 1021.
- [27] H.P. Fink, D. Fanter, B. Philipp, *Acta Polym.* 36 (1985) 1.
- [28] M.A. Singh, M.N. Groves, *Acta Crystallogr. Section A* 65 (2009) 190.
- [29] E. Kontturi, M. Suchy, P. Penttilä, B. Jean, K. Pirkkalainen, M. Torkkeli, R. Serimaa, *Biomacromolecules* 12 (2011) 770.
- [30] L. Nevot, P. Croce, *Rev. Phys. Appl.* 15 (1980) 761.
- [31] v.W. Scholtan, *Die Makromolekulare Chemie* 14 (1954) 169.
- [32] S. Mallam, F. Horkay, A.M. Hecht, E. Geissler, *Macromolecules* 22 (1989) 3356.
- [33] G. Cheng, Z.L. Liu, J.K. Murton, M. Jablin, M. Dubey, J. Majewski, C. Halbert, J. Browning, J. Ankner, B. Akgun, C. Wang, A.R. Esker, K.L. Sale, B.A. Simmons, M.S. Kent, *Biomacromolecules* 12 (2011) 2216.
- [34] J. Hine, C.H. Thomas, *J. Am. Chem. Soc.* 75 (1953) 739.
- [35] T.J. Su, J.R. Lu, R.K. Thomas, Z.F. Cui, J. Penfold, *J. Colloid. Interf. Sci.* 203 (1998) 419.
- [36] S.M. Notley, B. Pettersson, L. Wågberg, *J. Am. Chem. Soc.* 126 (2004) 13930.
- [37] E. Kontturi, P.C. Thune, J.W. Niemantsverdriet, *Langmuir* 19 (2003) 5735.
- [38] G. Garnier, M. Bertin, M. Smrckova, *Langmuir* 15 (1999) 7863.
- [39] M. Eriksson, S.M. Notley, L. Wågberg, *Biomacromolecules* 8 (2007) 912.
- [40] E. Kontturi, P.C. Thune, J.W. Niemantsverdriet, *Polymer* 44 (2003) 3621.
- [41] C. Aulin, S. Ahola, P. Josefsson, T. Nishino, Y. Hirose, M. Österberg, L. Wågberg, *Langmuir* 25 (2009) 7675.
- [42] E. Kontturi, T. Tammelin, M. Osterberg, *Chem. Soc. Rev.* 35 (2006) 1287.
- [43] S.M. Notley, M. Eriksson, L. Wågberg, S. Beck, D.G. Gray, *Langmuir* 22 (2006) 3154.
- [44] M. Ioelovich, *Bioresources* 4 (2009) 1168.
- [45] H. Tanaka, L. Ödberg, L. Wågberg, T. Lindström, *J. Colloid. Interf. Sci.* 134 (1990) 219.
- [46] L. Wågberg, *Nordic. Pulp. Paper Res. J.* 15 (2000) 586.
- [47] T.G.M.v.d. Ven, *Nordic. Pulp. Paper Res. J.* 15 (2000) 494.
- [48] S.M. Notley, M. Norgren, *Biomacromolecules* 9 (2008) 2081.
- [49] G. Wegner, V. Buchholz, L. Ödberg, S. Stemme, *Adv. Mater.* 8 (1996) 399.
- [50] A.T. Horvath, A.E. Horvath, T. Lindström, L. Wågberg, *Langmuir* 24 (2008) 10797.
- [51] H.-J. Butt, Karlheinz Graf, M. Kappl, in: (Eds.) 1st ed.; Wiley-VCH, 2003, p 373p.
- [52] L. Winter, L. Wågberg, L. Ödberg, T. Lindström, *J. Colloid. Interf. Sci.* 111 (1986) 537.
- [53] L. Wågberg, G. Pettersson, S. Notley, *J. Colloid. Interf. Sci.* 274 (2004) 480.